PART I. IMPROVEMENTS IN THE ROTATION-RATE STEP EXPERIMENT FOR THE EVALUATION OF DIFFUSION COEFFICIENTS AT ROTATING DISK ELECTRODES

PART II. ION-PAIRING AND ELECTRIC FIELD EFFECTS ON ELECTRON HOPPING IN THE NAFION-TRIS(2,2′-BIPYRIDINE)OSMIUM(3+/2+) SYSTEM

Thesis by

David N. Blauch

In Partial Fulfillment of the Requirements

for the Degree of

Doctor of Philosophy

California Institute of Technology

Pasadena, California

1991

(submitted August 1, 1990)

"I am afraid that I rather give myself away when I explain. Results without causes are much more impressive."

Sherlock Holmes in *The Stock-Broker's Clerk*
Sir Arthur Conan Doyle

Acknowledgments

As my graduate career at Caltech draws to a close, it seems fitting to acknowledge those individuals who have contributed to its success. First and foremost, I would like to thank my thesis advisor, Professor Fred Anson, for his patience, guidance, and ever enjoyable Christmas and July 4th gatherings. I have been privileged to work with Professor Jean-Michel Savéant, my graduate education having been greatly enriched by his penetrating insights and imagination. It has been a pleasure to know and interact with all of the individuals who have, at one time or another, been part of the Anson group. In particular, I wish to acknowledge Dr. Ching-Fong Shu, who performed the experimental measurements described in Part II, and Dr. David Malerba, who provided valuable technical assistance.

On a less serious note, life in southern California would have been considerably less tolerable without the highly entertaining distractions provided by the Hogs, GL, Dor Iaur, the Doctor, and Earthshaker, among others. Special thanks go to Colin Campbell for his friendship, not to mention his fine wine and outstanding cuisine, and to my E-Mail cronies, Anthony Kapolka and Leland Steinke, for the invigorating discussions, provocative opinions (some of which were even solicited), and sense of perspective they provided.

Finally, the past five years of graduate study would not have been possible without financial support, much of which was provided by the National Science Foundation and the Department of Education in the form of graduate fellowships.

Abstract

Part I

An improved description of the current transient produced by an abrupt change in the rate of rotation of a rotating disk electrode has been obtained by the method of orthogonal collocation. The procedure provides a formula that accurately describes the expected current transient for at least 90% of its duration. If the final rotation rate is chosen to be ca. 58% of the initial rotation rate, the resulting current transient exhibits simple exponential decay, thereby facilitating data analysis. A simple offset in the time scale of the experiment proves effective in compensating for the effects of both hydrodynamic relaxation and imperfections in the response of the electrode rotator.

Part II

The high ionic content and low dielectric constant that prevail in the interior of many redox polymers are expected to promote ionic association between the polyelectrolyte and counterions. The present study is an attempt to evaluate the influence of ion-pairing interactions on charge propagation within polyelectrolyte films. The system under investigation consists of the $Os(bpy)_3^{3+/2+}$ redox couple incorporated into Nafion, where ion-pairing between the osmium complex and pendant sulfonate groups is argued to be responsible for the irreversible retention of the complex within the film. The apparent diffusion coefficient characterizing the dynamics of electron propagation through the redox polymer exhibits a remarkably

sudden increase as the film approaches electrostatic saturation with the $Os(bpy)_3^{3+}$ complex. Existing models, even those taking into account the presence of electric fields within the film, do not account satisfactorily for the observed behavior of the apparent diffusion coefficients. The introduction of ion-pairing into the model for charge transport leads to predictions that are consistent with the observed behavior. Key ingredients in the successful model are the assumptions that the predominant forms of the $Os(bpy)_3^{3+/2+}$ complex incorporated in Nafion are neutral aggregates resulting from the formation of triple or double ion-pairs and that the triply ion-paired $Os(bpy)_3^{3+}$ species dissociates into a singly charged species containing the same number of sulfonate groups as the predominant form of the $Os(bpy)_3^{2+}$ complex, thereby providing a low-energy pathway for electron self-exchange. The dissociation of the triply ion-paired $Os(bpy)_3^{3+}$ complex provides a natural explanation for the steep increase in the apparent diffusion coefficient, i.e., the rate of electron propagation, as the concentration of the osmium complex comes close to saturation, because as saturation is approached the ion-pairing equilibrium shifts to favor the formation of the doubly ion-paired form of $Os(bpy)_3^{3+}$ that is the best partner for accepting an electron from the doubly ion-paired $Os(bpy)_3^{2+}$ complex. The inevitable presence of electric fields within the polyelectrolyte films also affects the observed behavior, especially as the concentration of the incorporated cation is increased.

TABLE OF CONTENTS

PART II. ION-PAIRING AND ELECTRIC FIELD EFFECTS ON ELECTRON HOPPING IN THE NAFION-TRIS(2,2′-BIPYRIDINE)OSMIUM(3+/2+) SYSTEM

List of Figures

List of Tables

Glossary of Symbols for Part I

Physical Quantities

C^*	bulk concentration of electroactive species (M)
$C(x,t)$	time-dependent concentration profile of electroactive species (M)
$C_0(x)$	initial steady-state concentration profile of electroactive species (M)
D	diffusion coefficient of electroactive species ($cm^2\ s^{-1}$)
F	Faraday constant ($C\ mol^{-1}$)
$i(t)$	time-dependent current (A)
n	number of electrons transferred in electrode reaction
S	electrode surface area (cm^2)
t	time (s)
t_D	delay time employed in finite difference simulation of imperfect motor response (s)
t_0	offset time required to compensate for nonideal effects (ms)
t_{HR}	delay time arising from hydrodynamic relaxation (ms)
t_{MR}	delay time arising from imperfect motor response (ms)
$v(x)$	time-independent hydrodynamic velocity function ($cm\ s^{-1}$)
$v(x,t)$	time-dependent hydrodynamic velocity function ($cm\ s^{-1}$)
x	distance from electrode surface (cm)
Δi	difference between initial and final steady-state currents (A)
υ	solution kinematic viscosity ($cm^2\ s^{-1}$)
ω_0	initial rotation rate of electrode (s^{-1})
ω_∞	final rotation rate of electrode (s^{-1})
$\omega(t)$	time-dependent rotation rate of electrode (s^{-1})

Dimensionless Quantities

$c(z,\tau)$	time-dependent concentration profile of electroactive species
$c_0(z)$	initial steady-state concentration profile of electroactive species
$f(\tau)$	fractional change in current

$H(z)$	time-independent hydrodynamic velocity function
$H(z,t)$	time-dependent hydrodynamic velocity function
$H_0(z)$	time-independent hydrodynamic velocity function describing the initial steady-state condition
S	Schmidt number of electroactive species
$u(\tau)$	function characterizing time-dependence of $\omega(\tau)$
v_a	coefficient in hydrodynamic velocity function
v_b	coefficient in hydrodynamic velocity function
v_c	coefficient in hydrodynamic velocity function
z	distance from electrode surface
ε	step size parameter
τ	time
τ_0	offset time required to compensate for non-ideal effects
τ_D	delay time employed in finite difference simulation of imperfect motor response
τ_{HR}	delay time arising from hydrodynamic relaxation
τ_{MR}	delay time arising from imperfect motor response

Orthogonal Collocation Quantities

$a_i(\tau)$	orthogonal collocation eigenfunction
$\vec{a}(\tau)$	vector containing eigenfunctions $a_i(\tau)$
$\mathbf{A}$	orthogonal collocation convection-diffusion operator
$\mathbf{A}_0$	orthogonal collocation convection-diffusion operator associated with the initial steady state
$\vec{b}_0$	vector describing initial steady-state boundary conditions
$\vec{b}_\infty$	vector describing final steady-state boundary conditions
$\mathbf{B}$	source matrix for the eigenvalue problem
f_i	orthogonal collocation coefficient
i	summation, matrix, or vector index
j	summation, matrix, or vector index
k_i	constants determined by boundary conditions
$\vec{k}$	vector containing constants k_i
m	matrix index
N	order of orthogonal collocation approximation
M	summation limit

P	EIGRF performance index
P_i	empirical constant relating λ_i to S
Q_i	empirical constant relating λ_i to S
$\mathbf{U}$	time-derivative matrix operator
$\mathbf{V}$	matrix whose columns are eigenvectors of the matrix **B**
$\vec{x}(\tau)$	exponential vector in the solution for $\vec{a}(\tau)$
α	parameter in exponential weight function
β	parameter in exponential weight function
λ_i	eigenvalue of the orthogonal collocation matrix **B**

Finite Difference Quantities

$c_{i,j}$	finite difference approximation of $c(z_i,\tau_j)$
$\vec{c}_j$	vector whose ith row contains $c_{i,j}$
$\vec{d}_j$	vector describing boundary conditions at time τ_j
h	spatial interval in finite difference mesh
k	temporal interval in finite difference mesh
$\mathbf{I}$	identity matrix
N	number of spatial intervals in finite difference mesh
$\mathbf{P}_j$	finite difference convection-diffusion operator at time τ_j
$\mathbf{Q}_j$	matrix employed in Crank-Nicolson procedure
$\mathbf{R}_j$	matrix employed in Crank-Nicolson procedure

Glossary of Symbols for Part II

Physical Quantities

A^+	$[Os(bpy)_3^{3+}\bullet(F^-)_2]^+$ ion-pair
B	$[Os(bpy)_3^{2+}\bullet(F^-)_2]$ ion-pair
C	$[Os(bpy)_3^{3+}\bullet(F^-)_3]$ ion-pair
C_i	concentration of species i (M)
C_E	total concentration of $Os(bpy)_3^{3+/2+}$ (M)
C_F^0	total concentration of Nafion sulfonate groups (M)
$C_{G,0}$	concentration of species G^+ at the electrode surface (M)
$C_{G,S}$	concentration of species G^+ in bulk solution (M)
D_{ap}	diffusion coefficient as measured experimentally ($cm^2\ s^{-1}$)
D_i	electron hopping diffusion coefficient ($cm^2\ s^{-1}$)
D_I	diffusion coefficient for physical displacement of species G^+ ($cm^2\ s^{-1}$)
D_{pd}	diffusion coefficient for physical displacement ($cm^2\ s^{-1}$)
E	electrode potential measured relative to bulk solution (V)
E_i	initial electrode potential in linear sweep voltammetry (V)
E^o	standard reduction potential (V)
F^-	Nafion sulfonate group not ion-paired with $Os(bpy)_3^{3+/2+}$
F	Faraday constant ($C\ mol^{-1}$)
G^+	mobile electroinactive counterion, H^+ or Na^+
i	current (A)
i_p	peak current (A)
k_{act}	second-order activation-limited rate constant ($M^{-1}\ s^{-1}$)
k_d	second-order diffusion-limited rate constant ($M^{-1}\ s^{-1}$)
k_i	second-order activation-limited rate constant for electron self-exchange ($M^{-1}\ s^{-1}$)
$\bar{k}_i$	second-order activation limited rate constant for electron self-exchange between adjacent sites on a fictitious lattice ($M^{-1}\ s^{-1}$)
K	ion-pairing association constant for species A^+ and F^- (M^{-1})
K*	ion-pairing association constant for species Q^{2+} and F^- (M^{-1})
P^+	$[Os(bpy)_3^{2+}\bullet F^-]^+$ ion-pair
Q^+	$[Os(bpy)_3^{3+}\bullet F^-]^{2+}$ ion-pair

Q_t	charge consumed in exhaustive electrolysis of Nafion-incorporated $Os(bpy)_3^{3+/2+}$ (C)
Q_t^0	charge consumed in exhaustive electrolysis of Nafion-incorporated $Os(bpy)_3^{3+/2+}$ at full loading (C)
R	gas constant (J mol^{-1} $K^{\circ -1}$)
s	slope from Q vs. $t^{1/2}$ of chronocoulometric data (C $s^{-1/2}$)
S	electrode surface area (cm^2)
t	time (s)
T	temperature (°K)
v	sweep rate in slow-scan linear sweep voltammetry (V s^{-1})
x	distance from electrode surface (cm)
x_c	coating thickness (cm)
δ	center-to-center distance between redox species during electron transfer (nm)
ΔE_-	voltammetric lower half-width at half-maxima (V)
ΔE_+	voltammetric upper half-width at half-maxima (V)
Φ	electric potential (V)
Φ_0	electric potential at the electrode surface (V)
Φ_E	potential of electrode (V)
Φ_N	potential of Nafion coating (V)
Φ_S	potential of bulk solution (V)

Dimensionless Quantities

a	concentration of A^+ multiplied by κ
a_0	value of a under conditions where $\rho=0$
b	concentration of B
c	concentration of C
f	concentration of F^-
f^0	total concentration of Nafion sulfonate groups
f(g)	characteristic function in general form of the boundary value problem
g	concentration of G^+
g_i	finite difference approximation of g at point z=hi
h	distance between points in finite difference simulation
i	index

IC	constant of integration
n	number of points in finite difference simulation
u	Boltzmann transformation variable
X_E	fractional loading
z	exponential transformation variable
z_i	point employed in finite difference simulation
α	scaling factor in exponential transformation
γ	ratio of k_2 to k_1, multiplied by κ
$\Delta\varepsilon_-$	voltammetric lower half-width at half-maxima
$\Delta\varepsilon_+$	voltammetric upper half-width at half-maxima
$\Delta\varepsilon_\pm$	voltammetric full-width at half-maxima
ε	electrode potential
ε_p	voltammetric peak potential
ε_-	electrode potential at lower half-maxima
ε_+	electrode potential at upper half-maxima
φ	current in slow-scan linear sweep voltammetry
φ_p	peak current in slow-scan linear sweep voltammetry
ϕ	electric potential
ϕ_0	electric potential at the electrode surface
κ	ion-pairing association constant
μ_i^0	standard chemical potential of species i
π	pi, 3.1415926536...
ρ	ratio of concentrations of $Os(bpy)_3^{2+}$ to $Os(bpy)_3^{3+}$
ρ_p	value of ρ at the peak potential
ρ_-	value of ρ at the lower half-maxima
ρ_+	value of ρ at the upper half-maxima
σ	ratio of D_I to D_1
ψ	chronoamperometric or chronocoulometric current

PART I

IMPROVEMENTS IN THE ROTATION-RATE STEP EXPERIMENT FOR THE EVALUATION OF DIFFUSION COEFFICIENTS AT ROTATING DISK ELECTRODES

Chapter 1

The Rotation-Rate Step Experiment

Introduction

A commonly encountered electrochemical problem is the need to determine diffusion coefficients without knowledge of concentration, number of electrons transferred, and electrode area. Albery et al.[1] have described a rotation-rate step experiment that permits such a determination. The experiment consists of changing the rotation rate of a rotating disk electrode instantaneously, under conditions where the current is mass-transport-limited, and recording the resulting current transient. Analysis of the time-dependence of the transient allows the diffusion coefficient of the reactant to be determined.

In our attempts to implement this technique, we encountered a number of discrepancies between the observed current transients and those predicted on the basis of the treatment of Albery et al..[1] For example, in experiments where ferrocyanide was oxidized at a rotating platinum disk electrode, the diffusion coefficient derived from the current transient deviated significantly from the accepted value, and the magnitude of the deviation varied with the size and direction of the change in rotation rate. We have, therefore, performed a more complete analysis of the expected current transients using orthogonal collocation and finite difference methods. These approaches require no assumptions regarding the magnitude or direction of the change in rotation rate and are, therefore, applicable to experiments involving large changes in rotation rate for which the approximate treatment in Reference 1 is unsuitable.

Two sources of deviant behavior in the rotation-rate step experiment are of concern. First, the velocity of the solution near the electrode surface requires time to adjust to the change in rotation

rate. This effect, known as hydrodynamic relaxation, has been modeled by Benton[2] for an impulsively rotated disk and by Chawla[3] for an impulsive change in the angular velocity of a rotating disk. The influence of hydrodynamic relaxation on the relaxation of the concentration profile resulting from the impulsive change in rotation rate of a rotating disk electrode has been modeled by Albery and co-workers.[1] Second, even the best available motor cannot change the rotation rate of an electrode instantaneously; imperfections in the desired step change in rotation rate are inevitable. Unlike the effects of hydrodynamic relaxation, however, the effects of imperfect motor response on the current transients obtained from an abrupt change in rotation rate have not been examined in detail. In fact, the effects arising from imperfect rotation rate steps are inextricably coupled with those arising from hydrodynamic relaxation. The former are likely to be most important at relatively high rotation rates, where the time required for the change in rotation rate is significant compared to the duration of the current transient. The latter, being independent of the rotation rate,[2,3] assume greater importance at low rotation rates, where imperfections in the motor response are less serious.

As we are interested in relatively high rotation rates and utilize rotators with relatively slow response times, our analysis assumes that hydrodynamic relaxation proceeds rapidly enough to be regarded as instantaneous on the time scale of the motor response time and the convective-diffusive relaxation within the Levich layer, which is the source of the transient current. After deriving the behavior to be expected in the absence of both hydrodynamic

relaxation and imperfections in the motor response, we demonstrate that a simple shift in the time scale in a manner similar to that proposed by Bruckenstein et al.[4] effectively compensates for these two sources of deviant behavior. The details of our analysis and comparison of its predictions with experimental current transients are the subject of Part I.

Theory

The time-dependent, convective-diffusion equation and associated boundary conditions describing the reduction or oxidation of a molecule at a rotating disk electrode are[5]

$$\frac{\partial C(x,t)}{\partial t} = D\frac{\partial^2 C(x,t)}{\partial x^2} - v(x)\frac{\partial C(x,t)}{\partial x} \tag{1.1}$$

and

$$C(0,t) = 0\ , \qquad \lim_{x\to\infty} C(x,t) = C^*\ , \qquad C(x,0) = C_0(x)\ , \tag{1.2}$$

where $C(x,t)$ is the concentration profile of the electroactive species, C^* is the bulk concentration, $C_0(x)$ is the initial steady-state concentration profile, x is the distance from the electrode surface, t is the time, and $v(x)$ is the hydrodynamic velocity function,[5] and D is the diffusion coefficient of the reacting molecule.

The experiment we wish to analyze involves an abrupt change in the electrode rotation rate from its initial value, ω_0, to a final value,

ω_∞ (s^{-1}). It is useful to define a step-size parameter, ε, to characterize the change in rotation rate.

$$\omega_\infty = \omega_0(1+\varepsilon)^2 \ . \tag{1.3}$$

In this formulation of the problem, the hydrodynamic velocity function, v(x), is time-independent and describes the steady-state condition associated with the final angular velocity ω_∞. The concentration profile at time t=0 is assumed to be the steady-state concentration profile associated with the angular velocity ω_0, consistent with the boundary conditions of Equation 1.2. This treatment is identical with the assumption that imperfections in the motor response and hydrodynamic relaxation are inconsequential.

For convenience, the following dimensionless quantities are introduced:

$$z = \left(\omega_\infty / \upsilon\right)^{1/2} x \ , \qquad \tau = \omega_\infty t \ , \tag{1.4}$$

$$c(z,\tau) = 1 - \frac{C(x,t)}{C^*} \ , \tag{1.5}$$

and

$$v(x) = (\omega_\infty \upsilon)^{1/2} H(z) \ , \tag{1.6}$$

where υ is the kinematic viscosity of the solution and H(z) is the dimensionless, steady-state hydrodynamic velocity function as described by Cochran[6] and by Benton.[2]

To characterize the magnitude of the current transient that results from the change in rotation rate in dimensionless form, the fractional change in current, $f(\tau)$, is defined:

$$f(\tau)=\frac{i(\tau)-i(0)}{i(\infty)-i(0)}=\frac{i(\tau)-i(0)}{\Delta i}\ . \tag{1.7}$$

$i(\tau)$ is the transient current that flows in response to the change in rotation rate; $i(0)$ and $i(\infty)$ are the initial and final steady-state currents, and Δi is the total change in current.

A three-term expression for H(z) accurate to better than 1% in the relevant region near the electrode surface is given by[2]

$$H(z)=v_a z^2+v_b z^3+v_c z^4, \tag{1.8}$$

where v_a=-0.51023, v_b=1/3, and v_c=-0.10265.

The boundary value problem represented by Equations 1.1 and 1.2 can be recast as

$$S\frac{\partial c(z,\tau)}{\partial \tau}=\frac{\partial^2 c(z,\tau)}{\partial z^2}-S\,H(z)\frac{\partial c(z,\tau)}{\partial z} \tag{1.9}$$

and

$$c(0,\tau)=1\ ,\quad \lim_{z\to\infty} c(z,\tau)=0\ ,\quad c(z,0)=c_0(z)\ , \tag{1.10}$$

where the Schmidt number S is defined by

$$S = \upsilon / D \cdot \tag{1.11}$$

Inspection of Equation 1.9 clearly reveals that the convective-diffusive behavior of the electroactive molecule is conveniently characterized by the Schmidt number. We therefore develop the theory for the rotation-rate step experiment in terms of the parameter S instead of D. Analysis of experimental current transients thus yields a value for the Schmidt number; knowledge of the solution kinematic viscosity, which may be readily measured, permits determination of the diffusion coefficient.

Chapter 2

Orthogonal Collocation Analysis

The Orthogonal Collocation Method

The solution of the boundary value problem represented by Equations 1.9 and 1.10 can be approximated by the method of orthogonal collocation.[7-10] In our implementation of the orthogonal collocation method, the time-dependent concentration $c(z,\tau)$ is assumed to be of the form

$$c(z,\tau) = \exp\left(-\alpha z^{\beta}\right) \sum_{i=0}^{N} a_i(\tau)\, z^i \,. \tag{2.1}$$

The parameters α and β are arbitrary; however, certain values for these parameters are advantageous, as explained in Appendix I. The boundary condition $c(0,\tau)=1$ (Equation 1.10) is satisfied by

$$a_0(\tau) = 1 \,, \tag{2.2}$$

providing $\beta>0$. The boundary condition $\lim_{z\to\infty} c(z,\tau) = 0$ is inherent in the expression for $c(z,\tau)$, because the exponential function dominates the expression at large z and forces convergence to zero as $z\to\infty$, providing $\alpha>0$.

The remaining functions, $a_i(\tau)$ for i= 1, 2, ..., N, are chosen so that the function c(z,t) in Equation 2.1 fulfills the requirements of the boundary value problem (Equations 1.9 and 1.10) at N collocation points, z_i for i= 1, 2, ..., N, at all times, τ. In principle, any set of N points can be employed in the orthogonal collocation procedure. The error associated with a particular approximation will, however, depend strongly upon the choice of collocation points, making it

advantageous to choose a set of collocation points that minimizes some measure of the error. In this project, the collocation points are chosen by means of Gaussian quadrature on the interval $[0,\infty)$ with respect to the weight function $\exp(-\alpha z^{\beta})$. The details of this procedure are provided by Caban and Chapman.[9]

Explicit differentiation of Equation 2.1 yields the following expressions for the derivatives of $c(z,\tau)$:

$$\frac{\partial c(z,\tau)}{\partial \tau} = \exp\left(-\alpha z^{\beta}\right) \sum_{i=0}^{N} \frac{da_i(\tau)}{d\tau} z^i \ , \tag{2.3}$$

$$\frac{\partial c(z,\tau)}{\partial z} = \exp\left(-\alpha z^{\beta}\right) \sum_{i=0}^{N} a_i(\tau) \left(i - \alpha \beta z^{\beta}\right) z^{i-1} \ , \tag{2.4}$$

and

$$\frac{\partial^2 c(z,\tau)}{\partial z^2} = \exp\left(-\alpha z^{\beta}\right) \sum_{i=0}^{N} a_i(\tau) \left(i\,(i-1) - \alpha \beta \,(2\,i + \beta - 1)\, z^{\beta} + \alpha^2 \beta^2 z^{2\beta}\right) z^{i-2} \ . \tag{2.5}$$

Substitution of Equations 2.3, 2.4, and 2.5 into the master differential equation (Equation 1.9) produces

$$\sum_{i=0}^{N} \frac{da_i(\tau)}{d\tau} S\, z^i =$$

$$\sum_{i=0}^{N} a_i(\tau) \left[i\,(i - 1 - S\,H(z)\,z) - \alpha \beta \,(2\,i + \beta - 1 - S\,H(z)\,z)\, z^{\beta} + \alpha^2 \beta^2 z^{2\beta}\right] z^{i-2} \ . \tag{2.6}$$

The equality in Equation 2.6 must be satisfied at each collocation point, *vide supra*, thereby leading to the linear system represented by

$$\mathbf{U}\frac{d\vec{a}(\tau)}{d\tau} = \mathbf{A}\,\vec{a}(\tau) - \vec{b}_{\infty}\,, \tag{2.7}$$

where the vectors are defined by

$$[\vec{a}(\tau)]_i = a_i(\tau) \tag{2.8}$$

and

$$[\vec{b}_{\infty}]_i = -\alpha\beta\left(\beta - 1 - S\,H(z_i)\,z_i\right)z_i^{\beta-2} + \alpha^2\beta^2 z_i^{2\beta-2} \tag{2.9}$$

and the matrices are defined by

$$[\mathbf{U}]_{i,j} = S\,z_i^{\,j} \tag{2.10}$$

and

$$[\mathbf{A}]_{i,j} = \left[j\left(j-1-S\,H(z_i)\,z_i\right) - \alpha\beta\left(2j+\beta-1-S\,H(z_i)\,z_i\right)z_i^{\beta} + \alpha^2\beta^2 z_i^{2\beta}\right]z_i^{\,j-2}\,. \tag{2.11}$$

Each row in Equation 2.7 corresponds to an evaluation of Equation 2.6 at a different collocation point.

The final steady-state solution, $\vec{a}(\infty)$, of the initial value problem represented by Equation 2.7 is the Levich solution corresponding to

the rotation rate ω_∞ and is obtained by solving Equation 2.7 under the condition $d\vec{a}(\tau)/d\tau = 0$:

$$\mathbf{A}\,\vec{a}(\infty) = \vec{b}_\infty \,. \tag{2.12}$$

The initial condition, characterized by $\vec{a}(0)$, is the Levich solution corresponding to the rotation rate ω_0. In order to evaluate $\vec{a}(0)$, it is necessary to alter the dimensionless hydrodynamic velocity function H(z), Equation 1.8, to describe the initial velocity profile, i.e., the velocity profile associated with the initial rotation rate, ω_0. (Recall that the variables have been normalized by the final rotation rate, ω_∞, which is related to the initial rotation rate by Equation 1.3.) The appropriate expression for the initial, dimensionless hydrodynamic velocity function is

$$H_0(z) = \frac{v_a (1+\varepsilon)^2 z^2 + v_b (1+\varepsilon) z^3 + v_c z^4}{(1+\varepsilon)^5} \,. \tag{2.13}$$

The subscript 0 is introduced to indicate that a matrix or vector is constructed by means of $H_0(z)$ instead of H(z) and hence is associated with the initial steady state. The initial steady-state solution is obtained by solution of the linear system

$$\mathbf{A}_0\,\vec{a}(0) = \vec{b}_0 \,. \tag{2.14}$$

Solution of the Eigenvalue Problem

The manipulations described in the preceding sections transform the original boundary value problem represented by Equations 1.9 and 1.10 into the eigenvalue problem represented by Equation 2.7. The reader is referred to standard mathematics texts for details regarding the solution of eigenvalue problems (see, for example, Strang[11] and Finizio and Ladas.[12]); we simply present the solution of Equation 2.7 in the form of Equations 2.15 and 2.16.

$$\vec{a}(\tau) = \vec{a}(\infty) + \mathbf{V}\,\vec{x} \tag{2.15}$$

$$[\vec{x}]_i = k_i \exp(\lambda_i \tau) \tag{2.16}$$

The columns of the matrix $\mathbf{V}$ are eigenvectors associated with the eigenvalues, λ_i, of the matrix $\mathbf{B}$, defined by

$$\mathbf{B} = \mathbf{U}^{-1}\mathbf{A}\ . \tag{2.17}$$

The constants k_i are chosen to satisfy the initial conditions by requiring

$$\mathbf{V}\,\vec{k} = \vec{a}(0) - \vec{a}(\infty)\ , \tag{2.18}$$

where

$$[\vec{k}]_i = k_i\ . \tag{2.19}$$

Calculation of Current Transients

The current that flows at the rotating disk electrode, $i(\tau)$, is related to the concentration gradient at the electrode surface by

$$i(\tau) = n\,F\,S\,D\left(\frac{\partial C(x,t)}{\partial x}\right)_{x=0} = n\,F\,S\,D\,C^{*}\left(\omega_{\infty}/\upsilon\right)^{1/2}\left(\frac{\partial c(z,\tau)}{\partial z}\right)_{z=0} . \qquad (2.20)$$

The electrode surface area is denoted by S and the Faraday constant by F; n is the number of electrons transferred in the electrode reaction. Combining Equations 2.4 and 2.15 with $z=0$ and $\beta>1$ yields the following expression for the gradient of $c(z,\tau)$ at the electrode surface:

$$\left(\frac{\partial c(z,\tau)}{\partial z}\right)_{z=0} = a_1(\tau) = a_1(\infty) + \sum_{i=1}^{N}[V]_{1,i}\,k_i\exp(\lambda_i\,\tau) . \qquad (2.21)$$

Utilization of Equations 2.20 and 2.21 permits the fractional change in current, $f(\tau)$, defined in Equation 1.7, to be recast in the form

$$f(\tau) = 1 + \sum_{i=1}^{N} f_i \exp(\lambda_i\,\tau) , \qquad (2.22)$$

where the collocation coefficients, f_i, are defined by

$$f_i = \frac{[V]_{1,i}\,k_i}{a_1(\infty) - a_1(0)} . \qquad (2.23)$$

Collocation Eigenvalues

The first step in the simulation of the current transient resulting from a step change in the rotation rate of a rotating disk electrode is to construct the matrices **A** and **U** from Equations 2.10 and 2.11. The matrix **B** is then computed by means of Equation 2.17 and its eigenvalues, λ_i, and a set of eigenvectors are determined. In this project, the IMSL subroutine EIGRF is utilized for the determination of the eigenvalues and eigenvectors. Technical details regarding the EIGRF subroutine may be found in the IMSL Reference Manual.[13] The elements of the matrices **A** and **U**, and hence **B**, depend upon the parameters α, β, and S but not upon the step-size parameter ε. For this reason, the eigenvalues, λ_i, are independent of the magnitude and direction of the change in rotation rate.

Typical sets of values for λ_i, evaluated for N= 2, 4, 6, 8, 10, 12 are shown in Table 2.1. The subscripts are assigned so that $\lambda_i > \lambda_j$ when $i<j$. As the order of the collocation, N, increases, the eigenvalues approach limiting values that are independent of α and β. For N=12, the limiting values of λ_i for i= 1, 2, 3, 4, 5, 6 have been essentially reached, as evidenced by the entries in Table 2.1. Higher collocation orders would be required to reach limiting values of λ_i for larger values of i. The limiting values of the collocation eigenvalues depend solely upon S and therefore provide a means of correlating the shape of a measured current transient with the Schmidt number, and thus the diffusion coefficient, of the electroactive species.

Relation of Collocation Eigenvalues to the Schmidt Number

Albery and co-workers[1] have derived a relationship between the Schmidt number and the exponential coefficients governing the shape and duration of the current transients produced by step changes in rotation rate. A modified form of the expression derived by Albery et al.[1] has been found empirically to provide an excellent approximation of the collocation eigenvalues. Expressed in terms of the λ_i values that are obtained from the orthogonal collocation procedure, the modified relationship takes the form

$$\lambda_i = P_i S^{-1/3}\left(1 - Q_i S^{-1/3}\right) . \qquad (2.24)$$

i	N						Ref. 1
	2	4	6	8	10	12	
1	-0.18980	-0.17770	-0.17781	-0.17781	-0.17781	-0.17781	-0.178
2	-0.41146	-0.42915	-0.43642	-0.43636	-0.43636	-0.43636	-0.460
3		-0.78242	-0.73870	-0.73681	-0.73681	-0.73681	
4		-2.18722	-1.08438	-1.06614	-1.06678	-1.06677	
5			-1.49876	-1.41641	-1.41992	-1.41991	
6			-7.12439	-1.94684	-1.79233	-1.79240	
7				-2.58211	-2.21307	-2.17825	
8				-17.15999	-2.84159	-2.58710	
9					-4.54126	-3.20933	
10					-34.46165	-3.87809	
11						-7.62335	
12						-61.31449	

Table 2.1. Collocation eigenvalues, λ_i, calculated for S=1500, α=250, and β=3.

The coefficients P_i and Q_i obtained by fitting the limiting values of λ_i, calculated from the orthogonal collocation procedure for a series of Schmidt numbers, to Equation 2.24 are listed in Table 2.2 for i= 1, 2, 3, 4. The corresponding coefficients estimated by Albery et al.[1] are also given; the moderately good agreement indicates that the approximations involved in the derivation in Reference 1 are not seriously in error.

i	Orthogonal Collocation		Reference 1	
	P_i	Q_i	P_i	Q_i
1	-2.2152 ± 0.0001	0.9290 ± 0.0005	-2.23	1.0
2	-5.571 ± 0.002	1.181 ± 0.002	-5.77	1.0
3	-9.563 ± 0.005	1.348 ± 0.004		
4	-14.03 ± 0.02	1.475 ± 0.007		

Table 2.2. Coefficients, P_i and Q_i, relating the collocation eigenvalues and the Schmidt numbers according to Equation 2.24.

Collocation Coefficients

Once the collocation eigenvalues are computed, the next step in the orthogonal collocation procedure is to compute the initial and final solutions, represented by $\vec{a}(0)$ and $\vec{a}(\infty)$, by means of Equations 2.14 and 2.12, respectively. Knowledge of $\vec{a}(0)$ and $\vec{a}(\infty)$ permit evaluation of the vector $\vec{k}$ from Equation 2.18. Finally, the collocation coefficients, f_i, are computed from the relation in Equation 2.23. Unlike the collocation eigenvalues, the collocation coefficients are functions of ε, in addition to α, β, and S, because the initial

steady-state solution, required in the computation of f_i, contains information regarding the initial rotation rate.

Relation of the Collocation Coefficients to the Schmidt Number

Typical sets of values for f_i, evaluated for N= 2, 4, 6, 8, 10, 12 are shown in Table 2.3. The subscript indicates the collocation eigenvalue with which the collocation coefficient is associated. As the order of the collocation, N, increases, the coefficients approach limiting values that are independent of α and β in the same manner as described for the collocation eigenvalues. For N=12, the limiting values of f_i for i= 1, 2, 3, 4, 5 have been essentially reached (see Table 2.3). Higher collocation orders would be required to reach limiting values of f_i for larger values of i.

i	N						Ref. 1
	2	4	6	8	10	12	
1	-1.93133	-1.72880	-1.72840	-1.72826	-1.72827	-1.72827	-1.57
2	0.93133	0.92104	0.94726	0.94726	0.94725	0.94725	0.57
3		-0.25469	-0.34284	-0.33650	-0.33652	-0.33652	
4		0.06245	0.16578	0.14967	0.14927	0.14927	
5			-0.04914	-0.05643	-0.05573	-0.05584	
6			-0.00734	0.03097	0.02709	0.02631	
7				-0.00848	-0.01163	-0.00890	
8				0.00179	0.00780	0.00571	
9					0.00013	-0.00362	
10					0.00061	0.00375	
11						0.00060	
12						0.00025	

Table 2.3. Collocation coefficients, f_i, calculated for S=1500, α=250, β=3, and ε=0.1.

The collocation coefficients, f_i, exhibit a weak dependence on the Schmidt number, as depicted in Figure 2.1, for a particular change in rotation rate. As is evident from the figure, the variation is also essentially linear with respect to $S^{-1/3}$. The variation is sufficiently small (e.g., f_1 increases by 3.2% as S increases from 300 to 48000 for ε=0.1) that for the purposes of this work it is possible to regard the coefficients, f_i, as independent of S. (The larger variation of f_i with the Schmidt number as i increases introduces negligible changes in calculated values of $f(\tau)$, because the multiplicative exponential term decreases rapidly toward zero as i increases.)

Relation of Collocation Coefficients to the Step-Size Parameter

The variation of a typical set of values of f_i with ε, the parameter characterizing the change in rotation rate (Equation 1.3), is shown in Figure 2.2 for i= 1, 2, 3, 4. It is found empirically that the dependences can be described reasonably accurately by simple polynomial functions of ε. The polynomials appropriate for a Schmidt number of 1500 are listed in Table 2.4. The equations given in Table 2.4 are utilized to calculate the collocation coefficients for other Schmidt numbers as well because of the insensitivity of the values of f_i to S (see above).

Complex Collocation Eigenvalues and Coefficients

For reasons discussed in Appendix I, it is advantageous to select α=S/6 and β=3. Empirically, utilization of these values for α and β in the orthogonal collocation analysis always leads to real values for λ_i and f_i. For other values for α and β, complex eigenvalues and

Figure 2.1. Variation of the first four collocation coefficients with the Schmidt number for ε=0.1. Straight lines are drawn through the calculated points. (○) f_1; (□) f_2; (△) f_3; (◇) f_4.

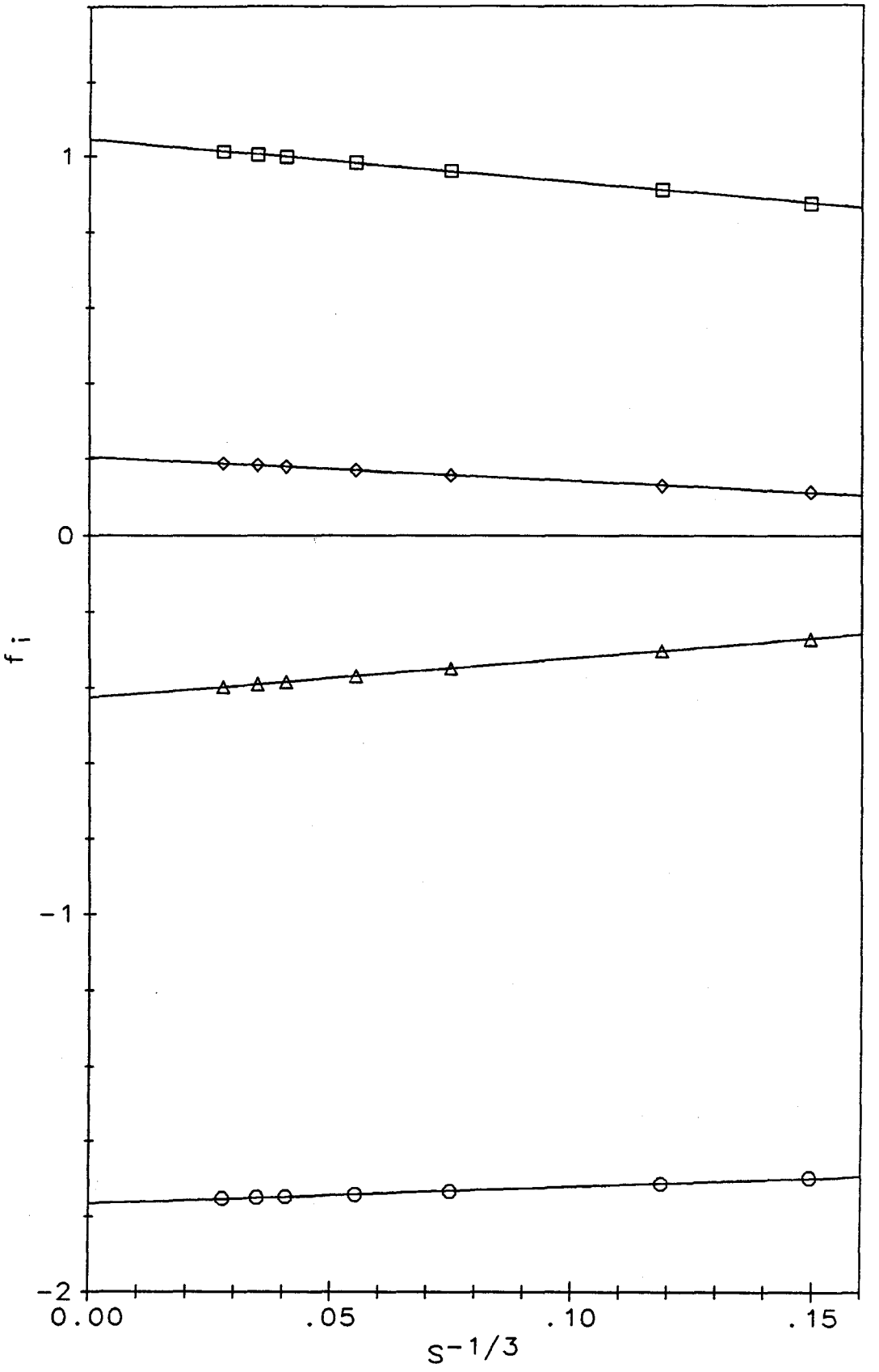
1
0
-1
-2
fi
0.00
.05
.10
.15
S-1/3

Figure 2.2. Variation of the first four collocation coefficients with the magnitude and sign of the change in rotation rate for a Schmidt number of 1500. Smooth curves were drawn through the calculated points. (○) f_1; (□) f_2; (△) f_3; (◇) f_4.

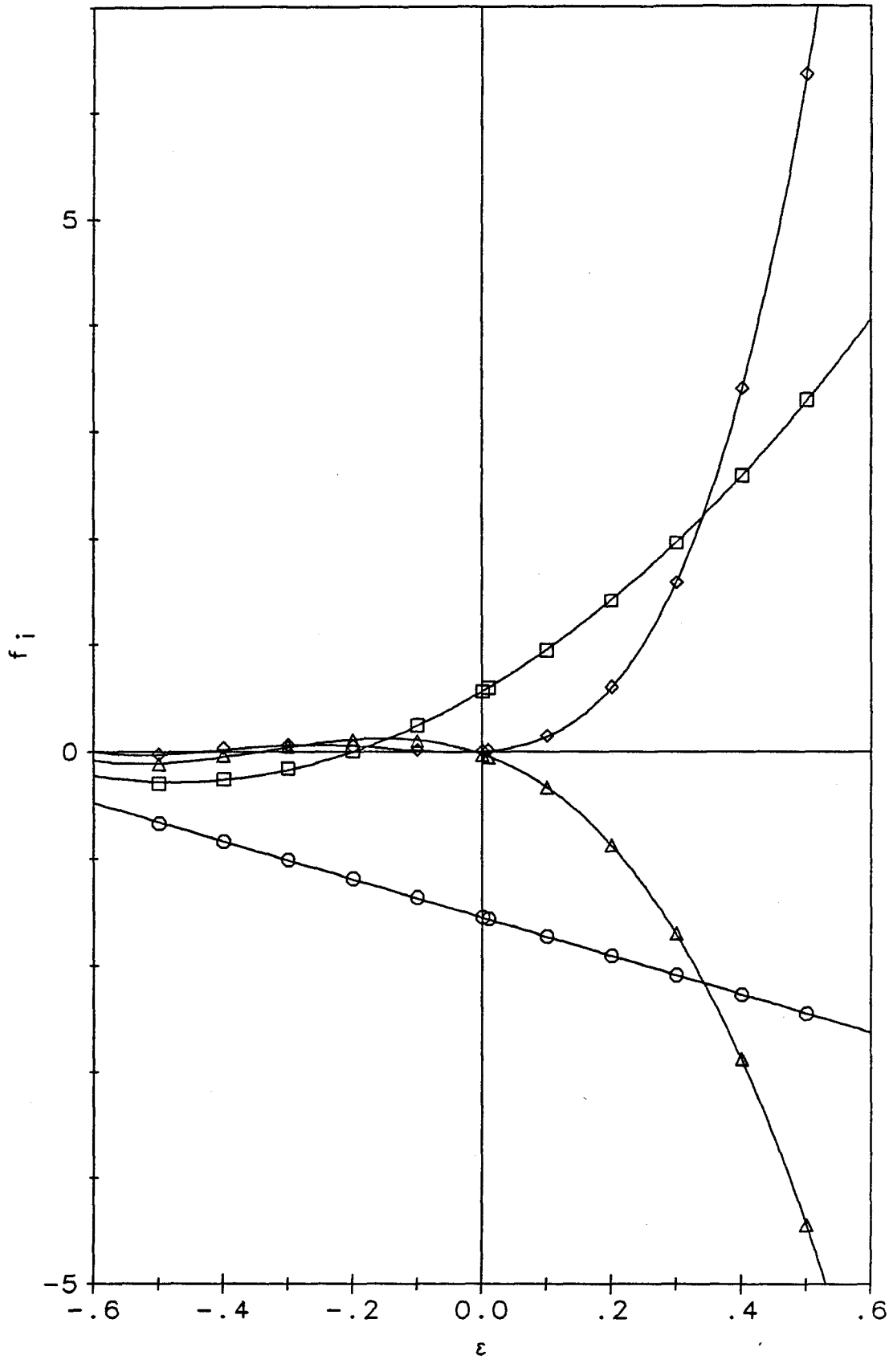
5
0
-5
f_i
-.6
-.4
-.2
0.0
.2
.4
.6
ε

coefficients are occasionally obtained. A typical example is provided in Table 2.5 for N=12, S=1500, α=100, β=3, and ε=0.1; the corresponding values for α=250 (Tables 2.1 and 2.3) are included for comparison. The subscripts re and im denote the real and imaginary components of the complex eigenvalues and coefficients.

f_1 =	-(1.551±0.002)	-(1.781±0.007)ε			
f_2 =	(0.562±0.006)	+(3.54 ±0.02)ε	+(3.68±0.07)ε^2		
f_3 =	-(0.029±0.006)	-(2.15±0.03)ε	-(8.8±0.1)ε^2	-(8.4±0.3)ε^3	
f_4 =	0	+(0.46±0.06)ε	+(7.4±0.2)ε^2	+(23.1±0.7)ε^3	+(20.±2.)ε^4

Table 2.4. Polynomial expressions relating f_i to ε for S=1500.

Complex eigenvalues and coefficients must necessarily occur as conjugate pairs, because the fractional change in current, $f(\tau)$, must be real. Under the heading α=100 in Table 2.5, the entries for i=7, 8 are conjugate pairs. For conjugate pairs of eigenvalues, λ and λ^*, and coefficients, f and f^*, the terms from Equation 2.22 involving these complex values may be rewritten as

$$f \exp(\lambda \tau) + f^* \exp(\lambda^* \tau) = 2\left(f_{re} \cos(\lambda_{im} \tau) - f_{im} \sin(\lambda_{im} \tau)\right) \exp(\lambda_{re} \tau) . \qquad (2.25)$$

For the example, the terms in Equation 2.22 involving the eigenvalues and coefficients for i=7,8 and α=100 in Table 2.5 may be rewritten as

$$f_7 \exp(\lambda_8 \tau) + f_8 \exp(\lambda_8 \tau) =$$

$$-0.00100\left(3.24368\cos(0.27643\,\tau) - \sin(0.27643\,\tau)\right)\exp(-2.16589\,\tau)\,. \qquad (2.26)$$

	α=250		α=100			
i	λ_i	f_i	$\lambda_{re,i}$	$\lambda_{im,i}$	$f_{re,i}$	$f_{im,i}$
1	-0.17781	-1.72827	-0.17781	0	-1.72827	0
2	-0.43636	0.94725	-0.43636	0	0.94725	0
3	-0.73681	-0.33652	-0.73681	0	-0.33652	0
4	-1.06677	0.14927	-1.06676	0	0.14929	0
5	-1.41991	-0.05584	-1.41954	0	-0.05560	0
6	-1.79240	0.02631	-1.79953	0	0.02501	0
7	-2.17825	-0.00890	-2.16589	0.27643	-0.00162	0.00050
8	-2.58710	0.00571	-2.16589	-0.27643	-0.00162	-0.00050
9	-3.20933	-0.00362	-2.46487	0	-0.00146	0
10	-3.87809	0.00375	-3.27689	0	-0.00019	0
11	-7.62335	0.00060	-4.01785	0	0.00330	0
12	-61.31449	0.00025	-33.30052	0	0.00043	0

Table 2.5. Collocation eigenvalues and coefficients for α=100 and α=250 with N=12, S=1500, β=3, and ε=0.1.

In this example, the period of the trigonometric functions is 22.7 radians, whereas the half-life of the exponential function is 0.320. Whenever complex eigenvalues and coefficients arise, the half-life of the exponential function is always observed to be at least one, frequently several, orders of magnitude smaller than the period of the trigonometric functions. The complex eigenvalues and coefficients therefore give rise to highly damped harmonic terms in the expression for the fractional change in current.

The limiting values of λ_i and f_i, i.e., those obtained for sufficiently large values of N, are never found, empirically, to be complex. The utilization of the results of the orthogonal collocation analysis described in the next section and in Chapter 4 involves only the limiting values of the collocation eigenvalues and coefficients; thus no complications associated with complex quantities exist. The limiting values of λ_i depend solely upon S, and the limiting values of f_i depend solely upon S and ε; the choice of α and β is arbitrary, provided $\alpha>0$ and $\beta>1$ as explained above.

Calculated Current Transients

Fractional changes in current may be calculated for a variety of experimental conditions from Equation 2.27,

$$f(\tau) = 1 + \sum_{i=1}^{M} f_i \exp(\lambda_i \tau) \,, \tag{2.27}$$

by utilizing λ_i and f_i values calculated by means of the orthogonal collocation procedure for S=1500, N=12, and M≤N. Representative results are shown in Figures 2.3 and 2.4 for steps to higher and lower rotation rates, respectively. Examination of these two figures shows that the fractional current changes resulting from steps to lower rotation rates can be described accurately with fewer summation terms in Equation 2.27 than those resulting from steps to higher rotation rates. In general, however, four terms, i= 1, 2, 3, 4, are adequate to describe with satisfactory accuracy all but the first 15% of the fractional current changes resulting from steps of either sign

Figure 2.3. Fractional changes in current calculated from Equation 2.27. From the top to the bottom curve, M = 2, 4, 6, 8, and 10 exponential terms are utilized in the calculation, with S=1500 and ε=0.3.

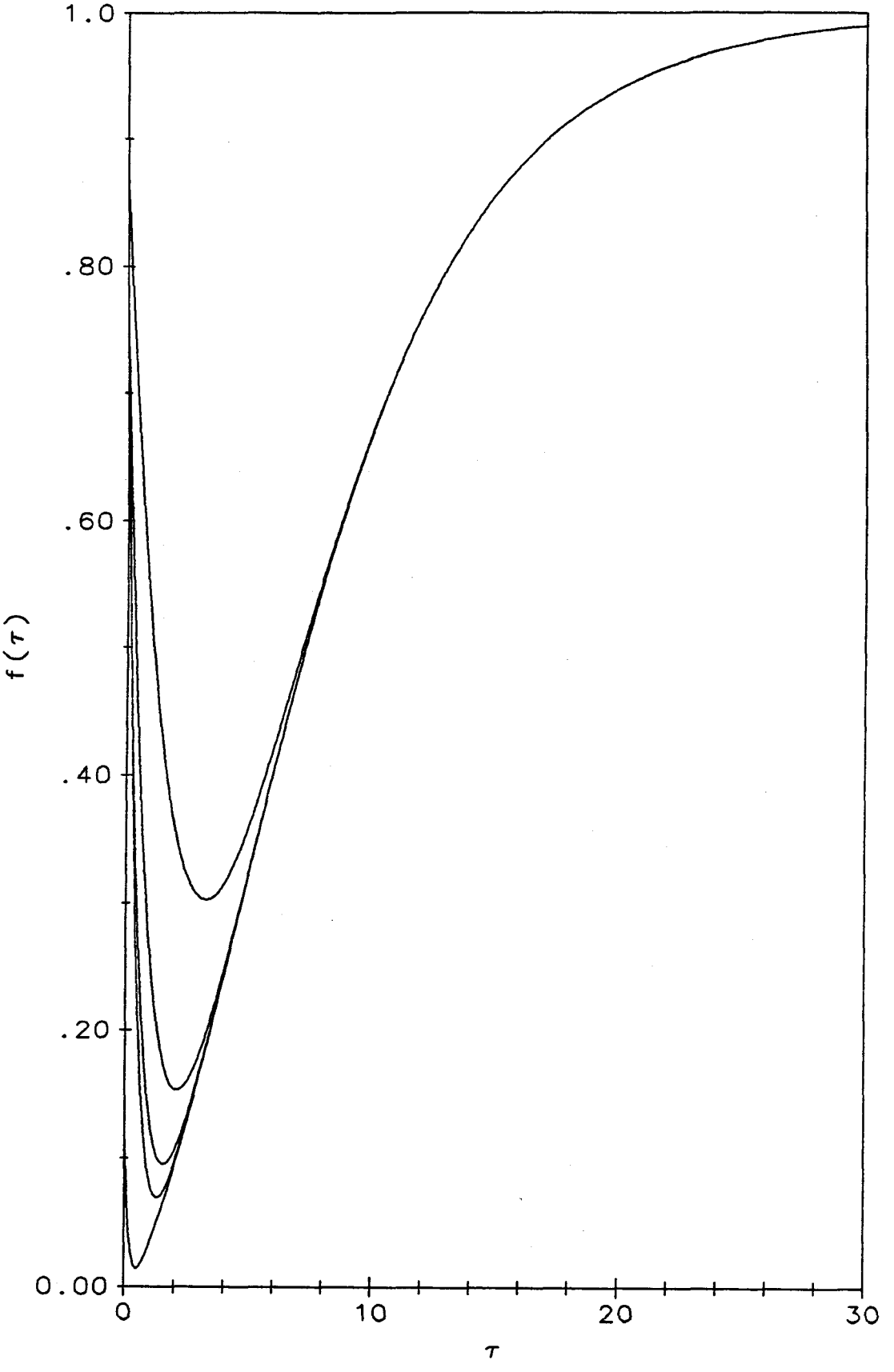
1.0
.80
.60
.40
.20
0.00
f(τ)
0
10
20
30
τ

Figure 2.4. Fractional changes in current calculated from Equation 2.27. From the bottom to the top curve, M = 2, 4, 6, 8, and 10 exponential terms are utilized in the calculation, with S=1500 and ε=-0.3. The last three curves are indistinguishable.

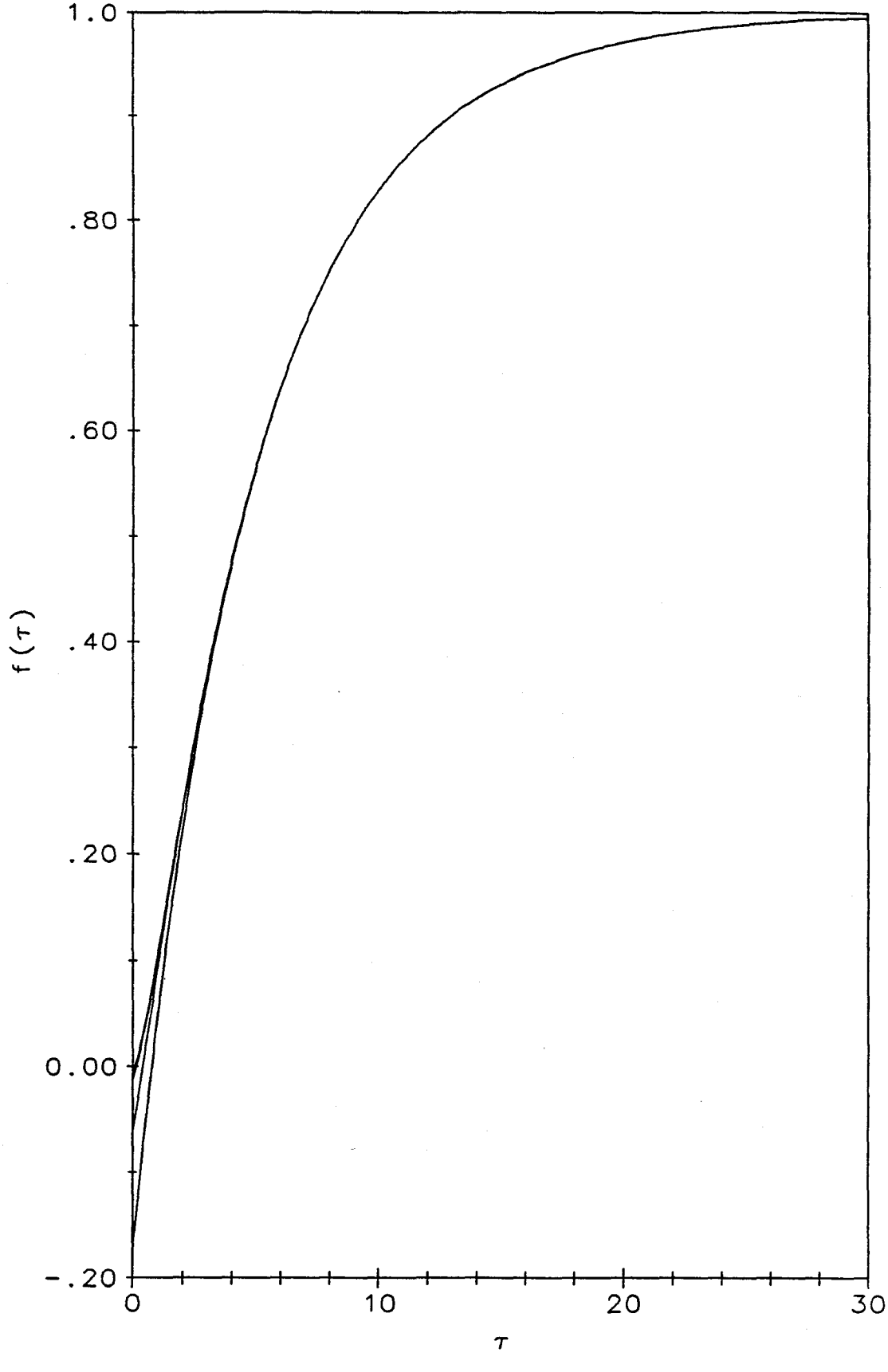
1.0
.80
.60
.40
.20
0.00
-.20
f(τ)
0
10
20
30
τ

with $|\varepsilon|<0.4$. For absolute values of ε outside this range or for times where $f(\tau)<0.15$, more terms are required in Equation 2.27 in order to calculate the current transient accurately.

The "Magic" Step Size

Inspection of Figure 2.2 reveals that for experiments in which the rotation rate is decreased by an amount corresponding to $\varepsilon=-0.24$ ($\omega_\infty/\omega_0=0.58$), the collocation coefficients for i= 2, 3, 4 are very close to zero. It follows from Equation 2.27 that the fractional current change obtained for this particular step change in rotation rate should be a simple exponential function of τ. This expectation is tested by calculating $f(\tau)$ from Equation 2.22 for $\varepsilon=-0.24$, S=1500, N=12, $\alpha=250$, and $\beta=3$ (Figure 2.5) and analyzing the calculated transient as if it were a simple exponential function. The results are shown in Figure 2.6, where the points represent a plot of $\ln[1-f(\tau)]$ vs. τ for the last 90% of the transient. The excellent linearity of the plot shows that current transients obtained from the "magic" step change in rotation rate, $\varepsilon=-0.24$, can be analyzed accurately as single exponential functions. This represents a considerable simplification in the data analysis when compared with the nonlinear curvefitting that is required to analyze the current transients obtained with any other value of the step change in rotation rate.

The value of λ_1 obtained from the slope of the least-squares line drawn through the points in Figure 2.6 may be used to calculate the Schmidt number from Equation 2.24. The value obtained, 1493, compares very favorably with the Schmidt number of 1500 used to simulate the current transient from which the points in Figure 2.6

Figure 2.5. Fractional change in current calculated from Equation 2.22 using N=12, S=1500, α=250, β=3, and ε=-0.24, the "magic" value.

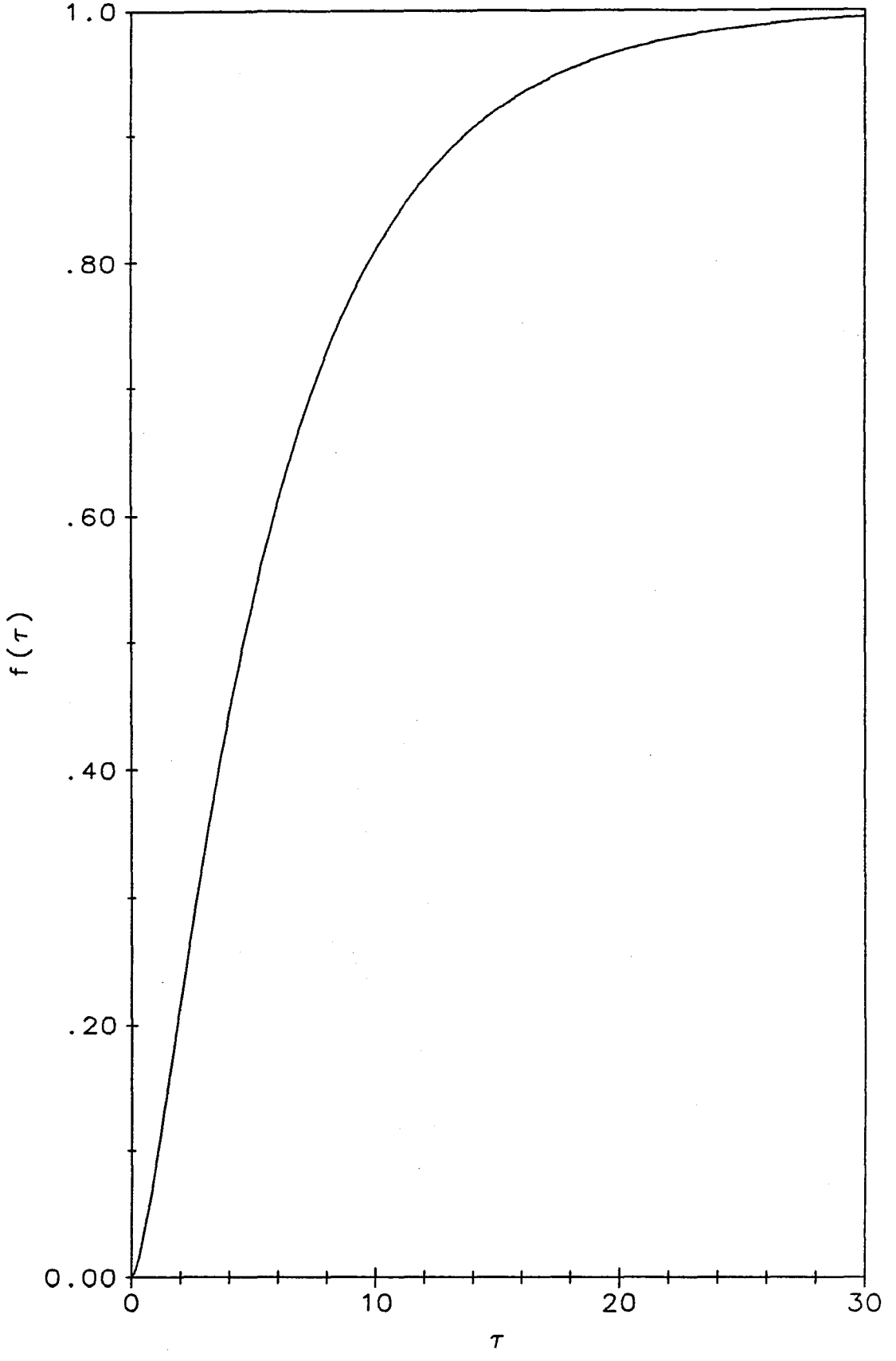
1.0
.80
.60
.40
.20
0.00
f(τ)
0
10
20
30
τ

Figure 2.6. Logarithmic analysis of the transient in Figure 2.5. The points are the calculated values and the line corresponds to a least-squares fit.

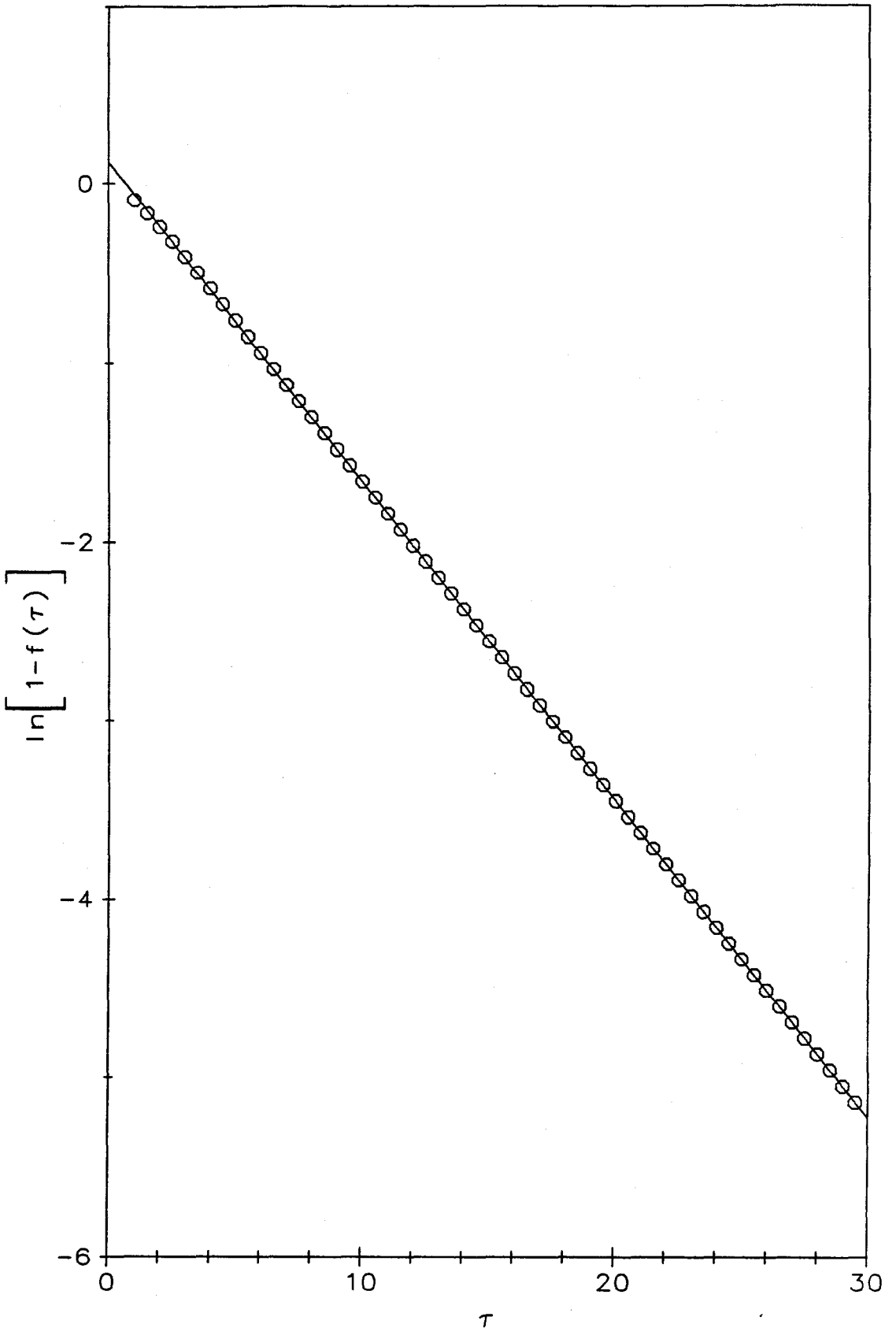
0
-2
-4
-6
0
10
20
30
τ
ln[1-f(τ)]

were derived. This agreement confirms that analysis of current transients resulting from the "magic" step change in rotation rate as simple exponential functions does not introduce significant error in the values of the Schmidt number obtained.

Chapter 3

Simulation of the Effects of Imperfect Motor Response

Simulation of the Effects of Imperfect Motor Response

A potentially significant source of error in the rotation-rate step experiment is the inability of the rotator to execute a perfect step change in rotation rate. In order to assess the extent to which finite motor response perturbs the current transient from that expected from a step change in rotation rate, we simulated the current transients resulting when the change in the rotation rate of a rotating disk electrode occurs over a nonzero time t_D.

Analysis of the effect of imperfect step changes in rotation rate is complicated by the coupling of this effect with that of hydrodynamic relaxation. Rigorous modeling of the current transients to be expected from the change in rotation rate actually applied to the rotated electrode by the motor, $\omega(t)$, requires use of the correct time-dependent velocity function, $v(x,t)$, obtained from solution of the Navier-Stokes equation using $\omega(t)$, in place of the time-independent velocity function, $v(x)$, in the boundary value problem of Equations 1.1 and 1.2. Such an analysis is too complicated and, fortunately, unnecessary for the purposes of this study. Albery and co-workers[1] have examined theoretically the effect of hydrodynamic relaxation on the current transient expected from a step change in rotation rate under conditions where imperfections in the motor response do not exist. We have performed the complementary study in which the effects of sluggish motor response are examined in the absence of effects arising from hydrodynamic relaxation.

We begin our investigation with the assumption that the velocity profile of the solution is, at all times, described by the steady-state velocity profile associated with the instantaneous angular velocity of

the electrode, $\omega(t)$; hydrodynamic relaxation is presumed to occur instantaneously. The theoretical framework presented in Chapter 1 is retained, the sole modification being the replacement of the function $v(x)$ in Equation 1.1 with the function $v(x,t)$ shown in Equation 3.1.

$$v(x,t) = (\omega(t)\,\upsilon)^{1/2}\left(v_a\left(\frac{\omega(t)}{\upsilon}\right)x^2 + v_b\left(\frac{\omega(t)}{\upsilon}\right)^{3/2}x^3 + v_c\left(\frac{\omega(t)}{\upsilon}\right)^2 x^4\right). \tag{3.1}$$

For consistency with the treatment presented in the preceding chapters, the normalizations shown in Equations 1.4, 1.5, and 1.6 are employed. The resulting expression for $H(z,\tau)$ is

$$H(x,\tau) = \left(\frac{\omega(\tau)}{\omega_\infty}\right)^{1/2}\left(v_a\left(\frac{\omega(t)}{\omega_\infty}\right)z^2 + v_b\left(\frac{\omega(t)}{\omega_\infty}\right)^{3/2}z^3 + v_c\left(\frac{\omega(t)}{\omega_\infty}\right)^2 z^4\right). \tag{3.2}$$

Additionally, the time-dependent angular velocity, $\omega(\tau)$, is defined in a manner analogous to that for the final rotation rate, ω_∞.

$$\omega(\tau) = \omega_0\,(1+\varepsilon\,u(\tau))^2 \tag{3.3}$$

Combining Equations 1.3 and 3.3 yields the following expression for the ratio $\omega(\tau)/\omega_\infty$:

$$\frac{\omega(\tau)}{\omega_\infty} = \left(\frac{1+\varepsilon\,u(\tau)}{1+\varepsilon}\right)^2. \tag{3.4}$$

The function $u(\tau)$ characterizes the time-dependence of the rotation rate of the electrode. For a perfect step change in rotation rate, $t_D=0$, $u(\tau)$ is defined by Equation 3.5.

$$u(\tau)=\begin{cases}0 & \tau<0\\ 1 & \tau\geq 0\end{cases} \tag{3.5}$$

The imperfection of the motor response is modeled by a linear change in $u(\tau)$ over a time period of $\tau_D=\omega_\infty t_D$ as expressed in Equation 3.6.

$$u(\tau)=\begin{cases}0 & \tau<0\\ \tau/\tau_D & 0\leq\tau<\tau_D\\ 1 & \tau\geq\tau_D\end{cases}. \tag{3.6}$$

A plot of the time-dependence of the rotation rate defined by Equations 3.3 and 3.6, such as that illustrated in Figure 3.1 for $\varepsilon=+0.414$, is nonlinear in the region $0<\tau<\tau_D$, though the degree of curvature is modest. The actual change in angular velocity performed by a motor attempting to execute a step change in rotation rate has been measured and published by Bruckenstein and co-workers.[4] While not providing an exact match, the expressions in Equations 3.3 and 3.6 provide a reasonable approximation of an actual motor response.

The master boundary value problem is similar to Equations 1.9 and 1.10. The function $H(z,\tau)$ that replaces $H(z)$ depends parametrically upon ε and τ_D.

Figure 3.1. The time-dependence of the rotation rate of a rotating disk electrode as defined by Equations 3.3 and 3.6 with ε=+0.414.

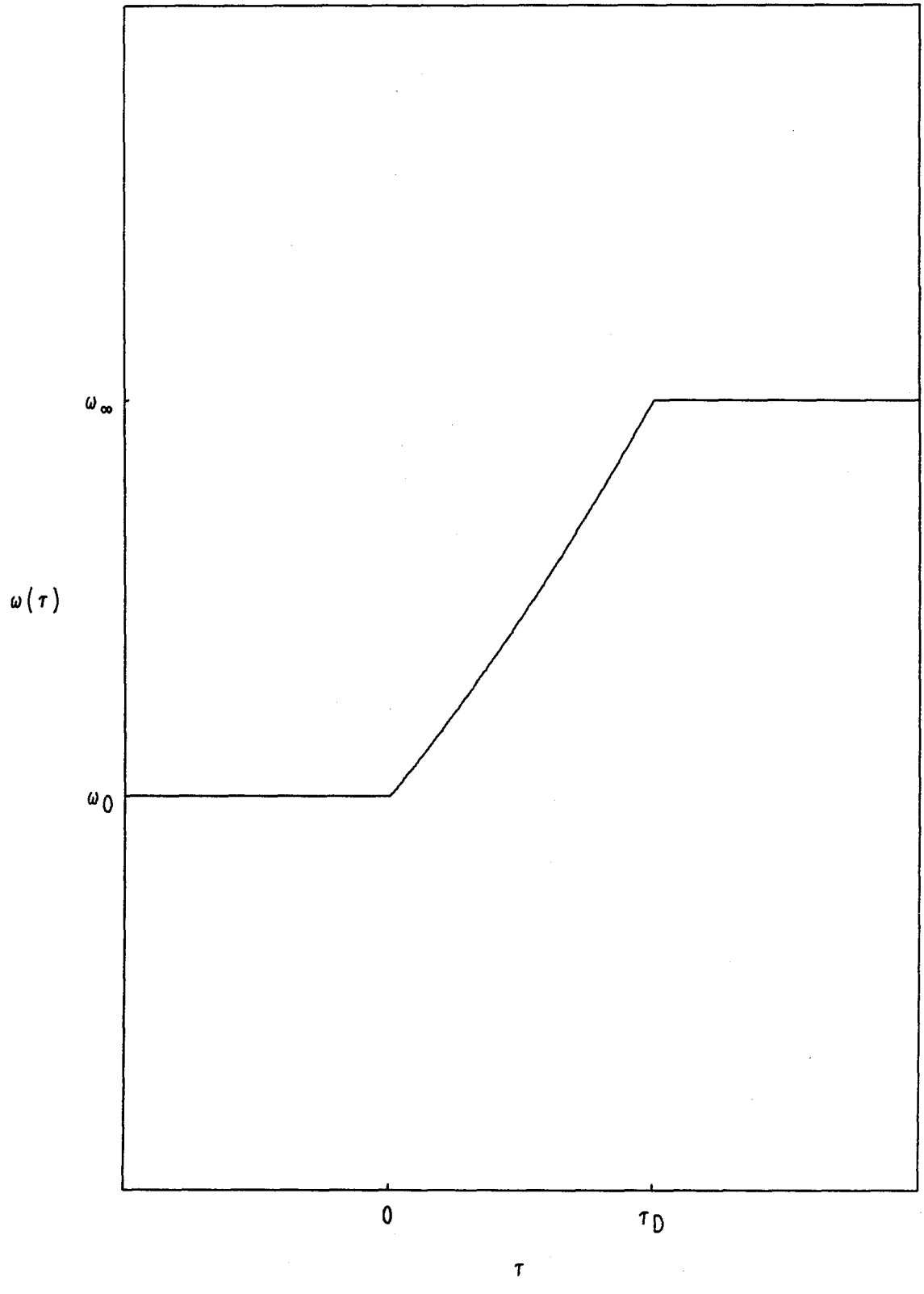
ω_∞
$\omega(\tau)$
ω_0
0
τ_D
τ

$$S\frac{\partial c(z,\tau)}{\partial \tau} = \frac{\partial^2 c(z,\tau)}{\partial z^2} - S\,H(z,\tau)\frac{\partial c(z,\tau)}{\partial z} \tag{3.7}$$

$$c(0,\tau) = 1\ , \qquad \lim_{z\to\infty} c(z,\tau) = 0\ , \qquad c(z,0) = c_0(z) \tag{3.8}$$

The Finite Difference Method

The simulation of current transients resulting from nonideal step changes in rotation rate involves a dimensionless hydrodynamic velocity function that is a function of both displacement and time. The existence of a time-dependence in the hydrodynamic velocity function destroys the separability of the differential Equation 3.7, thereby preventing formulation of a simple eigenvalue problem as part of the orthogonal collocation analysis described in Chapter 2. Because of the complications associated with applying the orthogonal collocation procedure to the problem involving a nonideal step change in rotation rate, we have resorted to the more general finite difference technique. The reader is referred to standard numerical analysis texts for detailed discussion of the finite difference method (see, for example, Kreyszig[14] and Burden, Faires, and Reynolds[15]).

Our implementation of the finite difference method utilizes six-point finite difference formulas (Equations 3.9 and 3.10) for approximation of the spatial derivatives of $c(z,\tau)$.

$$\left(\frac{\partial c(z,\tau)}{\partial z}\right)_{i,j} = \frac{-12\,c_{i-1,j} - 65\,c_{i,j} + 120\,c_{i+1,j} - 60\,c_{i+2,j} + 20\,c_{i+3,j} - 3\,c_{i+4,j}}{60\,h} \tag{3.9}$$

$$\left(\frac{\partial^2 c(z,\tau)}{\partial z^2}\right)_{i,j} = \frac{10\,c_{i-1,j} - 15\,c_{i,j} - 4\,c_{i+1,j} + 14\,c_{i+2,j} - 6\,c_{i+3,j} + c_{i+4,j}}{12\,h^2} \qquad (3.10)$$

The subscripts i and j signify evaluation of the function $c(z,\tau)$ or its derivative at the point z_i and τ_j. This scheme implements a square mesh with N+4 uniform spatial intervals of size h and an arbitrary number of uniform temporal intervals of size k. The approximations in Equations 3.9 and 3.10 have error terms of $O(h^5)$ and $O(h^4)$, respectively.

The Initial Conditions

The initial steady-state solution, $c_0(z)$, is described by the boundary value problem in Equations 3.11 and 3.12.

$$0 = \frac{d^2 c_0(z)}{dz^2} - S\,H(z,0)\,\frac{dc_0(z)}{dz} \qquad (3.11)$$

$$c_0(0) = 1\,, \qquad \lim_{z\to\infty} c_0(z) = 0 \qquad (3.12)$$

These equations follow directly from Equations 3.7 and 3.8 with $\partial c(z,\tau)/\partial\tau = 0$. Substitution of the finite difference formulas, Equations 3.9 and 3.10, into this boundary value problem leads to the N-dimensional linear system

$$\mathbf{P}_0\,\vec{c}_0 = \vec{d}_0\,. \qquad (3.13)$$

The vector subscript is the temporal index j; the initial steady-state solution corresponds to j=0. Row i of vector $\vec{c}_j$ consists of $c_{i,j}=c(z_i,\tau_j)$. The matrix **P** is defined by

$$\left[\mathbf{P}_j\right]_{i,m}=\begin{cases}50+12\,S\,h\,H_{i,j} & m=i-1;\ i=2,3,\ldots N\\ -75+65\,S\,h\,H_{i,j} & m=i;\ i=1,2,\ldots N\\ -20-120\,S\,h\,H_{i,j} & m=i+1;\ i=1,2,\ldots N-1\\ 70+60\,S\,h\,H_{i,j} & m=i+2;\ i=1,2,\ldots N-2\\ -30-20\,S\,h\,H_{i,j} & m=i+3;\ i=1,2,\ldots N-3\\ 5+3\,S\,h\,H_{i,j} & m=i+4;\ i=1,2,\ldots N-4\\ 0 & \text{all other i and m}\end{cases}, \qquad (3.14)$$

and the vector $\vec{d}_j$ imposes the spatial boundary conditions and is defined by

$$\left[\vec{d}_j\right]_i=\begin{cases}-50-12\,S\,h\,H_{1,j} & i=1\\ 0 & i=2,3,\ldots N\end{cases}. \qquad (3.15)$$

Implicit in these definitions are the relations $c_{0,j}=1$ and $c_{i,j}=0$ for $i>N$, which are consistent with the boundary conditions in Equation 3.8. The semi-infinite nature of the boundary value problem is accommodated by selecting the point z_N so that the concentration $c_{N,j}$ is essentially identical to the bulk concentration, which is zero.

The Time-Dependent Problem

Once the initial steady-state concentration profile has been obtained by solution of Equation 3.13, the time-evolution of the concentration profile is simulated by utilizing the finite difference formulas in Equations 3.9 and 3.10 in conjunction with the Crank-

Nicolson method.[14,15] The forward difference approximation of the time-dependent differential equation in Equation 3.7 is

$$\frac{60\,h^2}{k} S\left(\vec{c}_{j+1} - \vec{c}_j\right) = \mathbf{P}_j \vec{c}_j - \vec{d}_j \,. \tag{3.16}$$

The corresponding backward difference approximation is

$$\frac{60\,h^2}{k} S\left(\vec{c}_{j+1} - \vec{c}_j\right) = \mathbf{P}_{j+1} \vec{c}_{j+1} - \vec{d}_{j+1} \,. \tag{3.17}$$

The Crank-Nicolson approximation, obtained by addition of Equations 3.16 and 3.17, is

$$\frac{120\,h^2}{k} S\left(\vec{c}_{j+1} - \vec{c}_j\right) = \mathbf{P}_j \vec{c}_j - \vec{d}_j + \mathbf{P}_{j+1} \vec{c}_{j+1} - \vec{d}_{j+1} \,. \tag{3.18}$$

Introduction of the matrices $\mathbf{Q}_j$ and $\mathbf{R}_j$,

$$\mathbf{Q}_j = \frac{120\,h^2}{k} S\,\mathbf{I} - \mathbf{P}_j \tag{3.19}$$

and

$$\mathbf{R}_j = \frac{120\,h^2}{k} S\,\mathbf{I} + \mathbf{P}_j \,, \tag{3.20}$$

with $\mathbf{I}$ being the identity matrix, permits Equation 3.18 to be recast as

$$\mathbf{Q}_{j+1}\,\vec{c}_{j+1} = \mathbf{R}_j\,\vec{c}_j - \left(\vec{d}_j + \vec{d}_{j+1}\right) . \qquad (3.21)$$

Given the vector $\vec{c}_j$, the right side of Equation 3.21 may be evaluated; solution of the resulting linear system yields $\vec{c}_{j+1}$. The procedure for computing $\vec{c}_j$ for j=0 has been described above; from this starting point, the concentration profile at any time τ=jk may be calculated by recursive application of Equation 3.21. The error term for the Crank-Nicolson method is $O(k^2)$; thus the overall error of the finite difference simulation is $O(h^4+k^2)$. The finite difference procedure described above is unconditionally stable.

Calculation of Current Transients

The fractional change in current function $f(\tau)$, defined by Equations 1.7 and 2.20, is calculated by means of Equation 3.22.

$$f(\tau) = \frac{\left(\frac{\partial c(z,\tau)}{\partial z}\right)_{z=0,\tau} - \left(\frac{\partial c(z,\tau)}{\partial z}\right)_{z=0,\tau=0}}{\left(\frac{\partial c(z,\tau)}{\partial z}\right)_{z=0,\tau\to\infty} - \left(\frac{\partial c(z,\tau)}{\partial z}\right)_{z=0,\tau=0}} . \qquad (3.22)$$

From the concentration profile of $c(z,\tau)$ at a particular time τ=jk, the concentration gradient at the electrode surface is approximated by

$$\left(\frac{\partial c(z,\tau)}{\partial z}\right)_{z=0,\tau=jk} = \frac{-25 + 48\,c_{1,j} - 36\,c_{2,j} + 16\,c_{3,j} - 3\,c_{4,j}}{12\,h} . \qquad (3.23)$$

The concentration gradient associated with the initial steady-state problem is determined using the concentration profile for j=0, found

by solution of Equation 3.13. The concentration profile associated with the final steady-state condition may be found in one of two ways. First, the recursion in Equation 3.21 may be applied until the concentration profile becomes invariant, thereby indicating that the final steady state has been reached. Alternately, the linear system

$$\mathbf{P}_{\infty}\,\vec{\mathbf{c}}_{\infty} = \vec{\mathbf{d}}_{\infty} \tag{3.24}$$

may be solved. The ∞ subscript indicates that the conditions correspond to the final steady state, in which case the function $H(z,\tau)$ is evaluated using $\tau > \tau_D$.

Calculations

Finite difference simulations were performed on an AlphaNumeric PC2 computer (8088/8087) or a COMPAQ Deskpro computer (8086) using programs written in MicroSoft FORTRAN77 V3.20 or on a Digital Equipment MicroVAX 3500 using programs written in VAX FORTRAN V4.7. Simulations were performed using 40 to 100 spatial nodes and 100 to 3000 temporal nodes, depending upon the desired precision.

Fractional changes in current, $f(\tau)$, calculated by means of the orthogonal collocation procedure (Chapter 2) were identical to those calculated by means of the finite difference procedure using $\tau_D=0$ to the extent that each method had converged. Given the fundamentally different approximations of the orthogonal collocation and finite difference methods, it is virtually inconceivable that both methods would give, to as many as eight decimal places, the same

wrong answer. The agreement between the results of the two numerical methods therefore provides compelling verification of the veracity of the numerical techniques employed in this project.

Effect of Imperfect Motor Response

Imperfect motor response, like hydrodynamic relaxation, acts to delay the time when measured current transients conform to the behavior predicted when the presence of imperfections in the motor response is neglected. Bruckenstein and co-workers[4] have found that current transients resulting from rotation-rate steps of varying sizes can, once normalized, be superimposed by shifting the transients along the time axis. Theoretical arguments provided by Albery and co-workers[1] predict that the net effect of hydrodynamic relaxation is to shift the current transients along the time axis without a significant change in their shape.

Finite difference simulations of the rotation-rate step experiment using the "ramped" rotation-rate function, Equations 3.3 and 3.6, reveal that this particular imperfection in the step change in rotation rate also manifests itself as a simple time delay with little or no perturbation in the shape of the current transient. A set of six simulated transients is shown in Figure 3.2. As anticipated, all of the curves may be very nearly superimposed by shifting along the time axis.

To determine the effect of the presence of a delay time on the analysis of current transients for the evaluation of Schmidt numbers, the six simulated transients in Figure 3.2 are fitted to the modified version of Equation 2.27 given by

Figure 3.2. Effect of increasing the delay times on the fractional changes in current as determined from finite difference simulations. From left to right, the dimensionless delay times, τ_D, are 0, 1.0, 2.0, 3.0, 4.0, and 5.0 with S=2000 and ε=-0.24.

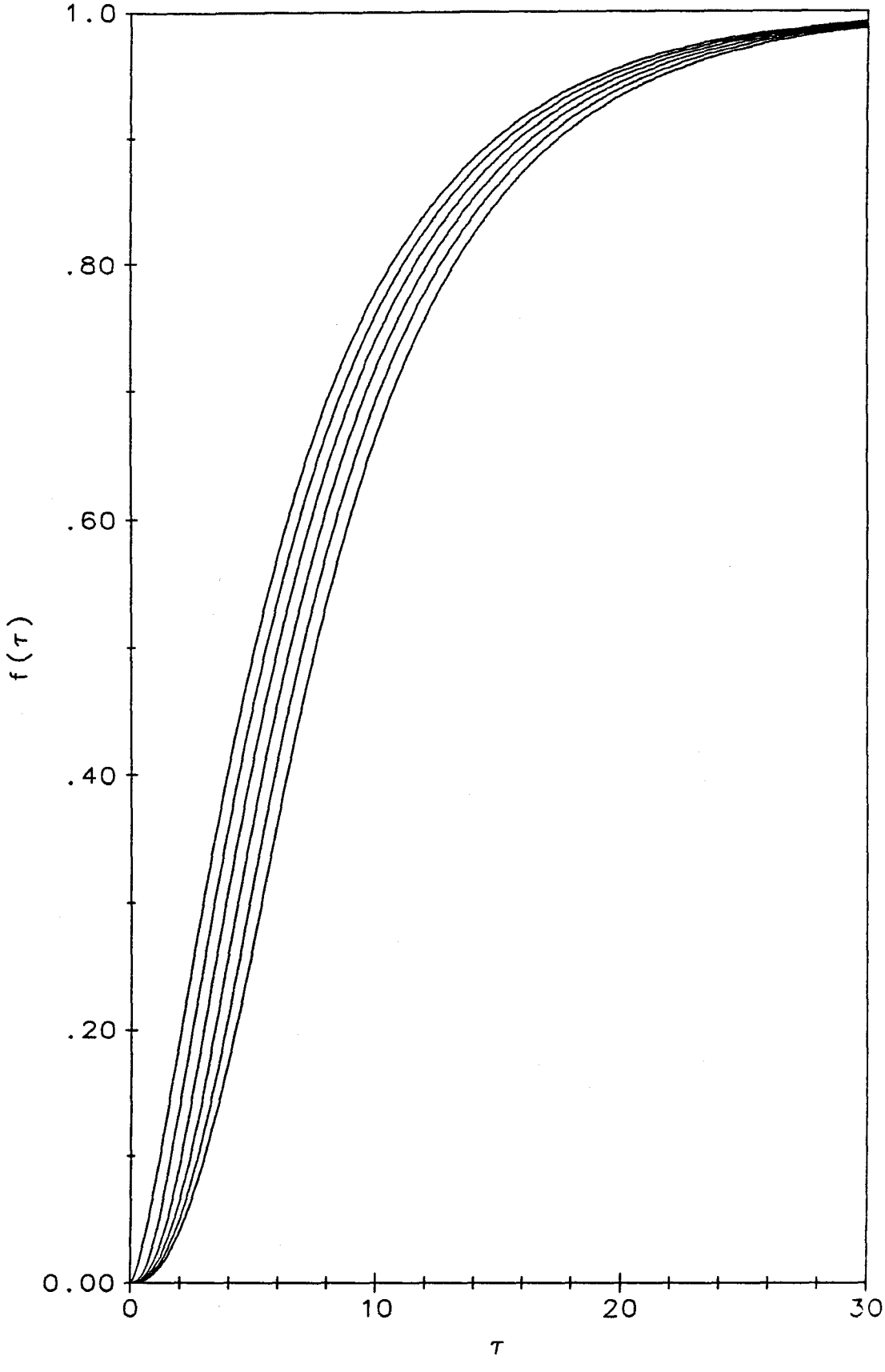
1.0
.80
.60
.40
.20
0.00
f(τ)
0
10
20
30
τ

$$f(\tau) = 1 + \sum_{i=1}^{4} f_i \exp\left(\lambda_i (\tau - \tau_0)\right) . \qquad (3.25)$$

The values of f_i are calculated using the polynomials in Table 2.4, and the expression in Equation 2.24 is substituted for λ_i in Equation 3.25. A nonlinear, least-squares fitting routine is employed with S and τ_0 adjusted to obtain the best fit. The resulting optimal values for S and τ_0 are listed in Table 3.1 for comparison with the actual values used in the simulation of the transients. The first 10% of each current transient was omitted from the least-squares procedure to avoid the imprecision of Equation 3.25 at short times as discussed in Chapter 2 (Figures 2.3 and 2.4). The entries in Table 3.1 show that for modest delay times the Schmidt number resulting from the least-squares fitting remains within 10% of its actual value. The values for τ_0 obtained from the fit are approximately half of the actual delay time used in the simulation, a fact that is not surprising. It appears that by restricting the analysis of current transients to data originating after the delay time, reasonably accurate estimates of Schmidt numbers can be obtained. Even fairly severe deviations of the change in rotation rate from a perfect step can be tolerated if the analysis of the resulting current transient is restricted to the appropriate portion of the transient.

Implications for the Analysis of Experimental Transients

The ability to determine Schmidt numbers, and hence diffusion coefficients, accurately from experimental current transients requires an efficacious strategy for accommodating the deviations

τ_D[a]	S[b]	τ_0[b]	τ_{min}[c]	min $f(\tau)$[c]
0.0	2000	-0.03	1.20	0.10
1.0	2014	0.42	1.68	0.10
2.0	2054	0.87	2.10	0.10
3.0	2138	1.30	2.46	0.10
4.0	2282	1.69	2.76	0.10
5.0	2528	2.04	3.00	0.10
5.0	2379	2.14	3.66	0.15
5.0	2277	2.22	4.26	0.20
5.0	2214	2.28	4.80	0.25
5.0	2181	2.31	5.22	0.30
5.0	2144	2.34	5.88	.0.35
5.0	2122	2.37	6.42	0.40

Table 3.1. Effect of delays during the application of changes in rotation rate on the Schmidt numbers obtained from analysis of current transients.

[a] Delay time used in simulation of the current transient for S=2000 and ε=-0.24.

[b] Optimum parameters obtained from nonlinear, least-squares fit to Eq. 3.25.

[c] The smallest values of τ and corresponding $f(\tau)$ that were employed in the nonlinear, least-squares fit of the current transients.

from ideal behavior arising from hydrodynamic relaxation and imperfect motor response. Albery et al.[1] have predicted that a simple shift along the time axis will compensate effectively for the effects of hydrodynamic relaxation in the absence of effects arising from finite motor response times. We have shown, in the preceding sections, that a simple offset along the time axis will also compensate

for the effects of imperfect motor response in the absence of effects arising from hydrodynamic relaxation. It is not implausible, therefore, to suggest that a simple offset in time will also compensate for the combined effects of both of these sources of deviant behavior. This notion is consistent with the observations of Bruckenstein et al.[4]

Given his analysis of the relaxation of the solution velocity profile produced by an impulsive angular velocity change for a rotated disk, Chawla[3] concluded that hydrodynamic relaxation occurs in two distinct stages. The immediate effect of the impulsive change in rotation rate is to generate a shear wave in the azimuthal flow, traveling away from the disk with dimensionless velocity 0.884. As the shear wave interacts with the existing von Karman flow, the radial outflow is altered, leading to a change in the axially flow. The system then develops toward the final steady state. The total time required for hydrodynamic relaxation is $\tau_{HR}=5$.

The analysis of Albery et al.[1] predicts that an offset time of $\tau_0=0.26$, independent of the Schmidt number, will effectively compensate for the effects of hydrodynamic relaxation. This value for the offset time appears too small, given the findings of Chawla.[3] The initial shear wave crosses the hydrodynamic boundary layer in a dimensionless time of approximately 1, and the offset time should be no less than half of this value. Alternately, one might expect the relevant offset time to be determined by the thickness of the Levich layer and thus to be dependent upon the Schmidt number. For S=1500, the initial shear wave crosses the Levich layer in a dimensionless time of 0.16. In this context, the value of $\tau_0=0.26$

reached by Albery et al.[1] might be reasonable, though their analysis does not consider the thickness of the Levich layer.

In addition to the uncertainty regarding the exact offset time, τ_{HR}, necessary to compensate for hydrodynamic relaxation, there is also uncertainty regarding the exact offset time, τ_{MR}, necessary to compensate for imperfect motor response. The correct value of τ_{MR} depends upon the actual performance of the rotator, which may be difficult to ascertain. Even were τ_{HR} and τ_{MR} accurately known, the delay time required for compensation of the combined effects of hydrodynamic relaxation and imperfect motor response is unlikely to be the simple sum of τ_{HR} and τ_{MR}. The preceding discussion clearly demonstrates the efficacy of an offset time in the analysis of experimental current transients but cannot provide the exact value to be used in the data analysis. For this reason, the real offset time, t_0, must be optimized, along with the Schmidt number S, in the curve fitting of experimental data.

Practical Limits on the Final Rotation Rate

Hydrodynamic relaxation occurs on a time frame that scales with the final rotation rate in the same way as the current transient. (This observation arises from the fact that τ_{HR} is a constant.) The degree to which hydrodynamic relaxation perturbs the current transient is therefore roughly independent of the choice of the final rotation rate.

Contributions arising from an imperfect rotator response, on the other hand, are strongly dependent upon the final rotation rate. The actual time required for many motors to execute an abrupt change in

angular velocity, t_{MR}, is relatively independent of the choice of final rotation rate. At low rotation rates, the value of $\tau_{MR}=\omega_\infty t_{MR}$ is likely to be negligibly small compared to the time scale of the current transient. The lower limit for the final rotation rate is therefore determined only by the operating limits of the rotating disk electrode technique. At high rotation rates, the time t_{MR} becomes significant compared to the time scale of the current transient; for sufficiently large values of ω_∞, the entire transient is dominated by the response of the motor. An inspection of Table 3.1 reveals that the maximum tolerable delay time is approximately $\tau_D=\omega_\infty t_{MR}=2$; for $\tau_D>2$, the error in S grows rapidly with increasing τ_D and becomes unacceptably large. The final rotation rate should, therefore, be chosen so that $\omega_\infty<2/t_{MR}$. If $t_{MR}=10$ ms, a functional upper limit for ω_∞ is 200 s^{-1} or 1900 rpm.

Chapter 4

Experimental Results and Discussion

Experimental

Reagents

Reagent-grade $K_4Fe(CN)_6$ and KCl were used without additional purification. Laboratory distilled water was purified by passage through a Barnstead Nanopure purification train. Measurements were conducted in 1.00 M KCl solutions containing approximately 2 mM $Fe(CN)_6^{4-}$. The solutions were maintained at 25.0±0.2°C. The kinematic viscosity of the solution was measured with an Ostwald viscosimeter; a value of $(8.56\pm0.03)\times10^{-3}$ cm^2 s^{-1} was obtained. All solutions were de-aerated with prepurified argon.

Apparatus and Procedures

The rotating electrode was a commercially available platinum disk electrode (Pine Instrument Co. or Oxford Electrodes Ltd.). A Pine Instrument MSR Rotator and Controller and Oxford Electrodes Model MC1/87 motor-controller were utilized. The overall response of the Pine Instrument system was somewhat faster than that of the Oxford system. The specifications for the latter indicate a response time of 50 ms. The unit we utilized met this specification for steps to higher rotation rates, but when stepping to lower rotation rates the response time appeared significantly longer, and considerable overshoot was evident.

Single current transients were recorded with a Tektronix Model 5223 Digitizing Oscilloscope and subsequently output on a Houston Omnigraphic X-Y recorder for measurement purposes. Experiments were conducted with conventional, commercially available instrumentation (PAR Model 173, 175, and 179 units). Multiple

transients were recorded with a computer-based digital acquisition and analysis system described previously.[16] Typically, 25 transients were recorded and ensemble-averaged to improve the signal-to-noise ratio.

Results

A typical current transient obtained by abruptly increasing the rotation rate of an electrode at which $Fe(CN)_6^{4-}$ was being oxidized to $Fe(CN)_6^{3-}$ is shown in Figure 4.1. The points correspond to the experimental measurements, and the line represents a weighted, nonlinear, least-squares fit of the data points to the Equation

$$i(t) - i(0) = \Delta i \left[1 + \sum_{i=1}^{4} f_i \exp\left(\lambda_i \omega_\infty (t - t_0)\right) \right], \qquad (4.1)$$

which is an expanded version of Equation 3.25. Δi, the difference between initial and final steady-state currents, was fitted along with λ_i (as expressed in Equation 2.24) and t_0 to allow for the fact that the final steady-state current had not been reached before the recording was terminated. The values of f_i were obtained from Table 2.2. The nonlinear, least-squares fitting procedure produced $\Delta i = +44.97 \pm 0.07$ μA, $t_0 = 11.3 \pm 0.3$ ms, and $S = 1260 \pm 40$. The value of Δi is in reasonable agreement with the value determined independently from the linear Levich plot (i vs. $\omega^{1/2}$) for the same solution, $\Delta i = +45.4 \pm 0.1$ μA. The least-squares value of t_0 is somewhat longer than half the estimated motor response time (10 ms), probably because of a contribution from hydrodynamic relaxation. The

Figure 4.1. Experimental current transient for the oxidation of 2 m M $Fe(CN)_6^{4-}$ at a platinum rotating disk electrode (S=0.17 cm^2), resulting from a step change in rotation rate from 52.4 s^{-1} to 104.8 s^{-1} (ε=+0.415). The points are experimental. The solid line is the result of a nonlinear, least-squares fit to Equation 4.1.

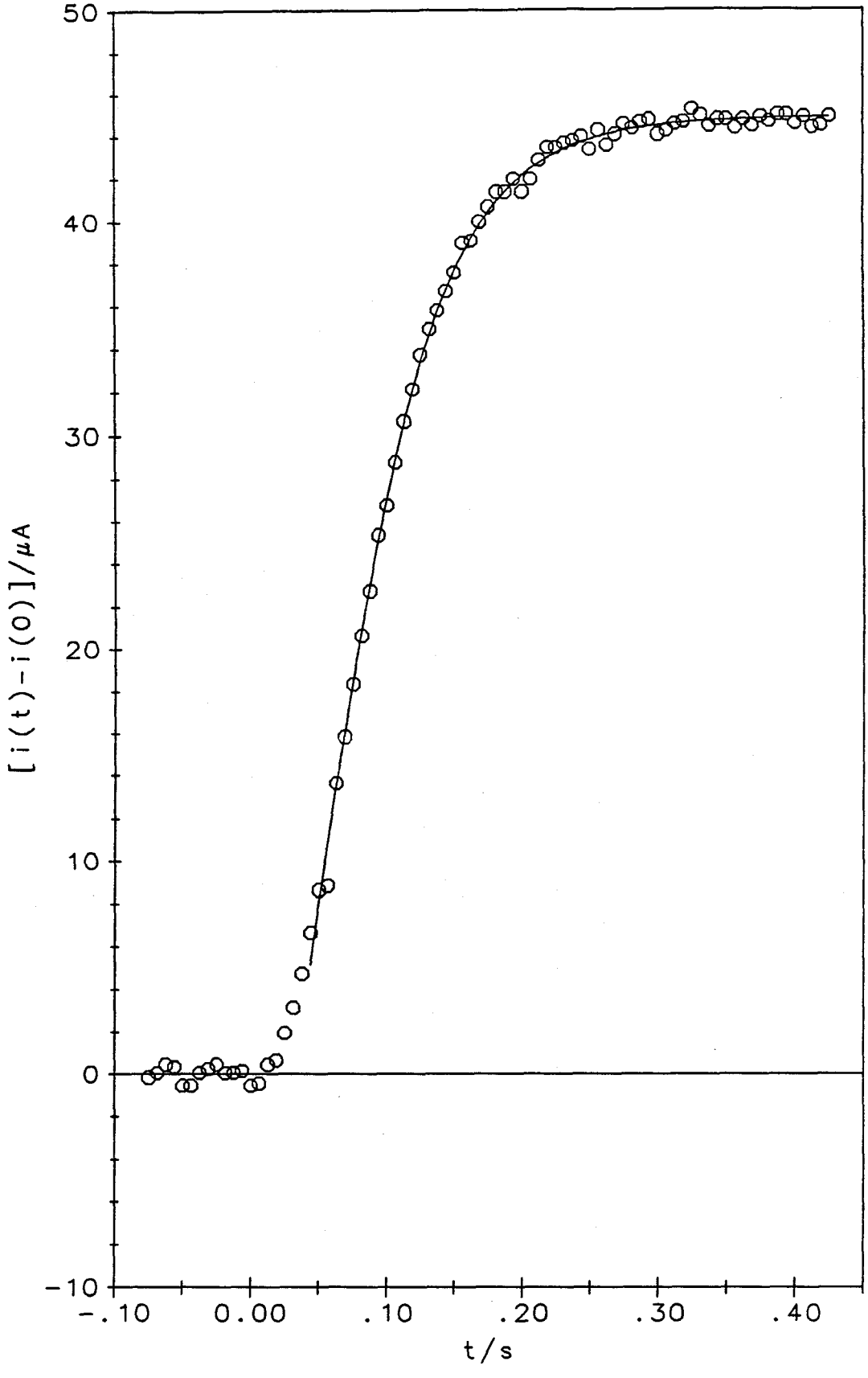
50
40
30
20
10
0
-10
[i(t)-i(0)]/μA
-.10
0.00
.10
.20
.30
.40
t/s

Schmidt number obtained from the least-squares fit corresponds to $D=(6.8\pm0.2)\times10^{-6}$ cm^2 s^{-1} and is in reasonable agreement with the accepted value for $Fe(CN)_6^{4-}$ in 1 M KCl at 25°C, $D=6.33\times10^{-6}$ cm^2 s^{-1} ($S=1352$).[17,18] This agreement and that of the calculated line with the experimental points in Figure 4.1 indicate the reliability of Equation 4.1 and the orthogonal collocation procedure that produced it.

"Magic" Step Experiments

When the rotation rate of the electrode was decreased from 42.3 s^{-1} to 24.4 s^{-1}, corresponding to $\varepsilon=-0.24$, the transient shown by the plotted points in Figure 4.2 resulted. The solid line, obtained by fitting the transient to Equation 4.1, corresponds to the least-squares values $\Delta i=-23.59\pm0.09$ μA, $t_0=17\pm2$ ms, and $S=1240\pm70$ ($D=(6.9\pm0.4)\times10^{-6}$ cm^2 s^{-1}). Because a step change in rotation rate corresponding to $\varepsilon=-0.24$ represents the "magic" step size described above, the transient is expected to obey Equation 4.1 with all but the first exponential term dropped. The same data points are plotted in a simple first-order decay plot in Figure 4.3 where the anticipated linearity is clearly evident. The weighted least-squares line drawn through the points corresponds to $t_0=15\pm3$ ms and $S=1340\pm50$ (using $\Delta i=-23.64$ μA as obtained from the Levich plot). The corresponding diffusion coefficient, $D=(6.4\pm0.2)\times10^{-6}$ cm^2 s^{-1}, is in good agreement with that obtained by means of Equation 4.1, demonstrating the utility of "magic" step experiments in simplifying the data analysis.

Figure 4.2. Experimental current transient for the oxidation of 2 m M $Fe(CN)_6^{4-}$ at a platinum rotating disk electrode (S=0.17 cm^2), resulting from a "magic" change in rotation rate: 42.3 s^{-1} to 24.4 s^{-1} (ε=-0.241). The points are experimental. The solid line is the result of a nonlinear, least-squares fit to Equation 4.1.

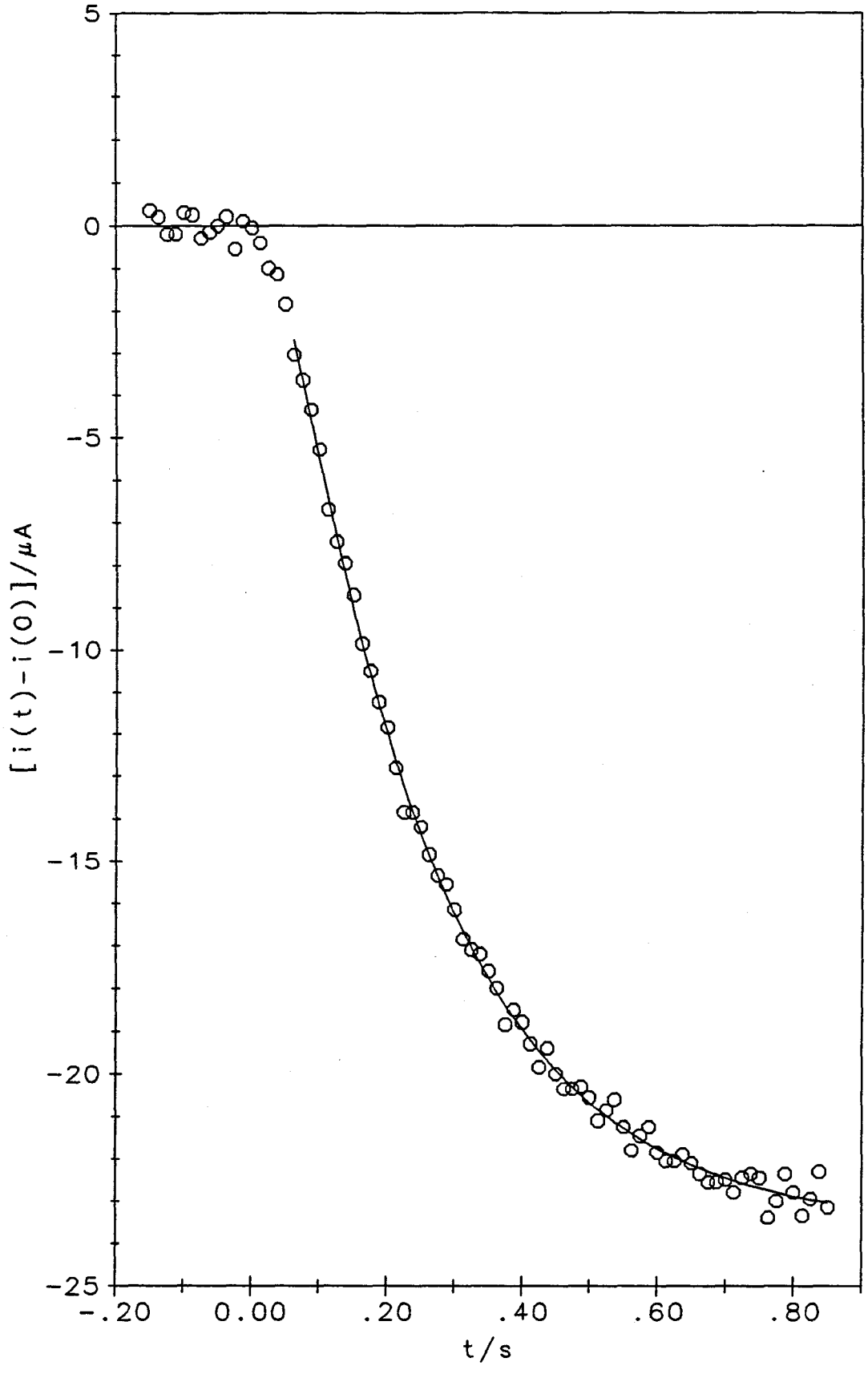
5
0
-5
-10
-15
-20
-25
[i(t)-i(0)]/μA
-.20
0.00
.20
.40
.60
.80
t/s

Figure 4.3. Logarithmic analysis of the transient in Figure 4.2. The straight line is a weighted, linear, least-squares fit of the experimental points.

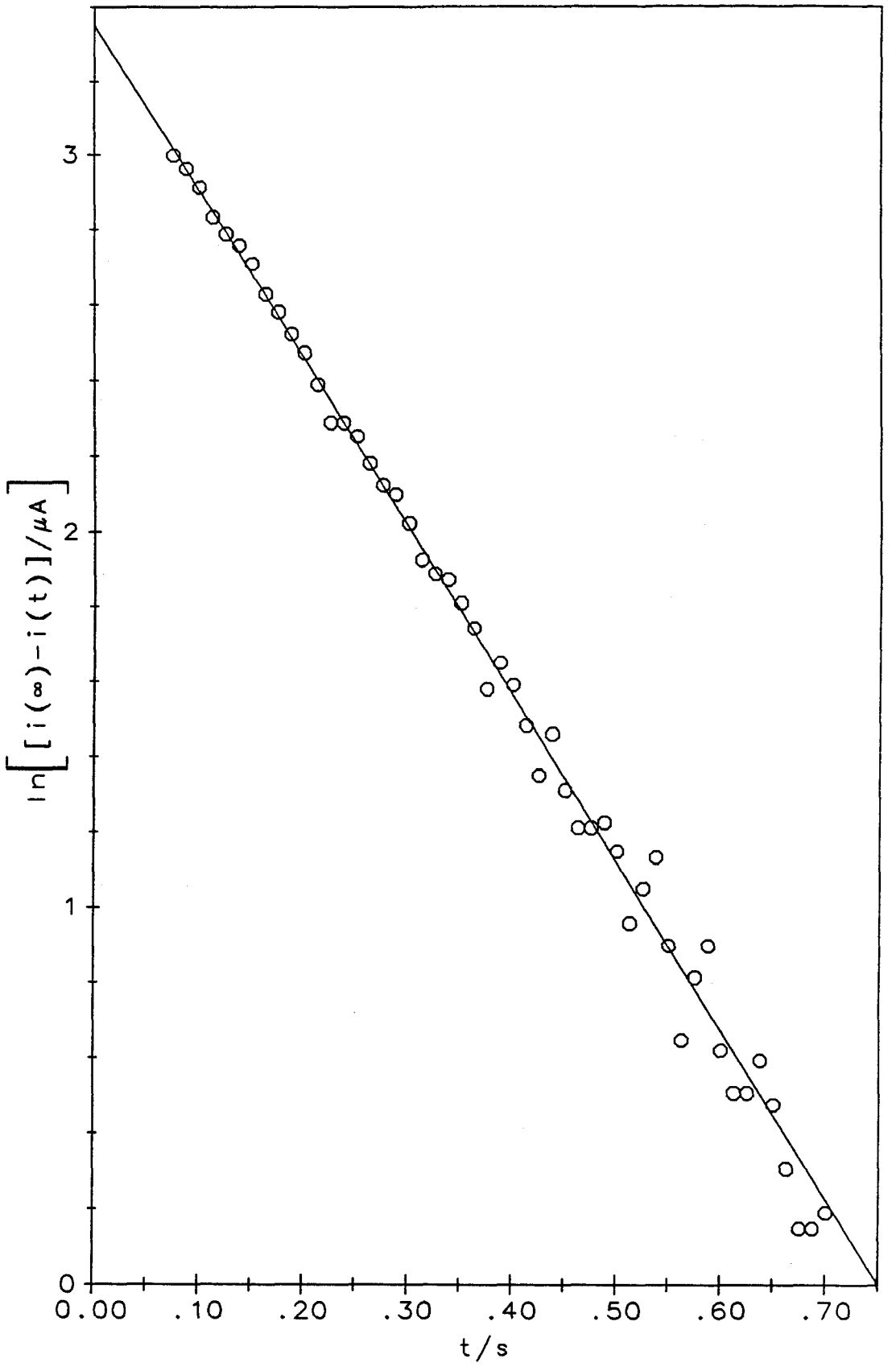
ln[[i(∞)-i(t)]/μA]
3
2
1
0
0.00
.10
.20
.30
.40
.50
.60
.70
t/s

A summary of results obtained from thirty-five experiments in which the rotation-rate changes varied from ε=-0.3 to +0.4 with ω_∞ values ranging from 6.3 to 105 s^{-1} is given in Table 4.1 along with the results of related experiments by others. The averages of the Schmidt numbers and diffusion coefficients obtained with the rotation-rate step experiments are in excellent agreement with the accepted values.[17,18] The higher standard deviations listed for the rotation-rate step method result from the poorer signal-to-noise ratio associated with the measurement of relatively small current changes at rotating disk electrodes. This factor will limit the precision attainable with this method, but a somewhat lower precision is often an acceptable price to pay for eliminating the need to know the electrode area and the reactant's concentration and n-value. The results in Table 4.1 also demonstrate clearly that the single exponential analysis that is possible with the "magic" change in rotation rate is no less reliable than the more detailed analysis required for other changes in rotation rate.

Discussion

In their earlier study, Albery et al.[1] derived an expression for $f(\tau)$ that was expected to be valid for small changes in rotation rate. The expression is similar in form to our Equation 2.22, but the series of exponential terms was truncated after the first two terms instead of the four that we found necessary to fit the transients over most of their duration. In addition, the pre-exponential and exponential numerical coefficients given by Albery et al.,[1] corresponding to f_i and λ_i values in Equation 2.22, differ somewhat from those that resulted

from the orthogonal collocation calculations. The values of the coefficients calculated by Albery et al.[1] are compared with those obtained in this work in Tables 2.1, 2.2, and 2.3.

Method	S	10^6 D/(cm^2 s^{-1})	Reference
Rotation-rate step experiment[a]	1330±30[a]	6.4 ±0.1[a]	this work
"Magic" rotation-rate step experiment[b]	1340±50[b]	6.4 ±0.2[b]	this work
Chronoamperometry	1354± 8	6.34±0.02	17
Exhaustive electrolysis at a rotating disk electrode	1350± 6	6.32±0.03	18

Table 4.1. Results of the evaluation of the Schmidt number and diffusion coefficient for $Fe(CN)_6^{4-}$ in 1 M KCl at 25.0°C by several experimental methods.

[a] Step sizes were in the range $-0.3 \leq \varepsilon \leq 0.4$. Four exponential terms were employed in the data analysis. The uncertainty is the standard deviation of the mean resulting from 35 determinations.

[b] The "magic" step size of ε=-0.24 was employed. One exponential term was employed in the data analysis. The uncertainty is the standard deviation of the mean resulting from 12 determinations.

The previous treatment, which was intended for small changes in rotation rate, neglected the dependence of f_i on ε. Since the present analysis demonstrates a considerable dependence of f_i on the magnitude and direction of the change in rotation rate (Figure 2.2), we compare, in Figure 4.4, the values of the diffusion coefficient calculated according to the equations of Albery et al.[1] with those obtained by fitting current transients to Equation 4.1. The present treatment is seen to yield diffusion coefficients that are essentially independent of the sign and magnitude of ε while the former, more

Figure 4.4 Effect of the magnitude and direction of the change in rotation rate on the diffusion coefficient obtained from analysis of the resulting current transient according to (O) Equation 4.1 or (□) Equation 4.5 of Reference 1. The solid horizontal line indicates the accepted value for the diffusion coefficient of $Fe(CN)_6^{4-}$ in 1 M KCl at 25°C (References 17 and 18).

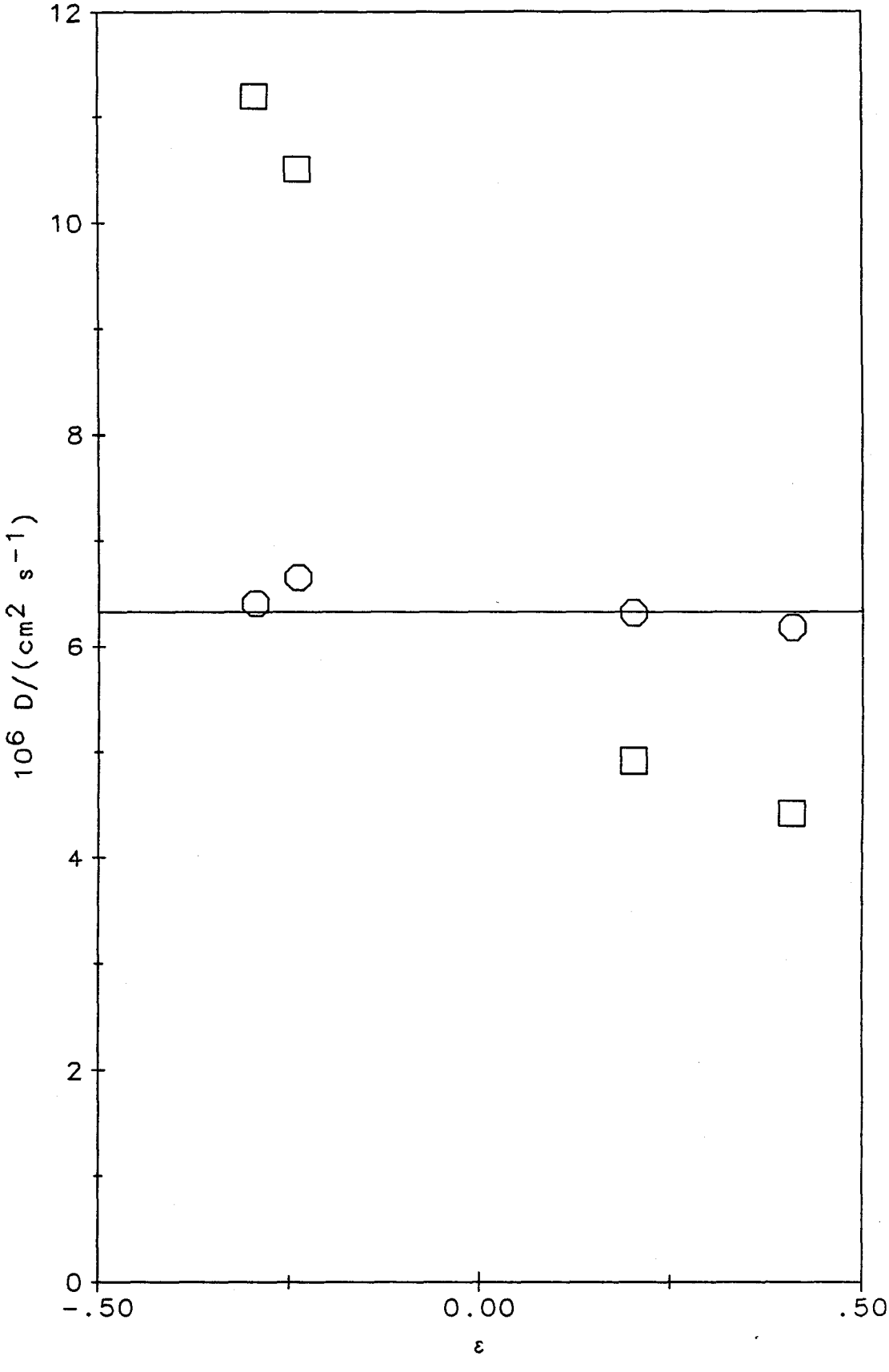
12
10
8
6
4
2
0
10^6 D/(cm^2 s^{-1})
-.50
0.00
.50
ε

approximate, treatment of Albery et al.[1] produces systematic errors in the evaluation of Schmidt numbers, and thus diffusion coefficients, except in the vicinity of $\varepsilon=0$. We also observe no dependence of the evaluated diffusion coefficients on the magnitude selected for the final rotation rate between ω_∞ = 6 to 100 s^{-1}.

It is essential to take account of the inevitable less-than-instantaneous motor response in analyzing the results of the experiment with which we have been dealing. In the first experimental description of the method,[1] a motor response time of 4 ms was quoted, but no currently commercially available motor responds so quickly. 10 to 50 ms is more typical, and failure to take this delay into account in the analysis of the current transients results in serious errors in estimates of Schmidt numbers. It is fortunate that a simple shift in the time axis as indicated in Equation 4.1 solves this potential problem as satisfactorily as it does. This approach is apparently also effective in correcting for the effects of hydrodynamic relaxation. The delay times, t_0, that are obtained from the least-squares fit to Equation 4.1 seem reasonable estimates for the combined effects of slow motor response and hydrodynamic relaxation. Previous empirical[4] and theoretical[1] attempts to deal with hydrodynamic relaxation have led to correction factors of widely different magnitudes. Another advantage of the present treatment is its apparent success in accounting simultaneously for the effects of hydrodynamic relaxation and imperfect motor response by the introduction of a single, least-squares fitted delay time.

Appendix I

Considerations Regarding the Choice of Values for the Parameters α and β

Considerations Regarding the Choice of Values for the Parameters α and β

In this appendix we address the choice of values for the parameters α and β. If the approximation $H(z)=v_a z^2$ is used in place of the expanded expression of Equation 1.8, the right side of Equation 2.6 may be rewritten as

$$\sum_{i=0}^{N} a_i(\tau)\left[i(i-1)-\alpha\beta(2i-\beta-1)z^{\beta}+\alpha^2\beta^2 z^{2\beta}-i v_a S z^3+\alpha\beta v_a S z^{\beta+3}\right]z^{i-2} . \quad (I.1)$$

It is advantageous to choose $\beta=3$, because this choice leads to the simplified expression

$$\sum_{i=0}^{N} a_i(\tau)\left[i(i-1)-(6\alpha(i+1)+i v_a S)z^3+3\alpha(3\alpha+v_a S)z^6\right]z^{i-2} . \quad (I.2)$$

This expression may be further simplified by choosing $\alpha=-v_a S/3$, in which case the coefficient associated with the term z^6 becomes zero. As indicated previously, $v_a=-0.51023$; thus $\alpha=-v_a S/3=0.17008S\approx S/6$.

In practice, the expanded expression in Equation 1.8 is employed for the calculation of H(z); thus the "simplifications" described in the preceding paragraph do not, strictly speaking, simplify the mathematical treatment. Nonetheless, choosing $\alpha \cong S/6$ and $\beta = 3$ will ensure that the expression in brackets on the right side of Equation 2.6 is dominated by two terms, one of which does not involve z and the other of which involves z^3. Under this condition, λ_i and f_i are always found to be real; other values for α and β sometimes lead to complex values for λ_i and f_i, *vide supra*.

Appendix II

Programs for the Simulation of Current Transients

Introduction

All programs for the simulation of current transients were written in FORTRAN and employed double-precision arithmetic. Orthogonal collocation computations were performed on a Digital Equipment VAX 11/750 or MicroVAX 3500. Finite difference computations were performed on a microcomputer (8086/8086 machine) or a Digital Equipment MicroVAX 3500.

OCWSTEP

The program OCWSTEP calculates the collocation eigenvalues and coefficients described in Chapter 2. When executed, the program prompts the user for the collocation order N, the Schmidt number S, the name of an output file (maximum 12 characters), the parameter α, and the parameter β. Floating point values are expected for S, α, and β; i.e., the entered values must include a decimal point. If no response or if a value of zero is provided for either α or β, the default values of α=S/6 and β=3 are used in the computations.

Given the simulation parameters N, S, α, and β, the collocation points z_i are selected and the eigenvalue problem is formulated and solved. The collocation points and collocation eigenvalues are written to the output file. The IMSL subroutine EIGRF computes a performance index, P; the program OCWSTEP displays the value of the performance index on the terminal, providing verification of the veracity of the computations. The performance index compares the magnitude of the residuals with the floating-point precision of the machine to assess the performance of the numerical algorithm. The performance index may be interpreted in the following manner:

$0<P<1$, excellent performance; $1<P<100$, good performance; $P>100$, poor performance or algorithm failure. In all cases examined in this study, the performance index lay in the interval $0<P<<1$, signifying that the residuals were as small as could be expected, given the numerical limits of the double precision arithmetic.

Once the eigenvalue problem has been solved, the user is prompted for the step size parameter ε. If a nonzero value is provided, the collocation coefficients corresponding to the specified step size are computed and written to the output file. If no value or a value of zero is entered at the prompt for ε, the output file is closed and program execution ends.

```
0001            PROGRAM OCWSTEP
0002
0003    C       David N. Blauch          March 1988, Revised June 1990
0004
0005    C       California Institute of Technology, Pasadena, CA 91125
0006
0007    C*****************************************************************
0008    C       Rotation-Rate Step Experiment:
0009    C             Current Transient Simulation by means of an
0010    C             Orthogonal Collocation Algorithm.
0011
0012    C       see D. N. Blauch, Ph.D. Thesis, Caltech, Chapter 2
0013
0014    C*****************************************************************
0015
0016            INTEGER I,N,PZ(20),PE(20),ICMPLX
0017            DOUBLE PRECISION A,B,E,Z(20),S
0018            COMPLEX*16 EVL(20),F(20)
0019            CHARACTER*12 FNAME
0020
0021            COMMON /ZNODE/Z/PAR/N,A,B,S/EVP/ICMPLX,EVL
0022
0023    10      FORMAT (A12)
0024    15      FORMAT (I8)
0025    20      FORMAT (D16.9)
0026
0027    C*****************************************************************
0028    C       Print Program Description and
0029    C       Obtain the Necessary Simulation Parameters.
0030
0031            WRITE (6,100)
0032    100     FORMAT (///25X,'Rotation-Rate Step Experiment',/11X,
0033         *       'Orthogonal Collocation Simulation of the ',
0034         *       'Current Transient',//1X,'Collocation Order ',
0035         *       '(integer, max. 20) ?  ',$)
0036            READ (5,15) N
0037
0038            WRITE (6,120)
0039    120     FORMAT (1X,'Schmidt Number ?  ',$)
0040            READ (5,20) S
0041
0042            WRITE (6,130)
0043    130     FORMAT (1X,'Output filename ?  ',$)
0044            READ (5,10) FNAME
0045
0046            WRITE (6,135)
0047    135     FORMAT (1X,'Parameter alpha ?  ',$)
0048            READ (5,20) A
0049            IF (A.EQ.0.D0) THEN
0050    C             *****  the default value is S/6
0051                  A=S/6.D0
0052            ENDIF
0053
0054            WRITE (6,137)
0055    137     FORMAT (1X,'Parameter beta ?  ',$)
0056            READ (5,20) B
```

```
0057            IF (B.EQ.0.D0) THEN
0058    C             *****  the default value is 3
0059                  B=3.D0
0060            ENDIF
0061
0062            WRITE (6,140) A,B
0063    140     FORMAT (/1X,'Simulation Parameters:',/10X,'alpha ',
0064         * 'parameter =  ',F10.2,/10X,'beta parameter =  ',F5.2)
0065
0066    C*****************************************************************
0067    C       Open the Output File
0068
0069            OPEN (1,FILE=FNAME,STATUS='NEW')
0070
0071    C*****************************************************************
0072    C       Save the Header Information
0073
0074            WRITE (1,160) N,S,A,B
0075    160     FORMAT (25X,'Rotation Rate Step Experiment',/11X,
0076         * 'Orthogonal Collocation Simulation of the Current ',
0077         * 'Transient',//22X,'Orthogonal Collocation Order =  ',I3,
0078         * /26X,'Schmidt Number =  ',F10.2,/25X,'Parameter ',
0079         * 'Alpha = ',F10.2,/28X,'Parameter Beta =  ',F5.2)
0080
0081    C*****************************************************************
0082    C       Determine the Optimal Nodes for the Simulation
0083    C             Program employs Gaussian Quadrature using the
0084    C             weight function is exp[-A z**B].
0085
0086            WRITE (6,200)
0087    200     FORMAT (/1X,'Determining Optimal Nodes ...')
0088
0089            CALL NODE
0090
0091    C       For output purposes, sort the nodes (make sure the
0092    C             order is smallest to largest).
0093
0094            CALL SORTZ(N,Z,PZ)
0095
0096    C*****************************************************************
0097    C       Save the optimal nodes
0098
0099            WRITE (1,220)
0100    220     FORMAT (/24X,'Nodes for Orthogonal Collocation',/27X,
0101         *        ' i',14X,'z[i]')
0102
0103            DO 250, I=1,N
0104                  WRITE (1,240) I,Z(PZ(I))
0105    240           FORMAT (27X,I2,10X,F13.10)
0106    250     CONTINUE
0107
0108    C*****************************************************************
0109    C       Solve the Final Steady State and Transient EVP
0110
0111            WRITE (6,300)
0112    300     FORMAT (1X,'Solving the Final Steady-State and ',
```

```
0113          *       'Transient Eigenvalue Problems ...')
0114
0115            CALL EIGEN
0116
0117      C     Again for output purposes, sort the eigenvalues
0118
0119            CALL SORTE(N,EVL,PE)
0120
0121      C*****************************************************************
0122      C     Save the eigenvalues
0123
0124            IF (ICMPLX.EQ.0) THEN
0125      C           ***** All eigenvalues are real
0126                  WRITE (1,320)
0127      320         FORMAT (/6X,'Eigenvalues Describing the Time-',
0128           *      'Dependence of the Current Transient',/28X,' i',
0129           *      10X,'e[i]')
0130                  DO 350, I=1,N
0131                        WRITE (1,340) I,DREAL(EVL(PE(I)))
0132      340               FORMAT (28X,I2,4X,F17.10)
0133      350         CONTINUE
0134            ELSE
0135      C     ***** Certain eigenvalues are complex
0136                  WRITE (1,360)
0137      360         FORMAT (/22X,'Chosen values of alpha, beta, and ',
0138           *      'the',/17X,'Schmidt number give rise to complex ',
0139           *      'eigenvalues',//6X,
0140           *      'Eigenvalues Describing the Time-Dependence of ',
0141           *      'the Current Transient',/18X,' i',10X,'real(e[i])',
0142           *      10X,'complex(e[i])')
0143
0144                  DO 380, I=1,N
0145                  WRITE (1,370) I,DREAL(EVL(PE(I))),DIMAG(EVL(PE(I)))
0146      370         FORMAT (18X,I2,7X,F17.10,4X,F17.10)
0147      380         CONTINUE
0148            ENDIF
0149
0150
0151      C*****************************************************************
0152      C     Solve the Initial Steady-State Problem for a Given Step-
0153      C           Size Parameter epsilon.
0154      C     Then compute the collocation coefficients f[i]
0155
0156            WRITE (6,400)
0157      400   FORMAT (/1X,'Enter a value for the step-size parameter ',
0158           *      'epsilon',/1X,'A value of zero will terminate ',
0159           *      'the program',/1X)
0160      450   WRITE (6,460)
0161      460   FORMAT (1X,'Next value of epsilon ?  ',$)
0162            READ (5,20) E
0163
0164            IF (E.EQ.0.D0) GOTO 1000
0165
0166            CALL FRAC(E,F)
0167
0168      C*****************************************************************
```

```
0169    C       Save the coefficients for this value of epsilon
0170
0171            WRITE (1,500) E
0172    500     FORMAT (/23X,'Coefficients for Exponential Terms',/30X,
0173         *       'Epsilon =  ',F8.5)
0174
0175            IF (ICMPLX.EQ.0) THEN
0176    C               ***** All collocation coefficients are real
0177                    WRITE (1,510)
0178    510             FORMAT (28X,' i',10X,'f[i]')
0179
0180                    DO 550, I=1,N
0181                          WRITE (1,340) I,DREAL(F(PE(I)))
0182    550             CONTINUE
0183            ELSE
0184    C               ***** Certain collocation coefficients are complex
0185                    WRITE (1,560)
0186    560             FORMAT (18X,' i',10X,'real(f[i])',10X,
0187         *                  'complex(f[i])')
0188                    DO 580, I=1,N
0189                    WRITE (1,370) I,DREAL(F(PE(I))),DIMAG(F(PE(I)))
0190    580             CONTINUE
0191            ENDIF
0192
0193
0194            GOTO 450
0195
0196    C***************************************************************
0197
0198    1000    CLOSE (1)
0199
0200            END

0001
0002    C***************************************************************
0003    C***************************************************************
0004
0005            SUBROUTINE NODE
0006
0007    C       ***** Node generation subroutine
0008    C             The "optimal" points for orthogonal collocation are
0009    C             determined.
0010
0011    C       ***** The subroutine generates a set of polynomials that
0012    C             are orthogonal on the interval z>=0 with respect to
0013    C             the weight function     exp[-A z**B]
0014
0015    C       ***** The "optimal" points are the roots of a polynomial
0016    C             of order NZ, which is also the order of the
0017    C             orthogonal collocation approximation
0018
0019    C       ***** Note:  This subroutine requires use of the gamma
0020    C             function.  The IMSL double precision function
0021    C             DGAMMA(X) is used.  If IMSL calls are not possible,
0022    C             a user-supplied gamma function must be available.
0023
```

```
0024    C*************************************************************
0025
0026          INTEGER I,J,K,NZ,MAX
0027          DOUBLE PRECISION A,B,Z(20),TMP,X,Y,C(20),C0,PREC,DGAMMA,S
0028          DOUBLE PRECISION MA(20,20),MA0(20),MA00,MB(20,20),MB0(20)
0029          DOUBLE PRECISION MB00
0030          EXTERNAL DGAMMA
0031          COMMON /ZNODE/Z/PAR/NZ,A,B,S
0032          PARAMETER (MAX=100)
0033          PARAMETER (PREC=1.D-12)
0034
0035    C*************************************************************
0036    C       Begin Gram-Schmidt Orthogonalization Procedure
0037    C             MA and MB are arrays used in this procedure
0038    C             MA0(I) and MB0(I) correspond to MA(I,0) and MB(I,0)
0039    C             MA00 corresponds to MA(0,0) and MB00 corresponds to
0040    C             MB(0,0).
0041    C             C is a vector used in the procedure, C0 corresponds
0042    C             to C(0)
0043
0044    C             MA(I,K) contains the coefficient for the z**K term
0045    C                   in the Ith-order polynomial
0046
0047    C             TMP, X, and Y are local variables
0048
0049    C       ***** Generate the 0th-order coefficient
0050          TMP=1.D0/B
0051          MB00=DSQRT((B*A**TMP)/DGAMMA(TMP))
0052          MA00=MB00
0053
0054    C       ***** Generate the 1st-order coefficients
0055          TMP=3.D0/B
0056          Y=DGAMMA(TMP)/(B*A**TMP)
0057          TMP=2.D0/B
0058          X=MA00*DGAMMA(TMP)/(B*A**TMP)
0059          MB(1,1)=1.D0/DSQRT(Y-X*X)
0060          MA(1,1)=MB(1,1)
0061          MB0(1)=-MB(1,1)*X
0062          MA0(1)=MB0(1)*MA00
0063
0064    C       ***** Each pass through the loop ending at line 100
0065    C             generates the Ith-order coefficients
0066          DO 100, I=2,NZ
0067                TMP=DBLE(I+1)/B
0068                C0=MA00*DGAMMA(TMP)/(B*A**TMP)
0069                X=C0*C0
0070                DO 20, K=1,I-1
0071                      C(K)=MA0(K)*DGAMMA(TMP)/(B*A**TMP)
0072                      DO 10, J=1,K
0073                            Y=DBLE(I+J+1)/B
0074                            C(K)=C(K)+MA(K,J)*DGAMMA(Y)/(B*A**Y)
0075    10                CONTINUE
0076                      X=X+C(K)*C(K)
0077    20          CONTINUE
0078
0079                TMP=DBLE(2*I+1)/B
```

```
0080                Y=DGAMMA(TMP)/(B*A**TMP)
0081                TMP=1.D0/DSQRT(Y-X)
0082                MB(I,I)=TMP
0083
0084                MB0(I)=-TMP*C0
0085                DO 30, K=1,I-1
0086                      MB(I,K)=-TMP*C(K)
0087    30          CONTINUE
0088
0089                MA(I,I)=TMP
0090                TMP=MB0(I)*MA00
0091                DO 40, J=1,I-1
0092                      TMP=TMP+MB(I,J)*MA0(J)
0093    40          CONTINUE
0094                MA0(I)=TMP
0095
0096                DO 60, K=1,I-1
0097                      MA(I,K)=0.D0
0098                      DO 50, J=K,I-1
0099                            MA(I,K)=MA(I,K)+MB(I,J)*MA(J,K)
0100    50                CONTINUE
0101    60          CONTINUE
0102
0103    100     CONTINUE
0104
0105    C*****************************************************************
0106    C       The coefficients of the polynomial of order NZ have been
0107    C       determined.  Now the roots, Z(), are found using a
0108    C       modified version of the Newton-Rapheson algorithm.
0109
0110    C       The roots are stored in the vector Z() as they are found
0111    C       The algorithm is designed to find the smallest roots
0112    C       first, though this order is not certain.
0113
0114    C       MAX is the maximum number of iterations permitted.
0115    C       PREC is the precision required for successful termination
0116    C             of the Newton-Rapheson algorithm.
0117
0118    C       ***** Each pass through the loop ending at line 200
0119    C             determines the Ith root;  the order is smallest to
0120    C             largest
0121          DO 200, I=1,NZ
0122
0123    C             ***** Always choose zero as the seed value
0124                  Z(I)=0.D0
0125
0126    C             ***** K is the iteration counter
0127                  K=0
0128
0129    130           IF (K.GT.MAX) THEN
0130                        WRITE (6,140)
0131    140                 FORMAT (//1X,'*****  Maximum Number of ',
0132         *                   'Iterations Exceeded in Subroutine NODE')
0133                        STOP
0134                  ENDIF
0135
```

```
0136                  K=K+1
0137
0138    C             ***** Horner's Algorithm is used to evaluate the
0139    C                   polynomial and its derivative at the current
0140    C                   root approximation.
0141                  X=MA(NZ,NZ)
0142                  Y=DBLE(NZ)*MA(NZ,NZ)
0143                  TMP=Z(I)
0144                  DO 160, J=NZ-1,1,-1
0145                        X=MA(NZ,J)+TMP*X
0146                        Y=DBLE(J)*MA(NZ,J)+TMP*Y
0147    160           CONTINUE
0148                  X=MA0(NZ)+TMP*X
0149
0150    C             ***** Factor out terms involving known roots
0151                  IF (I.NE.1) THEN
0152                        DO 180, J=1,I-1
0153                              Y=Y-X/(TMP-Z(J))
0154    180                 CONTINUE
0155                  ENDIF
0156
0157    C             ***** Obtain next approximation for the root using
0158    C                   the standard Newton-Rapheson formula
0159                  Z(I)=TMP-X/Y
0160                  TMP=DABS(TMP-Z(I))
0161                  IF (TMP.GT.PREC) GOTO 130
0162
0163    200     CONTINUE
0164
0165            RETURN
0166
0167            END

0001
0002    C*****************************************************************
0003    C*****************************************************************
0004
0005            SUBROUTINE EIGEN
0006
0007    C       David N. Blauch          September 1987
0008    C       Caltech, Pasadena, CA  91125
0009
0010    C       w-Step Experiment Simulation
0011    C       Orthogonal Collocation Algorithm combined with Eigenvalue
0012    C              Determination
0013
0014            INTEGER I,IJOB,IER,K,N,ICMPLX
0015            DOUBLE PRECISION A(20,20),B(20,20),C(20),W(20),Z(20)
0016            DOUBLE PRECISION TMP,H,S,PA,PB,E,EX,EXZ,ZB,HI,EIGRF
0017
0018    C       EISPACK subroutine is in IMSLD library (double precision)
0019            DOUBLE PRECISION AA(400),WK(440)
0020            COMPLEX*16 V(400),EVL(20),EVT(20,20)
0021
0022            EXTERNAL H,EIGRF
0023            COMMON /INVT/A,B,C,W/ZNODE/Z/PAR/N,PA,PB,S/EVP
```

```
0024            COMMON /ICMPLX,EVL,EVT
0025      C*****************************************************************
0026      C               N is the number of collocation points
0027      C               PA is alpha
0028      C               PB is beta
0029      C               S is the Schmidt number
0030
0031            DO 100, I=1,N
0032
0033      C               *****  Generate the EVP Matrices
0034      C               *****       SQ in A, V in B, and v in c
0035      C               *****       The time variable is normalized by the
0036      C               *****       final rotation rate (the Alberian
0037      C               *****       approach)
0038                      ZB=PA*Z(I)**PB
0039                      EX=DEXP(-ZB)
0040                      ZB=PB*ZB
0041                      EXZ=EX/(Z(I)*Z(I))
0042                      EX=EX*S
0043                      HI=S*H(Z(I),0.D0)*Z(I)
0044                      C(I)=EXZ*ZB*(-PB+1.D0+HI+ZB)
0045                      DO 80, K=1,N
0046                            EX=EX*Z(I)
0047                            EXZ=EXZ*Z(I)
0048                            A(I,K)=EX
0049                            TMP=DBLE(REAL(K))
0050                            B(I,K)=EXZ*(TMP*(TMP-1.D0-HI)
0051           *                       -ZB*(2.D0*TMP+PB-1.D0-HI)+ZB*ZB)
0052      80              CONTINUE
0053
0054      100     CONTINUE
0055
0056      C*****************************************************************
0057      C       Set up standard EVP by transforming SQ c' = V c + w
0058      C             into c' = A c + b.
0059      C       Carry out inversion procedure to obtain standard EVP
0060      C       A is in A and b is in w after subroutine call
0061
0062            CALL INVERT(N)
0063
0064      C*****************************************************************
0065      C       Calculate Offset Vector (i.e., final solution) for c
0066      C       Calculate vector INV(A) w = b
0067            DO 150, I=1,N
0068                  C(I)=W(I)
0069                  DO 130, K=1,N
0070                        B(I,K)=A(I,K)
0071      130             CONTINUE
0072      150     CONTINUE
0073
0074            CALL PIVOT(N)
0075
0076      C       *****  Move b from c to w
0077      C             The final solution is stored in W()
0078            DO 170, I=1,N
0079                  W(I)=C(I)
```

```
0080    170     CONTINUE
0081
0082
0083    C*****************************************************************
0084    C       Currently A is in A and b is in w
0085    C       Move the EVP matrix A into  AA
0086    C       EISPACK expects the characteristic matrix to be in vector
0087    C       form; AA is thus ready for EISPACK subroutine call
0088
0089            DO 200, K=1,N
0090                  DO 190, I=1,N
0091                        AA(N*(K-1)+I)=A(I,K)
0092    190           CONTINUE
0093    200     CONTINUE
0094
0095
0096    C*****************************************************************
0097    C       Solve the EVP using EISPACK (IMSL) Subroutines
0098    C       Call EIGRF to evaluate eigenvalues and eigenvectors for
0099    C             the real matrix AA
0100
0101    C       ***** IJOB=2 asks for eigenvalues, eigenvectors, and
0102    C             performance index
0103            IJOB=2
0104            CALL EIGRF(AA,N,N,IJOB,EVL,V,N,WK,IER)
0105            WRITE (6,250) WK(1)
0106    250     FORMAT (1X,'EIGRF Performance Index =  ',D16.9)
0107
0108    C       ***** The EISPACK subroutine returns the complex
0109    C                   eigenvalues in vector EVL and the complex
0110    C                   eigenvectors in vector V.
0111    C             Switch ICMPLX=1 if any eigenvalues or eigenvectors
0112    C                   are complex and 0 otherwise
0113            ICMPLX=0
0114            DO 270, I=1,N
0115                  IF (DIMAG(EVL(I)).NE.(0.D0)) THEN
0116                        ICMPLX=1
0117                  ENDIF
0118                  DO 260, K=1,N
0119                        EVT(K,I)=V(N*(I-1)+K)
0120                        IF (DIMAG(V(N*(I-1)+K)).NE.(0.D0)) THEN
0121                              ICMPLX=1
0122                        ENDIF
0123    260           CONTINUE
0124    270     CONTINUE
0125
0126            RETURN
0127
0128            END

0001
0002    C*****************************************************************
0003    C*****************************************************************
0004
0005            SUBROUTINE FRAC(E,F)
0006
```

```
0007    C       ***** Calculation of Initial Conditions, given the step-
0008    C             size parameter epsilon.
0009    C       ***** Also, calculation of coefficients f[i] for the
0010    C             fractional change in current function
0011
0012    C       ***** If the problem involves complex eigenvalues and
0013    C             eigenvectors, then complex arithmetic must be used
0014
0015            INTEGER I,K,N,ICMPLX
0016            DOUBLE PRECISION A(20,20),B(20,20),C(20),CF(20),Z(20)
0017            DOUBLE PRECISION C0(20),TMP,H,S,PA,PB,E,EX,ZB,HI
0018            COMPLEX*16 EVL(20),EVT(20,20),CA(20,20),CB(20,20),CC(20)
0019            COMPLEX*16 CCF(20),CC0(20),CTMP,F(20)
0020
0021            EXTERNAL H
0022            COMMON /INVT/A,B,C,CF/ZNODE/Z/PAR/N,PA,PB,S
0023            COMMON /CINVT/CA,CB,CC,CCF/EVP/ICMPLX,EVL,EVT
0024
0025    C***************************************************************
0026    C       Main Iterative Loop
0027    C       1) Compute initial solution (C0)
0028    C       2) Compute vector k
0029
0030    C***************************************************************
0031    C       Solve the initial steady-state problem (E<>0)
0032            DO 550, I=1,N
0033                  ZB=PA*Z(I)**PB
0034                  EX=DEXP(-ZB)/(Z(I)*Z(I))
0035                  ZB=PB*ZB
0036                  HI=S*H(Z(I),E)*Z(I)
0037                  C(I)=-EX*ZB*(-PB+1.D0+HI+ZB)
0038                  DO 530, K=1,N
0039                        EX=EX*Z(I)
0040                        TMP=DBLE(REAL(K))
0041                        B(I,K)=EX*(TMP*(TMP-1.D0-HI)
0042         *                        -ZB*(2.D0*TMP+PB-1.D0-HI)+ZB*ZB)
0043    530           CONTINUE
0044    550     CONTINUE
0045
0046            CALL PIVOT(N)
0047
0048    C       *****  Transfer the initial solution from c to c0
0049            IF (ICMPLX.EQ.0) THEN
0050                  DO 570, I=1,N
0051                        C0(I)=C(I)
0052    570           CONTINUE
0053            ELSE
0054                  DO 575, I=1,N
0055                        CC0(I)=DCMPLX(C(I),0.D0)
0056                        CCF(I)=DCMPLX(CF(I),0.D0)
0057    575           CONTINUE
0058            ENDIF
0059
0060    C***************************************************************
0061    C       Apply initial conditions; solve for k using A, c0, and b
0062
```

```
0063            IF (ICMPLX.EQ.0) THEN
0064                  DO 600, K=1,N
0065                        C(K)=C0(K)+CF(K)
0066                        DO 580, I=1,N
0067                              B(I,K)=DREAL(EVT(I,K))
0068    580                 CONTINUE
0069    600           CONTINUE
0070
0071                  CALL PIVOT(N)
0072            ELSE
0073                  DO 620, K=1,N
0074                        CC(K)=CC0(K)+CCF(K)
0075                        DO 610, I=1,N
0076                              CB(I,K)=EVT(I,K)
0077    610                 CONTINUE
0078    620           CONTINUE
0079
0080                  CALL CPIVOT(N)
0081            ENDIF
0082
0083    C*****************************************************************
0084    C       Output solution for current epsilon
0085    C       *****  TMP is the normalization constant for f(tau)
0086    C       *****  function
0087            IF (ICMPLX.EQ.0) THEN
0088                  TMP=-C0(1)-CF(1)
0089            ELSE
0090                  CTMP=-CC0(1)-CCF(1)
0091            ENDIF
0092
0093    C       ***** Calculation the coefficients, f[i], for the
0094    C             fractional change in current function
0095            IF (ICMPLX.EQ.0) THEN
0096                  DO 650, I=1,N
0097                        F(I)=DCMPLX(DREAL(EVT(1,I))*C(I)/TMP,0.D0)
0098    650           CONTINUE
0099            ELSE
0100                  DO 660, I=1,N
0101                        F(I)=EVT(1,I)*CC(I)/CTMP
0102    660           CONTINUE
0103            ENDIF
0104
0105            RETURN
0106
0107            END

0001
0002    C*****************************************************************
0003    C*****************************************************************
0004
0005            DOUBLE PRECISION FUNCTION H(Z,E)
0006
0007    C       Hydrodynamic Velocity Function
0008    C             Z = dimensionless displacement
0009    C             E = epsilon = step size parameter
0010    C             All parameters are normalized by the final rotation
```

```
0011    C                 rate
0012    C            E=0 corresponds to final velocity profile
0013    C            E<>0 corresponds to initial velocity profile
0014          DOUBLE PRECISION Z,E,X
0015
0016          X=Z/(1.D0+E)
0017
0018          H=X*X*(-0.51023D0+X*(1.D0-0.30795D0*X)/3.D0)/(1.D0+E)
0019
0020          RETURN
0021
0022          END

0001
0002    C*****************************************************************
0003    C*****************************************************************
0004
0005          SUBROUTINE PIVOT(N)
0006
0007    C     David N. Blauch          January 1987
0008    C     Caltech, Pasadena, CA  91125
0009
0010    C     Gaussian Elimination with Scaled Column Pivoting
0011
0012    C     The linear system A x = b is solved
0013    C           The matrix A is altered
0014    C           The solution is returned in the vector B
0015
0016          INTEGER I,J,N,NCOPY,P,NROW(20)
0017          DOUBLE PRECISION A(20,20),B(20),S(20),TMP,R(20,20),W(20)
0018
0019          COMMON /INVT/R,A,B,W
0020
0021    C     Initialize the Row Pointer NROW and
0022    C     Determine the Scaling Factors S
0023
0024          DO 100, I=1,N
0025
0026                S(I)=0.D0
0027
0028                DO 50, J=1,N
0029                      IF (S(I).LT.DABS(A(I,J))) THEN
0030                            S(I)=DABS(A(I,J))
0031                      ENDIF
0032    50            CONTINUE
0033
0034                IF (S(I).EQ.0.D0) THEN
0035                      WRITE (6,60)
0036    60                FORMAT (/X,'*****  No Unique Solution in ',
0037         *                      'Subroutine PIVOT')
0038                      STOP
0039                ENDIF
0040
0041                NROW(I)=I
0042
0043    100     CONTINUE
```

```
0044
0045    C       Begin the Gaussian Elimination Process
0046
0047            DO 200, I=1,N-1
0048
0049                  P=I
0050                  TMP=DABS(A(NROW(P),I))/S(NROW(P))
0051
0052                  DO 120, J=I+1,N
0053                  IF (TMP.LT.DABS(A(NROW(J),I))/S(NROW(J))) THEN
0054                        P=J
0055                        TMP=DABS(A(NROW(P),I))/S(NROW(P))
0056                  ENDIF
0057    120           CONTINUE
0058
0059                  IF (A(NROW(P),I).EQ.0.D0) THEN
0060                        WRITE (6,60)
0061                        STOP
0062                  ENDIF
0063
0064                  IF (NROW(I).NE.NROW(P)) THEN
0065                        NCOPY=NROW(I)
0066                        NROW(I)=NROW(P)
0067                        NROW(P)=NCOPY
0068                  ENDIF
0069
0070                  DO 160, J=I+1,N
0071                        IF (A(NROW(J),I).EQ.0.D0) GOTO 160
0072                        TMP=A(NROW(J),I)/A(NROW(I),I)
0073                        DO 140, K=I+1,N
0074                              A(NROW(J),K)=A(NROW(J),K)
0075         *                              -TMP*A(NROW(I),K)
0076    140                 CONTINUE
0077                        B(NROW(J))=B(NROW(J))-TMP*B(NROW(I))
0078    160           CONTINUE
0079
0080    200     CONTINUE
0081
0082            IF (A(NROW(N),N).EQ.0.D0) THEN
0083                  WRITE (6,60)
0084                  STOP
0085            ENDIF
0086
0087
0088    C       Begin Backward Substitution
0089
0090
0091            S(N)=B(NROW(N))/A(NROW(N),N)
0092
0093            DO 300, I=N-1,1,-1
0094
0095                  TMP=0.D0
0096                  DO 250, J=I+1,N
0097                        TMP=TMP+A(NROW(I),J)*S(J)
0098    250           CONTINUE
0099
```

```
0100                S(I)=(B(NROW(I))-TMP)/A(NROW(I),I)
0101
0102    300     CONTINUE
0103
0104            DO 400, I=1,N
0105                  B(I)=S(I)
0106    400     CONTINUE
0107
0108            RETURN
0109
0110            END

0001
0002
0003    C*****************************************************************
0004    C*****************************************************************
0005
0006            SUBROUTINE CPIVOT(N)
0007
0008    C       David N. Blauch          January 1987
0009    C       Caltech, Pasadena, CA  91125
0010
0011    C       Gaussian Elimination with Scaled Column Pivoting
0012
0013    C       The linear system A x = b is solved
0014    C             The matrix A is altered
0015    C             The solution is returned in the vector B
0016
0017    C       Subroutine written for complex variables
0018
0019    C*****************************************************************
0020
0021            INTEGER I,J,N,NCOPY,P,NROW(20)
0022            COMPLEX*16 A(20,20),B(20),S(20),TMP,R(20,20),W(20)
0023
0024            COMMON /CINVT/R,A,B,W
0025
0026    C       Initialize the Row Pointer NROW and
0027    C       Determine the Scaling Factors S
0028
0029            DO 100, I=1,N
0030
0031                  S(I)=DCMPLX(0.D0,0.D0)
0032
0033                  DO 50, J=1,N
0034                        IF (CDABS(S(I)).LT.CDABS(A(I,J))) THEN
0035                              S(I)=DCMPLX(CDABS(A(I,J)),0.D0)
0036                        ENDIF
0037    50                CONTINUE
0038
0039                  IF (S(I).EQ.0.D0) THEN
0040                        WRITE (6,60)
0041    60                  FORMAT (/X,'*****  No Unique Solution in ',
0042         *                        'Subroutine PIVOT')
0043                        STOP
0044                  ENDIF
```

```
0045
0046                NROW(I)=I
0047
0048    100     CONTINUE
0049
0050    C       Begin the Gaussian Elimination Process
0051
0052            DO 200, I=1,N-1
0053
0054            P=I
0055            TMP=DCMPLX(CDABS(A(NROW(P),I)/S(NROW(P))),0.D0)
0056
0057            DO 120, J=I+1,N
0058            IF (CDABS(TMP).LT.CDABS(A(NROW(J),I)/S(NROW(J)))) THEN
0059                  P=J
0060                  TMP=DCMPLX(CDABS(A(NROW(P),I)/S(NROW(P))),0.D0)
0061            ENDIF
0062    120     CONTINUE
0063
0064            IF (A(NROW(P),I).EQ.0.D0) THEN
0065                  WRITE (6,60)
0066                  STOP
0067            ENDIF
0068
0069            IF (NROW(I).NE.NROW(P)) THEN
0070                  NCOPY=NROW(I)
0071                  NROW(I)=NROW(P)
0072                  NROW(P)=NCOPY
0073            ENDIF
0074
0075            DO 160, J=I+1,N
0076                  IF (A(NROW(J),I).EQ.0.D0) GOTO 160
0077                  TMP=A(NROW(J),I)/A(NROW(I),I)
0078                  DO 140, K=I+1,N
0079                        A(NROW(J),K)=A(NROW(J),K)
0080          *                   -TMP*A(NROW(I),K)
0081    140           CONTINUE
0082                  B(NROW(J))=B(NROW(J))-TMP*B(NROW(I))
0083    160     CONTINUE
0084
0085    200     CONTINUE
0086
0087            IF (A(NROW(N),N).EQ.0.D0) THEN
0088                  WRITE (6,60)
0089                  STOP
0090            ENDIF
0091
0092
0093    C       Begin Backward Substitution
0094
0095
0096            S(N)=B(NROW(N))/A(NROW(N),N)
0097
0098            DO 300, I=N-1,1,-1
0099
0100                  TMP=DCMPLX(0.D0,0.D0)
```

```
0101                DO 250, J=I+1,N
0102                      TMP=TMP+A(NROW(I),J)*S(J)
0103    250         CONTINUE
0104
0105                S(I)=(B(NROW(I))-TMP)/A(NROW(I),I)
0106
0107    300     CONTINUE
0108
0109            DO 400, I=1,N
0110                  B(I)=S(I)
0111    400     CONTINUE
0112
0113            RETURN
0114
0115            END

0001
0002    C*****************************************************************
0003    C*****************************************************************
0004
0005            SUBROUTINE INVERT(N)
0006
0007    C       Matrix Inversion Subroutine
0008    C       Gaussian Elimination with Scaled Column Pivoting
0009
0010    C       Transforms the Linear System A x = B x + c  into
0011    C             x = U x + w with U in A and w in s
0012
0013            INTEGER I,J,K,N,P,NROW(20)
0014            DOUBLE PRECISION A(20,20),B(20,20),C(20),S(20),TMP,MAX
0015
0016            COMMON /INVT/A,B,C,S
0017
0018    C       Set Up Scaling Factors and Initialize Row Pointer NROW
0019
0020            DO 200, I=1,N
0021                  MAX=DABS(A(I,1))
0022                  DO 100, J=2,N
0023                        TMP=DABS(A(I,J))
0024                        IF (TMP.GT.MAX) THEN
0025                              MAX=TMP
0026                        ENDIF
0027    100           CONTINUE
0028                  IF (MAX.EQ.0.D0) GOTO 1000
0029                  S(I)=MAX
0030                  NROW(I)=I
0031    200     CONTINUE
0032
0033
0034            DO 300, I=1,N
0035
0036                  IF (I.EQ.N) GOTO 255
0037
0038    C             Find Pivots
0039
0040                  P=I
```

```
0041                MAX=DABS(A(NROW(I),I))/S(I)
0042                DO 250, J=I+1,N
0043                      TMP=DABS(A(NROW(J),I))/S(J)
0044                      IF (TMP.GT.MAX) THEN
0045                            P=J
0046                            MAX=TMP
0047                      ENDIF
0048    250         CONTINUE
0049
0050                IF (MAX.EQ.0.D0) GOTO 1000
0051
0052
0053    C           Carry Out Row Exchanges (if necessary)
0054
0055                IF (NROW(I).NE.NROW(P)) THEN
0056                      TMP=NROW(I)
0057                      NROW(I)=NROW(P)
0058                      NROW(P)=TMP
0059                ENDIF
0060
0061
0062    C           Normalize Row I in A
0063
0064    255         TMP=A(NROW(I),I)
0065                DO 260, K=1,N
0066                      IF (K.GE.I) THEN
0067                            A(NROW(I),K)=A(NROW(I),K)/TMP
0068                      ENDIF
0069                      B(NROW(I),K)=B(NROW(I),K)/TMP
0070    260         CONTINUE
0071                C(NROW(I))=C(NROW(I))/TMP
0072
0073
0074    C           Eliminate on the Remaining Rows
0075
0076                DO 290, J=1,N
0077
0078                   IF (J.NE.I) THEN
0079                      TMP=A(NROW(J),I)
0080                      DO 280, K=1,N
0081                      IF (K.GE.I) THEN
0082                      A(NROW(J),K)=A(NROW(J),K)-TMP*A(NROW(I),K)
0083                      ENDIF
0084                      B(NROW(J),K)=B(NROW(J),K)-TMP*B(NROW(I),K)
0085    280               CONTINUE
0086                      C(NROW(J))=C(NROW(J))-TMP*C(NROW(I))
0087                   ENDIF
0088
0089    290         CONTINUE
0090
0091    300    CONTINUE
0092
0093    C      Elimination Complete, return rows to original positions
0094
0095           DO 500, I=1,N
0096                 S(I)=C(NROW(I))
```

```
0097                DO 400, J=1,N
0098                     A(I,J)=B(NROW(I),J)
0099    400         CONTINUE
0100    500     CONTINUE
0101
0102            RETURN
0103
0104    C       Algorithm Failure Handler
0105
0106    1000    WRITE (6,1010)
0107    1010    FORMAT (/1X,'*****  Subroutine INVERT Aborted',/7X,
0108         *       'Matrix cannot be inverted or no unique ',
0109         *       'solution exists')
0110            STOP
0111
0112            END

0001
0002    C*****************************************************************
0003    C*****************************************************************
0004
0005            SUBROUTINE SORTZ(N,KY,P)
0006
0007    C       ***** Straight Insertion Sort
0008    C             algorithm refined for sorting collocation nodes
0009
0010    C       ***** The keys are in vector KY
0011    C       ***** The subroutine sets up the pointers in P
0012
0013    C       ***** The list is sorted so that the I-th smallest key is
0014    C             KY(P(I))
0015
0016    C       ***** The nodes are sorted from smallest to largest
0017
0018            INTEGER I,J,K,N,P(20)
0019            DOUBLE PRECISION KY(20)
0020
0021            P(1)=1
0022
0023    C       ***** Each pass adds the KY(I) to the list of sorted keys
0024            DO 100, I=2,N
0025
0026                 J=0
0027
0028    30           J=J+1
0029
0030    C            Have all sorted keys been checked?
0031                 IF (J.GE.I) GOTO 80
0032
0033    C            Is the current entry less than or equal to KY(I)?
0034                 IF ((KY(P(J))).LE.(KY(I))) GOTO 30
0035
0036    C            Insert the new key KY(I)
0037                 DO 60, K=I,J+1,-1
0038                      P(K)=P(K-1)
0039    60           CONTINUE
```

```
0040
0041    80          P(J)=I
0042
0043    100     CONTINUE
0044
0045            RETURN
0046
0047            END

0001
0002    C*****************************************************************
0003    C*****************************************************************
0004
0005            SUBROUTINE SORTE(N,KY,P)
0006
0007    C       ***** Straight Insertion Sort
0008    C             algorithm refined for sorting eigenvalues
0009
0010    C       ***** The keys are in vector KY
0011    C       ***** The subroutine sets up the pointers in P
0012
0013    C       ***** The list is sorted so that the I-th smallest key is
0014    C             KY(P(I))
0015
0016    C       ***** The eigenvalues are sorted from largest to smallest
0017    C             i.e., least negative to most negative based upon
0018    C             the real part of the eigenvalue
0019
0020            INTEGER I,J,K,N,P(20)
0021            COMPLEX*16 KY(20)
0022
0023            P(1)=1
0024
0025    C       ***** Each pass adds the KY(I) to the list of sorted keys
0026            DO 100, I=2,N
0027
0028                  J=0
0029
0030    30            J=J+1
0031
0032    C             Have all sorted keys been checked?
0033                  IF (J.GE.I) GOTO 80
0034
0035    C             Is the current entry >= KY(I)?
0036                  IF (DREAL(KY(P(J))).GE.DREAL(KY(I))) GOTO 30
0037
0038    C             Insert the new key KY(I)
0039                  DO 60, K=I,J+1,-1
0040                        P(K)=P(K-1)
0041    60            CONTINUE
0042
0043    80            P(J)=I
0044
0045    100     CONTINUE
0046
0047            RETURN
```

```
0048
0049            END
```

FDWSTEP

The program FDWSTEP simulates the current transient resulting from a step or "ramp" change in rotation rate using the finite difference method described in Chapter 3. When FDWSTEP is executed, the user is prompted for the Schmidt number S, the step size parameter ε, and the delay time τ_D. All three of these parameters must be entered as floating-point values; i.e., a decimal point must be included. The computer will then request the total number of spatial nodes N, the maximum dimensionless time τ_{max}, and the total number of temporal intervals M. The maximum dimensionless time τ_{max} must be a floating-point value; N and M are integers. Finally, the name of the output file is requested (maximum twelve characters).

The maximum displacement appropriate for the simulation is determined from the Schmidt number using the formula $z_N=5S^{-1/3}$. The temporal spacing is $k=\tau_{max}/M$. The initial and final steady-state concentration profiles are computed first; then the time-dependent problem is solved. After all computations are complete, the simulation parameters and results are written to the output file and program execution is terminated.

The subroutine BCROUT performs Crout's LU factorization of a "hexa-diagonal" matrix such as **P**, illustrated in Equation 3.14. No pivoting strategies are employed.

```
0001            PROGRAM FDWSTEP
0002
0003    C       David N. Blauch          March 1988, Revised June 1990
0004    C       Caltech, Pasadena, CA  91125
0005
0006    C***************************************************************
0007    C       Rotation-Rate Step Experiment
0008    C       Finite Difference Simulation of the Current Transient
0009
0010    C***************************************************************
0011    C       Algorithm includes the possibility of a nonperfect step
0012    C             change in rotation rate.
0013
0014            INTEGER I,J,L,N,M,LL
0015            DOUBLE PRECISION HV,A(200,6),B(200,6),Z,H,TMP,S,E,ZINF,T
0016            DOUBLE PRECISION DT,C(200),GRAD(5000),F(5000),GRAD0,R,TD
0017            DOUBLE PRECISION TAU(5000),GRADF,DGRAD
0018            CHARACTER*12 FNAME
0019
0020            COMMON /BCRTRED/A,C
0021            EXTERNAL HV,BCROUT
0022
0023    C***************************************************************
0024
0025    C       ***** System Parameters
0026
0027            WRITE (*,20)
0028    20      FORMAT (///25X,'Rotation-Rate Step Experiment',/13X,
0029           * 'Finite Difference Simulation of the Current Transient',
0030           * //1X,'System Parameters:',/10X,'Schmidt number ?  ',$)
0031            READ (*,30) S
0032    30      FORMAT (D16.9)
0033
0034            WRITE (*,40)
0035    40      FORMAT (10X,'Step-Size Parameter (epsilon) ?  ',$)
0036            READ (*,30) E
0037
0038            WRITE (*,60)
0039    60      FORMAT (10X,'Dimensionless Delay Time for Change in ',
0040           *       'Rotation Rate ?  ',$)
0041            READ (*,30) TD
0042            IF (TD.LT.0.D0) THEN
0043                  WRITE (*,70)
0044    70            FORMAT (/1X,'$$$$$  Delay Time Cannot be Negative')
0045                  STOP
0046            ENDIF
0047
0048    C       ***** Get Spatial Parameters
0049
0050            WRITE (*,100)
0051    100     FORMAT (/1X,'Simulation Parameters:',/10X,'Number of ',
0052           *       'Spatial Intervals (maximum 200) ?  ',$)
0053            READ (*,130) N
0054    130     FORMAT (I8)
0055
0056    C       ***** The maximum displacement is obtained from the
```

```
0057    C             Schmidt number
0058
0059            ZINF=5.D0/S**(1.D0/3.D0)
0060
0061    C       ***** Calculate the spatial step size
0062
0063            H=ZINF/DBLE(REAL(N))
0064
0065    C       ***** Get Temporal Parameters
0066
0067            WRITE (*,150)
0068    150     FORMAT (10X,'Final Dimensionless Time ?  ',$)
0069            READ (*,30) DT
0070
0071            WRITE (*,170)
0072    170     FORMAT (10X,'Number Temporal Intervals ?  ',$)
0073            READ (*,130) M
0074
0075    C       ***** Calculate the Temporal Step Size
0076
0077            DT=DT/DBLE(M)
0078
0079    C       ***** Get the file specification
0080
0081            WRITE (*,180)
0082    180     FORMAT (/1X,'Output Specifications:',/10X,'Name of ',
0083         *        'Output File ?  ',$)
0084            READ (*,190) FNAME
0085    190     FORMAT (A12)
0086
0087    C*****************************************************************
0088    C       *****  Compute the computational constant R
0089            R=120.D0*S*H*H/DT
0090
0091    C       *****  Create the Linear System for Determination of the
0092    C              Final Solution
0093
0094            T=TD+1.D0
0095            DO 250, I=1,N
0096                  Z=DBLE(I)*H
0097                  TMP=S*HV(Z,T,E,TD)*H
0098                  A(I,1)=50.D0+12.D0*TMP
0099                  A(I,2)=-75.D0+65.D0*TMP
0100                  A(I,3)=-20.D0-120.D0*TMP
0101                  A(I,4)=70.D0+60.D0*TMP
0102                  A(I,5)=-30.D0-20.D0*TMP
0103                  A(I,6)=5.D0+3.D0*TMP
0104                  C(I)=0.D0
0105    250     CONTINUE
0106            C(1)=-50.D0-12.D0*S*HV(H,T,E,TD)*H
0107
0108    C       ***** Solve the linear system;  the final concentration
0109    C             profile is returned in C().
0110
0111            CALL BCROUT(N)
0112
```

```
0113    C       ***** Determine the initial dimensionless gradient at the
0114    C             electrode surface
0115
0116            GRADF=(-3.D0*C(4)+16.D0*C(3)-36.D0*C(2)+48.D0*C(1)-25.D0)
0117         *       /(12.D0*H)
0118
0119    C*************************************************************
0120    C       *****  Create the Linear System for Determination of the
0121    C             Initial Solution
0122
0123            DO 280, I=1,N
0124                  Z=DBLE(I)*H
0125                  TMP=S*HV(Z,-1.D0,E,TD)*H
0126                  A(I,1)=50.D0+12.D0*TMP
0127                  A(I,2)=-75.D0+65.D0*TMP
0128                  A(I,3)=-20.D0-120.D0*TMP
0129                  A(I,4)=70.D0+60.D0*TMP
0130                  A(I,5)=-30.D0-20.D0*TMP
0131                  A(I,6)=5.D0+3.D0*TMP
0132                  TMP=S*HV(Z,0.D0,E,TD)*H
0133                  B(I,1)=50.D0+12.D0*TMP
0134                  B(I,2)=-75.D0+65.D0*TMP+R
0135                  B(I,3)=-20.D0-120.D0*TMP
0136                  B(I,4)=70.D0+60.D0*TMP
0137                  B(I,5)=-30.D0-20.D0*TMP
0138                  B(I,6)=5.D0+3.D0*TMP
0139                  C(I)=0.D0
0140    280     CONTINUE
0141            C(1)=-50.D0-12.D0*S*HV(H,-1.D0,E,TD)*H
0142
0143    C       ***** Solve the linear system;  the initial concentration
0144    C             profile is returned in C().
0145
0146            CALL BCROUT(N)
0147
0148    C       ***** Determine the initial dimensionless gradient at the
0149    C             electrode surface
0150
0151            GRAD0=(-3.D0*C(4)+16.D0*C(3)-36.D0*C(2)+48.D0*C(1)-25.D0)
0152         *       /(12.D0*H)
0153
0154            DGRAD=GRADF-GRAD0
0155
0156    C*************************************************************
0157    C       Main Loop
0158    C             B contains the iteration matrix, which is updated
0159    C                   at each iteration and is used to calculate A
0160
0161            DO 1000, J=1,M
0162                  T=DBLE(REAL(J))*DT
0163
0164                  Z=-100.D0-12.D0*S*H*(HV(H,T,E,TD)+HV(H,T-DT,E,TD))
0165                  DO 320, I=1,5
0166                        Z=Z-B(1,I+1)*C(I)
0167    320           CONTINUE
0168                  DO 360, I=2,N
```

```
                        TMP=0.D0
                        IF (I+4.GT.N) THEN
                              LL=N-I+2
                        ELSE
                              LL=6
                        ENDIF
                        DO 340, L=1,LL
                              TMP=TMP-B(I,L)*C(I+L-2)
340                     CONTINUE
                        C(I-1)=Z
                        Z=TMP
360               CONTINUE
                  C(N)=Z

C                 ***** The matrices need only be recalculated
C                       when T-2DT<TD; i.e., the hydrodynamic
C                       velocity profile is still changing with time

                  IF ((T-2.D0*DT).LE.TD) THEN
                  DO 400, I=1,N
                        Z=DBLE(I)*H
                        TMP=S*HV(Z,T,E,TD)*H
                        A(I,1)=50.D0+12.D0*TMP
                        A(I,2)=-75.D0+65.D0*TMP-R
                        A(I,3)=-20.D0-120.D0*TMP
                        A(I,4)=70.D0+60.D0*TMP
                        A(I,5)=-30.D0-20.D0*TMP
                        A(I,6)=5.D0+3.D0*TMP
                        DO 380, L=1,6
                              B(I,L)=A(I,L)
380                     CONTINUE
                        B(I,2)=B(I,2)+2.D0*R
400               CONTINUE
                  ELSE
                  DO 500, I=1,N
                        DO 480, L=1,6
                              A(I,L)=B(I,L)
480                     CONTINUE
                        A(I,2)=A(I,2)-2.D0*R
500               CONTINUE
                  ENDIF

C                 ***** Solve the linear system for this step

                  CALL BCROUT(N)

C                 ***** Save the results of this step (they will be
C                       stored in the output file later)

                  TAU(J)=T

                  GRAD(J)=(-3.D0*C(4)+16.D0*C(3)-36.D0*C(2)
     *                  +48.D0*C(1)-25.D0)/(12.D0*H)
                  F(J)=(GRAD(J)-GRAD0)/DGRAD

1000    CONTINUE
```

```
0225
0226    C*****************************************************************
0227    C       Open the Output File
0228
0229            OPEN (1,FILE=FNAME,STATUS='NEW')
0230
0231    C       ***** Store the Header and Simulation Information
0232
0233            WRITE (1,1200) S,E,TD,N,H,M,DT,GRAD0,GRADF,DGRAD
0234    1200    FORMAT (25X,'Rotation Rate Step Experiment',/13X,
0235         * 'Finite Difference Simulation of the Current Transient',
0236         * //25X,'Schmidt number =  ',F12.2,/21X,'Step Size ',
0237         * 'Parameter Epsilon =  ',F7.4,/8X,'Dimensionless ',
0238         * 'Delay Time for Change in Rotation Rate =  ',F7.4,
0239         * //19X,I4,' spatial intervals of size ',F10.8,/18X,
0240         * I5,' temporal intervals of size ',F12.6,
0241         * //20X,'Initial Gradient (z=0) = ',D16.9,
0242         * /20X,'Final Gradient (z=0) = ',D16.9,
0243         * /15X,'Total Change in Gradient (z=0) = ',D16.9,
0244         * //20X,'tau',14X,'gradient',9X,'f[tau]',/1X)
0245
0246    C       ***** Store the Initial Gradient, etc.
0247
0248            WRITE (1,1300) 0.D0,GRAD0,0.D0
0249    1300    FORMAT (16X,F12.6,5X,F13.8,5X,F12.10)
0250
0251    C       ***** Store the rest of the results
0252
0253            DO 1500, I=1,M
0254                  WRITE (1,1400) TAU(I),GRAD(I),F(I)
0255    1400          FORMAT (16X,F12.6,5X,F13.8,5X,F12.10)
0256    1500    CONTINUE
0257
0258            CLOSE (1)
0259
0260            END

0001
0002    C*****************************************************************
0003    C*****************************************************************
0004
0005            DOUBLE PRECISION FUNCTION HV(Z,T,E,TD)
0006
0007    C       Hydrodynamic Velocity Function
0008    C             Z  is the dimensionless displacement
0009    C             E  is the step-size parameter
0010    C             T  is the dimensionless time
0011    C             TD is the step delay time, i.e. ramp time
0012
0013            DOUBLE PRECISION Z,E,Y,T,X,VA,VB,VC,TD,U
0014
0015            PARAMETER (VA=-0.51023D0)
0016            PARAMETER (VB=1.D0)
0017            PARAMETER (VC=-0.30795D0)
0018
0019    C*****************************************************************
```

```
0020    C       The formulation of the rotation-rate step problem
0021    C             includes normalization by the final rotation rate.
0022
0023    C       ***** The function U; i.e., U[T], corresponds to the ramp
0024    C             function.  If TD=0, the U is a step function
0025            IF (T.LT.0.D0) THEN
0026                  U=0.D0
0027            ELSEIF (T.LT.TD) THEN
0028                  U=T/TD
0029            ELSE
0030                  U=1.D0
0031            ENDIF
0032
0033    C       ***** The variable X is the normalization factor used to
0034    C             scale the dimensionless displacement.  This factor
0035    C             is required to compensate for the fact that the
0036    C             current rotation rate is different from that used
0037    C             for the normalization.  Once the final rotation
0038    C             rate has been reached, X=1
0039
0040            X=(1.D0+E*U)/(1.D0+E)
0041
0042    C       ***** Y is the scaled dimensionless displacement
0043
0044            Y=X*Z
0045
0046    C       ***** HV is the dimensionless hydrodynamic velocity
0047    C             function as described by Cochran (Reference 6)
0048
0049            HV=X*Y*Y*(VA+Y*(VB+Y*VC)/3.D0)
0050
0051            RETURN
0052
0053            END

0001
0002    C*****************************************************************
0003    C*****************************************************************
0004
0005            SUBROUTINE BCROUT(N)
0006
0007    C       David N. Blauch          September 1987
0008    C       Caltech, Pasadena, CA 91125
0009
0010    C       Gaussian Elimination of an Assymetric "6-Diagonal" Matrix
0011
0012    C       ***** The finite difference algorithm implemented in the
0013    C       main program gives rise to a matrix whose only non-
0014    C       zero entries occur on the main diagonal, the diagonal
0015    C       immediately below the main diagonal, and the four
0016    C       diagonals immediately above the main diagonal.
0017
0018    C       ***** This subroutine is a direct factorization algorithm
0019    C       that takes advantage of this symmetry.
0020
0021    C       ***** No pivoting strategies are employed
```

```
0022
0023          INTEGER I,N,L,J
0024          DOUBLE PRECISION A(200,6),B(200),TMP,SUB
0025
0026          COMMON /BCRTRED/A,B
0027
0028    C*************************************************************
0029    C       Only the six nonzero diagonals of the relevant matrix
0030    C             are stored.
0031
0032    C       ***** If A() is the matrix as implemented in this program
0033    C             and M is the actual NxN matrix, then the storage
0034    C             format is as follows:
0035
0036    C             A(I,J) corresponds to M(I,I+J-2)
0037
0038    C       ***** Thus the main diagonal of M is stored as the column
0039    C             A( ,2)
0040
0041    C*************************************************************
0042    C       Normalization and Forward Elimination
0043          DO 100, I=1,N-1
0044                TMP=A(I,2)
0045                A(I,2)=1.D0
0046                SUB=A(I+1,1)
0047                IF (I+4.GT.N) THEN
0048                      L=N-I
0049                ELSE
0050                      L=4
0051                ENDIF
0052                DO 50, J=1,L
0053                      A(I,2+J)=A(I,2+J)/TMP
0054                      A(I+1,1+J)=A(I+1,1+J)-SUB*A(I,2+J)
0055    50          CONTINUE
0056                B(I)=B(I)/TMP
0057                B(I+1)=B(I+1)-SUB*B(I)
0058    100   CONTINUE
0059
0060    C       Backward Substitution
0061          B(N)=B(N)/A(N,2)
0062          DO 200, I=N-1,1,-1
0063                TMP=0.D0
0064                IF (I+4.GT.N) THEN
0065                      L=N-I
0066                ELSE
0067                      L=4
0068                ENDIF
0069                DO 150, J=1,L
0070                      TMP=TMP+A(I,2+J)*B(I+J)
0071    150         CONTINUE
0072                B(I)=B(I)-TMP
0073    200   CONTINUE
0074
0075          RETURN
0076
0077          END
```

Part I References

References

1. W. J. Albery, R. A. Hillman, and S. Bruckenstein, J. *Electroanal. Chem.*, **100** (1979) 687.

2. E. R. Benton, J. *Fluid Mech.*, **24** (1966) 781.

3. S. S. Chawla, *J. Fluid Mech.*, **78** (1976) 609.

4. S. Bruckenstein, M. I. Bellavance, and B. Miller, *J. Electrochem. Soc.*, **120** (1973) 1351.

5. A. J. Bard and L. R. Faulkner, Electrochemical Methods, Wiley, New York, 1980, Chapt. 8.

6. W. G. Cochran, *Proc. Cambridge Philos. Soc.*, **30** (1934) 365.

7. J. Villadsen and W. E. Stewart, *Chem. Eng. Sci.*, **22** (1967) 1483.

8. B. A. Finlayson, The Method of Weighted Residuals, Academic Press, New York, 1972.

9. R. Caban and T. W. Chapman, *Chem. Eng. Sci.*, **36** (1981) 849.

10. S.-C. Yen and T. W. Chapman, *Chem. Eng. Commun.*, **38** (1985) 159.

11. G. Strang, Linear Algebra and Its Applications, 2nd ed., Academic Press, New York, 1980, Chapt. 5.

12. N. Finizio and G. Ladas, Ordinary Differential Equations with Modern Applications, Wadsworth, Belmont, 1978, Chapt. 6.

13. IMSL Library Reference Manual, Vol. 2, IMSL, Houston, June 1982, p. E-1.

14. E. Kreyszig, Advanced Engineering Mathematics, 5th ed., Wiley, New York, 1983, Chapt. 21.

15. R. L. Burden, J. D. Faires, and A. C. Reynolds, Numerical Analysis, 2nd ed., Prindle, Weber and Schmidt, Boston, 1981, Chapts. 10 and 11.

16. G. Lauer, R. Abel, and F. C. Anson, *Anal. Chem.*, **39** (1967) 765.

17. M. von Stackelberg, M. Pilgram, and V. Toome, *Z. Elektrochem.*, **57** (1953) 342.

18. M. L. Hitchman and W. J. Albery, *Electrochim. Acta*, **17** (1972) 787.

PART II

ION-PAIRING AND ELECTRIC FIELD EFFECTS ON ELECTRON HOPPING IN THE NAFION-TRIS(2,2′-BIPYRIDINE)OSMIUM(3+/2+) SYSTEM

Chapter 5

The Electrochemical Behavior of the Tris(2,2′-bipyridine)osmium(3+/2+) Redox Couple Incorporated into Nafion

Introduction

The creation and characterization of polymeric electrode coatings containing covalently, coordinatively, or electrostatically bound redox centers have been a field of intense research during the past two decades.[1] In conjunction with the experimental work in this area, a theoretical framework describing the mechanisms and rate laws governing charge propagation within such coatings has been developed.[2-14] Beyond their intrinsic significance, the mechanisms of charge transport in "redox polymers" are important in light of their implications regarding the electrocatalytic properties of coated electrodes,[15] because charge propagation, together with kinetics and the rate of substrate permeation of the coating, is a potential rate-limiting factor in catalytic applications.[16]

Charge propagation across redox polymers requires the presence of a concentration gradient of the oxidized and reduced forms of the redox species. For this reason, the rates of charge propagation in redox polymer films have been investigated most often by electrochemical techniques,[17] the most commonly used techniques being chronocoulometry and chronoamperometry. In all cases, the chronocoulometric or chronoamperometric response has been observed to obey the Cottrell equation; i.e., the charge or current is proportional to the square root of time or to its inverse, respectively, providing the time scale is sufficiently short that the region of the film adjacent to the electrode surface in which a sizeable concentration gradient exists is small compared to the film thickness.[18] Such observations have led to the notion that charge propagation through redox polymers can be regarded as a diffusional

process, or at least equivalent to a diffusional process, which can be characterized by an apparent diffusion coefficient, D_{ap}.

Redox species attached to polymeric coatings by covalent or coordinative bonds are immobile; therefore, charge propagation must occur by means of electron hopping between adjacent pairs of oxidized and reduced redox centers. The way in which this sort of electron hopping can result in diffusion-like behavior was first explained by means of a stochastic model in which the redox centers are regarded as randomly distributed over a fictitious cubic lattice whose characteristic length is equal to the average hopping distance, δ.[13a,19] The electron hopping process is found to obey Fick's laws of diffusion with the rate of charge propagation being characterized by an electron hopping diffusion coefficient, D_1, defined by

$$D_1 = \bar{k}_1 \delta^2 C_E = \frac{k_1 \delta^2 C_E}{6} , \qquad (5.1)$$

where $\bar{k}_1$ is the second-order, activation-limited rate constant for electron transfer between two adjacent sites on the fictitious lattice, C_E is the total concentration of redox centers, and $k_1 = 6\bar{k}_1$ is the conventional, second-order, activation-limited rate constant for electron self-exchange. (The factor of six arises because each node of the lattice is surrounded by six neighbors.) In this case, the apparent diffusion coefficient for charge transport is simply the electron-hopping diffusion coefficient.

In the case of electrostatically bound redox species, physical diffusive displacement may contribute significantly to charge

propagation. The combined effects of physical displacement and electron hopping also result in overall diffusive behavior that obeys Fick's laws. The apparent diffusion coefficient in this case is the sum of the diffusion coefficients for physical displacement, D_{pd}, and electron hopping, D_1:[20]

$$D_{ap} = D_{pd} + D_1 = D_{pd} + \frac{k_1 \delta^2 C_E}{6} . \qquad (5.2)$$

Attempts to observe variations in the apparent diffusion coefficients with the concentration of redox sites have led to a variety of results, only some of which appear consistent with the predictions of Equation 5.2.[3e] Improvements in the theoretical model of charge propagation within redox polymers appear necessary.

A significant theoretical refinement arises from the observation that the maintenance of electroneutrality requires that electron movement be coupled with the physical displacement of electroinactive counterions, a situation analogous to that associated with ordinary solutions of electroactive reagents containing little or no supporting electrolyte, where migration of charged reactants in the electric field affects the rate of charge transport. Theoretical analysis[21] of such solution systems is based upon the classical Nernst-Planck-Fick equation. In the case of electron hopping in redox polymer films, low concentrations or mobilities of electroinactive counterions also produce electric fields that affect charge propagation rates. The "migration" of electrons, however, is not governed by the classical Nernst-Planck-Fick equation but by a

related equation derived by Saveant.[22a-b] Analyses of the responses expected in both steady-state[22c] and transient[22d] experiments show that the presence of an electric field always enhances the rate of electron hopping, and the enhancement grows as the mobility of the electroinactive counterion decreases. Thus, earlier suggestions,[1a,6,7a-c,9a] that charge propagation rates in redox polymer films might be controlled by the intrinsically slower of the two coupled processes of electron hopping and counterion displacement, seem incorrect. On the contrary, the slower the movement of the electroinactive ions, the faster the electron hopping and the larger the resulting current densities. In all cases, potential step experiments display Cottrellian behavior from which apparent diffusion coefficients can be evaluated. These apparent diffusion coefficients increase with the concentration of redox centers more steeply than the simple proportionality indicated in Equation 5.2. This feature has been used to interpret[22d] previous observations made with polyvinylpyridine copolymers containing coordinatively attached osmium and ruthenium redox centers.[11c]

In view of the high ionic content of typical redox polymers and of the hydrophobic character of large portions of their structures, ionic aggregation in redox polymers is expected to be commonplace.[23] A simple and convenient way to treat ionic interactions is in terms of ion-pairing equilibria. The ion-pairing equilibria under consideration involve the formation of tight, contact ion-pairs between the fixed, charged sites in the polyelectrolyte film and the electroactive counterions. Henceforth we will employ "ion-pair" and "ion-pairing" to designate this process. The basic relationships governing the ways

in which ion-pairing affects electron-hopping rates in redox polymers in the presence of electric fields have been established recently.[22b,24] These relationships predict apparent diffusion coefficients, obtained from steady-state responses, that show steep increases with the concentration of redox sites when the ion-pairing equilibrium constants are large.[22b]

The goals of the work reported in Part II of this thesis are to extend the relevant theoretical treatment for charge propagation in redox polymers and to test experimentally the occurrence of the predicted effects. For these purposes, redox polymers in which the electroactive ions are electrostatically attached to polyelectrolyte films in an irreversible fashion appear to be particularly attractive systems, because the very existence of irreversible electrostatic attachment implies a strong interaction between the electroactive counterions and the fixed ionic sites. (What else would prevent the loss of the incorporated counterions when the coatings are transferred to pure, supporting electrolyte?)

Electrode coatings prepared from the perfluorosulfonate electrolyte Nafion,[25] in which cationic reactants can be incorporated by ion-exchange, were chosen for this study. The excellent stability and high ionic permselectivity exhibited by such coatings have contributed greatly towards the attractiveness of Nafion for the purpose of immobilizing cationic species near the electrode surface, although problems with reproducibility, depending upon the source of the solutions of Nafion and the procedures employed to deposit the coatings, have been noted.[10b] The most extensive previous measurements have involved electroactive counterions consisting of

cationic complexes of 2,2'-bipyridine (bpy) with transition metals (e.g., Fe, Co, Ru, and Os), which are particularly strongly, and essentially irreversibly, bound by the Nafion coatings.[3b,4b-c,10a]

In one of the first studies, the diffusion coefficients of the $Ru(bpy)_3^{3+/2+}$ couple in Nafion were reported to show little dependence on the quantities of the complex incorporated into the coating, but large fractions of the incorporated complexes were found to be electroinactive.[4b] By contrast, in more recent studies of the same system, a very strong dependence of the diffusion coefficient on the concentration of the incorporated $Ru(bpy)_3^{3+/2+}$ was observed, and the same was reported for the $Os(bpy)_3^{3+/2+}$ couple.[8,14] We have observed similar behavior in the latter system. The preponderance of the evidence is that strong, nonlinear dependences of the apparent diffusion coefficients on the concentration of the redox centers is typical. The remainder of Part II is devoted to the exposition and experimental testing of an ion-pairing model that leads to predicted concentration dependences that agree with those observed experimentally.

Experimental

Materials

Solutions of Nafion (EW 1100) in an alcoholic solvent (4 wt.%) were obtained from the Aldrich Chemical Company. The concentration of sulfonate groups present in the solutions was determined by titration of the proton counter cations with standard base to be 34.2 mM. (The Nafion solution provided by the supplier was prepared by dissolution of the acid form of the polymer, so that

the acidity is a measure of the concentration of sulfonate groups in the Nafion stock solution.) This value was not far from that corresponding to the concentration specified by the supplier (39.7 mM) and agreed with the concentration estimated from the sulfur content of a dried sample of Nafion obtained by evaporation of an aliquot of the stock solution.

$Os(bpy)_3Cl_2 \cdot 6H_2O$ (bpy=2,2'-bipyridine) was prepared as described in the literature[26] with slight modifications: 1.0 g of K_2OsCl_6 and 1.28 g of 2,2'-bipyridine were added to 10 mL of glycerol, and the mixture was heated at 240°C for 1 hour. The volume was reduced to ca. 2 mL by heating at 180°C under vacuum. The residue was extracted with ether to remove excess 2,2'-bipyridine followed by dissolution in the minimum quantity of water. Lustrous, dark-green crystals were obtained from this solution upon cooling in the refrigerator.

Glassy-carbon electrodes (Tokai Carbon Co.) were mounted and polished as previously described.[27]

Instrumentation

Apparent diffusion coefficients were evaluated from chronocoulometric measurements[27] performed with a BAS 100 Electrochemical Analyzer (Bioanalytical Systems, Inc.). Cyclic voltammetry was carried out with PAR instrumentation (EG&G Instruments, Inc., PAR Model 173, 175, and 179 units) and an X-Y recorder. Conventional, two-compartment cells were employed. Potentials are reported with respect to a sodium chloride saturated calomel electrode (SSCE).

Procedures

Nafion coatings were applied to the glassy-carbon electrode surfaces either by spin-coating or by transfer of aliquots of the stock solution to the surface with a microsyringe. In both cases, the solvent was allowed to evaporate at room temperature to obtain adherent films. The results of experiments conducted with "solution processed"[10b] Nafion coatings were essentially similar to those obtained with unprocessed coatings. The spin-coated films exhibited the most reproducible behavior and were employed for measurements of relative diffusion coefficients. $Os(bpy)_3^{2+}$ was incorporated into coatings by immersing them for controlled times in a 0.5 mM solution of the complex in 0.05 M H_2SO_4. Measurements were started with the lowest concentration of $Os(bpy)_3^{2+}$ in the coatings. The concentration was increased gradually by re-exposure of the coating to the $Os(bpy)_3^{2+}$ solution for controlled periods. In this way, a series of diffusion coefficients was obtained for a wide range of reactant concentrations with a single Nafion coating. After each successive loading, the coating was soaked for 30 minutes in pure, supporting electrolyte to allow the reactant concentration profile to become uniform.

The experimental results were quite sensitive to the procedures employed to prepare the coatings of Nafion on polished glassy-carbon electrodes. After establishing an experimental protocol that yielded satisfactorily reproducible behavior, apparent diffusion coefficients for the $Os(bpy)_3^{2+}$-Nafion system were evaluated over a wide range of concentrations by means of potential-step

chronocoulometry. The quantity of reactant incorporated into the coating was determined by exhaustive oxidation of the complex to $Os(bpy)_3^{3+}$ followed by integration of the current required to reduce the oxidized complex to $Os(bpy)_3^{2+}$. This procedure was preferable to the simple oxidation of the $Os(bpy)_3^{2+}$, because corrections for background currents were smaller and more reproducible.

Results

Determination of the Fractional Loading

When the coatings were loaded to saturation with $Os(bpy)_3^{2+}$, the quantity of charge consumed during the first coulometric oxidation of the incorporated complex was greater than that required for the reduction of the resulting $Os(bpy)_3^{3+}$ and for all subsequent oxidation-reduction cycles, which produced essentially equal anodic and cathodic charge consumption. This behavior is consistent with expulsion of the osmium complex during the oxidation of $Os(bpy)_3^{2+}$ to $Os(bpy)_3^{3+}$. (The alternate incorporation of anions into the Nafion is strongly disfavored by its high cation permselectivity.) If electroneutrality were maintained exclusively by expulsion of $Os(bpy)_3^{3+}$ from the coating during the oxidation process, one would expect the first coulometric assay to consume 1.5 times as much charge as all subsequent assays, anodic or cathodic. If, on the other hand, electroneutrality were maintained by expulsion of $Os(bpy)_3^{2+}$ during the oxidation process, there would be no difference between the first anodic and all subsequent coulometric assays.

Experimentally, the ratio of the charges consumed in the first (anodic) and all subsequent assays was 1.4±0.1. It thus appears that

electroneutrality is maintained primarily by the expulsion of $Os(bpy)_3^{3+}$ during the oxidation of $Os(bpy)_3^{2+}$ in saturated coatings. The charge obtained in the subsequent coulometric assays, Q_t^o, was taken as a measure of the quantity of osmium complex in the film that corresponds to saturation of all the Nafion sulfonate groups by $Os(bpy)_3^{3+}$ and thus a fractional loading, X_E, of unity. The value of X_E for loadings below saturation was obtained from Equation 5.3,

$$X_E = \frac{3C_E}{C_F^0} = \frac{Q_t}{Q_t^0}, \qquad (5.3)$$

where Q_t is the measured charge for a coating containing the osmium complex at a concentration C_E. The total concentration of Nafion sulfonate sites is C_F^0.

The determination of X_E by this procedure assumes that the maximum quantity of $Os(bpy)_3^{3+}$ that can be incorporated in the coating corresponds to the complete replacement of the hydrogen counterions by the osmium complex. This assumption was checked for films deposited onto an electrode by transfer of measured aliquots of a solution of Nafion by the following procedure: The coating was exposed to a solution of $Os(bpy)_3^{2+}$ in 0.05 M H_2SO_4 until it was saturated with the osmium complex. The $Os(bpy)_3^{2+}$ was oxidized to $Os(bpy)_3^{3+}$, and the quantity of the oxidized complex present was determined by coulometric assay (as described above). The coulometrically measured value corresponded closely to one-third of the total quantity of sulfonate groups present, thereby supporting the use of Equation 5.3 in the evaluation of X_E.

A second assumption inherent in this procedure is that all of the incorporated osmium complex is electroactive. This assumption, which is supported by the observations reported in the preceding paragraph, was checked by means of a spectrophotometric assay. Platinum flag electrodes, from which it was easier to detach Nafion coatings, were coated with Nafion, loaded with $Os(bpy)_3^{2+}$, and a coulometric assay of the quantity of electroactive complex present performed. The coating was then dissolved in dimethylformamide by ultrasonically agitating the coated electrode in the absence of air. The concentration of $Os(bpy)_3^{2+}$ in the resulting solution was determined from its absorbance at 482 nm with $\varepsilon=1.4\times10^4\ \underline{M}^{-1}\ cm^{-1}$ as determined in separate calibration measurements. The quantities of $Os(bpy)_3^{2+}$ in the solution were found to be in excellent agreement with those obtained from the coulometric assays, thus confirming the complete electroactivity of the incorporated osmium complex.[28]

Determination of Apparent Diffusion Coefficients

The chronocoulometric plots of charge vs $(time)^{1/2}$ for data collected when the potential was stepped from 0.2 V, where no current flowed, to 0.9 V, where the incorporated $Os(bpy)_3^{2+}$ was oxidized to $Os(bpy)_3^{3+}$, were linear (Cottrell behavior) for all investigated values of X_E. Measurement times were typically 10 to 225 ms with film thicknesses on the order of 0.85 μm. Apparent diffusion coefficients were obtained from the slope, s ($C\ s^{-1/2}$), of the linear plots:

$$D_{ap} = \pi\left(\frac{s}{2FSC_E}\right)^2 = \pi\left(\frac{3s}{2FSC_F^0X_E}\right)^2. \qquad (5.4)$$

The electrode surface area is represented by S, and F is the Faraday constant. Uncertainties in the values of the fractional loadings result in corresponding uncertainties in the absolute values of D_{ap}, but the relative values of D_{ap} for a single coating with varying fractional loadings could be reproduced to ca. 10%. The assumption that the coating thickness, and hence C_F^0, did not change significantly with the fractional loading was based upon previous measurements[3e] in which Nafion coatings were loaded with varying quantities of $Co(bpy)_3^{2+}$. The determination of the absolute values of D_{ap} requires that C_F^0, the total concentration of sulfonate groups within the Nafion coating, be known. A value of 1.2 M was chosen for C_F^0.[10c] Uncertainties in C_F^0 result in corresponding uncertainties in the absolute values of D_{ap} but do not affect the relative variation of D_{ap} with changes in X_E, the central point of interest in the present investigation.

The results of a large number of measurements of D_{ap} originating from two different coated electrodes for a range of fractional loadings are shown in the data points plotted in Figure 5.1. The general trend in the data is similar to that reported recently by He and Chen[8] for similar experimental conditions. The present, more extensive, data set makes it clearer that the diffusion coefficient becomes very small as the loading approaches zero, that there is a relatively small region of intermediate loadings where it increases proportionately to the concentration of incorporated $Os(bpy)_3^{2+}$, and

Figure 5.1. Experimental values of the apparent diffusion coefficient for charge propagation in the Nafion-$Os(bpy)_3^{3+/2+}$ system plotted against the fractional loading.

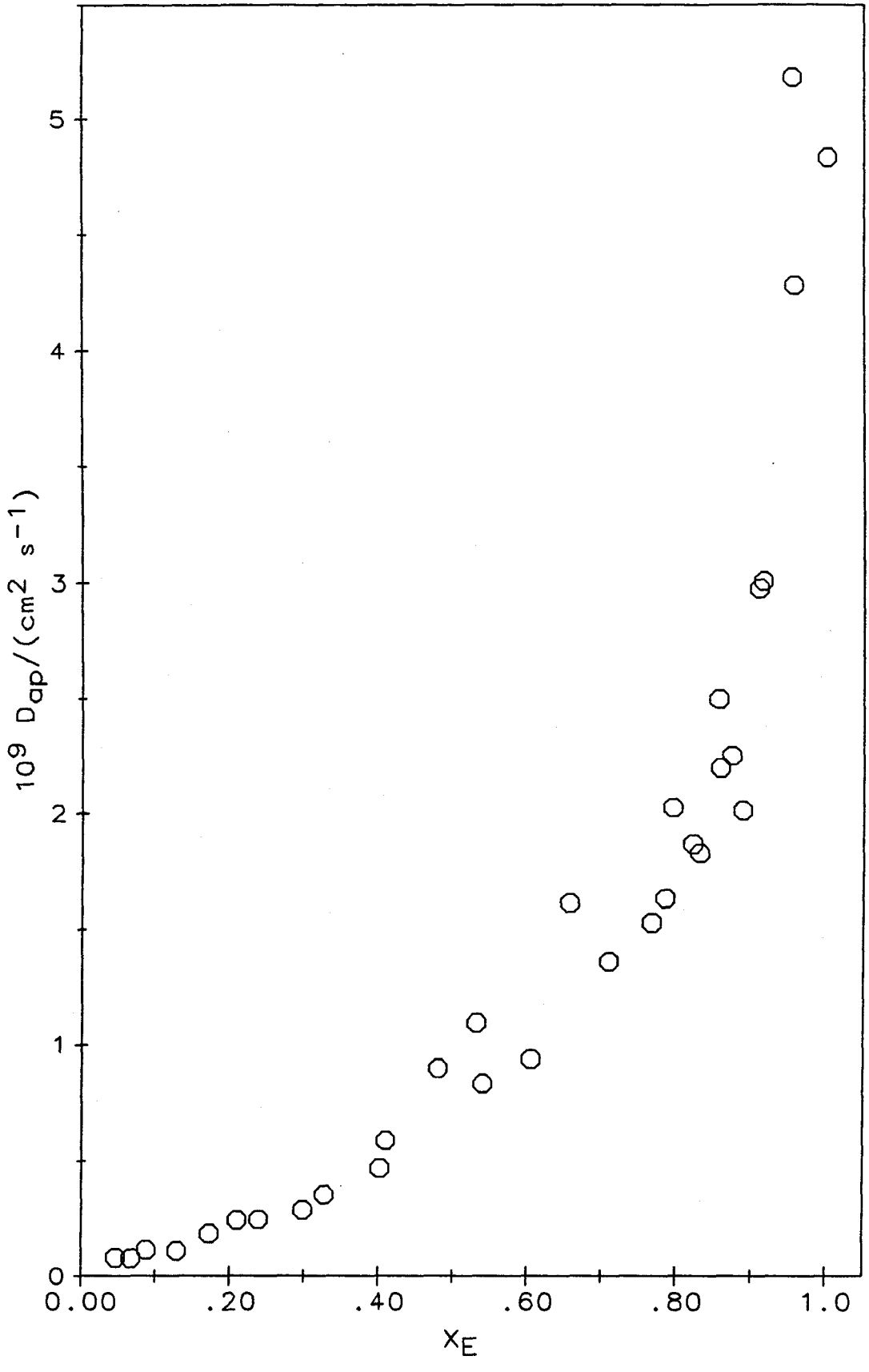
5
4
3
2
1
0
0.00
.20
.40
.60
.80
1.0
10^9 D_{ap}/(cm^2 s^{-1})
X_E

that it increases in a strikingly steep manner as the molar fraction approaches unity.[29] Very similar behavior has been reported very recently by Sharp et al.[14] for the same system under somewhat different conditions, where the electroinactive counterions were sodium ions instead of hydrogen ions. The features, evident in Figure 5.1, are not in accord with the simple model based on Equation 5.2[20] that has often been utilized in previous studies to account for the observed variations in apparent diffusion coefficients.[3b,4b,20] These studies, however, have not included as wide a range of loadings as the present measurements, nor has the electroactivity of all the incorporated complexes been independently verified. The ion-pairing model presented in Chapter 6 grew out of our attempts to understand the unusual behavior exhibited by the data in Figure 5.1.

Chapter 6

The Ion-Pairing Model

Proposed Ion-Pairing Reactions

Ions in polyelectrolyte films such as Nafion are likely to associate to form ion-pairs because of the high ionic concentrations, the reduced availability of water compared to ionic aqueous solutions, and the low dielectric constant of the organic polymer matrix.[30] The two-phase structure envisioned for Nafion (organic and aqueous ionic clusters)[31] leads one to expect cations such as $Os(bpy)_3^{2+}$ to be located in the interfacial region between the two phases where the local environment is particularly likely to favor ion-pairing.

One of the most striking features of dipositive transition metal complexes of 2,2'-bipyridine incorporated in Nafion coatings is the persistence of the complexes within the coatings for long periods after the loaded coatings are transferred to pure, supporting electrolyte solutions. This retention is most likely a result of an ionic aggregation of the cationic metal complex with the pendant sulfonate groups of the Nafion polymer, which we envision as a tight or contact ion-pair. In addition to the coulombic interactions leading to the formation of the ion-pair, other factors might also be operative. Because of the hydrophobic nature of the 2,2'-bipyridine ligand, the $Os(bpy)_3^{3+/2+}$ complex might be better solvated by the $-CF_2CF(CF_3)-O-CF_2CF_2SO_3^-$ pendant chains of the Nafion than by water. Solvation effects of this sort might encourage formation of contact ion-pairs. In the remainder of Part II, the terms "ion-pair" and "ion-pairing" refer to interactions of this type.

The strong retention of the $Os(bpy)_3^{3+/2+}$ complex by the Nafion coating suggests a very strong interaction between the complex and the polymer. For this reason we expect the predominant forms of

the $Os(bpy)_3^{2+}$ and $Os(bpy)_3^{3+}$ complexes inside the Nafion to be the uncharged ion-pairs $[Os(bpy)_3^{2+}\bullet(F^-)_2]$ and $[Os(bpy)_3^{3+}\bullet(F^-)_3]$, respectively, where F^- represents a Nafion sulfonate group.

The various possible ion-pairing equilibria involving the reduced and oxidized forms of the osmium complex are illustrated in Equations 6.1 through 6.5.

$$Os(bpy)_3^{2+} + F^- \rightleftharpoons [Os(bpy)_3^{2+}\bullet F^-]^+ \qquad (6.1)$$

$$[Os(bpy)_3^{2+}\bullet F^-]^+ + F^- \rightleftharpoons [Os(bpy)_3^{2+}\bullet(F^-)_2] \qquad (6.2)$$

$$Os(bpy)_3^{3+} + F^- \rightleftharpoons [Os(bpy)_3^{3+}\bullet F^-]^{2+} \qquad (6.3)$$

$$[Os(bpy)_3^{3+}\bullet F^-]^{2+} + F^- \rightleftharpoons [Os(bpy)_3^{3+}\bullet(F^-)_2]^+ \qquad (6.4)$$

$$[Os(bpy)_3^{3+}\bullet(F^-)_2]^+ + F^- \overset{K}{\rightleftarrows} [Os(bpy)_3^{3+}\bullet(F^-)_3] \qquad (6.5)$$

The coulombic attraction between the ion-paired complex and the Nafion sulfonate groups is expected to diminish as the charge on the ion-paired complex decreases. Additionally, steric crowding may discourage the formation of ion-pairs involving more than one or two sulfonate groups. For these reasons, the association constants for the reactions in Equations 6.1 through 6.5 are expected to decrease as the number of ion-paired sulfonate groups increases. To a first approximation, we consider that only three species, $[Os(bpy)_3^{2+}\bullet(F^-)_2]$, $[Os(bpy)_3^{3+}\bullet(F^-)_2]^+$, and $[Os(bpy)_3^{3+}\bullet(F^-)_3]$, are

present in sufficiently large concentrations to contribute significantly to the charge-transport process. As an alternative to the rather cumbersome formulas for these ion-pairs, we utilize the symbols A^+, B, and C in place of $[Os(bpy)_3^{3+}\bullet(F^-)_2]^+$, $[Os(bpy)_3^{2+}\bullet(F^-)_2]$, and $[Os(bpy)_3^{3+}\bullet(F^-)_3]$, respectively. The symbol G^+ represents the mobile, electroinactive counterions, i.e., H^+ or Na^+.

The ion-pairing model described above represents a simple, approximate method of dealing with variations in the activity coefficients for the tris(2,2'-bipyridine)osmium(3+/2+) complexes. The corresponding approach for dealing with variations in the activity coefficients for electroinactive counterions such as protons and sodium ions in Nafion is more troublesome. Cations such as sodium or hydrogen ions are likely to be located in the aqueous portion of the two-phase Nafion structure evoked earlier. Although sodium ions have been considered to engage in ion-pairing with the pendant sulfonate groups in Nafion,[30] the notion of significant quantities of $H^+\bullet F^-$ contact ion-pairs is not compatible with the strong acidity of Nafion membranes in their protonated form.[32] The fact that cations such as protons and sodium ions, unlike $Os(bpy)_3^{3+/2+}$, are not strongly retained in Nafion coatings suggests that interactions between H^+ and Na^+ and F^- are significantly different from those between $Os(bpy)_3^{3+/2+}$ and F^-. While a contact ion-pair between G^+ and F^- of the sort described above seems unlikely, a solvent-separated ion-pair might be plausible even in the case of protons. To proceed, we adopt the following strategy: We first develop a model based upon the ion-pairing reactions involving the tris(2,2'-bipyridine)osmium(3+/2+) complexes, described above,

that neglects possible variations in the activity coefficients for the electroinactive counterions. As will be shown later, this model is able to account for the salient feature of the experimental data in Figure 5.1, specifically, the steep rise in the apparent diffusion coefficient with the molar fraction of the redox centers present. The implications of interactions between the electroinactive counterions (H^+ or Na^+) and the Nafion sulfonate groups are then discussed qualitatively in terms of the variation of the activity coefficient of the ionic species with changes in the ionic strength of the system.

Proposed Pathways for Electron Hopping

Two pathways exist by which electron hopping can occur. The first pathway, illustrated in Equation 6.6,

$$\begin{array}{l} [Os(bpy)_3^{3+\bullet}(F^-)_2]^+ \; + \; [Os(bpy)_3^{2+\bullet}(F^-)_2] \\ \qquad\qquad k_1 \uparrow\downarrow k_1 \qquad\qquad , \\ [Os(bpy)_3^{2+\bullet}(F^-)_2] \; + \; [Os(bpy)_3^{3+\bullet}(F^-)_2]^+ \end{array} \tag{6.6}$$

involves the A^+-B redox pair and is a simple electron-transfer reaction. The second pathway, illustrated in Equation 6.7,

$$\begin{array}{l} [Os(bpy)_3^{3+\bullet}(F^-)_3] \; + \; [Os(bpy)_3^{2+\bullet}(F^-)_2] \\ \qquad\qquad k_2 \uparrow\downarrow k_2 \qquad\qquad , \\ [Os(bpy)_3^{2+\bullet}(F^-)_2] \; + \; [Os(bpy)_3^{3+\bullet}(F^-)_3] \end{array} \tag{6.7}$$

involves the C-B redox pair and consists of an electron-transfer reaction with concomitant transfer of a sulfonate group. We believe

the C-B pathway to be less facile than the A^+-B pathway for the following reasons: The main reaction coordinate for the C-B electron hopping pathway is the distance between the transferring sulfonate group and the metal centers. The potential energy for both the reactants and products consists of the sum of the energies for the B and the C moieties. The potential energy of the species C consists of a repulsive van der Waals contribution that increases rapidly as the metal-sulfonate distance decreases in the ($A^+ \bullet F^-$) ion-pair that constitutes species C and an attractive coulombic contribution that varies as the inverse of the metal-sulfonate distance. Upon increasing this distance, the van der Waals repulsive interaction between F^- and B comes into play and rises rapidly as the transferring sulfonate groups comes close to B. The ensuing activation barrier for F^- is certainly quite high, because the dissociation of the ($A^+ \bullet F^-$) ion-pair must take place inside a solvent cage, i.e., in a region of space where the dielectric constant is small. The barrier may be further increased by the F^--B van der Waals repulsion. Thus, the activation barrier is likely to be much larger than the energy required to dissociate the ionic aggregate represented by C into two solvated ions, A^+ and F^-. In contrast, the reaction barrier for the A^+-B electron-hopping pathway involves only the van der Waals repulsions associated with bringing the species A^+ and B sufficiently close for electron transfer to occur in addition to the reorganization energy associated with the electron-transfer process itself, contributions common to both the A^+-B and the C-B pathways.

On the basis of these arguments, the electron-hopping rate constant for the A^+-B pathway, k_1, is expected to be much larger than the corresponding rate constant, k_2, for the C-B pathway. One is therefore tempted to disregard the latter pathway in favor of the former. If the ion-pairing is exceptionally strong, however, the concentration of species C can be many orders of magnitude greater than that of species A^+, counteracting the kinetic considerations of the preceding paragraph. In light of this possibility, both electron-hopping pathways are included in the theoretical analysis.

Theory

The following notation is employed in addition to that previously described: C_i, concentration of species i (charges dropped); x, distance from the electrode surface; t, time; and Φ, electric potential. The transient behavior of the system under potentiostatic conditions is described by the following pair of differential equations:[22c-e,33]

$$\frac{\partial(C_A + C_C)}{\partial t} = \frac{D_1}{C_E}\frac{\partial}{\partial x}\left[C_B\frac{\partial C_A}{\partial x} - C_A\frac{\partial C_B}{\partial x} + \frac{F}{RT}C_A C_B\frac{\partial \Phi}{\partial x}\right]$$

$$+ \frac{D_2}{C_E}\frac{\partial}{\partial x}\left[C_B\frac{\partial C_C}{\partial x} - C_C\frac{\partial C_B}{\partial x} + \frac{F}{RT}C_B C_C\frac{\partial \Phi}{\partial x}\right] \qquad (6.8)$$

and

$$\frac{\partial C_G}{\partial t} = D_I\frac{\partial}{\partial x}\left[\frac{\partial C_G}{\partial x} + \frac{F}{RT}C_G\frac{\partial \Phi}{\partial x}\right]. \qquad (6.9)$$

The constants F, R, and T represent the Faraday constant, the gas constant, and the absolute temperature, respectively. D_I is the diffusion coefficient of the mobile electroinactive counterion. The electron-hopping diffusion coefficients, D_1 and D_2, are defined by the expression in Equation 5.1, using the rate constants k_1 and k_2, respectively.[34] It should be noted that the rate constants k_1 and k_2 are those operative in the absence of an electric field.

One should also note that Equation 6.8 neglects contributions to charge transport arising from physical displacement of the electroactive ions. The strong retention of the osmium complex by the Nafion coatings implies that the mobilities of the redox molecules are very small. The extremely small value observed for the apparent diffusion coefficient at very low fractional loadings, as compared to the values for the apparent diffusion coefficient at higher fractional loadings (see Figure 5.1), also suggests that D_{pd} is negligibly small for all but the lowest fractional loadings. The sulfonate groups are also regarded as being immobile; hence there is no migration of F^- or any ion-paired species under the influence of an electric field.

The permselectivity of Nafion and the conservation of charge principle require

$$C_F^0 = 3C_A + 2C_B + 3C_C + C_G \, . \qquad (6.10)$$

Conservation of mass for the electroactive complex requires

$$C_E = C_A + C_B + C_C \, . \qquad (6.11)$$

Given the composition of the ion-pairs and the stoichiometry of the ion-pairing reaction, the concentration of free sulfonate groups, C_F, i.e., those not ion-paired with the osmium complex, is given by

$$C_F = C_A + C_G \ . \tag{6.12}$$

The ion-pairing reaction of Equation 6.5 is assumed to remain at equilibrium throughout the time scale of the experiment; i.e., it is assumed to be fast compared to the rate of electron hopping. The relevant equilibrium expression is

$$K = \frac{C_C}{C_A C_F} \ , \tag{6.13}$$

where K is the ion-pairing association constant.

The boundary conditions for the potential step experiment described in the experimental section of Chapter 5 may be expressed in terms of C_B; all other quantities may be calculated by means of Equations 6.8 through 6.13.

$$t = 0, \ x \geq 0 \ \text{and} \ t \geq 0, \ x \rightarrow \infty: \quad C_B = C_E \tag{6.14}$$

$$t \geq 0, \ x = 0 \ \text{and} \ t \rightarrow \infty, \ x \geq 0: \quad C_B = 0 \tag{6.15}$$

The above boundary conditions correspond to the case where the Nafion coating is loaded with $Os(bpy)_3^{2+}$, which is then oxidized. The opposite case where the coating is loaded with $Os(bpy)_3^{3+}$, which is

then reduced, is accommodated by reversing the values for C_B in Equations 6.14 and 6.15.

In addition to the above boundary conditions, the flux of G^+ at the electrode surface must always be zero, because G^+ is neither consumed nor created at the electrode. This condition is imposed mathematically by

$$0 = \left[\frac{\partial C_G}{\partial x} + C_G \frac{\partial \Phi}{\partial x}\right]_{x=0} . \tag{6.16}$$

Introduction of Dimensionless Quantities

The mathematical notation is simplified by introduction of the following dimensionless quantities:

$$a = K C_F^0 \frac{C_A}{C_E} , \qquad b = \frac{C_B}{C_E} , \qquad c = \frac{C_C}{C_E} ,$$

$$f = \frac{C_F}{C_E} , \qquad f^0 = \frac{C_F^0}{C_E} = \frac{3}{X_E} , \qquad g = \frac{C_G}{C_E} , \tag{6.17}$$

$$\phi = \frac{F}{RT}\Phi , \qquad \kappa = K C_F^0 , \qquad \gamma = K C_F^0 \frac{k_2}{k_1} .$$

Note that the quantity f^0 is another measure of the fractional loading of the coating: $f^0 \rightarrow \infty$ corresponds to $X_E=0$, and $f^0=3$ corresponds to $X_E=1$.

A modified form of the Boltzmann transformation,

$$u = \left(K C_F^0\right)^{1/2} \frac{x}{\sqrt{D_1 t}} , \tag{6.18}$$

is effective in combining the spatial and temporal dependences of the concentrations into a single variable, thereby reducing the partial differential Equations 6.8 and 6.9 to the ordinary differential Equations 6.19 and 6.20:

$$0 = \frac{u}{2\kappa} \frac{d(a+\kappa c)}{du} + \frac{d}{du}\left[b \frac{d(a+\gamma c)}{du} - (a+\gamma c) \frac{db}{du} + b(a+\gamma c) \frac{d\phi}{du} \right] \tag{6.19}$$

and

$$0 = \frac{u}{2} \frac{dg}{du} + \sigma \frac{d}{du}\left[\frac{dg}{du} + g \frac{d\phi}{du} \right] , \tag{6.20}$$

where the parameter σ is defined by

$$\sigma = K C_F^0 \frac{D_I}{D_1} . \tag{6.21}$$

Introduction of the dimensionless quantities into Equations 6.10 through 6.13 yields

$$f^0 = \frac{3a}{\kappa} + 2b + 3c + g , \tag{6.22}$$

$$1 = \frac{a}{\kappa} + b + c , \tag{6.23}$$

$$f = \frac{a}{\kappa} + g , \tag{6.24}$$

and

$$af = cf^0 . \tag{6.25}$$

The dimensionless form of the boundary condition of Equation 6.16 is

$$0 = \left[\frac{dg}{du} + g\frac{d\phi}{du}\right]_{u=0} . \tag{6.26}$$

Determination of the Apparent Diffusion Coefficient

The current, i, that flows in response to the potential step is given by

$$i = FS\left[\frac{D_1}{C_E}\left(C_B\frac{\partial C_A}{\partial x} - C_A\frac{\partial C_B}{\partial x} + \frac{F}{RT}C_A C_B\frac{\partial \Phi}{\partial x}\right)\right.$$

$$\left. + \frac{D_2}{C_E}\left(C_B\frac{\partial C_C}{\partial x} - C_C\frac{\partial C_B}{\partial x} + \frac{F}{RT}C_B C_C\frac{\partial \Phi}{\partial x}\right)\right]_{x=0} , \tag{6.27}$$

where S represents the electrode surface area. Consistent with electrochemical convention, anodic currents are defined to be negative. Substitution of the dimensionless quantities of Equations 6.17 and 6.18 into Equation 6.27 yields

$$i = FSC_E\left(\frac{D_1}{t}\right)^{1/2}\left(KC_F^0\right)^{1/2}\psi , \tag{6.28}$$

where

$$\psi = \left[b \frac{d(a+\gamma c)}{du} - (a+\gamma c)\frac{db}{du} + b(a+\gamma c)\frac{d\phi}{du} \right]_{u=0} . \qquad (6.29)$$

The form of Equation 6.28 and the time-independent nature of the quantity ψ indicate that the chronoamperometric response will obey the Cottrell equation,

$$i = F S C_E \left(\frac{D_{ap}}{\pi t} \right)^{1/2} . \qquad (6.30)$$

This prediction is consistent with the observations reported in the experimental section of Chapter 5. Combining Equations 5.1, 5.3, 6.28, and 6.30, we obtain

$$D_{ap} = \frac{k_1 \delta^2 \pi}{18 K} \psi^2 X_E . \qquad (6.31)$$

Equation 6.31 is the working equation by which the values of the apparent diffusion coefficient are simulated. The corresponding analysis for the chronocoulometric response also leads to the expression in Equation 6.31 for the apparent diffusion coefficient.

The Expression for the Electric Potential

A diffusion coefficient of 3.5×10^{-6} cm^2 s^{-1} for protons in Nafion films has been measured by radiotracer techniques.[35] This value is at least two orders of magnitude larger than the values of D_1

encountered in this study. Moreover, the ion-pairing model developed above anticipates values for the ion-pairing association constant, K, considerably greater than unity. Given these considerations, it is reasonable to examine only the behavior expected in the limit $\sigma \rightarrow \infty$. This restriction is, in fact, stronger than necessary; Andrieux and Saveant[22e] have found that the chronoamperometric response for a simple electron-hopping system in a permselective medium is essentially independent of the value of σ for $\sigma > 1$.

As indicated in the previous chapter, Sharp and co-workers[14] have investigated the $Os(bpy)_3^{3+/2+}$-Nafion system using sodium ions as the mobile electroinactive counterions. The diffusion coefficient of sodium ions in Nafion has also been measured by radiotracer techniques and found to be 9.83×10^{-7} cm^2 s^{-1};[31] thus the limiting behavior for $\sigma \rightarrow \infty$ is also appropriate for the system investigated by Sharp et al..[14]

The derivative of the left hand side of Equation 6.32,

$$\frac{a}{\kappa} + c + g = f^0 - 2 \qquad (6.32)$$

(obtained from Equations 6.22 and 6.23), must be equal to zero; therefore, the sum of Equations 6.19 and 6.20 is

$$0 = \frac{d}{du}\left[b \frac{d(a+\gamma c)}{du} - (a+\gamma c)\frac{db}{du} + \sigma \frac{dg}{du} + \left(b(a+\gamma c) + \sigma g\right)\frac{d\phi}{du}\right]. \qquad (6.33)$$

Integration of Equation 6.33 produces

$$IC = b\frac{d(a+\gamma c)}{du} - (a+\gamma c)\frac{db}{du} + \sigma\frac{dg}{du} + \left(b(a+\gamma c)+\sigma g\right)\frac{d\phi}{du}. \tag{6.34}$$

The constant of integration, IC, must be equal to ψ, because Equation 6.34 evaluated at u=0 is equal to the sum of Equations 6.26 and 6.29. Rearrangement of Equation 6.34 produces

$$\frac{d\phi}{du} = \frac{\psi - b\frac{d(a+\gamma c)}{du} + (a+\gamma c)\frac{db}{du} - \sigma\frac{dg}{du}}{b(a+\gamma c)+\sigma g}, \tag{6.35}$$

which reduces to

$$\frac{d\phi}{du} = -\frac{1}{g}\frac{dg}{du} \tag{6.36}$$

in the limit $\sigma\rightarrow\infty$.

Integration of Equation 6.36 yields an expression for the electric potential:

$$\phi = \phi_0 + \ln\left[\frac{g_0}{g}\right], \tag{6.37}$$

or, in real quantities,

$$\Phi = \Phi_0 + \frac{RT}{F}\ln\left[\frac{C_{G,0}}{C_G}\right]. \tag{6.38}$$

The subscript 0 indicates that the quantity is evaluated at u=0. The choice of u=0 as the reference point is acceptable in all cases except

when $X_E=1$ and the coating is loaded with the reduced form of the complex, in which event $C_{G,0}=0$, and the logarithmic function is undefined. In this case, $x\rightarrow\infty$ can be used as the reference point, though this tactic does not circumvent the singularity at u=0.

Case 1: The General Problem, Arbitrary κ and γ

Substitution of Equation 6.36 into 6.19 and 6.29 leads to Equations 6.39 and 6.40, respectively.

$$0 = \frac{u}{2\kappa}\frac{d(a+\kappa c)}{du} + \frac{d}{du}\left[b\frac{d(a+\gamma c)}{du} - (a+\gamma c)\frac{db}{du} - \frac{b(a+\gamma c)}{g}\frac{dg}{du}\right] \qquad (6.39)$$

$$\psi = \left[b\frac{d(a+\gamma c)}{du} - (a+\gamma c)\frac{db}{du} - \frac{b(a+\gamma c)}{g}\frac{dg}{du}\right]_{u=0} \qquad (6.40)$$

The boundary conditions for this problem are:

<u>Coating loaded with osmium(2+) complex:</u>

u=0, b=1 ; $u\rightarrow\infty$, b=0 ; (6.41)

<u>Coating loaded with osmium(3+) complex:</u>

u=0, b=0 ; $u\rightarrow\infty$, b=1 . (6.42)

Manipulation of Equations 6.22 through 6.25 and 6.32 enables one to demonstrate that

$$b = g - \left(f^0 - 3\right), \qquad (6.43)$$

$$\frac{a}{\kappa} + c = \left(f^0 - 2\right) - g \,, \tag{6.44}$$

and

$$c = \left(\frac{a}{\kappa} + g\right)\frac{a}{f^0} \,, \tag{6.45}$$

from which one may solve for the quantity a in terms of g, f^0, and κ:

$$a = -\frac{1}{2}\left(f^0 + \kappa g\right) + \frac{1}{2}\left[\left(f^0 - \kappa g\right)^2 + 4\kappa f^0\left(f^0 - 2\right)\right]^{1/2} . \tag{6.46}$$

The master differential Equation, 6.39, can be reformulated as

$$0 = -\frac{u}{2}\frac{dg}{du} + \frac{d}{du}\left[f(g)\frac{dg}{du}\right] , \tag{6.47}$$

where

$$f(g) = \left(1 - \frac{\gamma}{\kappa}\right)\left[\left(g - \left(f^0 - 3\right)\right)\frac{da}{dg} + \left(\frac{f^0 - 3}{g} - 2\right)a\right]$$

$$+ \gamma\left(f^0 - 2\right)\left(\frac{f^0 - 3}{g} - 2\right) + \gamma g \,, \tag{6.48}$$

by utilization of Equations 6.43 through 6.45. The derivative $^{da}/_{dg}$ is obtained by explicit differentiation of Equation 6.46. The boundary conditions and appropriate simplified expression for ψ, obtained from Equation 6.40, are:

Coating loaded with osmium(2+) complex:

$u=0$, $g=f^0-3$; $u\rightarrow\infty$, $g=f^0-2$; (6.49)

$$a_0 = -\frac{1}{2}\left(\kappa\left(f^0-3\right)+f^0\right)+\frac{1}{2}\left[\left(\kappa\left(f^0-3\right)+f^0\right)^2+4\,\kappa\,f^0\right]^{1/2} ; \tag{6.50}$$

$$\psi = -\left(\gamma+\left(1-\frac{\gamma}{\kappa}\right)a_0\right)\left[\frac{dg}{du}\right]_{u=0} . \tag{6.51}$$

Coating loaded with osmium(3+) complex:

$u=0$, $g=f^0-2$; $u\rightarrow\infty$, $g=f^0-3$; (6.52)

$$\psi = -\left(\gamma+\left(1-\frac{\gamma}{\kappa}\right)\frac{\kappa\,f^0}{\kappa\left(f^0-2\right)+f^0}\right)\left[\frac{dg}{du}\right]_{u=0} . \tag{6.53}$$

The solution to the boundary value problem posed by Equations 6.47 and 6.49 or 6.52 was approximated by means of the finite difference procedure described in Appendix III.

Limiting Behavior for $X_E\rightarrow 0$

At very low fractional loadings, there is a large excess of both mobile electroinactive counterions, G^+, and free sulfonate groups, F^-. In fact, G^+ and F^- constitute essentially all of the ions present in the Nafion coating; thus

$$g \cong f \cong f^0 \tag{6.54}$$

and

$$\frac{dg}{du} \cong 0 \; . \tag{6.55}$$

Under these conditions, the equilibrium expression, Equation 6.25, and the conservation of mass expression, Equation 6.23, reduce to

$$c \cong a \tag{6.56}$$

and

$$b \cong 1 - \frac{1+\kappa}{\kappa} a \; . \tag{6.57}$$

Given these relations, the master differential Equation, 6.39, reduces to

$$0 = \frac{u}{2}\left(\frac{1+\kappa}{\kappa}\right)\frac{da}{du} + \frac{d^2a}{du^2} \tag{6.58}$$

for sufficiently small values of X_E; the corresponding boundary conditions being

<u>Coating loaded with osmium(2+) complex:</u>

$$u=0 \; , \quad a=\frac{\kappa}{1+\kappa} \; ; \qquad u \rightarrow \infty \; , \quad a=0 \; ; \tag{6.59}$$

<u>Coating loaded with osmium(3+) complex:</u>

$$u=0 \; , \quad a=0 \; ; \qquad u \rightarrow \infty \; , \quad a=\frac{\kappa}{1+\kappa} \; . \tag{6.60}$$

The analytic solution of this boundary value problem yields

$$\psi = (1+\gamma)\left[\frac{da}{du}\right]_{u=0} = \pm\left(\frac{1+\gamma}{\pi}\right)^{1/2}\left(\frac{\kappa}{1+\kappa}\right)^{1/2} . \qquad (6.61)$$

The positive sign applies to coatings loaded with $Os(bpy)_3^{3+}$ and the negative sign to coatings loaded with $Os(bpy)_3^{2+}$, as required by electrochemical convention.

Substitution of Equation 6.61 into 6.31 produces the following expression for the apparent diffusion coefficient:

$$D_{ap} = \frac{k_1 \delta^2}{18} C_F^0 \left(\frac{1+\gamma}{1+\kappa}\right) X_E = \frac{\delta^2}{18} C_F^0 \left(\frac{k_1 + k_2 K C_F^0}{1 + K C_F^0}\right) X_E . \qquad (6.62)$$

Given the form of Equation 6.62, a plot D_{ap} vs. X_E is predicted to be linear for sufficiently low fractional loadings. Also, note that the expressions for ψ and D_{ap}, and hence the values for these quantities, are the same regardless of whether the coating is loaded with $Os(bpy)_3^{2+}$ or $Os(bpy)_3^{3+}$.

Limiting Behavior for a Simple Electron-Hopping Model

The ion-pairing reaction in Equation 6.5 becomes irrelevant under three conditions: $\kappa=0$, $\kappa=\gamma$, and $\kappa>\gamma$ with $\kappa>100$. In the first situation, $\kappa=0$ means that the concentration of species C is zero, making the value of k_2, and hence γ, irrelevant and leading to a simple electron-hopping model involving only the reactants A^+ and B. In the second case, $k_1=k_2$ removes the relevance of the ion-pairing reaction, because species A^+ and C are equally reactive. In the third case, the

concentration of species A^+ is much smaller than that of species C, and the C-B pathway for electron hopping is inherently more facile than the A^+-B pathway; the system, therefore, resembles a simple electron-hopping scheme involving only reactants C and B. The fractional loading dependence of the apparent diffusion coefficient is the same in all three cases and is identical with that of the simple electron-hopping model examined by Andrieux and Saveant.[22e]

Case 2: A^+-B Pathway Only, $\gamma = 0$

As explained above, the rate constant associated with the C-B pathway for electron hopping, k_2, is expected to be orders of magnitude smaller than the rate constant associated with the A^+-B pathway for electron hopping, k_1. For modest values of the equilibrium constant K where the ratio C_C/C_A is not too large, it may be possible to disregard the C-B pathway for electron hopping, in which case, charge transport would occur exclusively via electron hopping between species A^+ and B.

By neglecting the C-B pathway, i.e., setting $\gamma=0$, the expression for f(g) simplifies to

$$f(g) = \left(g - \left(f^0 - 3\right)\right)\frac{da}{dg} + \left(\frac{f^0 - 3}{g} - 2\right)a \; ; \qquad (6.63)$$

a is still given by Equation 6.46, and da/dg is still found by explicit differentiation of that equation. The boundary conditions are unchanged from those for Case 1, but the expressions for ψ are simplified:

Coating loaded with osmium(2+) complex:

$$\psi = -a_0\left[\frac{dg}{du}\right]_{u=0}; \tag{6.64}$$

Coating loaded with osmium(3+) complex:

$$\psi = -\frac{\kappa f^0}{\kappa\left(f^0-2\right)+f^0}\left[\frac{dg}{du}\right]_{u=0}. \tag{6.65}$$

The quantity a_0 is found by means of Equation 6.50.

Limiting Behavior for $X_E \rightarrow 0$

The treatment for the low fractional loading limit presented in the general treatment for Case 1 also applies for Case 2. With $\gamma=0$, the appropriate expressions for ψ and D_{ap} are

$$\psi = \left[\frac{da}{du}\right]_{u=0} = \pm\frac{1}{\sqrt{\pi}}\left(\frac{\kappa}{1+\kappa}\right)^{1/2} \tag{6.66}$$

and

$$D_{ap} = \frac{k_1\delta^2}{18}\left(\frac{C_F^0}{1+K\,C_F^0}\right)X_E. \tag{6.67}$$

Limiting Behavior for $X_E \rightarrow 1$

At full fractional loading, $X_E=1$ and $f^0=3$, Equations 6.24, 6.25, and 6.42 reduce to

$$b = g\,, \tag{6.68}$$

$$f = 1-c\,, \tag{6.69}$$

and

$$c = \frac{a}{3+a}\,. \tag{6.70}$$

Using these equations, the master differential Equation, 6.39, can be written in the form of Equation 6.47 with

$$f(g) = \frac{6+\kappa g}{2} - \frac{(3-\kappa g)(6-\kappa g)+24\kappa}{2\sqrt{(3-\kappa g)^2+12\kappa}}\,. \tag{6.71}$$

The boundary conditions are identical to those for Case 1 with the provision that $f^0=3$. The appropriate expressions for ψ are

Coating loaded with osmium(2+) complex:

$$a_0 = -\frac{3}{2}+\frac{1}{2}\sqrt{9+12\kappa}\;; \tag{6.72}$$

$$\psi = -2a_0\left[\frac{dg}{du}\right]_{u=0}\,. \tag{6.73}$$

Coating loaded with osmium(3+) complex:

$$\psi = -\frac{3\kappa}{3+\kappa}\left[\frac{dg}{du}\right]_{u=0}\,. \tag{6.74}$$

Calculated Curves

The fractional loading dependences of the apparent diffusion coefficient for various values of the dimensionless equilibrium constant κ with $\gamma=0$ are illustrated in Figures 6.1 and 6.2 for coatings loaded with $Os(bpy)_3^{2+}$ and $Os(bpy)_3^{3+}$, respectively. These figures reveal that the larger the value of κ, the greater the curvature in the plot and the steeper the rise at full loading. The plots of $\log_{10}[\psi^2/\kappa]$ vs. $\log_{10}[\kappa]$ in Figures 6.3 and 6.4 for coatings fully loaded ($X_E=1$) with $Os(bpy)_3^{2+}$ and $Os(bpy)_3^{3+}$, respectively, reveal that increasing the equilibrium constant decreases the value of the apparent diffusion coefficient. (Bear in mind that the quantity ψ^2/κ is proportional to the apparent diffusion coefficient, as revealed by inspection of Equations 6.17 and 6.31.)

The rapid, non-linear increase in the apparent diffusion coefficient with increasing fractional loading parallels the rapid, nonlinear increase in the concentration of species A^+ as the fractional loading increases. The curves in Figure 6.5 show the variation of the equilibrium concentration of species A^+ with the fractional loading in a Nafion coating containing only $Os(bpy)_3^{3+}$ for several values of κ. As the fractional loading increases, the concentration of sulfonate groups not ion-paired with the osmium complex, C_F, diminishes, shifting the equilibrium in Equation 6.5 to the left. When $\gamma=0$, i.e., when $k_2=0$, electron hopping must occur exclusively via the reaction in Equation 6.6, which is the A^+-B pathway. The rate of the reaction in Equation 6.6 varies as the concentration of reactant A^+ varies. The decrease in the magnitude of the apparent diffusion coefficients with increasing values of the equilibrium constant at a given fractional

Figure 6.1. Variation of the apparent diffusion coefficient, normalized by its value at $X_E=1$, with the fractional loading for a coating loaded with $Os(bpy)_3^{2+}$ with $\gamma=0$. The curves from bottom to top, i.e., those possessing the greatest to the least amount of curvature, are calculated using $\kappa = 10^5, 10^3, 100, 10, 1, 0$.

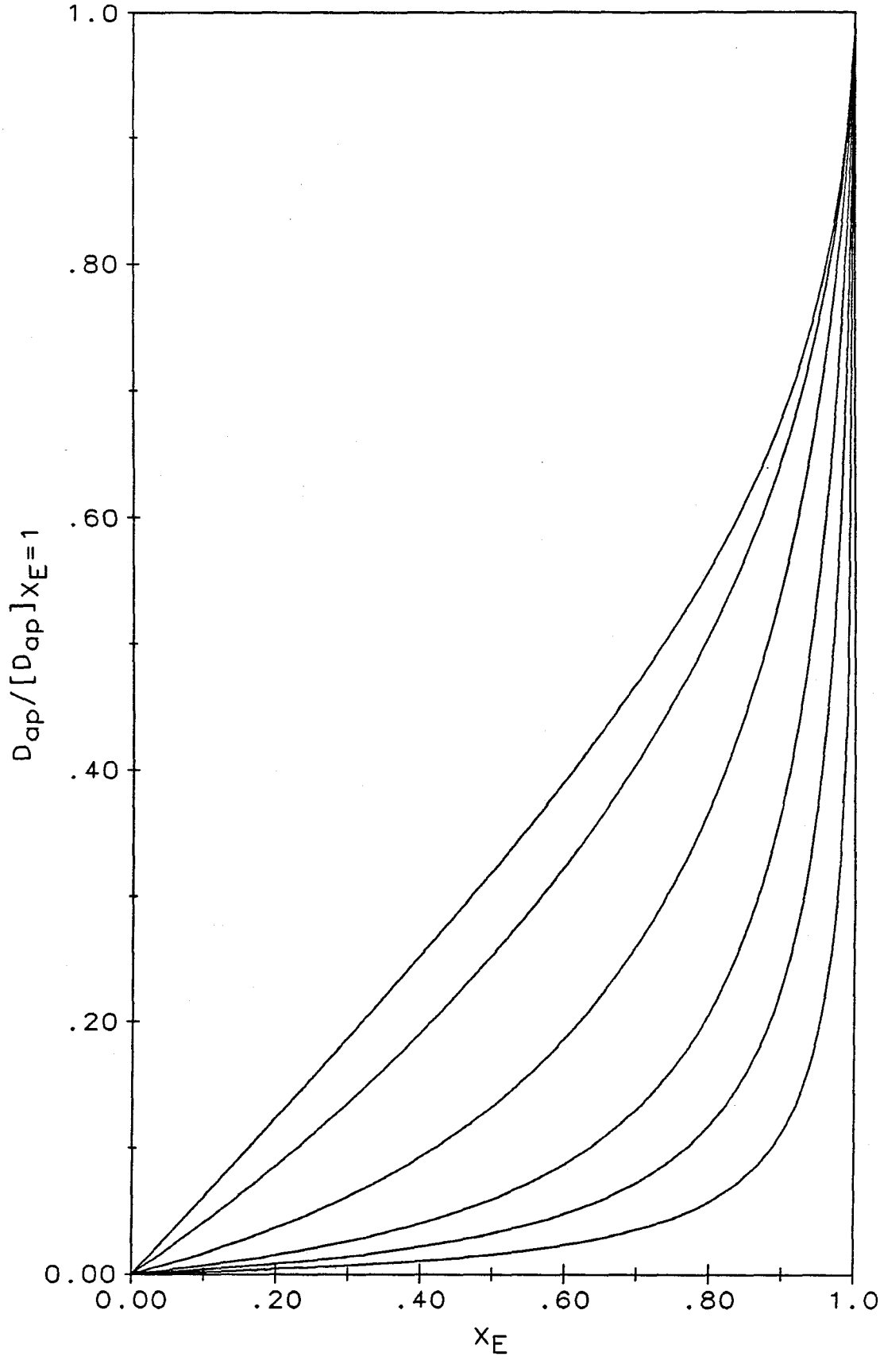
1.0
.80
.60
.40
.20
0.00
$D_{ap}/[D_{ap}]_{X_E=1}$
0.00
.20
.40
.60
.80
1.0
X_E

Figure 6.2. Variation of the apparent diffusion coefficient, normalized by its value at $X_E=1$, with the fractional loading for a coating loaded with $Os(bpy)_3^{3+}$ with $\gamma=0$. The curves from bottom to top, i.e., those possessing the greatest to the least amount of curvature, are calculated using $\kappa = 10^5, 10^3, 100, 10, 1, 0$.

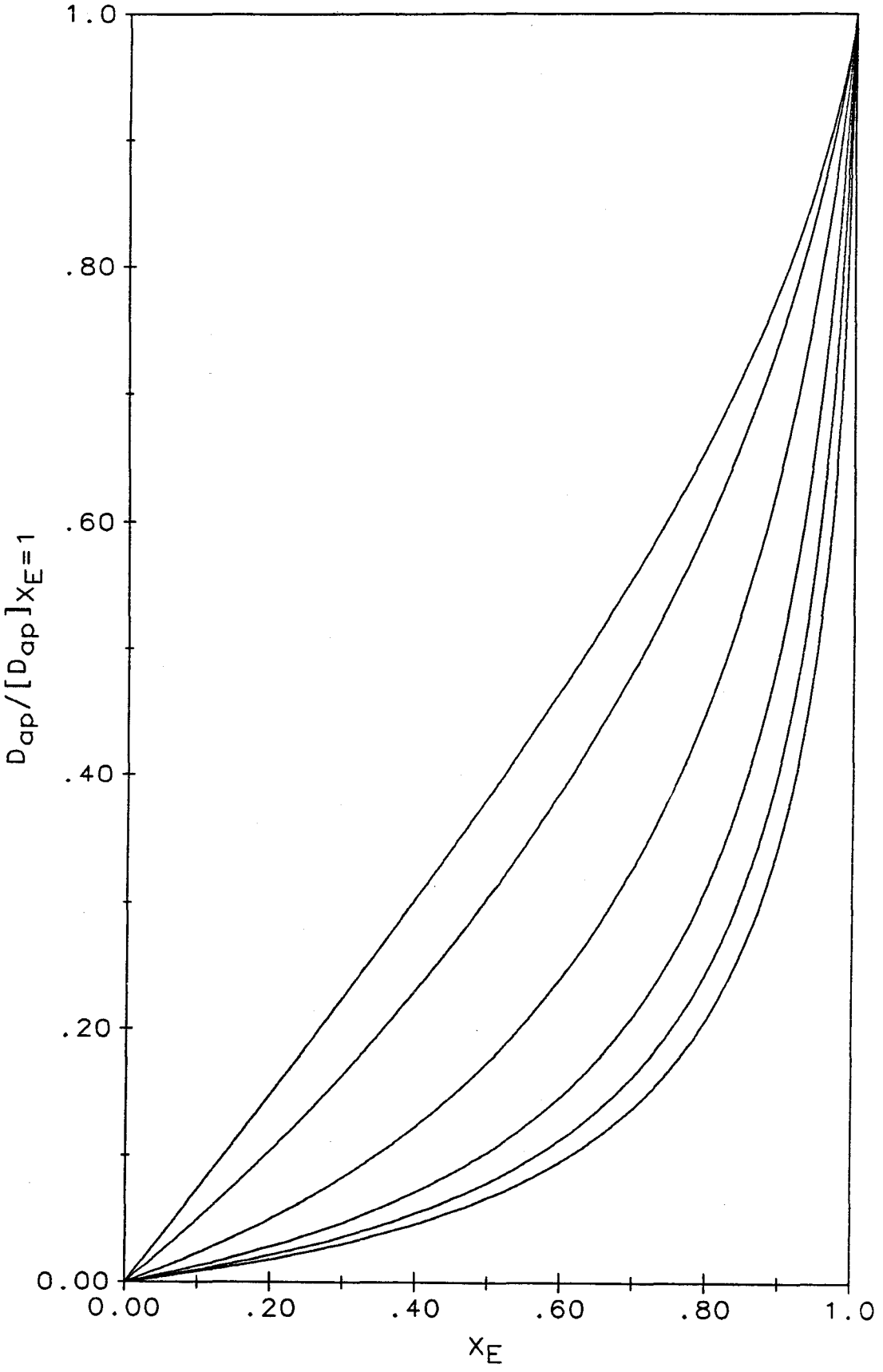
1.0
.80
.60
.40
.20
0.00
0.00
.20
.40
.60
.80
1.0
$D_{ap}/[D_{ap}]_{X_E=1}$
X_E

Figure 6.3. Variation of $\log_{10}[\psi^2/\kappa]$ with $\log_{10}[\kappa]$ for a coating loaded with $Os(bpy)_3^{2+}$ with $\gamma=0$ and $X_E=1$.

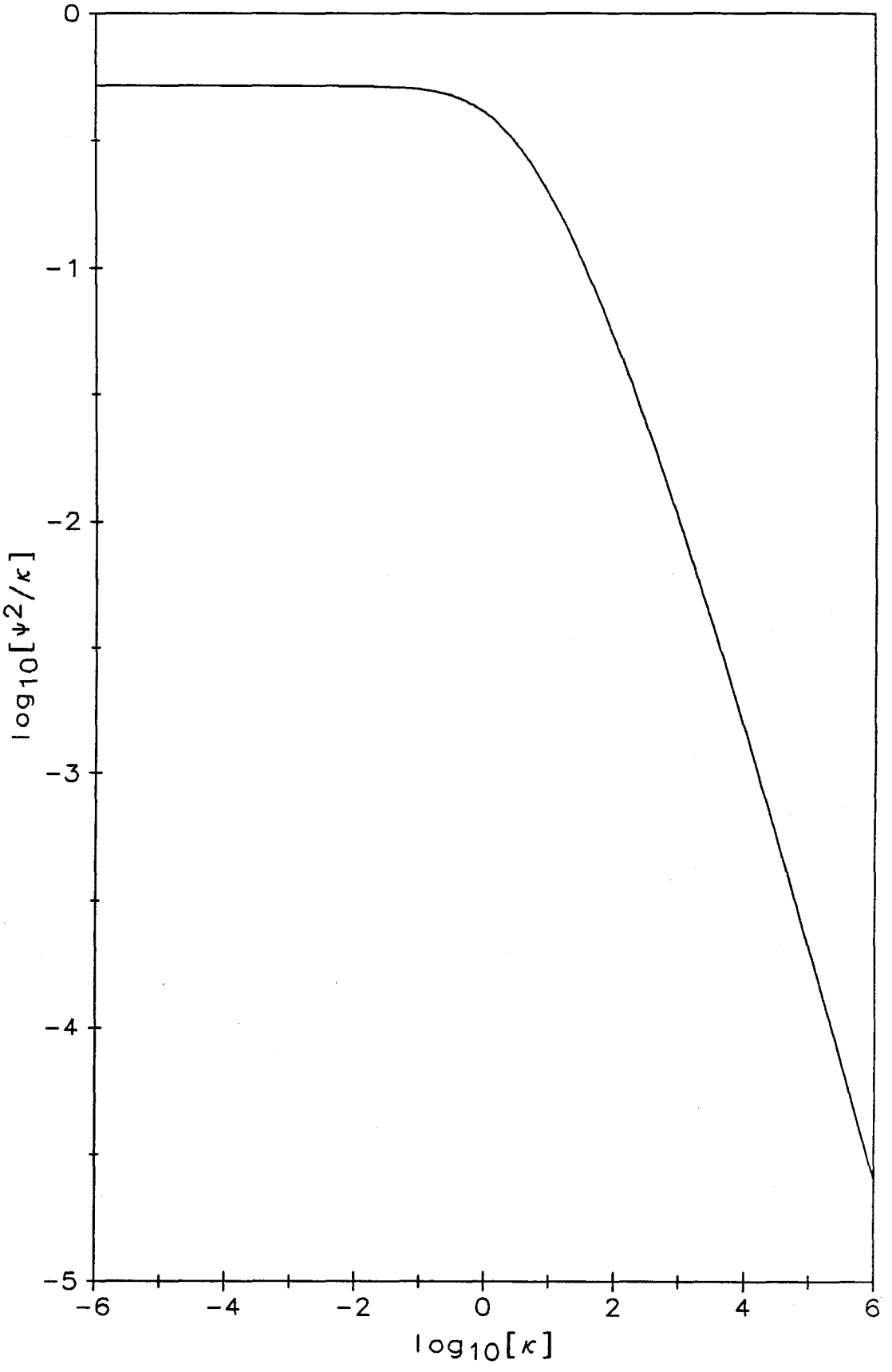
0
-1
-2
-3
-4
-5
-6
-4
-2
0
2
4
6
log10[ψ2/κ]
log10[κ]

Figure 6.4. Variation of $\log_{10}[\psi^2/\kappa]$ with $\log_{10}[\kappa]$ for a coating loaded with $Os(bpy)_3^{3+}$ with $\gamma=0$ and $X_E=1$.

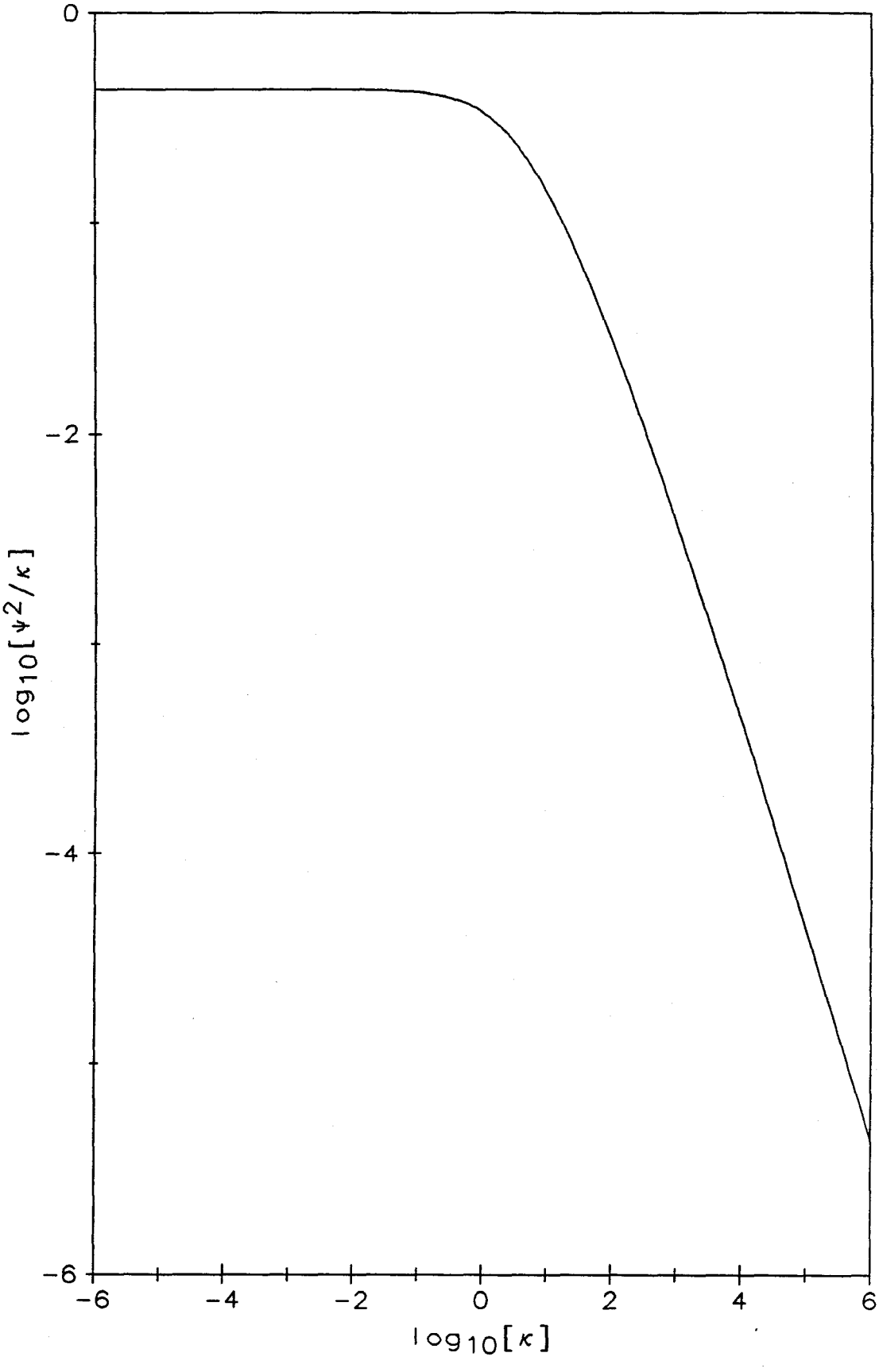
0
-2
-4
-6
-6
-4
-2
0
2
4
6
log10[ψ2/κ]
log10[κ]

Figure 6.5. Variation of the concentration of A^+, normalized by its value at $X_E=1$, with the fractional loading for a Nafion coating containing only $Os(bpy)_3^{3+}$. The curves from bottom to top, i.e., those possessing the greatest to the least amount of curvature, are calculated using $\kappa = 10^4, 10^3, 100, 10, 1$.

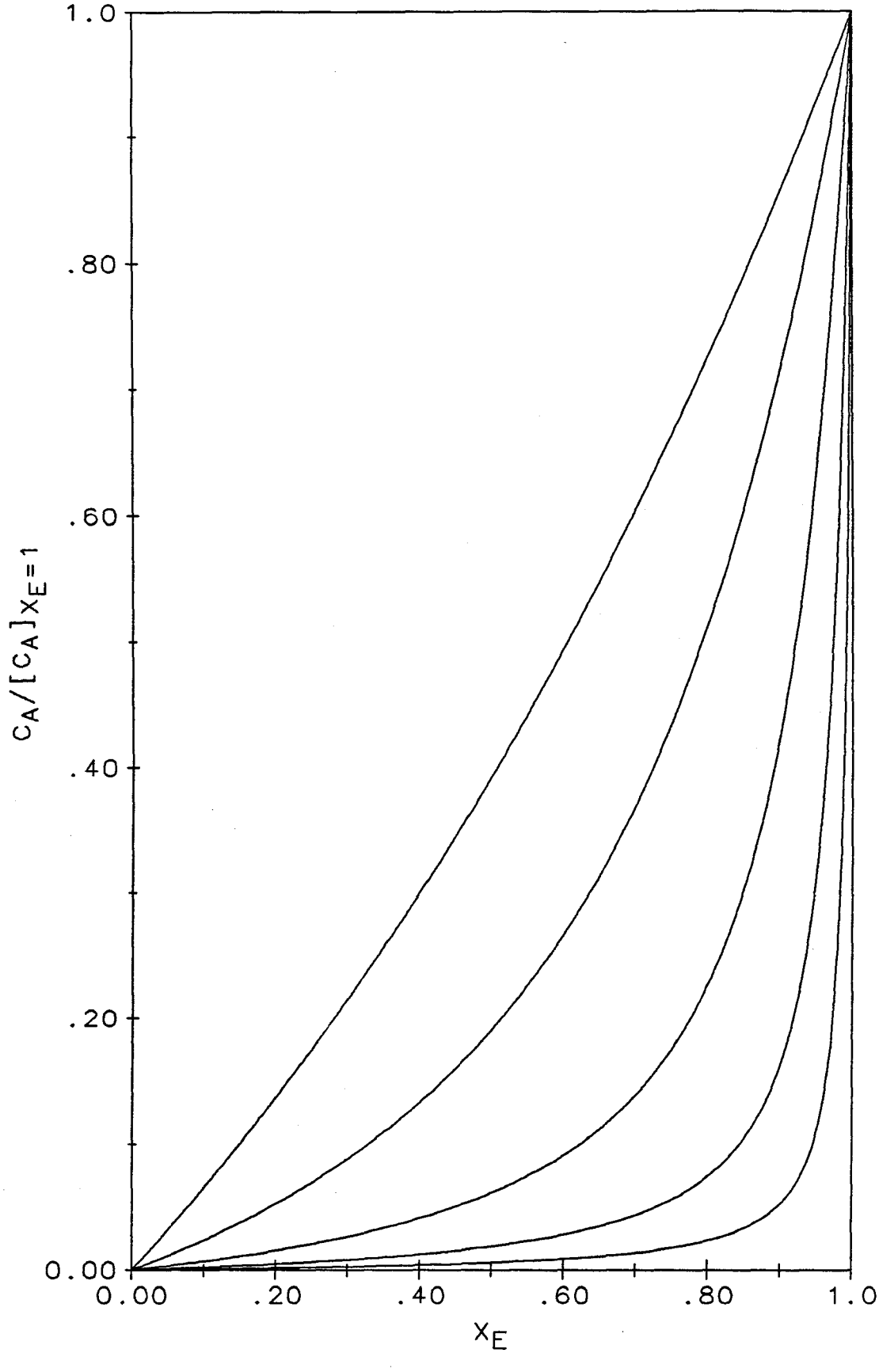
1.0
.80
.60
.40
.20
0.00
0.00
.20
.40
.60
.80
1.0
$C_A/[C_A]_{X_E=1}$
X_E

loading is due to the decrease in C_A with increasing κ for a constant value of X_E.

A noteworthy prediction of the ion-pairing model is that apparent diffusion coefficients determined from oxidations involving coatings loaded with $Os(bpy)_3^{2+}$ will differ from those determined from reductions involving coatings loaded with $Os(bpy)_3^{3+}$. This feature is illustrated in Figure 6.6 for the case where γ=0 and κ=1000. (Recall that at constant κ the quantity $\psi^2 X_E$ is proportional to D_{ap}.) When X_E=0, the values of D_{ap} determined from cathodic and anodic currents are identical, *vide supra*, but as X_E increases, the values of D_{ap} determined from cathodic and anodic currents differ by amounts that increase with X_E. This behavior arises from the influence of both the electric field and the ion-pairing equilibrium, both of which are asymmetric as regards cathodic vs. anodic experiments.

Fitting of the ion-pairing model to experimental data is facilitated by comparing the value of the apparent diffusion coefficient at a particular fractional loading with the slope of the plot of D_{ap} vs. X_E at very low fractional loadings. This quantity, defined as $S(X_E,\kappa,\gamma)$,

$$S(X_E, \kappa, \gamma) = D_{ap} \Big/ \left[\frac{dD_{ap}}{dX_E}\right]_{X_E=0}, \qquad (6.75)$$

depends solely upon the fractional loading at which D_{ap} is evaluated, the dimensionless equilibrium constant κ, and the parameter γ. If one chooses γ=0, the equilibrium constant associated with a particular value of D_{ap} is unambiguously identified. The greatest sensitivity is obtained by choosing X_E=1; plots of $S(1.0,\kappa,0)$ vs. $\log_{10}[\kappa]$ for coatings

Figure 6.6. Variation of $\psi^2 X_E$, which is proportional to D_{ap}, with X_E for γ=0 and κ=1000. The solid line applies to a coating loaded with $Os(bpy)_3^{2+}$; the dashed line applies to a coating loaded with $Os(bpy)_3^{3+}$.

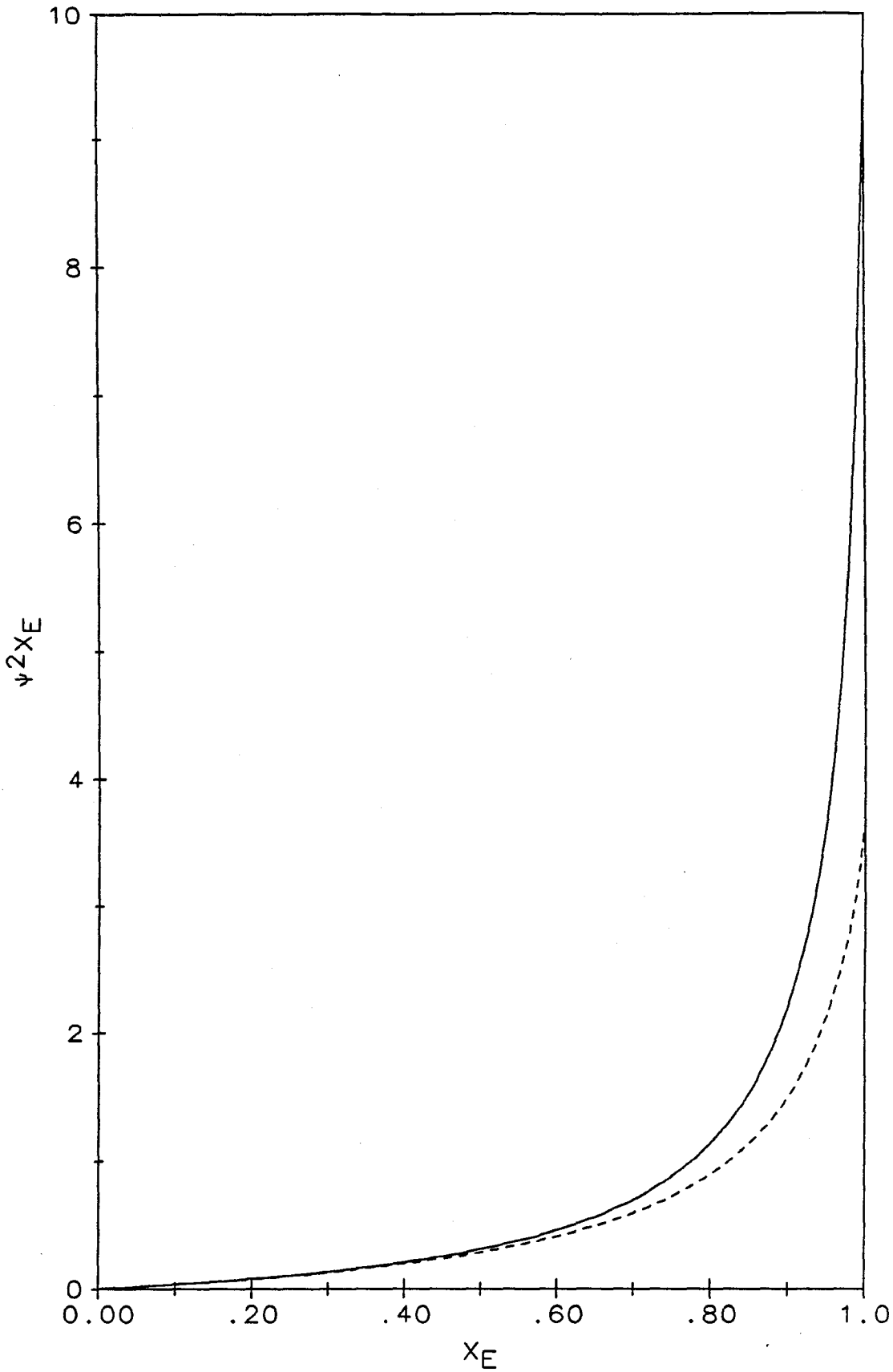
10
8
6
4
2
0
$\psi^2 x_E$
0.00
.20
.40
.60
.80
1.0
x_E

loaded with $Os(bpy)_3^{2+}$ and $Os(bpy)_3^{3+}$ are shown in Figures 6.7 and 6.8, respectively. Although measurements associated with $X_E = 1$ provide the greatest sensitivity, experimental values of D_{ap} at full loading are highly unreliable. In light of the poor quality of data taken at $X_E=1$, data analysis based upon plots of $S(0.9,\kappa,0)$ vs. $\log_{10}[\kappa]$, shown in Figures 6.9 and 6.10 for coatings loaded with $Os(bpy)_3^{2+}$ and $Os(bpy)_3^{3+}$, respectively, permits utilization of the more reliable data available at $X_E=0.90$ at the price of decreased sensitivity.

Once the value of κ has been determined from one of the Figures 6.7 through 6.10, the value k_1 may be determined from the experimental value of $\left[dD_{ap}/dX_E\right]_{X_E=0}$, and the expression in Equation 6.67.

Case 3: The Strong Ion-Pairing Limit, $\kappa > 100$

Computations based upon the general treatment for Case 1 reveal that as the value of the dimensionless equilibrium constant becomes increasingly large, the shapes of the curves D_{ap} vs. X_E become increasingly less insensitive to the value of κ, though the magnitude of the apparent diffusion coefficient continues to decrease with increasing κ. If we introduce the assumption that κ is large ($\kappa > 100$ roughly), simplified mathematical formulas describing the limiting shape of the D_{ap} vs. X_E curves can be derived. We call this limiting behavior the "strong ion-pairing limit."

In the strong ion-pairing limit, only minute quantities of the osmium(3+) complex exist in the form A^+; the predominance of species C over A^+ prevents us from neglecting the C-B pathway for

Figure 6.7. Variation of $S(1.0,\kappa,0)$ with $\log_{10}[\kappa]$ for coatings loaded with $Os(bpy)_3^{2+}$.

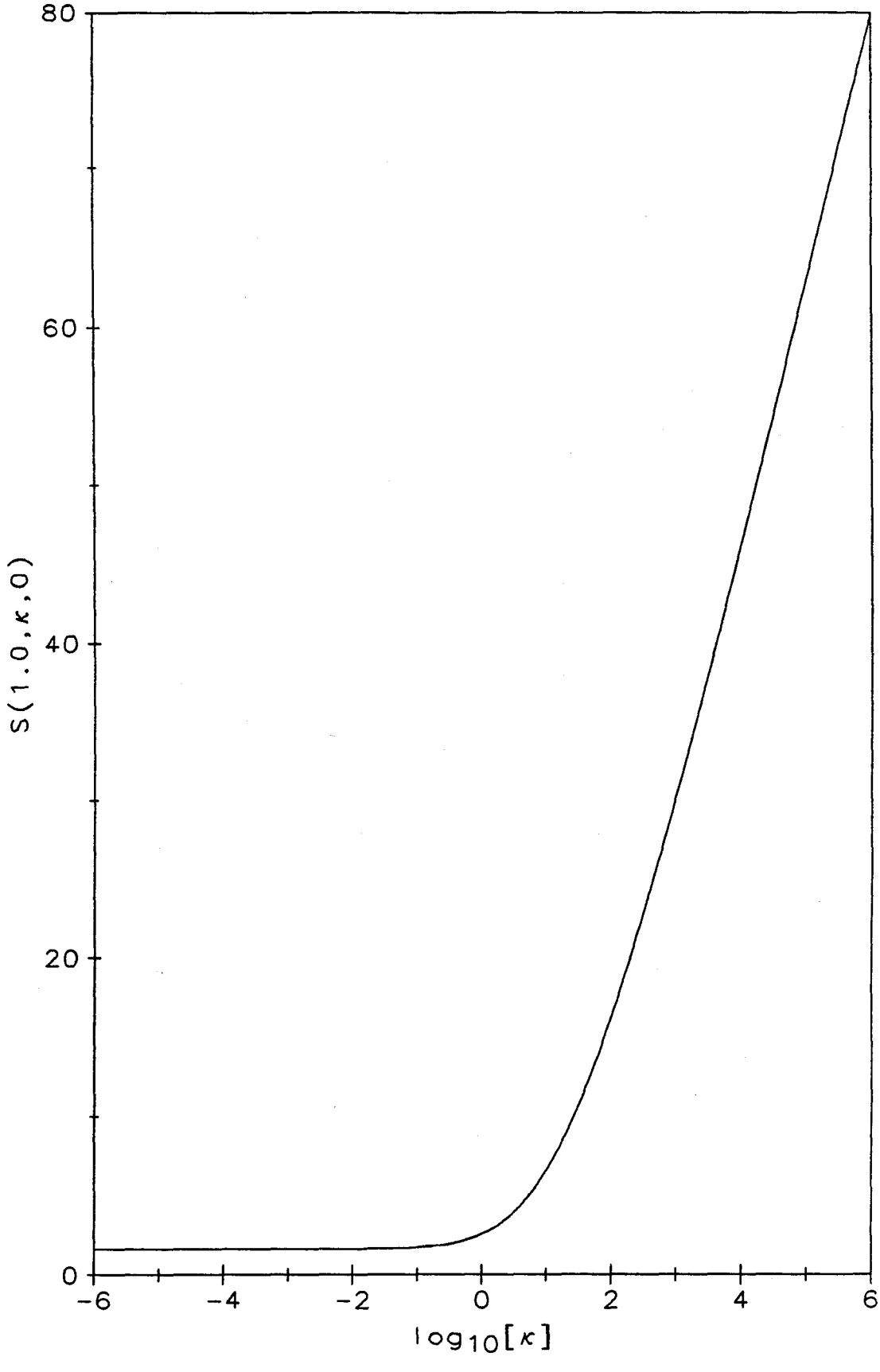
80
60
40
20
0
S(1.0,κ,0)
-6
-4
-2
0
2
4
6
log10[κ]

Figure 6.8. Variation of $S(1.0,\kappa,0)$ with $\log_{10}[\kappa]$ for coatings loaded with $Os(bpy)_3^{3+}$.

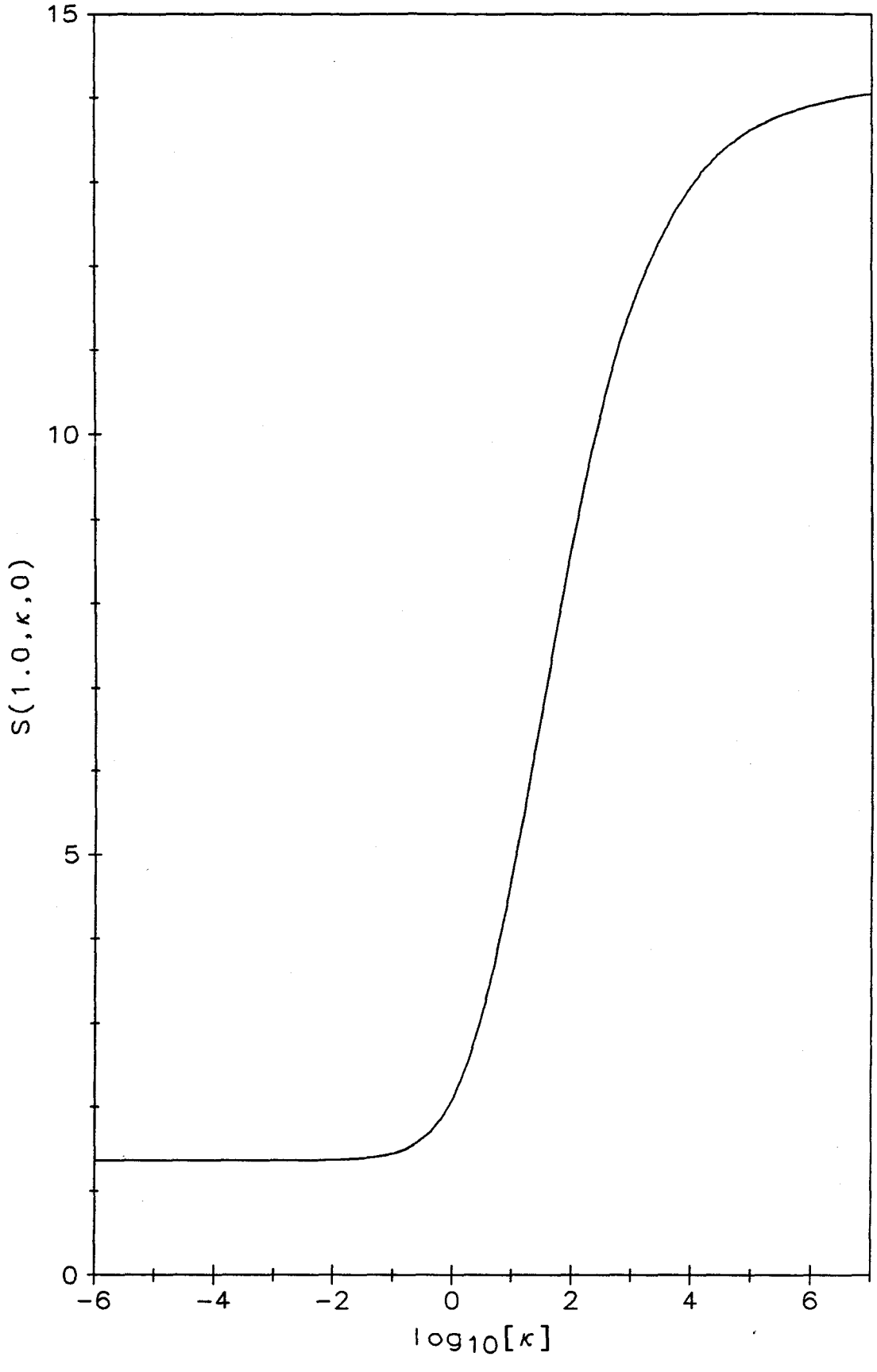
15
10
5
0
S(1.0,κ,0)
-6
-4
-2
0
2
4
6
log10[κ]

Figure 6.9. Variation of $S(0.9,\kappa,0)$ with $\log_{10}[\kappa]$ for coatings loaded with $Os(bpy)_3^{2+}$.

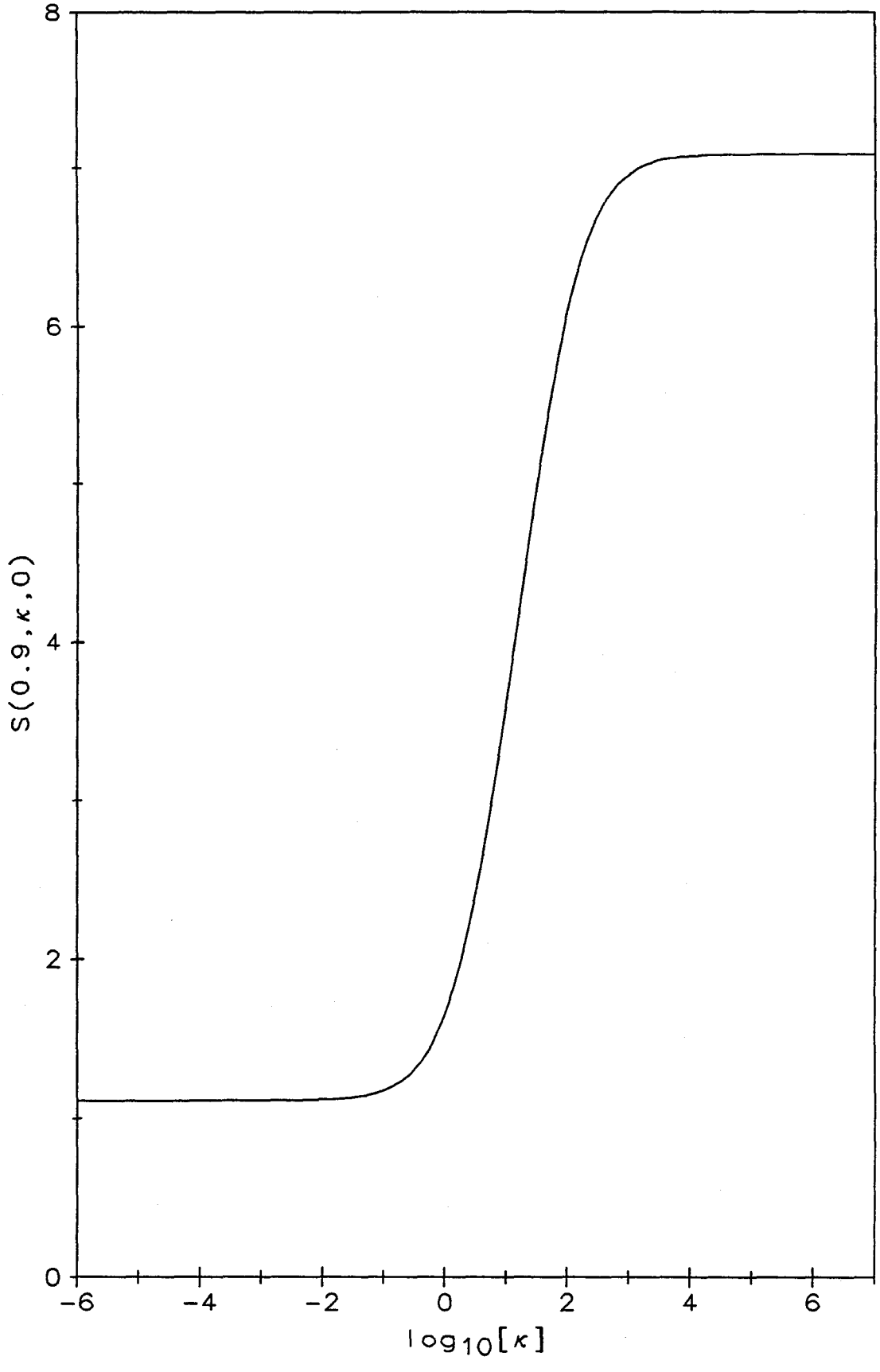
8
6
4
2
0
S(0.9,κ,0)
−6
−4
−2
0
2
4
6
log10[κ]

Figure 6.10. Variation of $S(0.9,\kappa,0)$ with $\log_{10}[\kappa]$ for coatings loaded with $Os(bpy)_3^{3+}$.

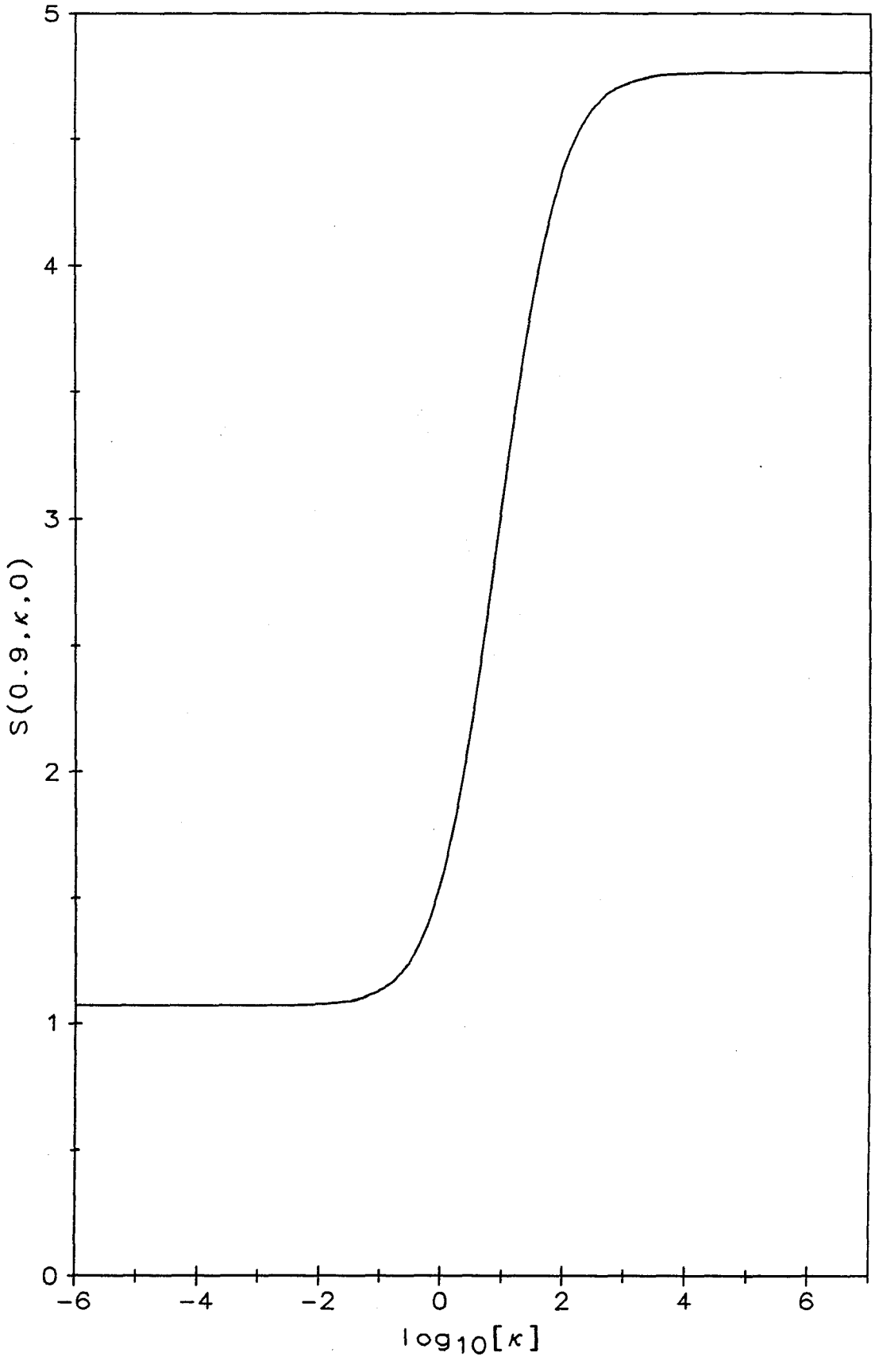
5
4
3
2
1
0
S(0.9,κ,0)
−6
−4
−2
0
2
4
6
log10[κ]

electron hopping in favor of the A^+-B pathway. We therefore derive limiting expressions for f(g) and ψ for arbitrary values of γ and κ>100.

When K is very large, we can assume that $C_A << C_C$, so that the sum $C_A + C_C$ may be accurately approximated by C_C. We introduce the further restriction that $C_A << C_G$. This second restriction can be met for all fractional loadings except $X_E=1$ by insisting that κ be above a certain limit. The following equations are invalid when $X_E=1$ but are accurate at all other fractional loadings.

The approximations described in the preceding paragraph allow Equations 6.44 and 6.45 to be rewritten as

$$c \equiv \left(f^0 - 2\right) - g \tag{6.76}$$

and

$$a \equiv \frac{\left(f^0 - 2\right) - g}{g} f^0 . \tag{6.77}$$

Combining Equations 6.76 and 6.77 yields

$$a + \gamma c = \left(\left(f^0 - 2\right) - g\right)\left(\frac{f^0}{g} + \gamma\right). \tag{6.78}$$

Substitution of Equations 6.78 into the general expression for f(g), Equation 6.48, produces the simplified expression

$$f(g) = 2f^0 + \left(g - 2\left(f^0 - 2\right)\right)\gamma + \frac{\left(f^0 - 2\right)\left(f^0 - 3\right)\gamma - \left(4f^0 - 9\right)f^0}{g}$$

$$+ \frac{2\left(f^0 - 2\right)\left(f^0 - 3\right)f^0}{g^2} \qquad (6.79)$$

for f(g), and the following simplified expressions for ψ:

Coating loaded with osmium(2+) complex:

$$\psi = -\left(\gamma + \frac{f^0}{f^0 - 3}\right)\left(\frac{dg}{du}\right)_{u=0}; \qquad (6.80)$$

Coating loaded with osmium(3+) complex:

$$\psi = -\left(\gamma + \frac{f^0}{f^0 - 2}\right)\left(\frac{dg}{du}\right)_{u=0}. \qquad (6.81)$$

Limiting Behavior for $X_E \rightarrow 0$

The simplifying considerations associated with low fractional loading have been explained in detail in the corresponding section under Case 1. When κ is large, ψ and D_{ap} can be approximated by means of

$$\psi = (1+\gamma)\left[\frac{da}{du}\right]_{u=0} = \pm\sqrt{\frac{1+\gamma}{\pi}}, \qquad (6.82)$$

where the positive sign applies to coatings loaded with $Os(bpy)_3^{3+}$ and the negative sign to coatings loaded with $Os(bpy)_3^{2+}$, and

$$D_{ap} = \frac{k_1 \delta^2}{18\,K}(1+\gamma)\,X_E \,. \qquad (6.83)$$

Calculated Curves

The fractional loading dependences of the apparent diffusion coefficient for various values of the parameter γ are illustrated in Figures 6.11 and 6.12 for coatings loaded with $Os(bpy)_3^{2+}$ and $Os(bpy)_3^{3+}$, respectively. When γ=0, the D_{ap} vs. X_E curve is highly nonlinear and rises very sharply as full loading is approached. As explained above, this behavior is attributable to the variation of C_A with X_E for large values of κ. For nonzero values of γ, there is a contribution from the C-B pathway to the charge-transport process. Just as the contribution from the A^+-B pathway varies with C_A, the contribution from the C-B pathway varies with C_C. In the strong ion-pairing limit, essentially all of the osmium(3+) complex exists as species C; hence, the variation in C_C with the fractional loading is linear. The contribution from the C-B pathway for charge propagation, therefore, is also linear. (It is not rigorously linear because of the influence of the electric field.) This linear contribution is evident in the increasing slope and the prolonged linear behavior of the D_{ap} vs. X_E plot at low fractional loadings as the value of γ increases. In the limit $\gamma \to \infty$, the D_{ap} vs. X_E plot is identical to that obtained by Andrieux and Saveant[22e] when ion-pairing is

Figure 6.11. Variation of the apparent diffusion coefficient, normalized by its value at X_E=0.999, with the fractional loading for a coating loaded with $Os(bpy)_3^{2+}$ in the strong ion-pairing limit, i.e., κ>100. The curves from bottom to top, i.e., those possessing the greatest to the least amount of curvature, are calculated using γ = 10^6, 10^3, 100, 30, 10, 1, 0.

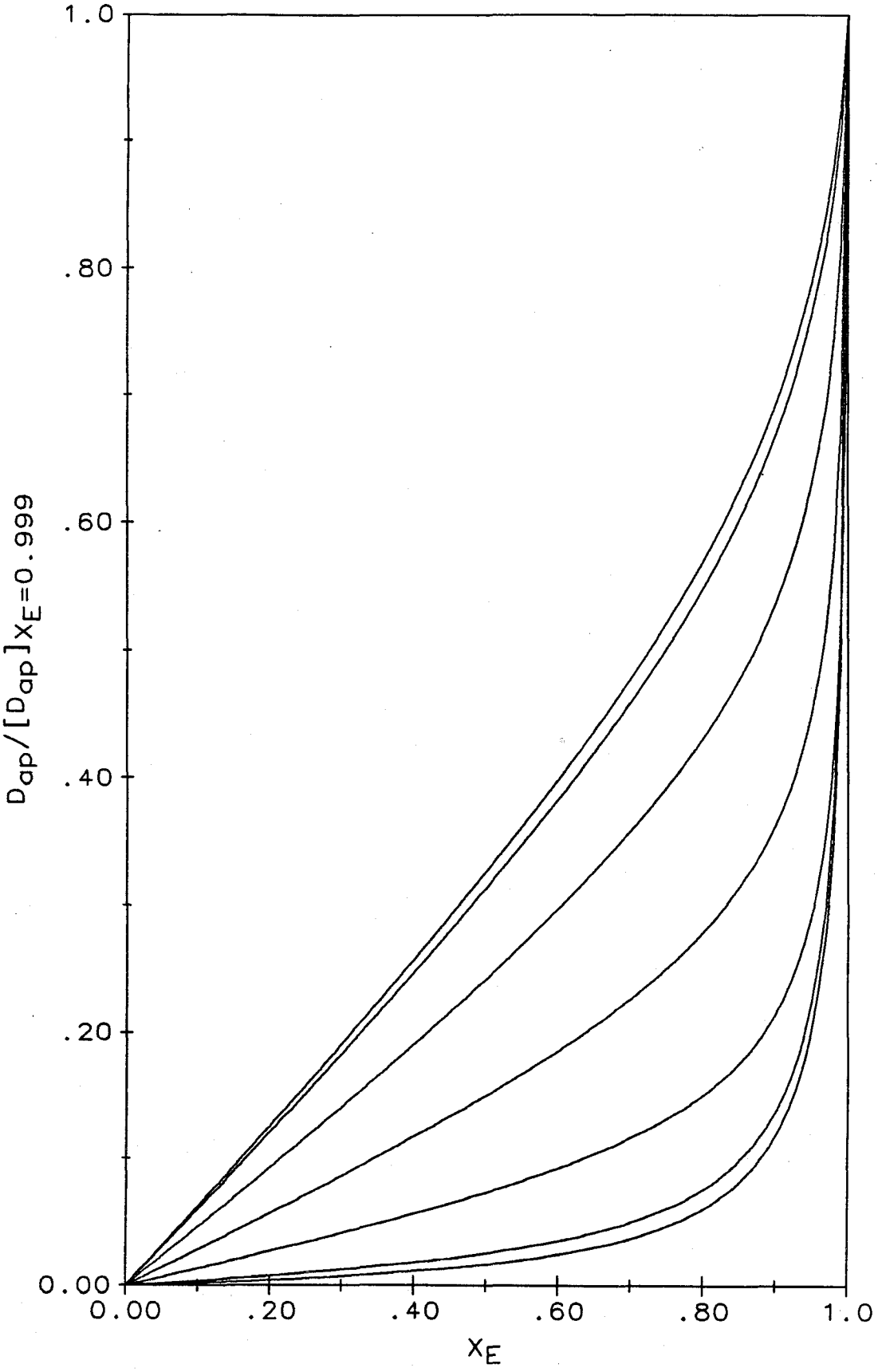
1.0
.80
.60
.40
.20
0.00
0.00
.20
.40
.60
.80
1.0
$D_{ap}/[D_{ap}]_{X_E=0.999}$
X_E

Figure 6.12. Variation of the apparent diffusion coefficient, normalized by its value at X_E=0.999, with the fractional loading for a coating loaded with $Os(bpy)_3^{3+}$ in the strong ion-pairing limit, i.e., κ>100. The curves from bottom to top, i.e., those possessing the greatest to the least amount of curvature, are calculated using γ = 10^6, 100, 30, 10, 3, 1, 0.

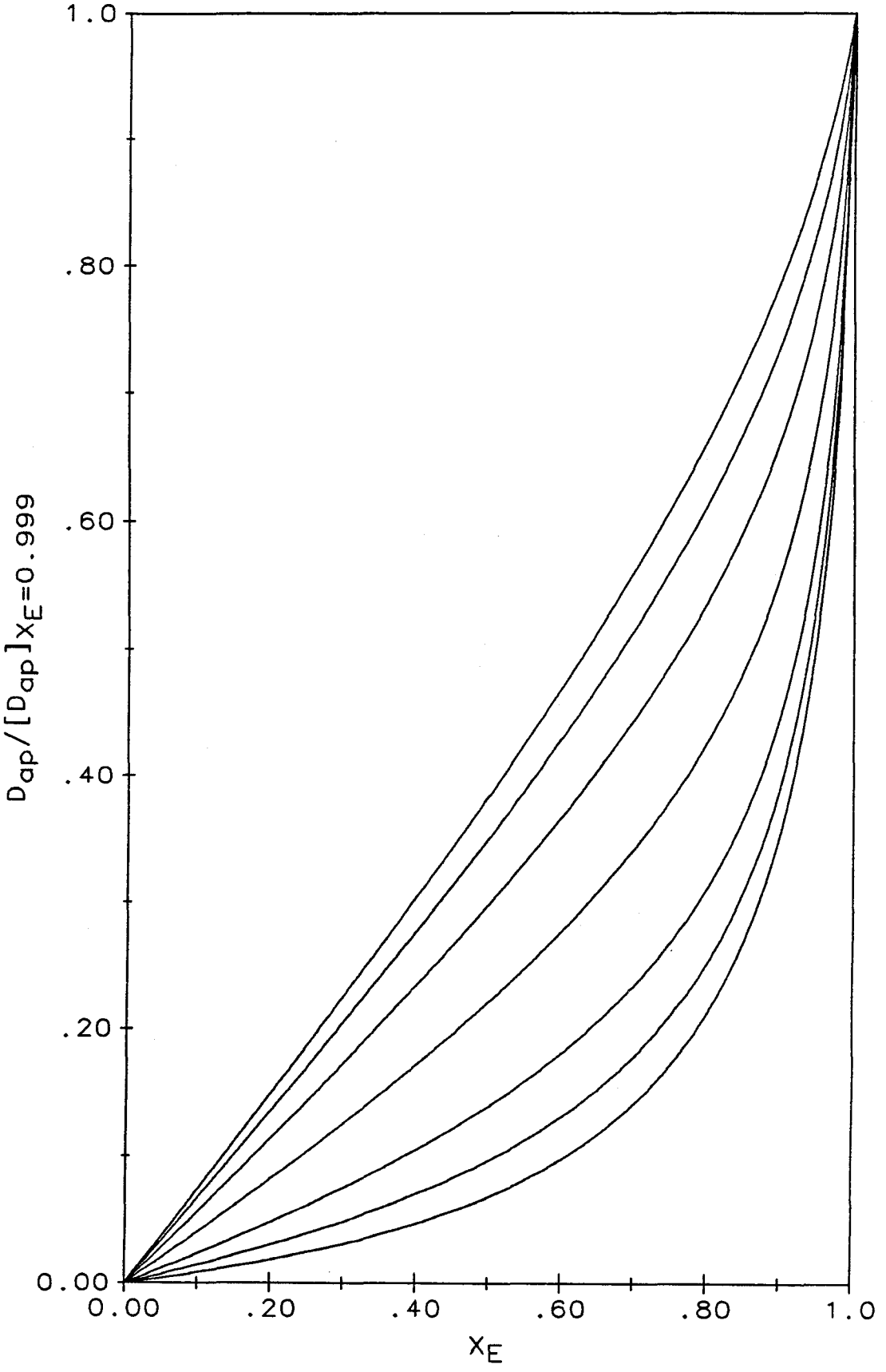
1.0
.80
.60
.40
.20
0.00
0.00
.20
.40
.60
.80
1.0
$D_{ap}/[D_{ap}]_{X_E=0.999}$
X_E

neglected, i.e., the case where $\kappa=0$; the modest curvature at high loadings under these conditions is attributable solely to the influence of the electric field.

In a manner similar to that described for Case 2, fitting of the ion-pairing model for the strong ion-pairing limit to experimental data is facilitated by comparing the value of the apparent diffusion coefficient at a particular fractional loading with the slope of the plot of D_{ap} vs. X_E at very low fractional loadings. Plots of $S(0.9,\kappa>100,\gamma)$ vs. $\log_{10}[\gamma]$ for coatings loaded with $Os(bpy)_3^{2+}$ and $Os(bpy)_3^{3+}$ are shown in Figures 6.13 and 6.14, respectively.

Once the value of γ has been determined from Figure 6.13 or 6.14, the value of k_1/K can be determined from the value of $\left[dD_{ap}/dX_E\right]_{X_E=0}$ and the expression in Equation 6.83. The value of k_2 is uniquely determined, given values for γ and the ratio k_1/K. The nature of the approximations associated with the mathematical treatment for the strong ion-pairing limit prevent resolution of the contributions from k_1 and K, both of which affect only the magnitude of D_{ap}. A change in the value of either k_1 or K may be offset by a proportionate change in the value of the other. In order to assign individual values to k_1 and K, it is necessary to employ the general treatment using nonlinear curve-fitting techniques to optimize k_1, k_2, and K simultaneously. Although feasible in principle, the insensitivity of the apparent diffusion coefficient to the relative values of k_1 and K for large values of K prevents an accurate determination of these two quantities. In short, the variation of the apparent diffusion coefficient with the fractional loading of the coating is not an

Figure 6.13. Variation of $S(0.9,\kappa>100,\gamma)$ with $\log_{10}[\gamma]$ for coatings loaded with $Os(bpy)_3^{2+}$.

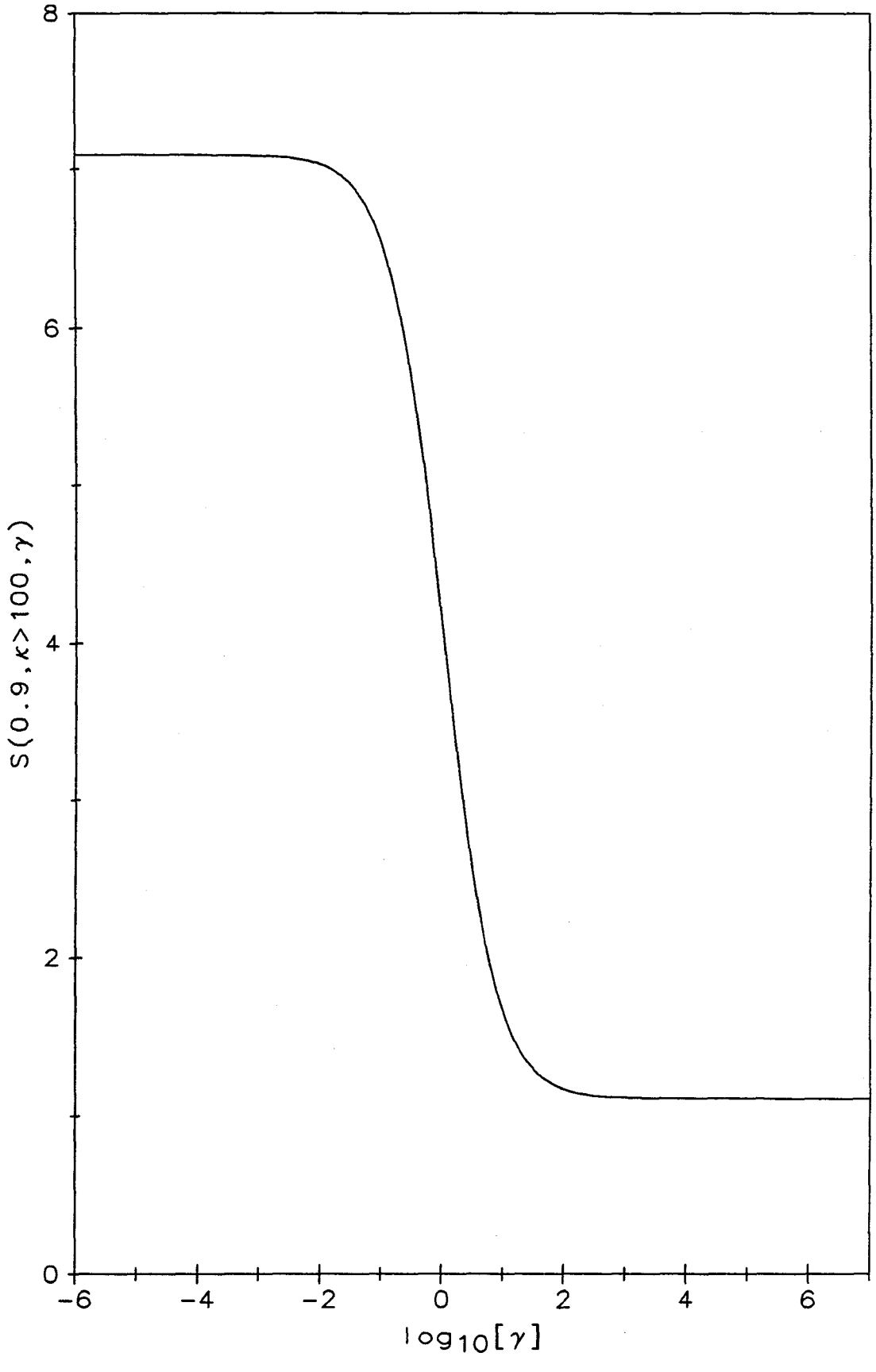
8
6
4
2
0
S(0.9,κ>100,γ)
−6
−4
−2
0
2
4
6
log10[γ]

Figure 6.14. Variation of $S(0.9,\kappa>100,\gamma)$ with $\log_{10}[\gamma]$ for coatings loaded with $Os(bpy)_3^{3+}$.

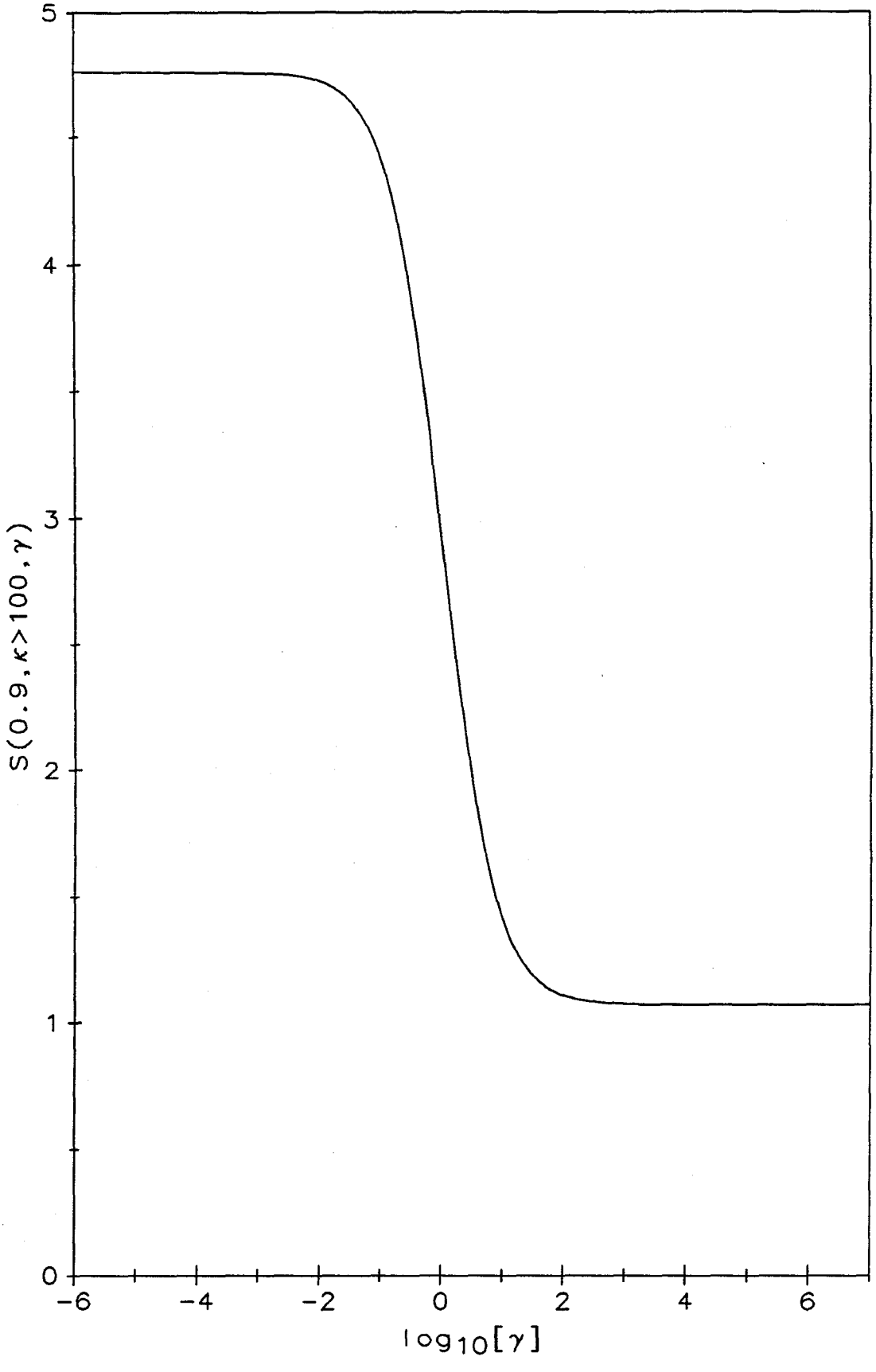
5
4
3
2
1
0
S(0.9,κ>100,γ)
−6
−4
−2
0
2
4
6
log10[γ]

effective means for distinguishing between various combinations of values for the parameters k_1 and K when K is large.

The Effect of the Electric Field

As a comparison with the analysis and computations associated with the preceding cases, the relevant theory is extended to include the case where the electric-field enhancement of the rate of electron hopping is neglected. Influences arising from the electric field are quite simply eliminated by setting $\partial\Phi/\partial x = d\phi/du = 0$ and omitting the Nernst-Planck-Fick equation for the electroinactive counterions (Equation 6.9). The appropriate differential equation describing charge propagation through the $Os(bpy)_3^{3+/2+}$-loaded Nafion coating is

$$0 = \frac{u}{2\kappa}\frac{d(a+\kappa c)}{du} + \frac{d}{du}\left[b\frac{d(a+\gamma c)}{du} - (a+\gamma c)\frac{db}{du}\right], \tag{6.84}$$

which can also be written in the form of Equation 6.47. The boundary conditions and expressions for a, a_0, and ψ associated with various limiting behaviors are identical to those described for Cases 1 through 3. The only differences are the expressions for f(g), which are summarized below:

Case 1: General Treatment, Arbitrary κ and γ

$$f(g) = \left(1-\frac{\gamma}{\kappa}\right)\left(\left(g-\left(f^0-3\right)\right)\frac{da}{dg} - a\right) - \gamma\ ; \tag{6.85}$$

Case 2: A^+-B Pathway Only, $\gamma=0$

$$f(g) = \left(g-\left(f^0-3\right)\right)\frac{da}{dg} - a \; ; \tag{6.86}$$

Case 3: The Strong Ion-Pairing Limit, $\kappa>100$

$$f(g) = f^0 - 2f^0\frac{\left(f^0-2\right)}{g} + f^0\frac{\left(f^0-2\right)\left(f^0-3\right)}{g^2} - \gamma \; . \tag{6.87}$$

The limiting behavior for $X_E \rightarrow 0$ is identical to that described for Case 1. When the fractional loading is small, there is a large excess of supporting electrolyte; i.e., free sulfonate groups and electroinactive counterions, under which condition electric field effects, if considered, would be negligible.

The formulas in Equations 6.85 and 6.86 are valid when $X_E=1$. The caveat associated with the strong ion-pairing limit also applies to Equation 6.87.

Calculated Curves

For comparison with the results for Case 2, the fractional loading dependences of the apparent diffusion coefficient for various values of the dimensionless equilibrium constant κ with $\gamma=0$ are illustrated in Figures 6.15 for a coating loaded with $Os(bpy)_3^{2+}$. Qualitatively, this set of curves is very similar to that of Figure 6.1. Noteworthy is the linear dependence of D_{ap} upon X_E when $\kappa=0$, which is the

Figure 6.15. Variation of the apparent diffusion coefficient, normalized by its value at $X_E=1$, with the fractional loading for a coating loaded with $Os(bpy)_3^{2+}$ with $\gamma=0$. Contributions to the electron-hopping process arising from the electric field are omitted from the computations. The curves from bottom to top, i.e., those possessing the greatest to the least amount of curvature, are calculated using $\kappa = 10^5, 10^3, 100, 10, 1, 0$.

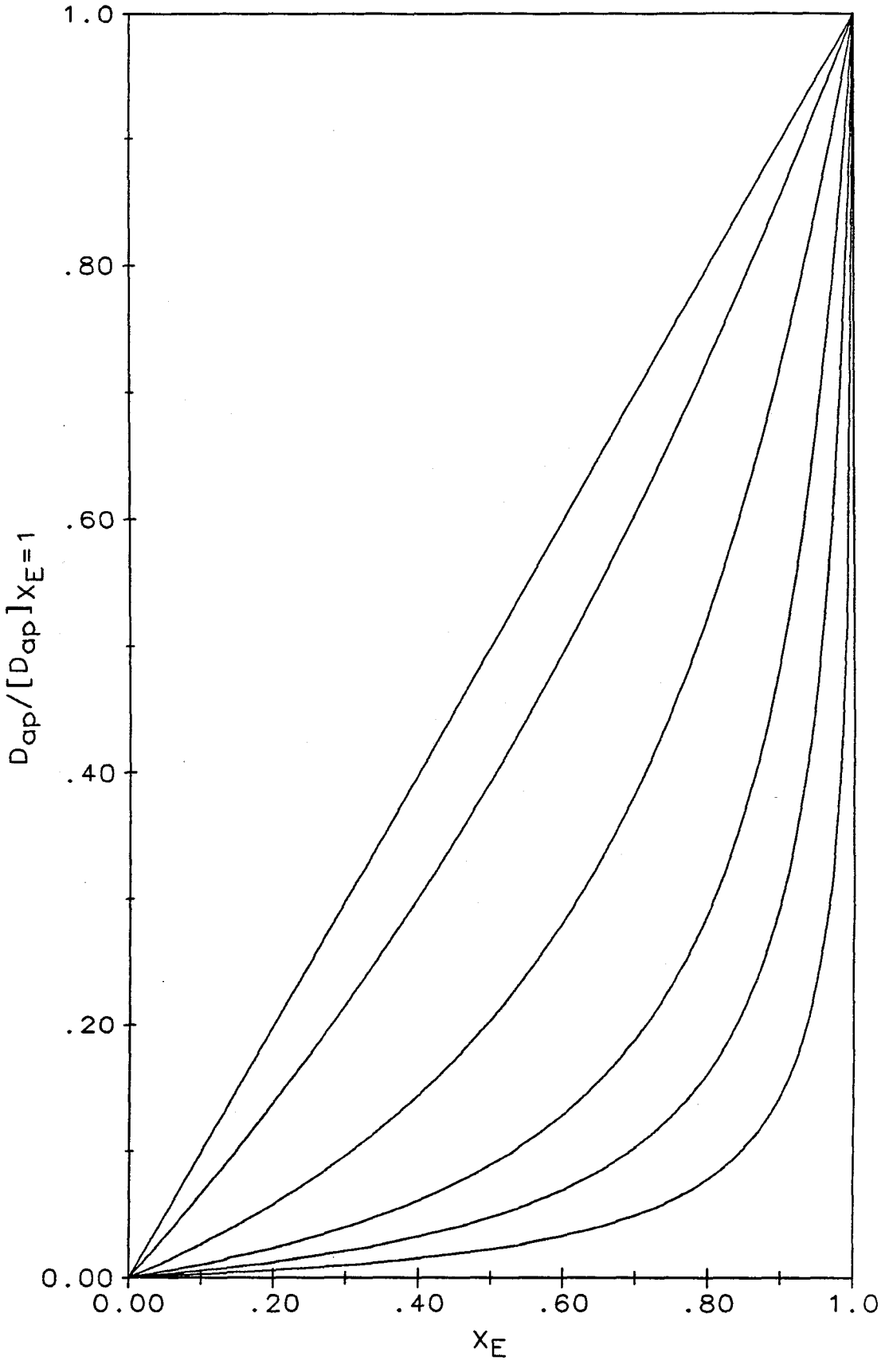
1.0
.80
.60
.40
.20
0.00
0.00
.20
.40
.60
.80
1.0
$D_{ap}/[D_{ap}]_{X_E=1}$
X_E

behavior predicted by Equation 5.1 when both electric field and ion-pairing effects are absent. Inclusion of the influence of the electric field in the theoretical treatment leads to significant quantitative differences in the calculated values of D_{ap}, but the gross features of the plots of D_{ap} vs. X_E are attributable to the ion-pairing equilibrium, not to the electric field. This is illustrated more clearly in Figure 6.16 where curves are plotted for κ=1000 and γ=0 in which electric field effects are included (solid line) and omitted (dashed line). Although these two curves are clearly different, both display a sharp upward curvature at full loading. Given the obvious quantitative importance of accounting for the influence of the electric field on the rate of electron hopping, we base our analysis of the experimental plot of D_{ap} vs. X_E, presented in Chapter 7, upon computations that include contributions to charge propagation arising from the electric field.

Figure 6.16. Variation of $\psi^2 X_E$, which is proportional to D_{ap}, with X_E for γ=0, κ=1000, and a coating loaded with $Os(bpy)_3^{2+}$. Electric field effects were included in the computation of the solid line, whereas electric field effects were neglected in the computation of the dashed line.

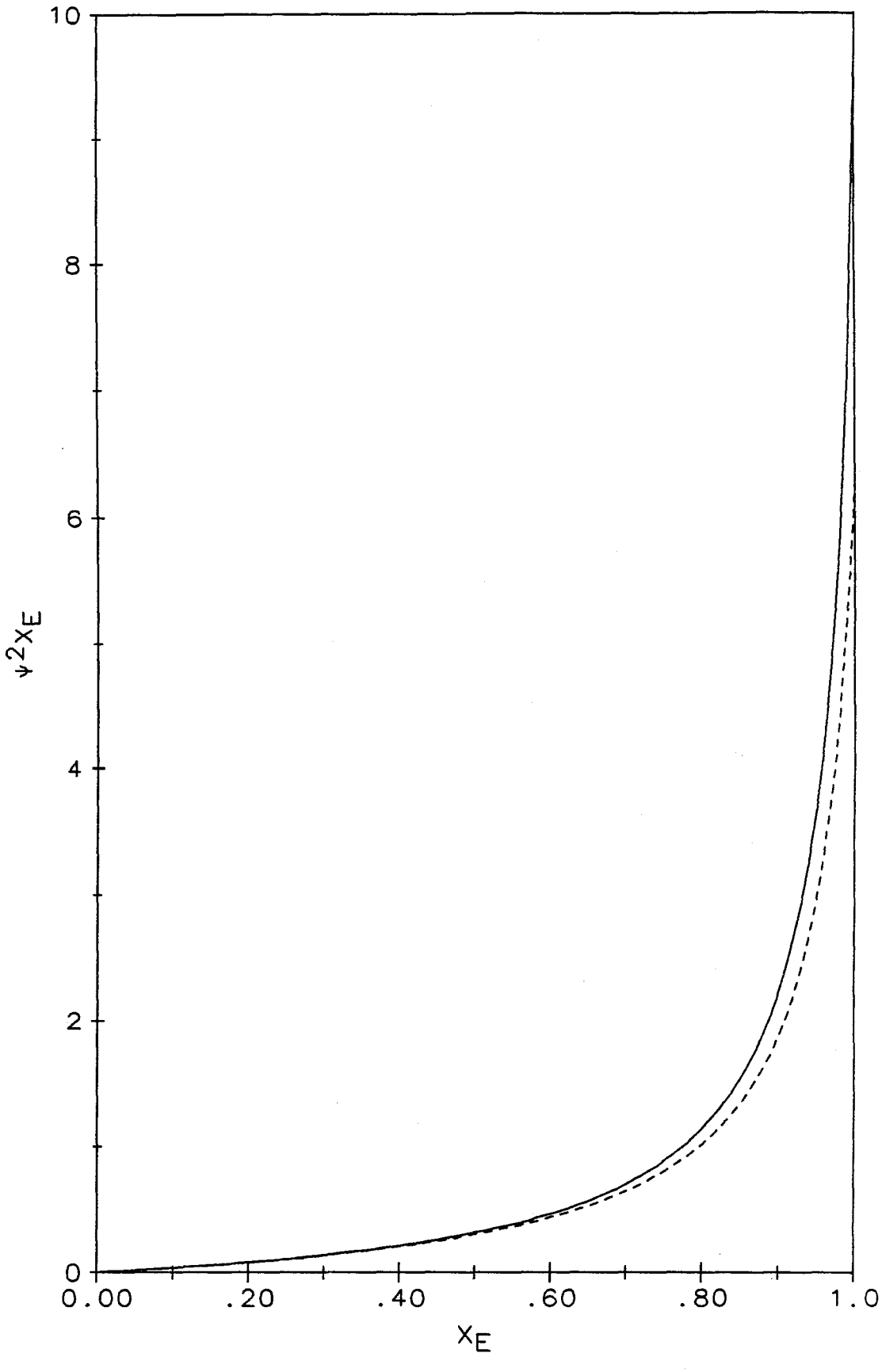
10
8
6
4
2
0
$\psi^2 x_E$
0.00
.20
.40
.60
.80
1.0
x_E

Chapter 7

Comparison of Theoretical and Experimental Results

Characterization of the Experimental Data

As described in Chapter 6, experimentally measured plots of D_{ap} vs. X_E can be analyzed by comparing the value of D_{ap} at relatively high fractional loading with the slope of the plot at low fractional loading. The experimentally measured values for the apparent diffusion coefficient shown in Figure 5.1 are proportional to the fractional loading for $X_E<0.25$. A linear, least-squares fit of the data in this low loading region yields

$$D_{ap} = (2\pm2)\times10^{-11}\ cm^2\ s^{-1} + (1.0\pm0.1)\times10^{-9}\ cm^2\ s^{-1}\ X_E\ . \qquad (7.1)$$

The intercept corresponds to the diffusion coefficient for physical displacement of $Os(bpy)_3^{2+}$, because at infinite dilution the oxidized and reduced reactants never encounter each other, leaving physical displacement as the only mechanism for charge transport. The value of $2\times10^{-11}\ cm^2\ s^{-1}$ for D_{pd} is sufficiently small compared to the values of D_{ap} for $X_E>0.1$ that the omission of physical displacement from the theoretical analysis of Chapter 6 seems justified. (In fact, statistically, the intercept in Equation 7.1 is not significantly different from zero.)

The value of D_{ap} at $X_E=1$ is estimated to be $(6.6\pm0.7)\times10^{-9}\ cm^2\ s^{-1}$ by extrapolation from the data at the highest fractional loadings. At $X_E=0.9$, the measured value of D_{ap} is $(2.0\pm0.2)\times10^{-9}\ cm^2\ s^{-1}$. Substitution of these values and the slope from Equation 7.1 into Equation 6.75 yields $S(1.0,\kappa,\gamma)=7\pm1$ and $S(0.9,\kappa,\gamma)=3.0\pm0.4$.

Characterization of the D_{ap} vs. X_E Data Reported by Sharp, et al.[14]

The D_{ap} vs. C_E data reported by Sharp and co-workers[14] for the $Os(bpy)_3^{3+/2+}$-Nafion system with $G^+=Na^+$ is linear for C_E up to 0.25 M, the linear, least-squares line of best fit being

$$D_{ap} = (0.9\pm1.2)\times10^{-11}\ cm^2\ s^{-1} + (6.5\pm0.7)\times10^{-10}\ cm^2\ s^{-1}\ C_E\ . \qquad (7.2)$$

These D_{ap} vs. C_E data display a nearly vertical rise at C_E=0.415 M, which is the concentration corresponding to full fractional loading. The corresponding value for C_F^0 is 1.25 M; thus from Equation 7.2 we find $\left[dD_{ap}/dX_E\right]_{X_E=0}=(2.7\pm0.3)\times10^{-10}\ cm^2\ s^{-1}$. The values of D_{ap} at X_E=1.0 and X_E=0.9, $(1.9\pm0.2)\times10^{-9}\ cm^2\ s^{-1}$ and $(5.0\pm0.5)\times10^{-10}\ cm^2\ s^{-1}$, respectively, lead to $S(1.0,\kappa,\gamma)=7\pm1$ and $S(0.9,\kappa,\gamma)=1.9\pm0.3$. A summary of the characterization of the experimental data is provided in Table 7.1.

Comparison of Theoretical and Experimental Results

Utilizing the procedure for data analysis described in Chapter 6 in conjunction with the characterizations listed in Table 7.1, the entries in Table 7.2 for k_1, k_2, and K are obtained. Our calculations employ δ=1.4 nm[34,36], C_F^0=1.2 M for the analysis of data acquired in this study, and C_F^0=1.25 M for analysis of the data acquired by Sharp and co-workers.[14] Comparisons of the experimental D_{ap} vs. X_E data with various theoretical curves are provided in Figures 7.1 through 7.6.

Figure 7.1. Comparison of experimental D_{ap} vs. X_E data (circles) with a theoretical curve (solid line) computed using $\kappa=11$ ($K=9$ $\underline{M}^{-1}$), $k_1=8x10^6$ M^{-1} s^{-1}, $\gamma=0$ ($k_2=0$), $\delta=1.4$ nm, and $C_F^0=1.2$ $\underline{M}$. Data were collected as part of this study using $G^+=H^+$ as the electroinactive counterion.

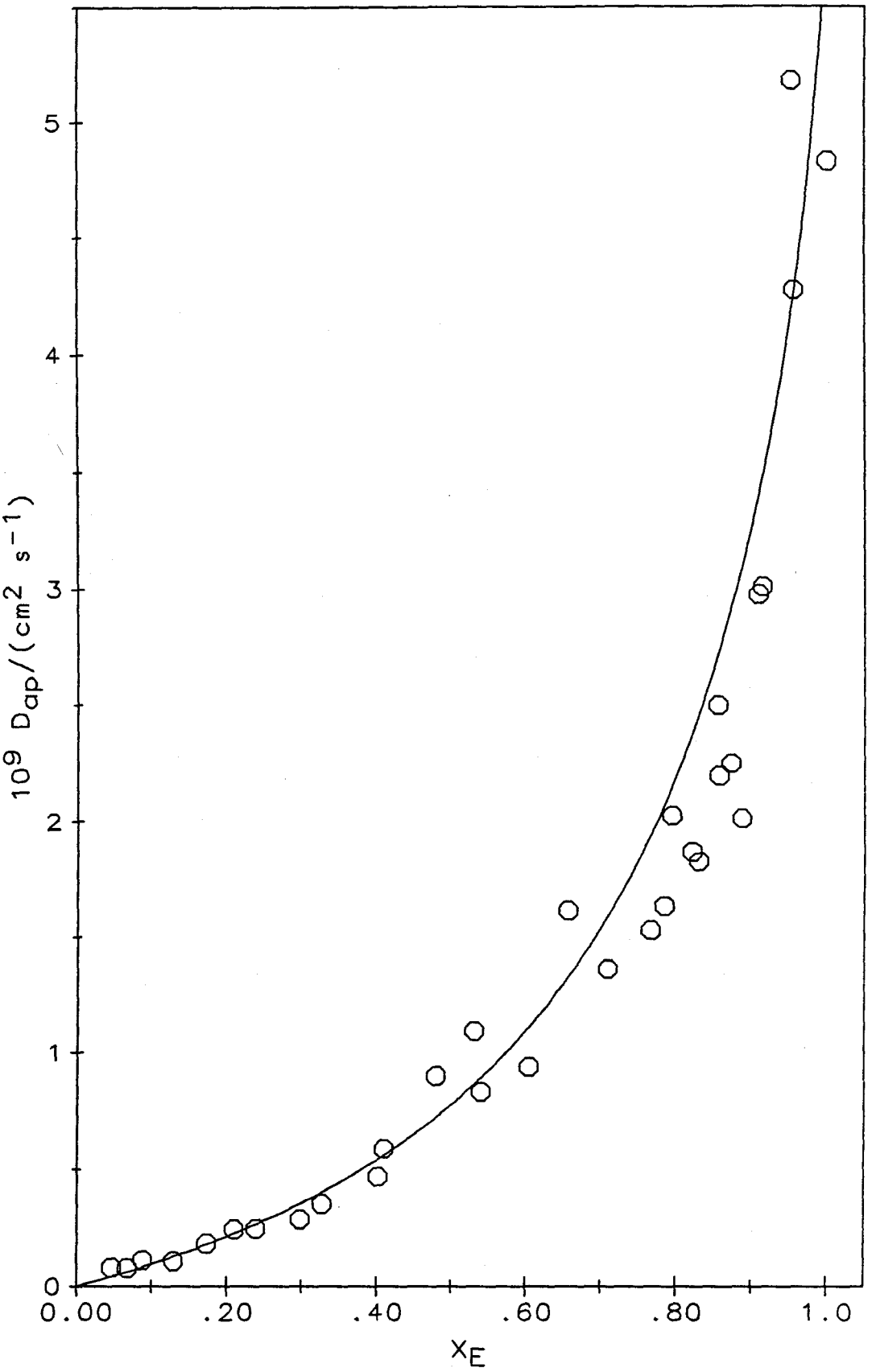
5
4
3
2
1
0
10^9 D_{ap}/(cm^2 s^{-1})
0.00
.20
.40
.60
.80
1.0
X_E

Figure 7.2. Comparison of experimental D_{ap} vs. X_E data (circles) with a theoretical curve (solid line) computed using $\kappa=6$ ($K=5$ $\underline{M}^{-1}$), $k_1=5x10^6$ M^{-1} s^{-1}, $\gamma=0$ ($k_2=0$), $\delta=1.4$ nm, and $C_F^0=1.2$ $\underline{M}$. Data were collected as part of this study using $G^+=H^+$ as the electroinactive counterion.

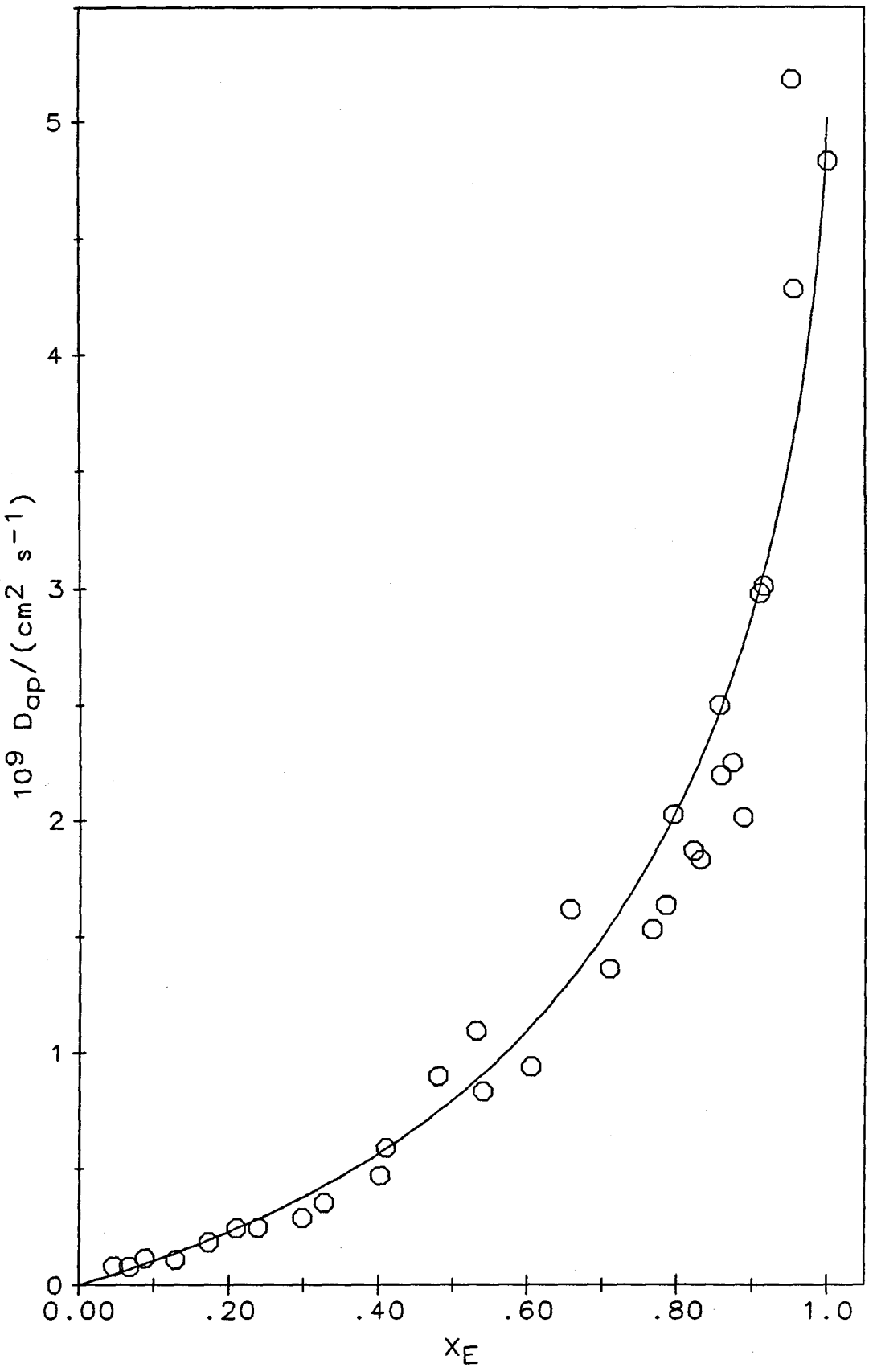
5
4
3
2
1
0
10^9 D_{ap}/(cm^2 s^{-1})
0.00
.20
.40
.60
.80
1.0
x_E

Figure 7.3. Comparison of experimental D_{ap} vs. X_E data (circles) with a theoretical curve (solid line) computed using the strong ion-pairing limit (κ>100), $k_1/K=2.7\times10^5$ s^{-1}, γ=2.2 ($k_2=5.0\times10^5$ $\underline{M}^{-1}$ s^{-1}), δ=1.4 nm, and C_F^0=1.2 $\underline{M}$. Data were collected as part of this study using $G^+=H^+$ as the electroinactive counterion.

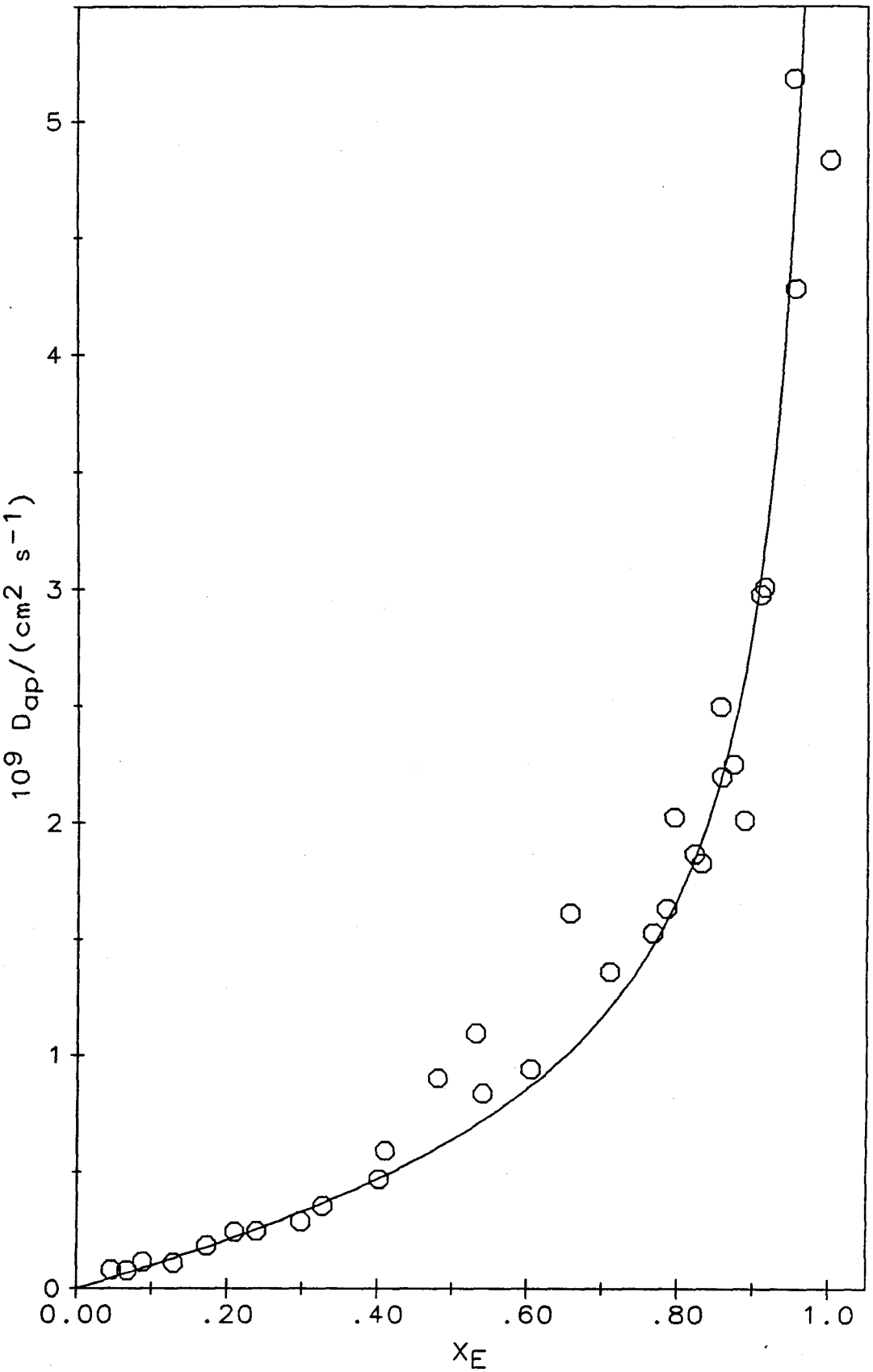
5
4
3
2
1
0
10^9 D_{ap}/(cm^2 s^{-1})
0.00
.20
.40
.60
.80
1.0
X_E

Figure 7.4. Comparison of experimental D_{ap} vs. X_E data (circles) with a theoretical curve (solid line) computed using $\kappa=12$ ($K=10$ $\underline{M}^{-1}$), $k_1=2.6\times10^6$ M^{-1} s^{-1}, $\gamma=0$ ($k_2=0$), $\delta=1.4$ nm, and $C_F^0=1.25$ $\underline{M}$. Data were collected by Sharp and co-workers[14] using $G^+=Na^+$ as the electroinactive counterion.

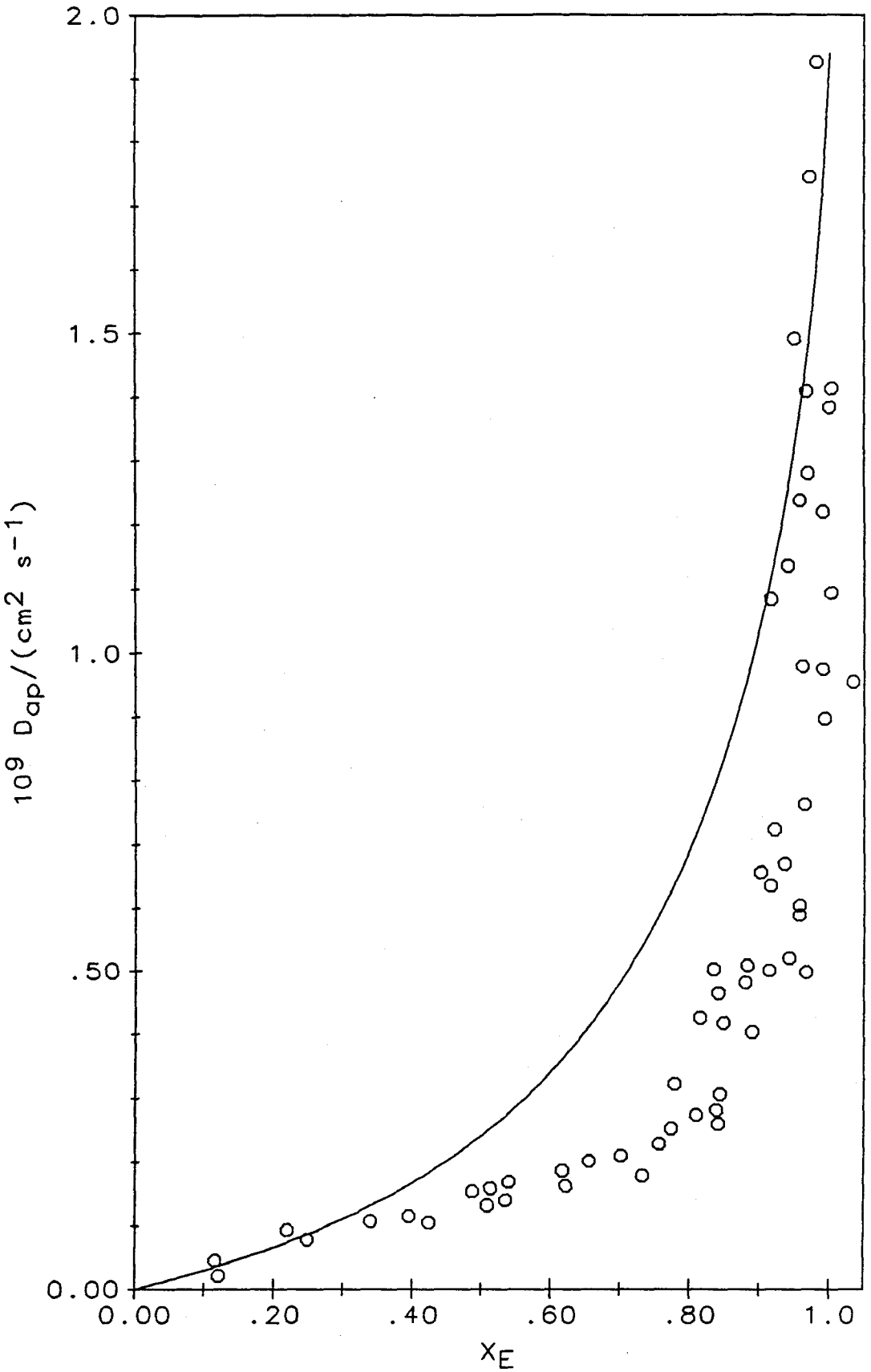
2.0
1.5
1.0
.50
0.00
0.00
.20
.40
.60
.80
1.0
10^9 D_{ap}/(cm^2 s^{-1})
X_E

Figure 7.5. Comparison of experimental D_{ap} vs. X_E data (circles) with a theoretical curve (solid line) computed using κ=1.6 (K=1.3 $\underline{M}^{-1}$), k_1=5.2x10^5 M^{-1} s^{-1}, γ=0 (k_2=0), δ=1.4 nm, and C_F^0=1.25 $\underline{M}$. Data were collected by Sharp and co-workers[14] using $G^+ = Na^+$ as the electroinactive counterion.

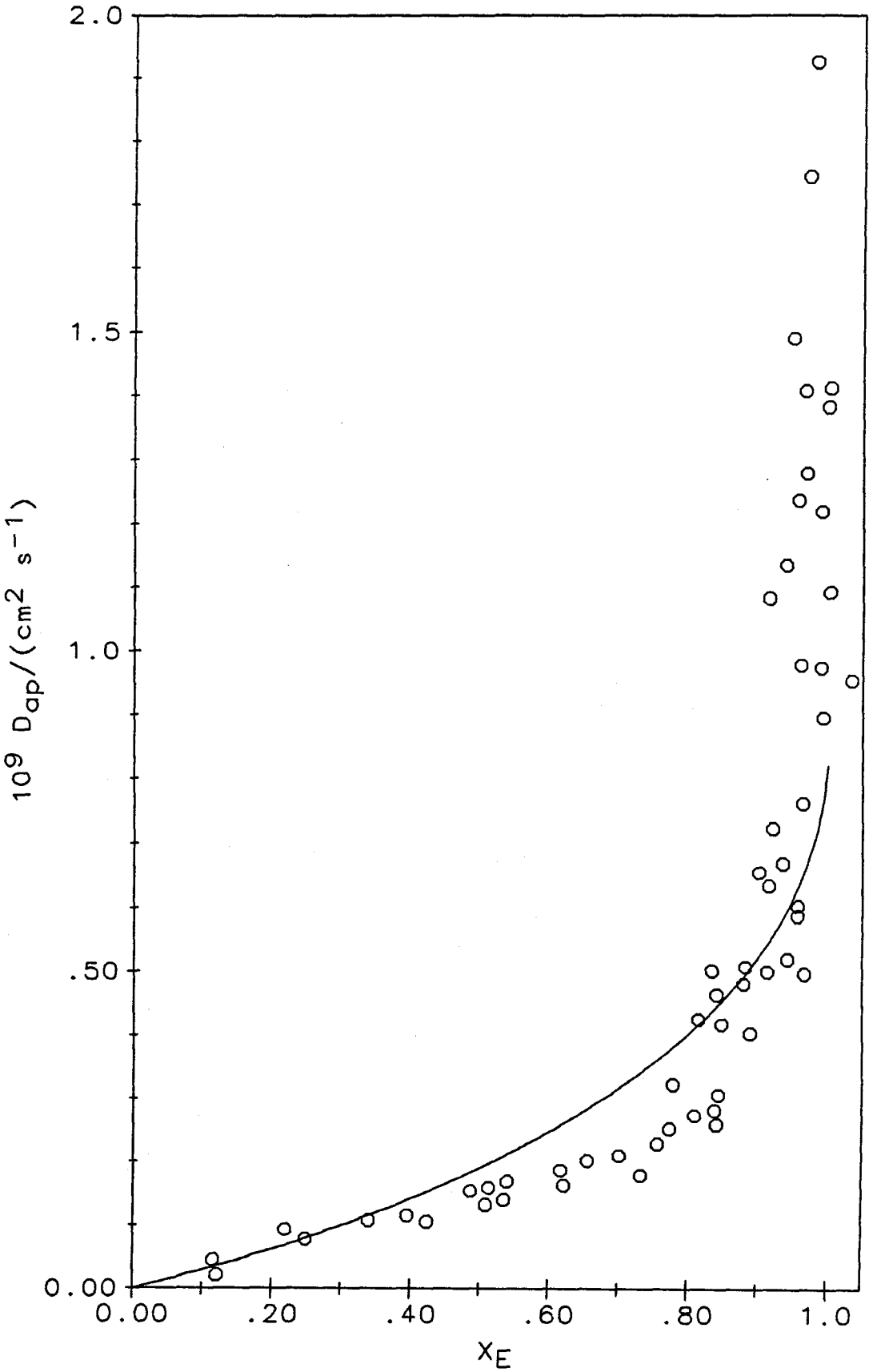
2.0
1.5
1.0
.50
0.00
0.00
.20
.40
.60
.80
1.0
10^9 D_{ap}/(cm^2 s^{-1})
X_E

Figure 7.6. Comparison of experimental D_{ap} vs. X_E data (circles) with a theoretical curve (solid line) computed using the strong ion-pairing limit ($\kappa>100$), $k_1/K=2.9\times10^4$ s^{-1}, $\gamma=7$ ($k_2=1.7\times10^5$ $\underline{M}^{-1}$ s^{-1}), $\delta=1.4$ nm, and $C_F^0=1.25$ $\underline{M}$. Data were collected by Sharp and co-workers[14] using $G^+=Na^+$ as the electroinactive counterion.

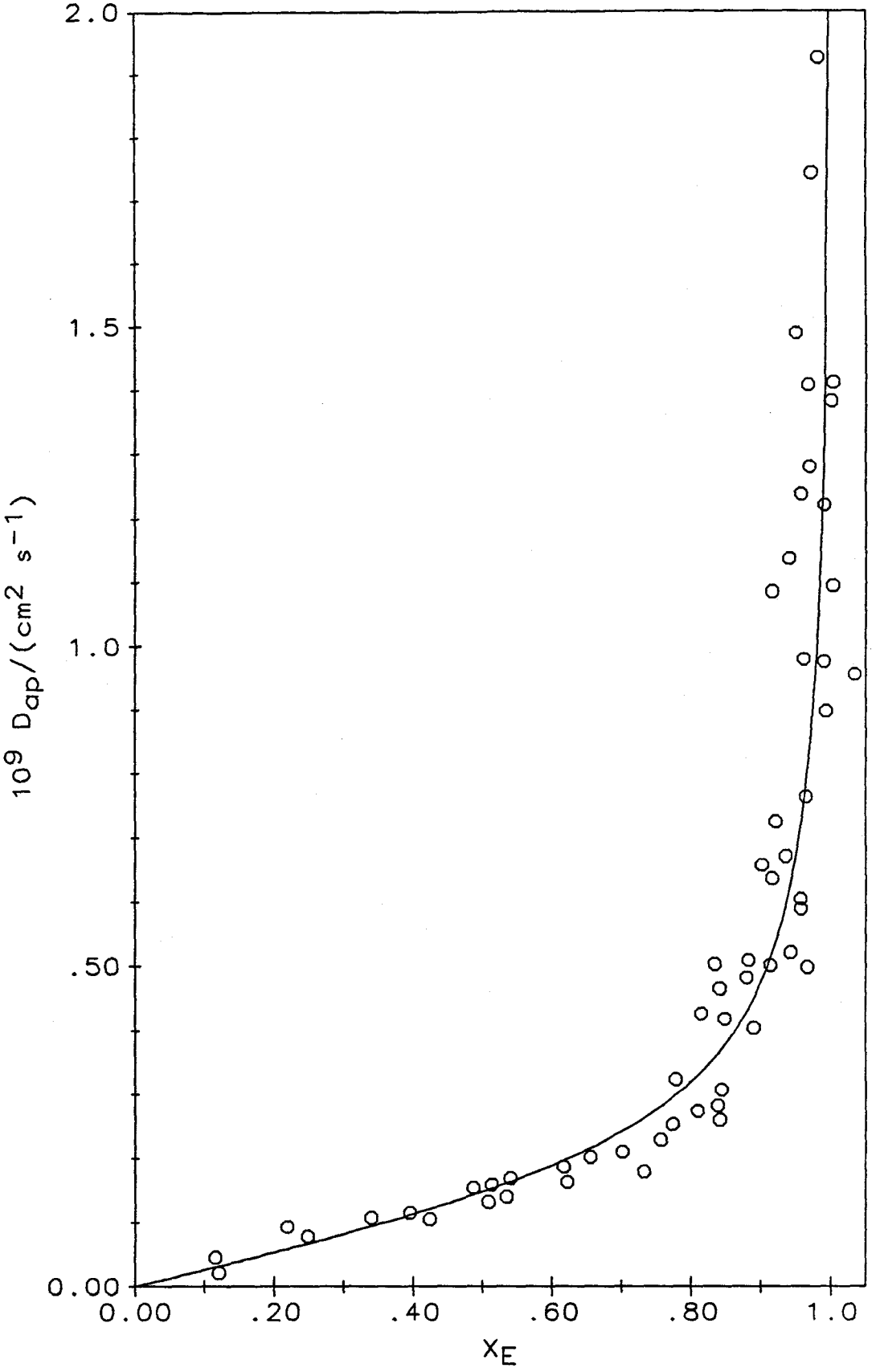
2.0
1.5
1.0
.50
0.00
0.00
.20
.40
.60
.80
1.0
10^9 D_{ap}/(cm^2 s^{-1})
x_E

Quantity	D_{ap} vs. X_E Data from this Study	D_{ap} vs. X_E Data from Reference 14
$10^9 \left[\frac{dD_{ap}}{dX_E}\right]_{X_E=0}$	1.0±0.1	0.27±0.03
$10^9 \left[D_{ap}\right]_{X_E=1.0}$	6.6±0.7	1.9±0.2
$10^9 \left[D_{ap}\right]_{X_E=0.9}$	2.9±0.2	0.50±0.05
$S(1.0,\kappa,\gamma)$	7±1	7±1
$S(0.9,\kappa,\gamma)$	3.0±0.4	1.9±0.3

Table 7.1. Summary of results for the characterization of experimental D_{ap} vs. X_E data.

Discussion

There is clearly excellent agreement between the predictions of the ion-pairing model and the empirical D_{ap} vs. X_E data of this study, as is readily evident upon inspection of Figures 7.1, 7.2, and 7.3. As it happens, the versatility of the ion-pairing model is sufficiently great that the experimental data can be accurately fit by more than one set of values for k_1, k_2, and K. Given the experimental error, the observed variation of the apparent diffusion coefficient with the fractional loading does not distinguish effectively between the various mechanistic options inherent in the ion-pairing model. The data analysis strongly suggests that ion-pairing plays a major role in the charge-transport process within Nafion; unfortunately, it is not

possible to resolve the relative contributions to that process from the A^+-B and C-B pathways.

Theory	Fit of D_{ap} vs. X_E Data from This Study[a]		Fit of D_{ap} vs. X_E Data from Reference 14[b]	
Case 2 using $S(1.0,\kappa,\gamma)$	κ=11±3 γ=0	k_1=(9±3)x10^6 $\underline{M}^{-1}$ s^{-1} k_2=0 K=9±3 $\underline{M}^{-1}$	κ=12±3 γ=0	k_1=(2.5±0.7)x10^6 $\underline{M}^{-1}$ s^{-1} k_2=0 K=10±2 $\underline{M}^{-1}$
Case 2 using $S(0.9,\kappa,\gamma)$	κ=6±2 γ=0	k_1=(5±2)x10^6 $\underline{M}^{-1}$ s^{-1} k_2=0 K=5±2 $\underline{M}^{-1}$	κ=1.6 ±0.8 γ=0	k_1=(5±3)x10^5 $\underline{M}^{-1}$ s^{-1} k_2=0 K=1.3±0.6 $\underline{M}^{-1}$
Case 3 using $S(0.9,\kappa,\gamma)$	κ>100 γ=2.2±0.7	k_1/K=(2.6±0.6)x10^5 s^{-1} k_2=(5±2)x10^5 $\underline{M}^{-1}$ s^{-1}	κ>100 γ=7±3	k_1/K=(3±1)x10^4 s^{-1} k_2=(2±1)x10^5 $\underline{M}^{-1}$ s^{-1}

Table 7.2. Summary of values for parameters employed in fitting theoretical curves to experimental data.

[a] Calculations utilize C_F^0=1.2 $\underline{M}$.

[b] Calculations utilize C_F^0=1.25 $\underline{M}$.

In contrast to the good agreement between theory and experiment evident in Figures 7.1 through 7.3, the calculated curves in Figures 7.4 and 7.5 provide poor fits to the experimental data. The ion-pairing model under the conditions of Case 2 (γ=0) is unable to account accurately for the variation of the apparent diffusion coefficient with the fractional loading observed by Sharp and co-workers.[14] The assumption of strong ion-pairing and inclusion of the C-B pathway in addition to the A^+-B pathway as a possible route for

electron hopping in the model, however, leads to an excellent match between theoretical and experimental data as shown in Figure 7.6. A large value for the equilibrium constant is essential in order to obtain the extremely steep rise in D_{ap} as $X_E \rightarrow 1$. A substantial contribution from the C-B pathway to the charge-transport process is necessary to obtain the prolonged linear dependence of D_{ap} upon X_E for fractional loadings below 50%; hence, the nonzero value for γ.

Discussion

As discussed in the preceding section, the ion-pairing model accurately describes the D_{ap} vs. X_E data obtained in this study using protons as the mobile electroinactive counterions for a variety of combinations of k_1, k_2, and K, three of these combinations being shown in Table 7.2. The circumstantial evidence strongly suggests that ion-pairing interactions have a major influence on charge transport in the $Os(bpy)_3^{3+/2+}$-Nafion system. Within the framework of the model described in this report, it appears that the ion-pairing interactions of Equations 6.1 through 6.5 are relatively strong with K unlikely to be less than 6 $\underline{M}^{-1}$ and possibly much larger. It is not possible to assess with any degree of certainty the relative importance of the A^+-B and C-B pathways for electron hopping, except to say that the larger the value of K, the greater the significance of the C-B pathway.

The D_{ap} vs. X_E data reported by Sharp and co-workers[14] using sodium ions as the mobile electroinactive counterions is fit in a compelling manner only by assuming that the ion-pairing equilibrium in Equation 6.5 lies strongly to the right. Within the

context of the ion-pairing model, we conclude that the data of Sharp, et al.[14] arises from very strong ion-pairing between the Nafion sulfonate groups and the tris(2,2'-bipyridine)osmium(3+/2+) complex such that essentially all of the complex exists as neutral, fully ion-paired moieties regardless of the oxidation state of the complex; only a trace quantity of the osmium(3+) complex exists in a doubly ion-paired state. Two pathways for electron hopping are operative: electron hopping between doubly ion-paired osmium(2+) and osmium(3+) species (the A^+-B pathway) and electron hopping between fully ion-paired osmium(2+) and osmium(3+) species (the C-B pathway). At low fractional loadings both pathways participate significantly in the charge transport process, though the C-B pathway is somewhat more dominant, as indicated by $\gamma>1$. At high fractional loading, however, the A^+-B pathway becomes the dominant pathway for electron hopping; the sharp increase in the value of the apparent diffusion coefficient as the fractional loading approaches unity reflects the equally sharp increase in C_A under the same conditions.

The Rate Constant for Electron Self-Exchange

The electron self-exchange rate constant for the $Os(bpy)_3^{3+/2+}$ redox couple in solution has been measured to be approximately 10^7 $\underline{M}^{-1}$ s^{-1}.[1a] This value is well below the bimolecular diffusion-limited rate constant in solution and probably represents the activation-limited rate constant under aqueous conditions. Fits of the experimental data based upon the assumptions of Case 2 yield $k_1=10^6$ to 10^7 $\underline{M}^{-1}$ s^{-1} (see Table 7.2). Fits of the experimental data based upon the treatment for the strong ion-pairing limit, Case 3 in

Figure 7.2, yield $k_1/K=10^4$ to 10^5 s^{-1} and $k_2 \cong 10^5$ $\underline{M}^{-1}$ s^{-1}. The strong ion-pairing limit applies only when $K>100$ $\underline{M}^{-1}$, roughly, which indicates that $k_1>10^6$ $\underline{M}^{-1}$ s^{-1}.

Interestingly, the various analyses of both sets of experimental data all suggest that the electron self-exchange rate constant for the $Os(bpy)_3^{3+/2+}$ redox couple incorporated into Nafion is within an order of magnitude of its value in aqueous solution. It is important to note that this value applies to the A^+-B pathway, i.e., electron hopping between reactants each ion-paired with the same number of sulfonate groups. The rate constant, k_2, for the C-B pathway is considerably smaller than that for the A^+-B pathway consistent with our earlier arguments.

Comparison of Results for Different Electroinactive Counterions

Within the framework of the ion-pairing model described in Chapter 6, the identity of the electroinactive counterion is irrelevant provided it is monovalent and diffuses rapidly compared to the rate of electron hopping; the value of the apparent diffusion coefficient should therefore be independent of species G^+. A comparison of the apparent diffusion coefficients obtained when hydrogen ions are employed as the electroinactive counterion, i.e., data acquired as part of this study, with those obtained when sodium ions are employed as the electroinactive counterion, i.e., the data of Sharp and co-workers,[14] reveals substantial differences in the magnitude of D_{ap} and in the shape of the D_{ap} vs. X_E plots (compare Figures 7.1 and 7.4, for example). Clearly, one must question whether these differences are attributable solely to the different species serving as the

electroinactive counterions or whether the differences could have other origins, such as different sources and ages of the Nafion or methods of coating preparation. Uncertainties in the determination of the apparent diffusion coefficients and the fractional loadings could also be responsible, at least in part, for the discrepancies.

If differences between the experimental results of this study and those of Sharp and co-workers[14] are not experimental artifacts, and it appears they are not, then one must conclude that the electroinactive counterions participate in propagating charge across the coating in a manner that goes beyond their role in the electric-field enhancement of the rate of electron hopping.[22b] One likely possibility is that the electroinactive counterions also interact with the Nafion sulfonate groups.

Activity Effects Associated with Species G^+ and F^-

A rigorous, quantitative treatment of interactions between the electroinactive counterion and the sulfonate groups is, in principle, feasible, but such a treatment would introduce additional adjustable parameters, complicating the analysis and detracting from the persuasiveness of the model. As an alternative, we provide a qualitative assessment of the likely implications of G^+-F^- interactions.

First, we observe that the equilibrium constant K for the reaction of Equation 6.5 should be regarded as an apparent equilibrium constant that depends on the nature of the mobile, electroinactive counterion. In fact, in the ion-pairing equilibrium (Equation 6.5), the concentration of the free sulfonate groups, C_F, should be multiplied by an activity coefficient that depends on the interactions of the

sulfonate groups with the mobile, electroinactive counterions. The activity coefficient, which is smallest when X_E approaches zero, will increase as X_E increases, and more and more of the sulfonate ions have the osmium complex as their counterions and less and less free sulfonate ions are available, thereby enhancing the ion-pairing between the osmium complex and the sulfonate groups. As a result, the point where the initially linear dependence of D_{ap} upon X_E becomes nonlinear (because of lack of sufficient F^- to ion-pair with A^+) occurs at larger values of X_E than would otherwise be true.

This behavior can also be explained as follows: The ionic interactions between the electroinactive counterions, H^+ or Na^+, and the sulfonate groups that are responsible for the variation in activity coefficients cause the initial slope of the D_{ap} vs. X_E plot to be smaller than would be the case if the activity coefficient were unity at all values of X_E. The experimental behavior one expects to observe is a steeper increase of D_{ap} with X_E as $X_E \rightarrow 1$ than is predicted by a model in which variations in the activity coefficients of the electroinactive counterions with X_E are neglected.

Contributions from other Ion-Paired Species

Ion-paired species other than A^+, B, and C might conceivably participate in the electron-hopping process. Suppose, contrary to our earlier assumptions, that the $[Os(bpy)_3^{3+}\cdot(F^-)_2]^+$ and $[Os(bpy)_3^{2+}\cdot F^-]^+$ ions are not strongly ion-paired but that the $[Os(bpy)_3^{3+}\cdot(F^-)]^{2+}$ and $Os(bpy)_3^{2+}$ ions are. Electron hopping should occur between reactants possessing the same number of ion-paired sulfonate groups for the same reasons that electron hopping between species A^+ and B

should predominate over electron hopping between species C and B, provided the equilibrium concentrations of A^+ and C are not widely different. If we introduce the representations $Q^{2+}= [Os(bpy)_3{}^{3+}\bullet F^-]^{2+}$ and $P^+=[Os(bpy)_3{}^{2+}\bullet(F^-)]^+$, then from the conservation conditions

$$C_F^0 = C_Q + C_P + 2\,C_A + C_F \tag{7.3}$$

and

$$C_E = C_Q + C_P + C_A\ , \tag{7.4}$$

we can write

$$C_F = C_Q + C_E + C_G\ . \tag{7.5}$$

The concentrations of species Q^{2+} and P^+ are represented by C_Q and C_P, respectively. The ion-pairing equilibrium condition is

$$K^* = \frac{C_A}{C_Q\,C_F}\ , \tag{7.6}$$

which may be re-written as

$$K^* = \frac{C_A}{C_Q\left(C_Q + C_E + C_G\right)}\ ; \tag{7.7}$$

the corresponding expression for the ion-pairing model presented in Chapter 6 is

$$K = \frac{C_C}{C_A (C_A + C_G)} . \tag{7.8}$$

The underlying cause of the sharp rise in D_{ap} as X_E approaches unity for large K (Figure 6.1) is the sharp increase in C_A as C_G approaches zero (Figure 6.5). (Recall that $C_G \rightarrow 0$ as $X_E \rightarrow 1$ in regions containing only the oxidized osmium complex.) At full loading when K is large and $C_G=0$, the fraction of osmium(3+) complex existing as species A^+ is

$$\frac{C_A}{C_E} \cong \sqrt{\frac{1}{K}} , \tag{7.9}$$

whereas at low loadings when K is large and $C_G=C_F^0$, the fraction of osmium(3+) complex existing as species A^+ is

$$\frac{C_A}{C_E} \cong \frac{1}{K C_F^0} . \tag{7.10}$$

It is obvious that for large K the fraction of osmium(3+) complex existing as the charge-carrying species A^+ varies by orders of magnitude as the fractional loading varies from low to high values. The variation in D_{ap} mirrors the variation in C_A/C_E, *vide supra.*

In the alternate scheme involving species Q^{2+}, P^+, and A^+, the variation in C_Q/C_E with changing fractional loading is less drastic, because the denominator in Equation 7.7 never reduces to C_Q^2. At full loading when K is large and $C_G=0$, the fraction of osmium(3+) complex existing as species Q^{2+} is

$$\frac{C_Q}{C_E} = \frac{1}{K^* C_E} = \frac{3}{K^* C_F^0}, \qquad (7.11)$$

whereas at low loadings when K is large and $C_G = C_F^0$, the fraction of osmium(3+) complex existing as species Q^{2+} is

$$\frac{C_Q}{C_E} = \frac{1}{K^* C_F^0}. \qquad (7.12)$$

The fraction of species Q^{2+}, therefore, varies by at most a factor of three as X_E ranges from zero to unity; the variation in D_{ap} over this same range of fractional loadings will be correspondingly modest.

One might also imagine a system containing only $Os(bpy)_3^{2+}$, $Os(bpy)_3^{3+}$, and $[Os(bpy)_3^{3+} \bullet (F^-)]^{2+}$. This possibility can also be rejected, because there is no dramatic change in the fraction of charge-carrying species upon going from low to high fractional loadings, and thus no steeply rising D_{ap} vs. X_E plots are to be expected. In addition, if the osmium(2+) species were not ion-paired, one would expect the complex to rapidly leak out of the Nafion coating into pure, supporting electrolyte in opposition to the experimental observations.

Other Charge-Transport Models

Although the ion-pairing model discussed above is in reasonably good agreement with the experimental data, it is worth considering whether the observed variation of D_{ap} with X_E could originate from other phenomena. Curved D_{ap} vs. X_E plots have been predicted in an alternative model in which the redox centers are assumed to be

strictly located at the nodes of a real, perfect cubic lattice.[33b] As already noted, redox polymers such as those involved in the present study seem unlikely to have structures that match this model.

Another, quite different, model recently proposed to explain the sharp rise of the D_{ap} vs. X_E plots observed with the $Os(bpy)_3^{3+/2+}$ and $Ru(bpy)_3^{3+/2+}$ couples in Nafion is based upon the original Dahms-Ruff notion of charge propagation as a diffusional process that combines physical displacement of the redox centers with electron hopping between them.[8] The overall diffusion coefficient is expressed as usual by Equation 5.2, but the constant k_1 is itself regarded as possibly limited either by the rate of diffusion of the redox centers toward one another or by the activation requirements of the reaction according to

$$k_1 = \frac{k_{act}\, k_d}{k_{act} + k_d}, \qquad (7.13)$$

where k_{act} is the activation-limited, electron self-exchange rate constant and k_d is the diffusion-limited, bimolecular rate constant. The suggestion originally proposed by Ruff and Friedrich[20b] and later, in a different formulation, by He and Chen,[8] is that k_d is a function of both the diffusion coefficient for physical displacement, D_{pd}, and that for electron hopping, D_1, leading to a concentration dependence for k_1. This reasoning, however, is difficult to understand, because both k_{act} and k_d are bimolecular rate constants; the combination of these two rate constants in Equation 7.13 should therefore be independent of the concentration of redox sites. As it

happens, the rate constant k_1 in Equation 5.2 is the activation-limited electron self-exchange rate constant, and the first term on the right side of Equation 5.2 entirely accounts for the contributions from physical diffusion.[20d-f] We thus conclude that the observed dependence of the apparent diffusion coefficient upon the fractional loading show in Figure 5.2 is not satisfactorily explained by these alternative models.

Chapter 8

Slow-Scan Linear-Sweep Voltammetry

Slow-Scan Linear-Sweep Voltammetry

An interesting consequence of the ion-pairing model is the predicted effects of the ion-pairing reaction on the shapes of current-potential curves recorded under conditions where Nernstian equilibrium is attained. The system under investigation involves three phases: the electrode, the Nafion film, and the supporting electrolyte. Phase equilibrium at the Nafion-electrode interface is established when

$$\mu_A^0 + \mu_e^0 + R\,T \ln C_A + F\left(\Phi_N - \Phi_E\right) = \mu_B^0 + R\,T \ln C_B \,. \tag{8.1}$$

Similarly, phase equilibrium at the Nafion-solution interface is established when

$$\mu_G^0 + R\,T \ln C_G + F\,\Phi_N = \mu_{G,S}^0 + R\,T \ln C_{G,S} + F\,\Phi_S \,. \tag{8.2}$$

The standard chemical potential of species i is represented by μ_i^0. The subscripts E, N, and S signify the electrode, Nafion film, and supporting electrolyte, respectively; the subscript e represents an electron. $C_{G,S}$ is the concentration of electroinactive counterions, G^+, in the bulk solution. All other symbols possess the same significance as previously defined.

The expressions in Equations 8.1 and 8.2 may be combined to yield E, the electrode potential measured relative to bulk solution:

$$E = \Phi_E - \Phi_S = E^0 + \frac{R\,T}{F} \ln \frac{C_A\,C_{G,S}}{C_B\,C_G} \,, \tag{8.3}$$

where the standard reduction potential, E^0, is defined by

$$E^0 = \frac{\mu_A^0 + \mu_e^0 + \mu_{G,S}^0 - \mu_B^0 - \mu_G^0}{F} . \qquad (8.4)$$

Substituting the conservation conditions of Equations 6.10 through 6.12, the equilibrium expression of Equation 6.13 and the dimensionless quantities defined in Equation 6.17 into Equation 8.3 lead to

$$\varepsilon = \frac{F}{RT} \ln\left[E - E^0\right] - \ln\frac{3\,C_{G,S}}{C_F^0} = \ln\frac{a}{b\,g\,\kappa\,X_E} , \qquad (8.5)$$

where ε is the dimensionless potential difference between the electrode and bulk solution.

The time-dependent electrode potential in the linear-sweep voltammetry experiment can be written as

$$E = E_i + v\,t , \qquad (8.6)$$

where the initial electrode potential E_i is well positive or well negative of the voltammetric wave, and v is the sweep rate (V s^{-1}). The treatment presented in this chapter presumes that the sweep rate is small enough that the system is never far from equilibrium.

The current, i, that flows in response to the change in electrode potential is described by

$$i = \frac{dq}{dt} = F\,S\,x_c \frac{dC_B}{dt} = F\,S\,C_E\,x_c\,v \frac{F}{RT} \frac{db}{d\varepsilon} , \qquad (8.7)$$

where x_C is the thickness of the Nafion coating. The dimensionless current, φ, is defined by

$$\varphi = -\frac{i R T}{F Q_t v} = -\frac{db}{d\varepsilon}, \tag{8.8}$$

where $Q_t = FSC_E x_C$ is the total charge required to exhaustively oxidize or reduce the Nafion-incorporated complex. A positive sweep rate gives rise to anodic currents (negative i), whereas a negative sweep rate gives rise to cathodic currents (positive i). The shape of the voltammetric wave is independent of the direction of the linear sweep; we therefore choose to define the dimensionless current as always positive, hence the negative sign in Equation 8.8.

Introducing the parameter ρ characterizing the oxidation state of the redox system,

$$\rho = \frac{C_B}{C_A + C_C} = \frac{\kappa b}{a + \kappa c}, \tag{8.9}$$

the quantities a, b, and g may be calculated by means of

$$a = -\frac{1}{2}\left(\kappa\left(f^0 - \frac{3+2\rho}{1+\rho}\right) + f^0\right)$$

$$+\frac{1}{2}\left[\left(\kappa\left(f^0 - \frac{3+2\rho}{1+\rho}\right) + f^0\right)^2 + \frac{4\kappa f^0}{1+\rho}\right]^{1/2}, \tag{8.10}$$

$$b = \frac{\rho}{1+\rho}, \tag{8.11}$$

and

$$g = f^0 - \frac{3+2\rho}{1+\rho} . \tag{8.12}$$

Substitution, with differentiation where necessary, of Equations 8.10 through 8.12 into Equations 8.5 and 8.8 yields

$$\varepsilon = \ln\left[\frac{a}{\kappa X_E}\right] - \ln\left[\frac{\rho}{1+\rho}\left(f^0 - \frac{3+2\rho}{1+\rho}\right)\right] \tag{8.13}$$

and

$$\varphi = \frac{\rho}{1+\rho}\left[\frac{a+f^0}{(1+\rho)a^2+\kappa f^0}\kappa\rho + \frac{(f^0-1)\rho+(f^0-3)}{(f^0-2)\rho+(f^0-3)}\right]^{-1} . \tag{8.14}$$

Equations 8.13 and 8.14 permit calculation of the values of ε and φ associated with a particular oxidation state of the redox polymer, ion-pairing equilibrium constant, and fractional loading. The appropriate value for a is calculated by means of Equation 8.10. Equations 8.10, 8.13, and 8.14, therefore, enable the computation of dimensionless linear-sweep voltammograms, i.e., plots of φ vs. ε, corresponding to slow-scan conditions.

Characterization of Voltammetric Waves

A convenient means of characterizing the voltammetric wave is to identify the value of the peak current, φ_p, and the potential at which the peak current occurs, ε_p. The current maximum coincides with the

point where $d\varphi/d\rho = 0$, because $d\rho/d\varepsilon$ never vanishes. Equating the derivative of Equation 8.8 with respect to ρ with zero yields a complex expression, one of the roots of which, ρ_p, is the oxidation state of the redox polymer at the peak current and uniquely identifies φ_p and ε_p.

The full-width, $\Delta\varepsilon_{\pm}$, and half-widths, $\Delta\varepsilon_-$ and $\Delta\varepsilon_+$, of the voltammetric wave at half-maximum provide a measure of the wave's symmetry or lack thereof. The positions of the half-maxima, which correspond to the points where $\varphi=\varphi_p/2$, are identified by $\rho=\rho_-$ and $\rho=\rho_+$ or, alternately, $\varepsilon=\varepsilon_-$ and $\varepsilon=\varepsilon_+$. The full-width at half-maximum is defined by

$$\Delta\varepsilon_{\pm} = \varepsilon_+ - \varepsilon_- , \tag{8.15}$$

and the half-widths are defined by

$$\Delta\varepsilon_- = \varepsilon_p - \varepsilon_- \tag{8.16}$$

and

$$\Delta\varepsilon_+ = \varepsilon_+ - \varepsilon_p . \tag{8.17}$$

Voltammetric Behavior under Limiting Conditions

Limiting Behavior for $\kappa=0$

It is instructive to examine the slow-scan, linear-sweep voltammetric response expected when no ion-pairing equilibria exist,

$\kappa=0$, because this is the behavior predicted by a simple electron-hopping model.[22e] When $\kappa=0$, the parameter ρ is simply the ratio C_B/C_A; thus

$$\lim_{\kappa\to 0}\frac{a}{\kappa} = \frac{1}{1+\rho}, \tag{8.18}$$

and the dimensionless potential and current are defined by

$$\varepsilon = -\ln\left[\rho\left(f^0 - \frac{3+2\rho}{1+\rho}\right)X_E\right] \tag{8.19}$$

and

$$\varphi = \frac{\rho}{1+\rho}\left[\frac{(f^0-2)\rho+(f^0-3)}{(f^0-2)\rho^2+2(f^0-2)\rho+(f^0-3)}\right]. \tag{8.20}$$

Equating the derivative of φ, as defined in Equation 8.20, with respect to ρ with zero yields

$$0 = \rho_p^4 + 2\frac{f^0-3}{f^0-2}\rho_p^3 - \frac{2}{f^0-2}\rho_p^2 - 2\frac{f^0-3}{f^0-2}\rho_p - \left(\frac{f^0-3}{f^0-2}\right)^2. \tag{8.21}$$

The limiting behaviors at low ($f^0\to\infty$) and full ($f^0=3$) fractional loadings are described below.

Limiting behavior for low fractional loading

$$\varepsilon = -\ln[3\rho] \tag{8.22}$$

$$\varphi = \frac{\rho}{(1+\rho)^2} \tag{8.23}$$

The peak current and potential correspond to $\rho_p = 1$ and are approximately φ_p=0.2500 and ε_p=-1.0986; the full- and half-widths at half-maximum are $\Delta\varepsilon_{\pm}$=3.5255 and $\Delta\varepsilon_{-}=\Delta\varepsilon_{+}$=1.7627.

Limiting behavior for full fractional loading

$$\varepsilon = \ln\left[\frac{1+\rho}{\rho^2}\right] \tag{8.24}$$

$$\varphi = \frac{\rho}{(1+\rho)(2+\rho)} \tag{8.25}$$

The peak current and potential correspond to $\rho_p = \sqrt{2}$ and are approximately φ_p=0.1716 and ε_p=0.1882; the full- and half-widths at half-maximum are $\Delta\varepsilon_{\pm}$=5.1062, $\Delta\varepsilon_{-}$=2.2065, and $\Delta\varepsilon_{+}$=2.8997.

At low fractional loading the voltammetric wave is symmetric about the peak current with a full-width at half-maximum of 90.6 mV at 25°C, consistent with the classical voltammetric behavior for surface-confined, one-electron redox species.[37] The symmetry of the wave arises from the presence of a large excess of supporting electrolyte in the form of G^+ and F^- when X_E is near zero. Changes in the oxidation state of the redox system result in negligible changes in the concentration of G^+; hence there is no change in the Donnan potential.[38] At high fractional loadings, however, the concentration

of G^+ changes drastically leading to corresponding changes in the Donnan potential and the introduction of dissymmetry in the voltammetric wave.

Limiting Behavior for $\kappa > 100$

In examining the voltammetric behavior expected for large values of the ion-pairing equilibrium constant, we employ the approximations described for the strong ion-pairing limit, Case 3 in Chapter 6. In the strong ion-pairing limit, the rather cumbersome expression for a in Equation 8.10 simplifies to

$$a = \frac{f^0}{(f^0-2)\rho+(f^0-3)} . \tag{8.26}$$

Substitution of this expression into Equations 8.13 and 8.14 yields

$$\varepsilon = \ln\left[\frac{1}{3\rho}\left(\frac{(1+\rho)f^0}{(f^0-2)\rho+(f^0-3)}\right)^2\right] - \ln[\kappa] \tag{8.27}$$

and

$$\varphi = \frac{\rho}{1+\rho}\left[\frac{(f^0-2)\rho+(f^0-3)}{(f^0-2)\rho^2+(2f^0-3)\rho+(f^0-3)}\right] . \tag{8.28}$$

Notice that the position of the voltammetric wave shifts with $\ln[\kappa]$, consistent with classical voltammetric behavior.[39] Although the value of κ influences the position of the wave, it has no influence on

the shape of the wave or the shifts in the wave attributable to changes in the fractional loading.

Equating the derivative of φ, as defined in Equation 8.28, with respect to ρ with zero yields

$$0 = \rho_p^4 + 2\frac{f^0-3}{f^0-2}\rho_p^3 - \frac{2f^0-3}{(f^0-2)^2}\rho_p^2 - 2\frac{f^0-3}{f^0-2}\rho_p - \left(\frac{f^0-3}{f^0-2}\right)^2 . \tag{8.29}$$

The limiting behaviors at low ($f^0 \rightarrow \infty$) and full ($f^0=3$) fractional loadings are described below.

Limiting behavior for low fractional loading

$$\varepsilon = -\ln[3\rho] - \ln[\kappa] \tag{8.30}$$

$$\varphi = \frac{\rho}{(1+\rho)^2} \tag{8.31}$$

The peak current and potential correspond to $\rho_p = 1$ and are approximately φ_p=0.2500 and ε_p=-1.0986-ln[κ]; the full- and half-widths at half-maximum are $\Delta\varepsilon_{\pm}$=3.5255 and $\Delta\varepsilon_{-}=\Delta\varepsilon_{+}$=1.7627.

Limiting behavior for full fractional loading

$$\varepsilon = \ln\left[\frac{3(1+\rho)^2}{\rho^3}\right] - \ln[\kappa] \tag{8.32}$$

$$\varphi = \frac{\rho}{(1+\rho)(3+\rho)} \tag{8.33}$$

The peak current and potential correspond to $\rho_p = \sqrt{3}$ and are approximately φ_p=0.1340 and ε_p=1.4608-ln[κ]; the full- and half-widths at half-maximum are $\Delta\varepsilon_{\pm}$=6.4820, $\Delta\varepsilon_{-}$=2.5479, and $\Delta\varepsilon_{+}$=3.9342.

At low fractional loading, the voltammetric behavior is identical to that described for the case where κ=0 with the exception that the voltammetric wave shifts with ln[κ], *vide supra*. The insensitivity of the low fractional loading behavior, apart from the shift in the position of the wave, to the value of the equilibrium constant is attributable to the presence of a large excess of species G^+ and F^-. As the oxidation state of the redox system changes, there is no appreciable change in the concentration of F^-, and, therefore, no change in the ratio C_A/C_C.

In presenting the approximations associated with the strong ion-pairing limit in Chapter 6, it was noted that these approximations are not rigorously applicable when X_E=1. To be more precise, these approximations apply when X_E=1 only in the limit $\kappa\rightarrow\infty$, a condition with physically unrealistic implications. (For other values of X_E, it is only necessary that κ be large.) Our interest in writing Equations 8.32 and 8.33 is to examine a particular type of limiting behavior; within this context, predictions associated with $\kappa\rightarrow\infty$ are acceptable.

Limiting Behavior for X_E=0

The approximations appropriate for fractional loadings approaching zero have been described in detail in Chapter 6 in conjunction with the behavior of D_{ap} vs. X_E curves when $X_E\rightarrow 0$.

Utilization of these approximations in conjunction with Equations 6.22, 8.9, and 8.11 leads to

$$a = \frac{1}{1+\rho}\left(\frac{\kappa}{1+\kappa}\right). \tag{8.34}$$

Substitution of Equation 8.34 into Equations 8.13 and 8.14 yields

$$\varepsilon = -\ln[3\rho] - \ln[1+\kappa] \tag{8.35}$$

and

$$\varphi = \frac{\rho}{(1+\rho)^2}. \tag{8.36}$$

The peak current and potential always correspond to $\rho_p = 1$ and are approximately φ_p=0.2500 and ε_p=-1.0986-ln[κ+1]; the full- and half-widths at half-maximum are $\Delta\varepsilon_{\pm}$=3.5255 and $\Delta\varepsilon_{-}=\Delta\varepsilon_{+}$=1.7627.

Summary of Limiting Behaviors

A summary of the characteristics of slow-scan, linear-sweep voltammograms under various limiting conditions is presented in Table 8.1. In going from low to high fractional loading, there is a shift in the position of the peak current, a reduction in the magnitude of the peak current, and a distortion of the wave from the symmetric shape observed for small X_E. These effects arise from both the permselectivity of Nafion films and the ion-pairing reaction, though

ion-pairing with a large value for K produces the most extreme effect.

Quantity	Limiting Conditions				
	$\kappa=0$		κ	$\kappa>100$	
	$X_E=0$	$X_E=1$	$X_E=0$	$X_E=0$	$X_E=1$
ρ_p	1.0000	1.4142	1.0000	1.0000	1.7321
φ_p	0.2500	0.1716	0.2500	0.2500	0.1340
ε_p	-1.0986	0.1882	-1.0986-ln[1+κ]	-1.0986-ln[κ]	1.4608-ln[κ]
$\Delta\varepsilon_-$	1.7627	2.2065	1.7627	1.7627	2.5479
$\Delta\varepsilon_+$	1.7627	2.8997	1.7627	1.7627	3.9342
$\Delta\varepsilon_\pm$	3.5255	5.1062	3.5255	3.5255	6.4820

Table 8.1. Summary of the characteristics of slow-scan, linear-sweep voltammetric waves under various limiting conditions.

Calculated Voltammograms

Slow-scan, linear-sweep voltammograms calculated for X_E= 0.0, 0.5, 0.8, 0.9, 1.0 and κ= 0, 0.01, 0.1, 1.0, 10., ∞ are presented in Figure 8.1. The voltammograms in Figure 8.1 are plotted with reference to ε^*, which is defined by

$$\varepsilon^* = -\ln[3(1+\kappa)] . \tag{8.37}$$

The shift and decrease in the peak current and distortion of the voltammetric wave in going from low to high fractional loading are clearly evident. The magnitude of the ion-pairing equilibrium

Figure 8.1. Linear-sweep voltammograms calculated for κ= 0, 0.01, 0.1, 1.0, 10.0, ∞. The curves in each window correspond, from left to right (highest to lowest peak currents), to X_E = 0.0, 0.5, 0.8, 0.9, 1.0.

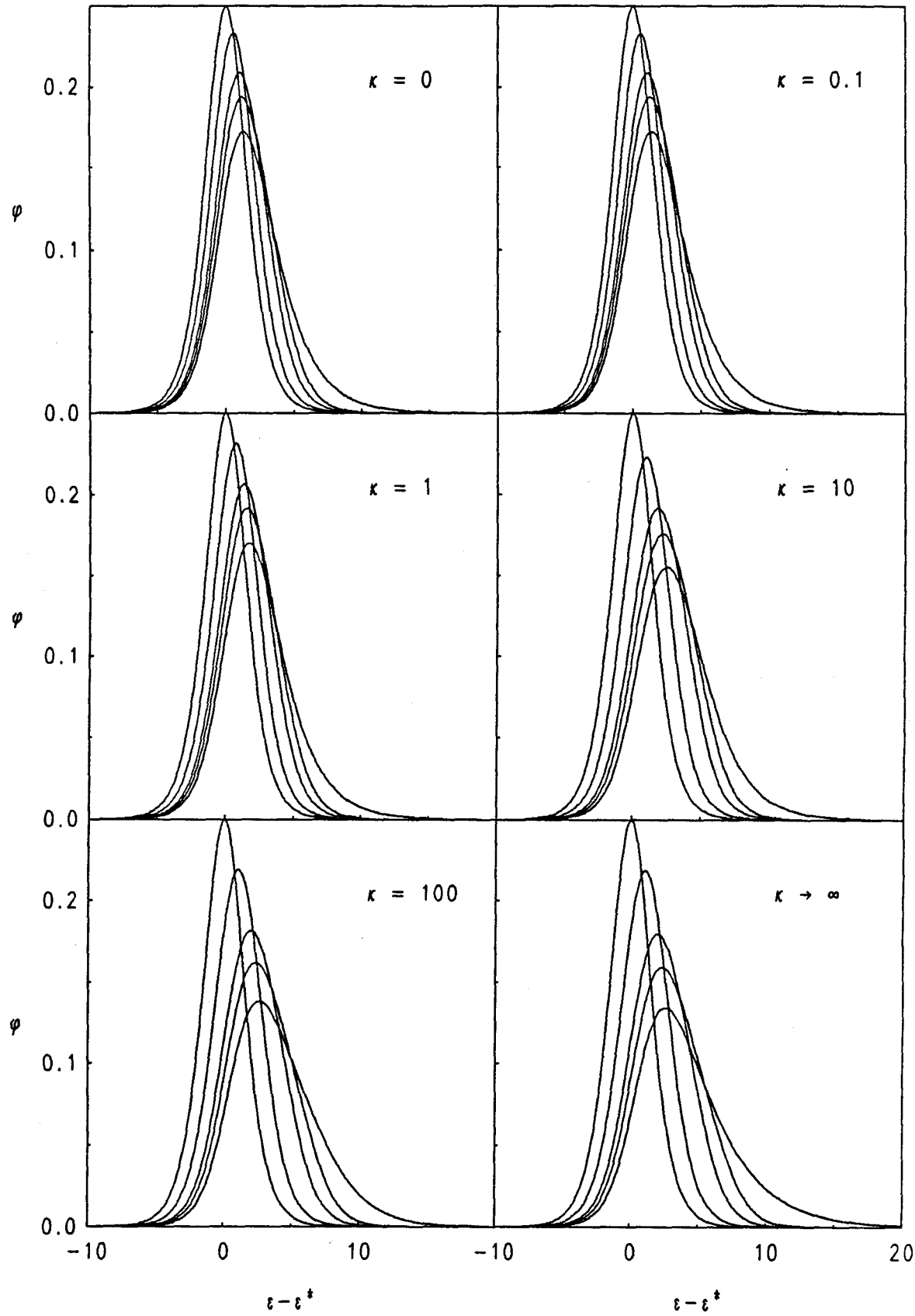
κ = 0
κ = 0.1
κ = 1
κ = 10
κ = 100
κ → ∞
φ
0.0
0.1
0.2
−10
0
10
20
ε − ε*

constant has a marked effect upon the shape of the curves. In principle, therefore, the analysis of the fractional loading dependence of experimental slow-scan, linear-sweep voltammograms could yield useful information regarding the degree of ion-pairing within the Nafion coating.

Comparison of Theoretical with Experimental Results

Three representative slow-scan cyclic voltammograms recorded using a Nafion-coated electrode containing electrostatically incorporated $Os(bpy)_3^{2+}$ at a fractional loading of X_E=0.88 are shown in Figure 8.2. These voltammograms do not correspond exactly to the achievement of equilibrium conditions, even at the lowest scan rates (2 mV s^{-1}), as is evident from the persistent difference, of the order of 15 to 20 mV, between the anodic and cathodic peak potentials. Although this deficiency prevents a rigorous quantitative testing of the validity of Equations 8.10, 8.13, and 8.14, a qualitative comparison of the predicted with the observed behavior seems worthwhile.

The variation of the observed peak currents of slow-scan voltammetric waves with the scan rate and with the fractional loading are compared with the predictions of the ion-pairing model in Table 8.2; a similar comparison of the half-widths at half-maximum is made in Table 8.3. The experimental peak currents, i_p, are presented in the normalized form, φ_p, defined in Equation 8.38.

$$\varphi_p = \frac{i_p R T}{F Q_t v} \tag{8.38}$$

Figure 8.2. Experimental slow-scan cyclic voltammograms recorded using a Nafion-coated electrode containing electrostatically bound $Os(bpy)_3^{2+}$. The fractional loading is X_E=0.88. The curves correspond, from smallest to largest peaks currents, to sweep rates of 2, 5, and 10 mV s^{-1}.

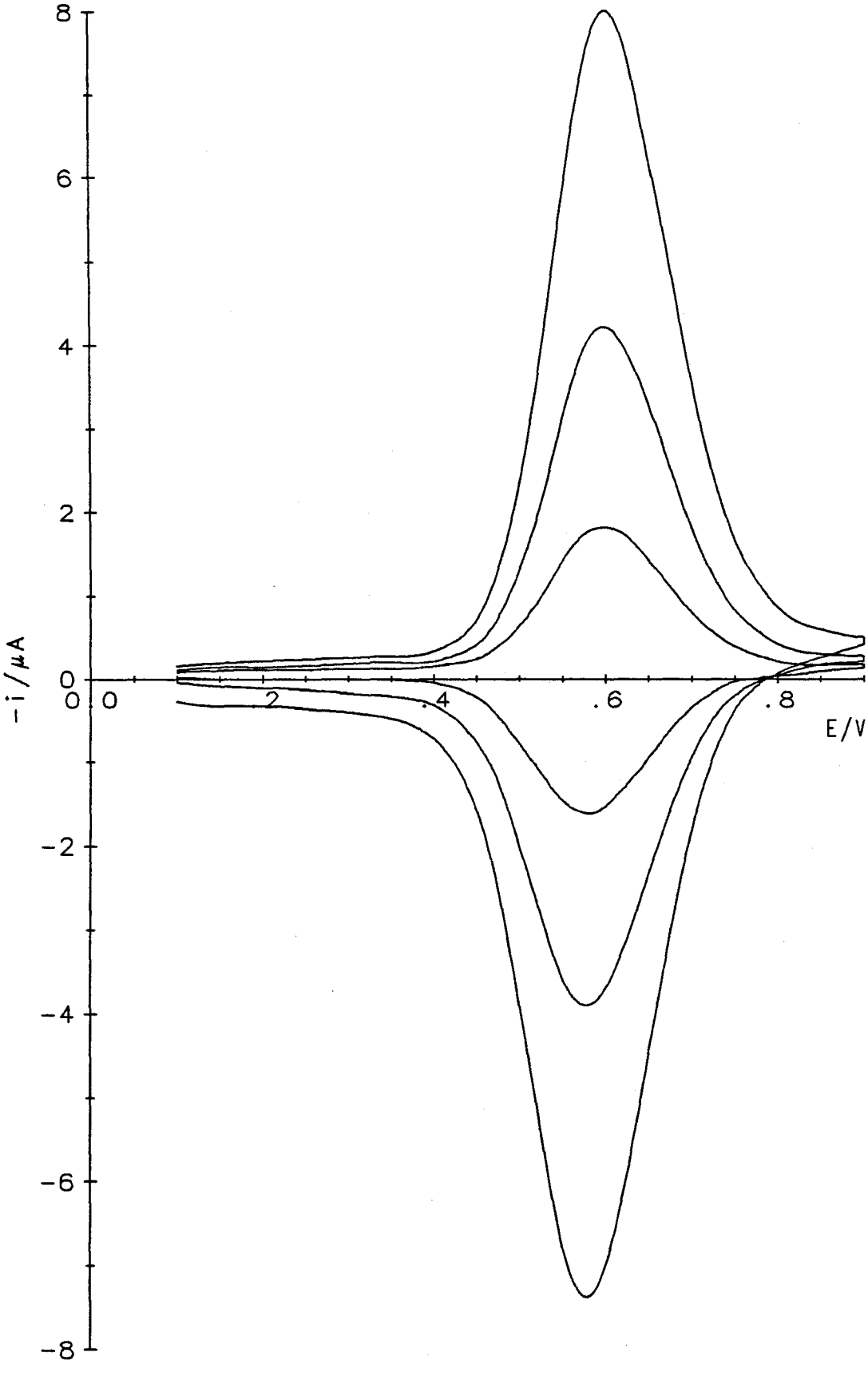
8
6
4
2
0
-2
-4
-6
-8
-i / μA
0.0
.2
.4
.6
.8
E/V

X_E	Q_t (μC)	Experimental			Theoretical	
		φ_p			φ_p	
		$v = 2$ mV s^{-1}	$v = 5$ mV s^{-1}	$v = 10$ mV s^{-1}	$\kappa = 11$	$\kappa > 100$
0.18	37	0.17	0.16	0.15	0.24	0.24
0.47	95	0.15	0.15	0.14	0.22	0.22
0.70	142	0.16	0.15	0.14	0.20	0.20
0.88	180	0.16	0.15	0.15	0.18	0.16
1.00	206	0.13	0.13	0.12	0.15	0.13

Table 8.2. Comparison of experimental and theoretical peak currents. Experimental data are taken from the anodic sweep of slow-scan cyclic voltammograms.

The experimental half-widths, measured in millivolts, are related to the dimensionless half-widths, $\Delta\varepsilon_-$ and $\Delta\varepsilon_+$, by

$$\Delta E_- = \frac{R\,T}{F}\Delta\varepsilon_- = \frac{R\,T}{F}(\varepsilon_m - \varepsilon_-) \tag{8.39}$$

and

$$\Delta E_+ = \frac{R\,T}{F}\Delta\varepsilon_+ = \frac{R\,T}{F}(\varepsilon_+ - \varepsilon_m)\,. \tag{8.40}$$

The experimental half-widths of the experimental waves at half-maximum are of the same order as predicted by the ion-pairing model. The voltammetric waves are almost symmetric at low fractional loading, but as X_E increases the waves become clearly dissymmetric in the direction predicted by the model (see Figure 8.1

and Table 8.3). The quantitative agreement between the observed and calculated values is not perfect, but inasmuch as true equilibrium conditions were not achievable, the behavior seems compatible with the ion-pairing model discussed in this report.

X_E	Experimental		Theoretical			
			$\kappa = 11$		$\kappa > 100$	
	ΔE_- (mV)	ΔE_+ (mV)	ΔE_- (mV)	ΔE_+ (mV)	ΔE_- (mV)	ΔE_+ (mV)
0.18	70	75	47.0	47.0	47.2	47.2
0.47	65	75	51.1	51.7	51.8	52.8
0.70	75	85	56.2	59.3	57.9	63.1
0.88	75	93	61.7	72.6	63.8	84.0
1.00	83	145	64.2	85.1	65.6	102.4

Table 8.3. Comparison of experimental and theoretical half-widths at half-maximum for voltammetric waves. Experimental data are taken from the anodic sweep of slow-scan, cyclic voltammograms recorded at v=2 mV s^{-1}.

Appendix III

Numerical Techniques

The Boundary Value Problem

As indicated previously, the mathematical description of the potential-step experiment leads to a boundary value problem of the form

$$0 = -\frac{u}{2}\frac{dg}{du} + \frac{d}{du}\left[f(g)\frac{dg}{du}\right], \qquad \text{(III.1)}$$

$$u = 0, \; g = g_0; \qquad u \to \infty, \; g = g_\infty . \qquad \text{(III.2)}$$

For many values of X_E, κ, and γ, the boundary value problem of Equations III.1 and III.2 is stiff, thereby creating considerable numerical difficulties. This feature of the problem, coupled with the inherently awkward nature of the semi-infinite boundary conditions, led us to employ the exponential transformation

$$z = \left(f^0 - 3\right) + \exp(-\alpha u) . \qquad \text{(III.3)}$$

The scaling factor, α, is a positive number that scales the value of dg/dz at $z=f^0-2$, i.e., the gradient of g at the electrode surface. Although the value of α is, in principle, arbitrary, choosing α so that dg/dz lies between 0.5 and 2.0 reduces the numerical difficulties encountered in the solution of the boundary value problem.

Introduction of the exponential transformation of Equation III.3 in the original boundary value problem (Equations III.1 and III.2) produces a new boundary value problem:

$$0 = \left(f(g) - \frac{1}{2\alpha^2} \ln\left[z - \left(f^0 - 3 \right) \right] \right) \frac{dg}{dz}$$

$$+ \left(z - \left(f^0 - 3 \right) \right) \left(f(g) \frac{d^2 g}{dz^2} + \frac{df(g)}{dg} \left(\frac{dg}{dz} \right)^2 \right), \qquad \text{(III.4)}$$

$$z = f^0 - 3, \quad g = g_\infty; \qquad z = f^0 - 2, \quad g = g_0 . \qquad \text{(III.5)}$$

The formulas presented in Chapter 6 require knowledge of the gradient of g with respect to u at the electrode surface. This quantity is given by

$$\left[\frac{dg}{du} \right]_{u=0} = -\alpha \left[\frac{dg}{dz} \right]_{z = f^0 - 2} . \qquad \text{(III.6)}$$

Finite Difference Methods

The boundary value problem posed by Equations III.4 and III.5 was solved numerically by means of the finite-difference technique. Our implementation of the finite-difference technique employed the center-difference formulas

$$\left[\frac{dg}{dz} \right]_i \cong \frac{g_{i+1} - g_{i-1}}{2h} \qquad \text{(III.7)}$$

and

$$\left[\frac{d^2 g}{dz^2} \right]_i \cong \frac{g_{i+1} - 2 g_i + g_{i-1}}{h^2} , \qquad \text{(III.8)}$$

where the subscript i indicates evaluation of the function at the point z_i. The points z_i for i= 0, 1,. .., n+1 are equally spaced on the interval [0,1]; the spacing between nodes is h=1/(n+1). The values of g_0 and g_{n+1} are established by the boundary conditions of Equation III.5 and are fractional-loading dependent. The error associated with the center-difference formulas of Equations III.7 and III.8 is of $O(h^2)$.

Substitution of the center-difference formulas into the differential Equation III.4 yields a nonlinear system of n equations:

$$0 = \left(f(g_i) - \frac{1}{2\alpha^2}\ln\left[i\,h - \left(f^0 - 3\right)\right]\right)\frac{g_{i+1} - g_{i-1}}{2h}$$

$$+\left(i\,h - \left(f^0 - 3\right)\right)\left(f(g_i)\frac{g_{i+1} - 2\,g_i + g_{i-1}}{h^2} + \left(\frac{df(g)}{dg}\right)_{g_i}\left(\frac{g_{i+1} - g_{i-1}}{2h}\right)^2\right) \qquad \text{(III.9)}$$

for i=1,2,...,n. The solution of this nonlinear system, g_i for i= 1, 2, ..., n, is the finite difference approximation of the solution of the relevant boundary value problem.

Once the numerical solution has been obtained, the gradient of g at the electrode surface ($z=f^0-2$) is approximated by

$$\left[\frac{dg}{dz}\right]_{z=f^0-2} = \frac{-3\,g_0 + 4\,g_1 - g_2}{2h}, \qquad \text{(III.10)}$$

which also has an error of $O(h^2)$.

The nonlinear system of equations, Equation III.9, was solved using Newton's method.[40] The derivatives $df(g)/dg$ and $d^2f(g)/dg^2$ were obtained by explicit differentiation of the appropriate expression for

f(g). The Jacobian matrix for this system is tridiagonal, permitting use of fast, direct-factorization techniques at each iteration of Newton's method; Crout's method[41] was employed in this study. In certain cases, particularly at high fractional loadings, convergence-acceleration techniques (Richardson extrapolation[42] and Shanks transformation[43]) were employed.

Computations

Computations were performed on a Digital Equipment VAX 11/750 or MicroVAX 3500 using programs written in VAX FORTRAN V4.7. Between 100 and 5000 nodes were utilized in the computations; all numerical solutions were computed to an accuracy of at least 0.01%.

Appendix IV

Programs for the Calculation of Apparent Diffusion Coefficients and Slow-Scan Linear-Sweep Voltammograms

Introduction

The programs for the calculation of apparent diffusion coefficients and slow-scan linear-sweep voltammograms were written in FORTRAN, employed double-precision arithmetic, and were executed on a Digital Equipment VAX 11/750 or MicroVAX 3500.

IONPAIR

The program IONPAIR computes ψ, $\psi^2 X_E$, and profiles for the dimensionless concentrations a, b, c, and g as well as the electric potential ϕ. The quantity $\psi^2 X_E$ is proportional to D_{ap}, as can be seen by inspection of Equation 6.31

Upon executing the program, the operator is asked to provide information regarding the initial loading of the Nafion coating, whether or not electric field effects are to be included in the computations, and the extent of ion-pairing. The responses to these questions are used to identify the limiting formulas from Chapter 6 to be used in the computations. If necessary, the operator is prompted for values for κ and/or γ. Next, the fractional loading, X_E, is requested.

Once the parameters for the ion-pairing model have been provided, the computer requests the parameters relating to the finite difference simulation: the tolerance, the maximum number of iterations, the number of points in the simulation, and the scaling parameter α. The tolerance is the convergence criterion for successful termination of Newton's method and is based upon the relative root-mean-square correction applied at a particular iteration. NOTE: the tolerance does NOT refer to the error in ψ! The

error in ψ is best estimated by examining the convergence of these quantities as the number of points in the finite difference simulation, n, is increased. If the maximum number of iterations is exceeded before the tolerance criterion is met, the program terminates. All parameters must be supplied as floating point quantities, with the exception of the maximum number of iterations and the number of simulation points that are integers. Finally, the user is requested to supply the names of the output files.

The program first performs the finite difference simulation, apprising the operator at each pass of the progress of Newton's method. Upon convergence, the values of ψ and $\psi^2 X_E$ are displayed along with the recommended value for α; the last task performed by the computer is to write the simulation results to the specified file and save the concentration and potential profiles, if so requested. The recommended value of α is reliable except for very large values of κ, in which case it can be too large.

The quantity ψ and the concentration profile a have the same significance as that described in Chapter 6 except when the limiting behavior for κ=0 (ion-pairing option "Z") is specified. In this case,

$$a = \frac{C_A}{C_E} \qquad \text{(IV.1)}$$

instead of the definition of Equation 6.17, and the chronoamperometric current and apparent diffusion coefficient are given by

$$i = FS\,C_E\left(\frac{D_1}{t}\right)^{1/2}\psi \qquad \text{(IV.2)}$$

and

$$D_{ap} = \frac{k_1 \delta^2 \pi}{18} C_F^0 \psi^2 X_E \,, \qquad \text{(IV.3)}$$

respectively. When electric field effects are taken into account (electric field option "E" and ion-pairing option "Z"), the results are identical with those obtained by Andrieux and Saveant[22e]; when electric field effects are not taken into account (electric field option "N" and ion-pairing option "Z"), the results are identical with those predicted by Equation 5.1; i.e., ψ is independent of X_E.

```
0001            PROGRAM IONPAIR
0002
0003      C     David N. Blauch          March 1989, Revised June 1990
0004      C     Caltech, Pasadena, CA  91125
0005      C
0006      C     For a discussion of the Contact Ion-Pairing Model
0007      C           D. N. Blauch, Ph.D. Thesis, Caltech, 1991
0008      C
0009      C     Electrochemical System:
0010      C           Nafion-coated electrode with 3+/2+ redox couple
0011      C           incorporated
0012      C
0013      C     Potential Step Experiment
0014      C           Oxidation of M(2+) to M(3+) or
0015      C           Reduction of M(3+) to M(2+)
0016      C
0017      C*************************************************************
0018      C
0019      C     GAMMA is the parameter gamma = K CF0 k2/k1
0020      C     KAPPA is the parameter kappa = K CF0
0021      C     G(i) is the finite difference approximation of g at z(i)
0022      C     J(i,j) is the Jacobian (which is tri-diagonal)
0023      C           i=1 points to the diagonal below the main diagonal
0024      C           i=2 points to the main diagonal
0025      C           i=3 points to the diagonal above the main diagonal
0026      C           j is the row number
0027      C     R(i) is the residual vector
0028      C     XE is the fractional loading of the Nafion film
0029      C     F0 is the dimensionless concentration of
0030      C           free sulfonate sites
0031      C     CA, CB, and CC are the dimensionless concentrations a or
0032      C           CA/CE, b, and c, respectively
0033      C     P is the dimensionless electric potential
0034      C     FI, DFI, and DDFI correspond to f(g), df/dg, and d2f/dg2
0035      C
0036      C*************************************************************
0037            INTEGER I,IERR,CNT,N,MAX
0038            DOUBLE PRECISION G(5000),J(5000,3),R(5000)
0039            DOUBLE PRECISION KAPPA,K2,K3,K4,GAMMA,CON
0040            DOUBLE PRECISION XE,F0,F2,F3
0041            DOUBLE PRECISION H,H2,H4,HH,HH2,HH4,Z,ZZ,DG,G0,GNP1
0042            DOUBLE PRECISION PREC,ERR,SLOPE,A,AA,AA2
0043            DOUBLE PRECISION PSI,D,TMP,A0
0044            DOUBLE PRECISION U,CA,CB,CC,P
0045            DOUBLE PRECISION FI,DFI,DDFI
0046            CHARACTER*1 SEXP,SEF,SIP,SOUT
0047            CHARACTER*12 FOUT,FOUTA,FOUTB,FOUTC,FOUTG,FOUTP
0048
0049            EXTERNAL CROUT,FG
0050            COMMON /OPT/SEXP,SEF,SIP,SOUT/CRTRED/J,R/FUNC/FI,DFI,DDFI
0051            COMMON /COND/XE,F0,F2,F3,KAPPA,K2,K3,K4,GAMMA,CON
0052
0053      C*************************************************************
0054            WRITE (6,10)
0055      10    FORMAT (//25X,'Apparent Diffusion Coefficients',
0056           *       /19X,'for Charge Propagation in a Nafion Coating',
```

```
0057          *       /24X,'Containing a Metal(3+/2+) Complex',
0058          *       //1X,'Initial experimental conditions:',
0059          *       /10X,'R - coating loaded with M(2+) complex',
0060          *       /10X,'O - coating loaded with M(3+) complex',
0061          *       /1X,'Option for initial conditions ?  ',$)
0062                  READ (5,20) SEXP
0063      20          FORMAT (A1)
0064                  IF ((SEXP.NE.'R').AND.(SEXP.NE.'O')) THEN
0065                        WRITE (6,30)
0066      30                FORMAT (1X,'Invalid Response')
0067                        STOP
0068                  ENDIF
0069
0070                  WRITE (6,35)
0071      35          FORMAT (/1X,'Options regarding Electric Field Effects:',
0072          *       /10X,'E - Electric Field Effects Included',
0073          *       /10X,'N - Electric Field Effects Not Included',
0074          *       /1X,'Option ? ',$)
0075                  READ (5,20) SEF
0076                  IF ((SEF.NE.'E').AND.(SEF.NE.'N')) THEN
0077                        WRITE (6,30)
0078                        STOP
0079                  ENDIF
0080
0081                  WRITE (6,40)
0082      40          FORMAT (/1X,'Options regarding Ion-Pairing: ',
0083          * /10X,'G - Case 1:  general treatment, arbitrary kappa',
0084          * /10X,'A - Case 2:  A+/B pathway only, gamma=0',
0085          * /10X,'S - Case 3:  strong, ion-pairing limit, kappa>100',
0086          * /10X,'Z -          limiting behavior for kappa=0',
0087          * /1X,'Option ?  ',$)
0088                  READ (5,20) SIP
0089                  IF ((SIP.EQ.'A').OR.(SIP.EQ.'G')) THEN
0090                        WRITE (6,50)
0091      50                FORMAT (1X,'Value of kappa ?  ',$)
0092                        READ (5,60) KAPPA
0093      60                FORMAT (D16.9)
0094                        IF (KAPPA.LE.0.D0) THEN
0095                              WRITE (6,30)
0096                              STOP
0097                        ENDIF
0098                  ENDIF
0099                  IF ((SIP.EQ.'G').OR.(SIP.EQ.'S')) THEN
0100                        WRITE (6,70)
0101      70                FORMAT (1X,'Value of gamma ?  ',$)
0102                        READ (5,60) GAMMA
0103                        IF (GAMMA.LE.0.D0) THEN
0104                              GAMMA=0.D0
0105                        ENDIF
0106                  ENDIF
0107                  IF ((SIP.NE.'G').AND.(SIP.NE.'A').AND.(SIP.NE.'S')
0108              *       .AND.(SIP.NE.'Z')) THEN
0109                        WRITE (6,30)
0110                        STOP
0111                  ENDIF
0112
```

```
0113            WRITE (6,80)
0114     80     FORMAT (/1X,'Fractional loading ?  ',$)
0115            READ (5,60) XE
0116            IF ((XE.LE.0.D0).OR.(XE.GT.1.D0).OR.
0117           * (XE.EQ.1.D0).AND.((SIP.EQ.'S').OR.(SIP.EQ.'G'))) THEN
0118                  WRITE (6,30)
0119                  STOP
0120            ENDIF
0121
0122            WRITE (6,100)
0123     100    FORMAT (/1X,'Options for finite difference simulations:',
0124           *       /1X,'Tolerance (relative rms error) ?  ',$)
0125            READ (5,60) PREC
0126            IF (PREC.LE.0.D0) THEN
0127                  PREC=1.D-8
0128            ENDIF
0129            WRITE (6,110)
0130     110    FORMAT (1X,'Maximum number of iterations ?  ',$)
0131            READ (5,120) MAX
0132     120    FORMAT (I8)
0133            IF (MAX.LE.0) THEN
0134                  MAX=20
0135            ENDIF
0136            WRITE (6,130)
0137     130    FORMAT (1X,'Number of points in simulation ?  ',$)
0138            READ (5,120) N
0139            IF (N.LE.0) THEN
0140                  N=1000
0141            ELSE IF (N.GT.5000) THEN
0142                  N=5000
0143            ENDIF
0144            WRITE (6,140)
0145     140    FORMAT (1X,'Value for scaling parameter alpha ?  ',$)
0146            READ (5,60) A
0147            IF (A.LE.0D0) THEN
0148                  A=1.D0
0149            ENDIF
0150
0151            WRITE (6,145)
0152     145    FORMAT (/1X,'Filename for simulation results ?  ',$)
0153            READ (5,170) FOUT
0154            WRITE (6,150)
0155     150    FORMAT (1X,'Save conc. and potential profiles ?  ',$)
0156            READ (5,20) SOUT
0157            IF (SOUT.EQ.'Y') THEN
0158                  WRITE (6,160)
0159     160          FORMAT (10X,'Filename for profile of a ?  ',$)
0160                  READ (5,170) FOUTA
0161     170          FORMAT (A12)
0162                  WRITE (6,180)
0163     180          FORMAT (10X,'Filename for profile of b ?  ',$)
0164                  READ (5,170) FOUTB
0165                  IF (SIP.NE.'Z') THEN
0166                  WRITE (6,190)
0167     190          FORMAT (10X,'Filename for profile of c ?  ',$)
0168                  READ (5,170) FOUTC
```

```
0169                ENDIF
0170                WRITE (6,200)
0171    200         FORMAT (10X,'Filename for profile of g ?  ',$)
0172                READ (5,170) FOUTG
0173                IF (SEF.EQ.'E') THEN
0174                WRITE (6,210)
0175    210         FORMAT (10X,'Filename for potential profile ?  ',$)
0176                READ (5,170) FOUTP
0177                ENDIF
0178          ENDIF
0179
0180          WRITE (6,250)
0181    250   FORMAT (1X)
0182
0183    C*****************************************************************
0184    C     Perform various preliminary tasks
0185    C
0186    C     Initialize the iteration counter
0187          CNT=0
0188
0189    C     Determine the interval size
0190          H=1.D0/DBLE(REAL(N+1))
0191
0192    C     Calculate various constants which appear in the formulas
0193          F0=3.D0/XE
0194          F2=F0-2.D0
0195          F3=F0-3.D0
0196          IF ((SIP.EQ.'A').OR.(SIP.EQ.'G')) THEN
0197                K2=KAPPA*KAPPA
0198                K3=K2*KAPPA
0199                K4=K3*KAPPA
0200          ENDIF
0201          H2=2.D0*H
0202          H4=4.D0*H
0203          HH=H*H
0204          HH2=2.D0*HH
0205          HH4=4.D0*HH
0206          AA2=2.D0*A*A
0207          IF (SIP.EQ.'A') THEN
0208                CON=1.D0
0209                GAMMA=0.D0
0210          ELSE IF (SIP.EQ.'G') THEN
0211                CON=1.D0-GAMMA/KAPPA
0212          ENDIF
0213
0214    C     Establish the boundary conditions
0215    C           G0 corresponds to z0=f0-3
0216    C           GNP1 corresponds to zNP1=f0-2
0217          IF (SEXP.EQ.'R') THEN
0218    C           Film is loaded with M(2+)
0219                G0=F2
0220                GNP1=F3
0221          ELSE
0222    C           Film is loaded with M(3+)
0223                G0=F3
0224                GNP1=F2
```

```
0225            ENDIF
0226
0227    C       The initial approximation is a straight line
0228    C             The slope depends upon the boundary conditions
0229            DO 300, I=1,N
0230                  IF (SEXP.EQ.'R') THEN
0231    C                   Film is loaded with M(2+)
0232    C                         the slope is negative
0233                        G(I)=F2-H*DBLE(REAL(I))
0234                  ELSE
0235    C                   Film is loaded with M(3+)
0236    C                         the slope is positive
0237                        G(I)=F3+H*DBLE(REAL(I))
0238                  ENDIF
0239    300     CONTINUE
0240
0241
0242    C*************************************************************
0243    C       Finite Difference Approximation of the Solution
0244    C             The vector G() contains the current approximation
0245    C             for g(z);  each pass revises the approximation
0246
0247    C       Newton's Method is employed at each pass to obtain the
0248    C             next approximation.  The residuals vector, R(), and
0249    C             the Jacobian, J(,), are computed.  The correction
0250    C             vector, x, is found by solving the linear system:
0251    C                         J x = R
0252    C       Crout Reduction is used to obtain x.  The EXTERNAL
0253    C             SUBROUTINE CROUT uses the data in COMMON BLOCK
0254    C             /CRTRED/J,R.  The algorithm alters the contents of
0255    C             J and returns the vector x in R.
0256
0257    C       Note that since J is tri-diagonal, only the central
0258    C             diagonals are stored.
0259
0260    C       re-entry point for each iteration
0261    500     CONTINUE
0262
0263    C       increment the loop counter
0264            CNT=CNT+1
0265
0266    C       have we exceeded the iteration limit?
0267            IF (CNT.GT.MAX) THEN
0268                  WRITE (6,550)
0269    550           FORMAT (/1X,'%%  Max. nbr. of iterations exceeded')
0270                  STOP
0271            ENDIF
0272
0273    C       element i is G0
0274    C       The subroutine FG(G) calculates the values f(g), f'(g),
0275    C             and f''(g)
0276            CALL FG(G(1))
0277            DG=G(2)-G0
0278
0279    C       Evaluate element 1 of vector R
0280            R(1)=(DLOG(H)/AA2-FI)*DG/H2-H*FI*(G(2)-2.D0*G(1)+G0)/HH
```

```
0281          *       -H*DFI*DG*DG/HH4
0282
0283      C     Construct row 1 of the Jacobian
0284            J(1,1)=0.D0
0285            J(1,2)=-DFI*DG/H2+2.D0*FI/H-DFI*(G(2)-2.D0*G(1)+G0)/H
0286          *       -DDFI*DG*DG/H4
0287            J(1,3)=(DLOG(H)/AA2-FI)/H2-FI/H-DFI*DG/H2
0288
0289      C     Construct the interior elements
0290            DO 600, I=2,N-1
0291                  Z=F3+H*DBLE(REAL(I))
0292                  ZZ=Z-F3
0293      C           Evaluate FI, DFI, and DDFI
0294                  CALL FG(G(I))
0295                  DG=G(I+1)-G(I-1)
0296
0297      C           Evaluate element I of vector R
0298                  R(I)=(DLOG(ZZ)/AA2-FI)*DG/H2
0299          *             -ZZ*FI*(G(I+1)-2.D0*G(I)+G(I-1))/HH
0300          *             -ZZ*DFI*DG*DG/HH4
0301
0302      C           Construct row I of the Jacobian
0303                  J(I,1)=(FI-DLOG(ZZ)/AA2)/H2
0304          *             -ZZ*FI/HH+ZZ*DFI*DG/HH2
0305                  J(I,2)=-DFI*DG/H2+2.D0*ZZ*FI/HH
0306          *             -ZZ*DFI*(G(I+1)-2.D0*G(I)+G(I-1))/HH
0307          *             -ZZ*DDFI*DG*DG/HH4
0308                  J(I,3)=(DLOG(ZZ)/AA2-FI)/H2
0309          *             -ZZ*FI/HH-ZZ*DFI*DG/HH2
0310
0311      600   CONTINUE
0312
0313      C     element N+1 is FNP1
0314            ZZ=1.D0-H
0315            CALL FG(G(N))
0316            DG=GNP1-G(N-1)
0317
0318      C     Evaluate element N of vector R
0319            R(N)=(DLOG(ZZ)/AA2-FI)*DG/H2-ZZ*FI*(GNP1-2.D0*G(N)
0320          *       +G(N-1))/HH-ZZ*DFI*DG*DG/HH4
0321
0322      C     Construct row N of the Jacobian
0323            J(N,1)=(FI-DLOG(ZZ)/AA2)/H2-ZZ*FI/HH+ZZ*DFI*DG/HH2
0324            J(N,2)=-DFI*DG/H2+2.D0*ZZ*FI/HH-ZZ*DFI*
0325          *       (GNP1-2.D0*G(N)+G(N-1))/HH-ZZ*DDFI*DG*DG/HH4
0326            J(N,3)=0.D0
0327
0328
0329      C     Obtain the next approximation
0330      C     The correction vector is returned in R()
0331            CALL CROUT(N)
0332
0333      C     Compute the revised conc. profile and estimate the error
0334            ERR=0.D0
0335            IERR=0
0336            DO 700, I=1,N
```

```
0337    C             Add the correction vector to the old approximation
0338    C                   to obtain the new approximation
0339                  G(I)=G(I)-R(I)
0340    C             Estimate the relative error
0341    C             If G(I)=0, drop that point from the error estimate
0342                  IF (G(I).NE.0.D0) THEN
0343                        ERR=ERR+(R(I)/G(I))**2
0344                        IERR=IERR+1
0345                  ENDIF
0346    700     CONTINUE
0347    C       Estimate the root mean square of the relative error
0348            ERR=DSQRT(ERR/DBLE(REAL(IERR)))
0349
0350            WRITE (6,720) CNT,ERR
0351    720     FORMAT (1X,'Pass ',I3,10X,'rel. rms error =  ',D16.9)
0352
0353    C       Are we within tolerance?
0354    C       If not, repeat the iteration loop
0355            IF (ERR.GT.PREC) GOTO 500
0356
0357    C*************************************************************
0358    C       Finite Difference Simulation has converged to within the
0359    C             specified precision.  Compute the final quantities
0360    C
0361    C       Calc. the slope dg/dz at the electrode surface (z=f0-2)
0362    C             recall that dg/du = - alpha dg/dz
0363            SLOPE=(3.D0*GNP1-4.D0*G(N)+G(N-1))/H2
0364
0365    C       formulas for PSI for all cases are the same regardless of
0366    C             whether or not electric field effects are included
0367            IF (SIP.EQ.'Z') THEN
0368    C       No ion-pairing, kappa=0
0369            IF ((XE.EQ.1.D0).AND.(SEXP.EQ.'R').AND.(SEF.EQ.'E')) THEN
0370                  PSI=2.D0*A*SLOPE
0371            ELSE
0372                  PSI=A*SLOPE
0373            ENDIF
0374            ELSE IF (SIP.EQ.'S') THEN
0375    C             Strong ion-pairing limit, kappa>100
0376                  PSI=A*(GAMMA+F0/GNP1)*SLOPE
0377            ELSE IF (SEXP.EQ.'R') THEN
0378    C       Coating loaded with M(2+)
0379            TMP=F0+KAPPA*F3
0380            A0=(DSQRT(TMP*TMP+4.D0*KAPPA*F0)-TMP)/2.D0
0381            IF ((XE.EQ.1.D0).AND.(SIP.EQ.'A').AND.(SEF.EQ.'E')) THEN
0382    C             Special conditions for full loading
0383                  PSI=2.D0*A*A0*SLOPE
0384            ELSE
0385                  PSI=A*(GAMMA+CON*A0)*SLOPE
0386            ENDIF
0387            ELSE
0388    C             Coating loaded with M(3+)
0389                  PSI=A*(GAMMA+CON*KAPPA*F0/(F0+KAPPA*F2))*SLOPE
0390            ENDIF
0391
0392    C       Calculate the dimensionless diffusion coefficient
```

```
0393            D=XE*PSI*PSI
0394
0395      C     Compute the optimal value for alpha
0396            IF (SEXP.EQ.'R') THEN
0397                  AA=DABS(2.D0*A*SLOPE)
0398            ELSE
0399                  AA=DABS(0.5D0*A*SLOPE)
0400            ENDIF
0401
0402      C*************************************************************
0403      C     Print the results
0404      C
0405            WRITE (6,1000) PSI,D,AA
0406      1000  FORMAT (//1X,'psi =  ',D16.9,/1X,'psi*psi*XE =  ',D16.9,
0407           *      //1X,'recommended value for alpha =  ',D16.9)
0408
0409            OPEN (1,FILE=FOUT,STATUS='NEW')
0410
0411            WRITE (1,1100)
0412      1100  FORMAT (11X,'Finite Difference Simulation of a ',
0413           *      'Potential Step Experiment',
0414           *      /24X,'for the Contact Ion-Pairing Model')
0415            IF (SEXP.EQ.'R') THEN
0416                  WRITE (1,1105)
0417      1105        FORMAT (/1X,'Coating loaded with M(2+) complex')
0418            ELSE
0419                  WRITE (1,1106)
0420      1106        FORMAT (/1X,'Coating loaded with M(3+) complex')
0421            ENDIF
0422            IF (SIP.EQ.'Z') THEN
0423                  WRITE (1,1110)
0424      1110        FORMAT (/1X,'Limiting behavior for kappa=0')
0425            ELSE IF (SIP.EQ.'S') THEN
0426                  WRITE (1,1120) GAMMA
0427      1120        FORMAT (/1X,'Strong ion-pairing limit, kappa>100',
0428           *            /10X,'gamma =  ',D16.9)
0429            ELSE IF (SIP.EQ.'A') THEN
0430                  WRITE (1,1140) KAPPA
0431      1140        FORMAT (/1X,'A+/B pathway only, gamma=0',
0432           *            /10X,'kappa =  ',D16.9)
0433            ELSE
0434                  WRITE (1,1150) KAPPA,GAMMA
0435      1150        FORMAT (/1X,'General treatment',
0436           *            /10X,'kappa =  ',D16.9,
0437           *            /10X,'gamma =  ',D16.9)
0438            ENDIF
0439            IF (SEF.EQ.'E') THEN
0440                  WRITE (1,1160)
0441      1160        FORMAT (/1X,'Calculations include the effect of ',
0442           *            'the electric field')
0443            ELSE
0444                  WRITE (1,1170)
0445      1170        FORMAT (/1X,'Calculations do not include the ',
0446           *            'effect of the electric field')
0447            ENDIF
0448            WRITE (1,1180) XE
```

```
0449    1180   FORMAT (/1X,'Fractional loading =  ',F8.6)
0450           WRITE (1,1200) N,PREC,MAX,CNT,A,PSI,D,AA
0451    1200   FORMAT (/1X,'Simulation parameters:',
0452         *       /10X,'Number of points =  ',I5,
0453         *       /10X,'Relative rms tolerance for convergence =  ',
0454         *       D16.9,/10X,'Maximum number of iterations =  ',I5,
0455         *       /10X,'Number of iterations required =  ',I5,
0456         *       /10X,'scaling parameter alpha =  ',D16.9,
0457         *       //1X,'psi =  ',D16.9,
0458         *       /1X,'psi*psi*XE =  ',D16.9,
0459         *       //1X,'recommended value for alpha =  ',D16.9)
0460
0461           CLOSE (1)
0462
0463    C*****************************************************************
0464    C      Save the concentration and potential profiles, if
0465    C           necessary
0466    C      All concentration profiles are dimensionless
0467    C      the values of b=CB/CE, c=CC/CE, and g=CG/CE are saved
0468    C      the value of a=kappa*CA/CE is saved, except for option
0469    C      Z where a=CA/CE is saved
0470    C      The potential profile is dimensionless
0471    C      The independent variable in the output files is u not z
0472    C
0473           IF (SOUT.EQ.'Y') THEN
0474                 OPEN (1,FILE=FOUTA,STATUS='NEW')
0475                 OPEN (2,FILE=FOUTB,STATUS='NEW')
0476                 IF (SIP.NE.'Z') THEN
0477    C                  Open file for C only if kappa is non-zero
0478                       OPEN (3,FILE=FOUTC,STATUS='NEW')
0479                 ENDIF
0480                 OPEN (4,FILE=FOUTG,STATUS='NEW')
0481                 IF (SEF.EQ.'E') THEN
0482    C                  save the electric potential profile only if
0483    C                  computations include electric field effects
0484                       OPEN (5,FILE=FOUTP,STATUS='NEW')
0485                 ENDIF
0486
0487    1500         FORMAT (1X,D14.7,',',D14.7)
0488
0489    C            The last point corresponds to the electrode surface
0490                 IF (SEXP.EQ.'R') THEN
0491    C                  Coating loaded with M(2+)
0492                       IF (SIP.EQ.'Z') THEN
0493                             WRITE (1,1500) 0.0,1.0
0494                       ELSE
0495                             IF (SIP.EQ.'S') THEN
0496                                   CA=F0/F3
0497                                   CC=1.D0
0498                             ELSE
0499                                   TMP=KAPPA*F3+F0
0500                                   CA=(DSQRT(TMP*TMP+4.D0*KAPPA
0501         *                                *F0)-TMP)/2.D0
0502                                   CC=1.D0-CA/KAPPA
0503                             ENDIF
0504                             WRITE (1,1500) 0.0,CA
```

```
0505                              WRITE (3,1500) 0.0,CC
0506                        ENDIF
0507                        WRITE (2,1500) 0.0,0.0
0508                        WRITE (4,1500) 0.0,F3
0509                        IF ((SEF.EQ.'E').AND.(XE.NE.1.D0)) THEN
0510                              WRITE (5,1500) 0.0,0.0
0511                        ENDIF
0512                  ELSE
0513     C                  Coating loaded with M(3+)
0514                        WRITE (1,1500) 0.0,0.0
0515                        WRITE (2,1500) 0.0,1.0
0516                        IF (SIP.NE.'Z') THEN
0517                              WRITE (3,1500) 0.0,0.0
0518                        ENDIF
0519                        WRITE (4,1500) 0.0,F2
0520                        IF (SEF.EQ.'E') THEN
0521                              WRITE (5,1500) 0.0,0.0
0522                        ENDIF
0523                  ENDIF
0524
0525                  DO 2000, I=N,1,-1
0526                        Z=F3+H*DBLE(REAL(I))
0527                        U=-DLOG(Z-F3)/A
0528
0529                        CB=G(I)-F3
0530
0531                        IF (SIP.EQ.'Z') THEN
0532                              CA=1.D0-CB
0533                        ELSE
0534                              IF (SIP.EQ.'S') THEN
0535                                    CA=(F2-G(I))*F0/G(I)
0536                                    CC=1.D0-CB
0537                              ELSE
0538                                    TMP=F0-KAPPA*G(I)
0539                                    CA=(DSQRT(TMP*TMP+4.D0*KAPPA
0540           *                        *F0*F2)-F0-KAPPA*G(I))/2.D0
0541                                    CC=1.D0-CB-CA/KAPPA
0542                              ENDIF
0543                              WRITE (3,1500) U,CC
0544                        ENDIF
0545
0546                        WRITE (1,1500) U,CA
0547                        WRITE (2,1500) U,CB
0548                        WRITE (4,1500) U,G(I)
0549
0550                        IF (SEF.EQ.'E') THEN
0551                        IF ((XE.EQ.1.D0).AND.(SEXP.EQ.'R')) THEN
0552                              P=-DLOG(G(I))
0553                        ELSE
0554                              P=DLOG(GNP1/G(I))
0555                        ENDIF
0556                        WRITE (5,1500) U,P
0557                        ENDIF
0558
0559     2000           CONTINUE
0560
```

```
0561    C             Bulk solution possesses u -> infinity and
0562    C                   hence cannot be written
0563
0564                  CLOSE (1)
0565                  CLOSE (2)
0566                  IF (SIP.NE.'Z') THEN
0567                        CLOSE (3)
0568                  ENDIF
0569                  CLOSE (4)
0570                  IF (SEF.EQ.'E') THEN
0571                        CLOSE (5)
0572                  ENDIF
0573            ENDIF
0574
0575            END

0001
0002    C$$$$$$$$$$$$$$$$$$$$$$$$$$$$$$$$$$$$$$$$$$$$$$$$$$$$$$$$$$$$$$$$$$$
0003
0004            SUBROUTINE FG(G)
0005
0006    C       evaluation of
0007    C             FI   = f(g)
0008    C             DFI  = (df/dg)
0009    C             DDFI = d2f/dg2
0010    C
0011    C***************************************************************
0012            DOUBLE PRECISION XE,F0,F2,F3,KAPPA,K2,K3,K4,GAMMA
0013            DOUBLE PRECISION FI,DFI,DDFI
0014            DOUBLE PRECISION A,DA,DDA,DDDA,TMP,SQ,CON
0015            DOUBLE PRECISION G,G2,G3,G4
0016            CHARACTER*1 SEXP,SEF,SIP,SOUT
0017
0018            COMMON /OPT/SEXP,SEF,SIP,SOUT/FUNC/FI,DFI,DDFI
0019            COMMON /COND/XE,F0,F2,F3,KAPPA,K2,K3,K4,GAMMA,CON
0020
0021    C***************************************************************
0022            G2=G*G
0023            G3=G2*G
0024            G4=G3*G
0025
0026            IF (SIP.EQ.'Z') THEN
0027    C             No Ion Pairing Case, kappa=0
0028                  IF (SEF.EQ.'N') THEN
0029    C                   Omit Electric Field Effects
0030                        FI=-1.D0
0031                        DFI=0.D0
0032                        DDFI=0.D0
0033                  ELSE IF (XE.EQ.1.D0) THEN
0034    C                   Full Loading Case with Electric Field Effects
0035                        FI=G-F0+1.D0
0036                        DFI=1.D0
0037                        DDFI=0.D0
0038                  ELSE
0039    C                   Fractional Loading less than unity
0040    C                         with Electric Field Effects Included
```

```
0041                    FI=G-2.D0*F2+F2*F3/G
0042                    DFI=1.D0-F2*F3/G2
0043                    DDFI=2.D0*F2*F3/G3
0044                ENDIF
0045              ELSE IF (SIP.EQ.'S') THEN
0046    C               Strong Ion-Pairing Limit
0047                IF (SEF.EQ.'N') THEN
0048    C                   Electric Field Effects Not Included
0049                    FI=F0*(1.D0+F2*(-2.D0+F3/G)/G)-GAMMA
0050                    DFI=2.D0*F0*F2*(1.D0-F3/G)/G2
0051                    DDFI=2.D0*F0*F2*(-2.D0+3.D0*F3/G)/G3
0052                ELSE
0053    C                   Electric Field Effects Included
0054                    FI=2.D0*F0+(G-2.D0*F2)*GAMMA
0055           *                +(-(4.D0*F0-9.D0)*F0
0056           *                +F2*F3*(GAMMA+2.D0*F0/G))/G
0057                    DFI=GAMMA+((4.D0*F0-9.D0)*F0
0058           *                -F2*F3*(GAMMA+4.D0*F0/G))/G2
0059                    DDFI=2.D0*(-(4.D0*F0-9.D0)*F0
0060           *                +F2*F3*(GAMMA+6.D0*F0/G))/G3
0061                ENDIF
0062              ELSE IF ((XE.EQ.1.D0).AND.(SIP.EQ.'A')
0063           *       .AND.(SEF.EQ.'E')) THEN
0064    C               Full loading with Case 2 and E-Field effects incl.
0065                TMP=DSQRT(12.D0*KAPPA+(3.D0-KAPPA*G)**2)
0066                FI=(6.D0+KAPPA*G)/2.D0-(K2*G2-9.D0*KAPPA*G
0067           *            +18.D0+24.D0*KAPPA)/(2.D0*TMP)
0068                DFI=0.5D0*KAPPA-(K3*G3-9.D0*K2*G2+27.D0*KAPPA
0069           *             *G-27.D0-36.D0*KAPPA)*KAPPA/(2.D0*TMP**3)
0070                DDFI=-18.D0*K4*G*(KAPPA*G-3.D0)/(TMP**5)
0071              ELSE
0072    C               Both of the remaining ion-pairing cases, G and A,
0073    C                   require calculating a and its derivatives
0074    C                   regardless of whether or not electric field
0075    C                   effects are included in the computations
0076                TMP=F0-KAPPA*G
0077                SQ=DSQRT(TMP*TMP+4.D0*F0*KAPPA*F2)
0078                A=(SQ-KAPPA*G-F0)/2.D0
0079                DA=-KAPPA*(1.D0+TMP/SQ)/2.D0
0080                DDA=2.D0*F0*K3*F2/(SQ**3)
0081                DDDA=6.D0*F0*K4*F2*TMP/(SQ**5)
0082                IF (SIP.EQ.'A') THEN
0083    C                   A+/B pathway only, gamma=0
0084                    IF (SEF.EQ.'N') THEN
0085    C                       Electric Field Effects Omitted
0086                        FI=(G-F3)*DA-A
0087                        DFI=(G-F3)*DDA
0088                        DDFI=DDA+(G-F3)*DDDA
0089                    ELSE
0090    C                       Electric Field Effects Included
0091                        FI=(G-F3)*DA+((F3/G)-2.D0)*A
0092                        DFI=(G-F3)*DDA+((F3/G)-1.D0)*DA-F3*A/G2
0093                        DDFI=(G-F3)*DDDA+F3*DDA/G
0094           *                    -2.D0*F3*DA/G2+2.D0*F3*A/G3
0095                    ENDIF
0096                ELSE
```

```
0097    C                   General treatment
0098                        IF (SEF.EQ.'N') THEN
0099    C                         Electric Field Effects Omitted
0100                              FI=CON*((G-F3)*DA-A)-GAMMA
0101                              DFI=CON*(G-F3)*DDA
0102                              DDFI=CON*(DDA+(G-F3)*DDDA)
0103                        ELSE
0104    C                         Electric Field Effects Included
0105                              FI=CON*(G-F3)*DA+GAMMA*G
0106         *                          +((F3/G)-2.D0)*(CON*A+GAMMA*F2)
0107                              DFI=CON*((G-F3)*DDA+((F3/G)-1.D0)*DA)
0108         *                          -F3*(CON*A+GAMMA*F2)/G2
0109                              DDFI=CON*(G-F3)*DDDA+F3*(CON*DDA+2.D0*
0110         *                           (-DA*CON+(CON*A+GAMMA*F2)/G)/G)/G
0111                        ENDIF
0112                  ENDIF
0113            ENDIF
0114
0115            RETURN
0116
0117            END

0001
0002    C$$$$$$$$$$$$$$$$$$$$$$$$$$$$$$$$$$$$$$$$$$$$$$$$$$$$$$$$$$$$$$$$$$
0003
0004            SUBROUTINE CROUT(N)
0005
0006    C       David N. Blauch          November 6, 1986
0007    C       Caltech, Pasadena, CA  91125
0008
0009    C       Solution of the Linear System of Equations Mx=v
0010    C       Using Crout Reduction (i.e., direct factorization)
0011
0012    C       Note that M must be tri-diagonal:
0013    C             the diagonal elements are in column 2
0014    C             the off-diagonal elements i-1 and i+1 are in
0015    C             columns 1 and 3 resp.
0016
0017            INTEGER I,N
0018            DOUBLE PRECISION M(5000,3),V(5000)
0019
0020            COMMON /CRTRED/M,V
0021
0022            M(1,3)=M(1,3)/M(1,2)
0023            DO 100, I=2,N-1
0024                  M(I,2)=M(I,2)-M(I,1)*M(I-1,3)
0025                  M(I,3)=M(I,3)/M(I,2)
0026    100     CONTINUE
0027            M(N,2)=M(N,2)-M(N,1)*M(N-1,3)
0028
0029            V(1)=V(1)/M(1,2)
0030            DO 200, I=2,N
0031                  V(I)=(V(I)-M(I,1)*V(I-1))/M(I,2)
0032    200     CONTINUE
0033
0034            DO 300, I=N-1,1,-1
```

```
0035                    V(I)=V(I)-M(I,3)*V(I+1)
0036     300      CONTINUE
0037
0038              RETURN
0039
0040              END
```

SSLSV

The program SSLSV calculates the slow-scan, linear-sweep voltammogram predicted by the ion-pairing model for a particular value of κ and X_E. When executed, the operator is prompted for information regarding the extent of ion-pairing and the fractional loading, specific values of κ and X_E being requested where necessary. This information determines which formulas from Chapter 8 will be utilized in the calculations. The initial and final values for the dimensionless potential, ε, are then requested, along with the resolution in ε. The convergence criterion and maximum number of iterations for Steffensen's algorithm,[44] used to solve for ρ given ε, are requested. The resolution in ε indicates the spacing between points on the voltammogram; at each point the value of ρ is calculated to the relative precision of the convergence criterion. Because quadratic interpolation is employed in the determination of the values for the peak current, peak potential, and the full- and half-widths at half-maximum, the actual accuracy of ε_p, $\Delta\varepsilon_{\pm}$, $\Delta\varepsilon_{-}$, and $\Delta\varepsilon_{+}$ are considerably better than the specified resolution in ε. All user-supplied numbers are floating point variables, except the maximum number of iterations. Finally, name(s) for the output file(s) must be provided.

The computer first constructs the entire voltammogram and then analyzes the voltammogram, locating the peak current and peak potential, potentials for the half-maximum currents, and the full- and half-widths. These voltammetric characterizations are then displayed on the terminal and written to disk; the voltammogram is then saved, if so requested.

```
0001            PROGRAM SSLSV
0002
0003    C       David N. Blauch          March 1989     Revised June 1990
0004    C       Caltech, Pasadena, CA  91125
0005    C
0006    C       Slow-Scan Linear-Sweep Voltammetry
0007    C             at a Nafion Modified Electrode
0008    C       See David N. Blauch, Ph.D. Thesis, Chapter 8 for a
0009    C             discussion of the relevant theory and nomenclature
0010    C
0011    C*****************************************************************
0012    C
0013    C       XE is the fractional loading
0014    C       KAPPA is the dimensionless, ion-pairing equil. constant
0015    C       RHO is the ratio of total concentrations of reduced to
0016    C             oxidized forms of the redox species
0017    C       CURRENT is the dimensionless current theta
0018    C       E is the dimensionless potential epsilon
0019    C
0020    C*****************************************************************
0021            INTEGER I,IP,CNT,MAX,NE
0022            DOUBLE PRECISION E(10000),C(10000),CP,CHALF,EP,HWPOS
0023            DOUBLE PRECISION XE,KAPPA,RHO,EI,EF,DE,F0,HWNEG,FW
0024            DOUBLE PRECISION EPSILON,CURRENT,PREC,ERR,X1,X2,X3
0025            CHARACTER*1 SIP,SXE,SLSV
0026            CHARACTER*12 FLSV,FCHR
0027
0028            EXTERNAL EPSILON,CURRENT
0029
0030    C*****************************************************************
0031    C       Get the simulation parameters
0032    C
0033            WRITE (6,10)
0034    10      FORMAT (//23X,'Slow-Scan Linear-Sweep Voltammetry',
0035         *        //1X,'Available ion-pairing limits:',
0036         *        /10X,'Z - no ion-pairing, kappa=0',
0037         *        /10X,'G - general treatment, arbitrary kappa',
0038         *        /10X,'S - strong ion-pairing limit, kappa>100',
0039         *        /10X,'(kappa is the dimensionless ion-pairing ',
0040         *        'equilibrium constant.)',
0041         *        /1X,'Option for extent of ion-pairing ?  ',$)
0042            READ (5,20) SIP
0043    20      FORMAT (A1)
0044            IF ((SIP.NE.'Z').AND.(SIP.NE.'S')) THEN
0045    C             'G' is the default option
0046                  SIP='G'
0047                  WRITE (6,30)
0048    30            FORMAT (1X,'Value for kappa ?  ',$)
0049                  READ (5,40) KAPPA
0050    40            FORMAT (D16.9)
0051                  IF (KAPPA.LE.0.D0) THEN
0052                        SIP='Z'
0053                  ENDIF
0054            ENDIF
0055
0056            WRITE (6,50)
```

```
0057    50      FORMAT (/1X,'Available fractional loading limits:',
0058           *       /10X,'Z - limiting behavior for XE=0',
0059           *       /10X,'G - general treatment, arbitrary XE',
0060           *       /10X,'F - limiting behavior for XE=1'
0061           *       /10X,'(XE is the fractional loading.)',
0062           *       /1X,'Option for fractional loading ?  ',$)
0063            READ (5,20) SXE
0064            IF ((SXE.NE.'Z').AND.(SXE.NE.'F')) THEN
0065                  SXE='G'
0066                  WRITE (6,60)
0067    60            FORMAT (1X,'Value for XE ?  ',$)
0068                  READ (5,40) XE
0069                  IF (XE.LE.0.D0) THEN
0070                        SXE='Z'
0071                  ELSE IF (XE.GE.1.D0) THEN
0072                        SXE='F'
0073                  ELSE
0074    C                   Fractional loading expressed as f0
0075                        F0=3.0/XE
0076                  ENDIF
0077            ENDIF
0078
0079            WRITE (6,70)
0080    70      FORMAT (/1X,'Limits for epsilon:',
0081           *       /1X,'Initial value for epsilon ?  ',$)
0082            READ (5,40) EI
0083            IF (EI.EQ.0.D0) THEN
0084                  IF (SIP.EQ.'G') THEN
0085                        EI=-10.D0-DLOG(3.D0*(1.D0+KAPPA))
0086                  ELSE
0087                        EI=-10.D0
0088                  ENDIF
0089            ENDIF
0090            WRITE (6,80)
0091    80      FORMAT (1X,'Final value for epsilon ?  ',$)
0092            READ (5,40) EF
0093            IF (EF.EQ.0.D0) THEN
0094                  IF (SIP.EQ.'G') THEN
0095                        EF=20.D0-DLOG(3.D0*(1.D0+KAPPA))
0096                  ELSE
0097                        EF=20.D0
0098                  ENDIF
0099            ENDIF
0100            WRITE (6,90)
0101    90      FORMAT (1X,'Absolute resolution of epsilon ?  ',$)
0102            READ (5,40) DE
0103            IF (DE.LE.0.D0) THEN
0104                  DE=0.01
0105            ENDIF
0106
0107            WRITE (6,100)
0108    100     FORMAT (/1X,'Computational parameters:',/1X,'Relative ',
0109           *       'tolerance for the Steffensen algorithm ?  ',$)
0110            READ (5,40) PREC
0111            IF (PREC.LE.0.D0) THEN
0112                  PREC=1.D-6
```

```
0113            ENDIF
0114            WRITE (6,110)
0115    110     FORMAT (1X,'Max. nbr. of Steffensen iterations ?  ',$)
0116            READ (5,120) MAX
0117    120     FORMAT (I8)
0118            IF (MAX.LE.0) THEN
0119                  MAX=20
0120            ENDIF
0121
0122            WRITE (6,123)
0123    123     FORMAT (/1X,'Filename for results ?  ',$)
0124            READ (5,140) FCHR
0125            WRITE (6,125)
0126    125     FORMAT (1X,'Save voltammogram ?  ',$)
0127            READ (5,20) SLSV
0128            IF ((SLSV.EQ.'Y').OR.(SLSV.EQ.'y')) THEN
0129                  WRITE (6,130)
0130    130           FORMAT (/1X,'Filename for the voltammogram ?  ',$)
0131                  READ (5,140) FLSV
0132    140           FORMAT (A12)
0133            ENDIF
0134
0135    C*****************************************************************
0136    C       Perform initializations
0137    C
0138    C       Number of points in the simulation
0139            NE=IDINT((EF-EI)/DE)
0140
0141    C*****************************************************************
0142
0143    C       Select the seed value for RHO, based upon initial
0144    C             potential for all points except the first, the seed
0145    C             value is the previous value of RHO
0146            RHO=DEXP(-EI)
0147
0148            DO 500, I=1,NE+1
0149                  E(I)=EI+DE*DBLE(REAL(I-1))
0150
0151    C             ***** Steffensen's algorithm is used to determine
0152    C                    the value of RHO that gives rise to E
0153    C             initialize the iteration counter
0154                  CNT=0
0155
0156    C             re-entry point for next iteration
0157    C                   increment iteration counter
0158    300                 CNT=CNT+1
0159
0160    C                   Are we wasting our time?
0161                        IF (CNT.GT.MAX) THEN
0162    C                         we have exceeded MAX iterations
0163    C                         algorithm has failed
0164                              WRITE (6,320)
0165    320                       FORMAT (/1X,'MAX exceeded')
0166                              STOP
0167                        ENDIF
0168
```

```
0169    C                  save the current value of RHO
0170                       X1=RHO
0171    C                  two passes of fixed-point iteration
0172    C                        the system is such that fixed-point
0173    C                        iteration always converges
0174                       X2=DEXP(EPSILON(X1,KAPPA,F0,SIP,SXE)-E(I))*X1
0175                       X3=DEXP(EPSILON(X2,KAPPA,F0,SIP,SXE)-E(I))*X2
0176    C                  calculate the fixed-point error
0177                       ERR=DABS((X3-X2)/X3)
0178    C                  are we within tolerance?
0179                       IF (ERR.GT.PREC) THEN
0180    C                        best estimate is outside of tolerance
0181    C                        Aitken's algorithm is used to speed
0182    C                        convergence
0183                             RHO=(X1*X3-X2*X2)/(X3-2.D0*X2+X1)
0184    C                        return for another iteration
0185                             GOTO 300
0186                       ELSE
0187    C                        RHO has been calculated to a
0188    C                        satisfactory precision
0189                             RHO=X3
0190                       ENDIF
0191
0192    C             calculate the current
0193                  C(I)=CURRENT(RHO,KAPPA,F0,SIP,SXE)
0194    500           CONTINUE
0195
0196    C*************************************************************
0197    C       Save the voltammogram
0198    C
0199            IF ((SLSV.EQ.'Y').OR.(SLSV.EQ.'y')) THEN
0200                  OPEN (1,FILE=FLSV,STATUS='NEW')
0201
0202                  DO 600, I=1,NE+1
0203                        WRITE (1,620) E(I),C(I)
0204    620                 FORMAT (1X,D14.7,',',D14.7)
0205    600           CONTINUE
0206
0207                  CLOSE (1)
0208            ENDIF
0209
0210    C*************************************************************
0211    C       Pass 1:  Locate the peak current
0212    C
0213                  I=1
0214    700           CONTINUE
0215                  I=I+1
0216                  IF (I.GT.NE) THEN
0217    C                   we ran out of points and have found no maxima
0218                        WRITE (6,720)
0219    720                 FORMAT (1X,'Peak Current Not Found')
0220                        STOP
0221                  ELSE
0222    C                   the peak current is always above 0.1
0223    C                   scan voltammogram until current is above 0.1
0224                        IF (C(I).LT.0.1) GOTO 700
```

```
0225                ENDIF
0226    C           is the curve still rising?
0227                IF (C(I)-C(I-1)) 750,750,700
0228    750     CONTINUE
0229    C       Determine the peak current and potential
0230    C           the peak current lies between points I-2 and I
0231    C           use quadratic interpolation to estimate the peak
0232    C           current and peak potential
0233    C       save the position, roughly, of the maxima
0234            IP=I
0235    C       calculate the peak current and peak potential
0236            CP=C(I-1)-0.125D0*((C(I)-C(I-2))**2)/(C(I)
0237         *       -2.D0*C(I-1)+C(I-2))
0238            EP=E(I-1)-0.5D0*DE*(C(I)-C(I-2))/(C(I)
0239         *       -2.D0*C(I-1)+C(I-2))
0240    C*************************************************************
0241    C       Pass 2:  Locate one of the half-maxima
0242    C           examine portion of the curve with points I > IP
0243    C
0244    C       value of the current at half-maxima
0245            CHALF=CP/2.D0
0246    C       initialize the pointer
0247            I=IP+1
0248    800         CONTINUE
0249                I=I+1
0250                IF (I.GT.NE) THEN
0251    C               we have run out of points and the current is
0252    C               still above CHALF
0253                    WRITE (6,820)
0254    820             FORMAT (1X,'First Half-Maxima Not Found')
0255                    STOP
0256                ENDIF
0257                IF (C(I)-CHALF) 850,850,800
0258    850     CONTINUE
0259    C       use quadratic interpolation to locate the potential at
0260    C           half-maxima
0261    C       have we found the upper (positive) or lower (negative)
0262    C           half of the wave?
0263            IF (E(I).GT.EP) THEN
0264                HWPOS=E(I-1)+DE*(CHALF-C(I-1))/(C(I)-C(I-1))-EP
0265            ELSE
0266                HWNEG=EP-E(I-1)-DE*(CHALF-C(I-1))/(C(I)-C(I-1))
0267            ENDIF
0268
0269    C*************************************************************
0270    C       Pass 3:  Locate the other half-maxima
0271    C           examine portion of the curve with points I < IP
0272    C
0273    C       initialize the pointer
0274            I=IP
0275    900         CONTINUE
0276                I=I-1
0277                IF (I.GT.NE) THEN
0278    C               we have run out of points and the current is
0279    C               still above CHALF
0280                    WRITE (6,920)
```

```
0281    920               FORMAT (1X,'Second Half-Maxima Not Found')
0282                      STOP
0283                ENDIF
0284    C           is the current less than half the peak current?
0285                IF (C(I)-CHALF) 950,950,900
0286    950     CONTINUE
0287    C       use quadratic interpolation to locate the potential at
0288    C           half-maxima
0289    C       have we found the upper (positive) or lower (negative)
0290    C           half of the wave?
0291            IF (E(I).GT.EP) THEN
0292                HWPOS=E(I)+DE*(CHALF-C(I))/(C(I+1)-C(I))-EP
0293            ELSE
0294                HWNEG=EP-E(I)-DE*(CHALF-C(I))/(C(I+1)-C(I))
0295            ENDIF
0296
0297    C       Calculate the full-width at half-maxima
0298    C           the full-width is the sum of the half-widths
0299            FW=HWPOS+HWNEG
0300
0301    C*************************************************************
0302    C       Print the results at the terminal
0303    C
0304            WRITE (6,1000) EP,CP,HWNEG,HWPOS,FW
0305    1000    FORMAT (/10X,'peak potential =  ',F10.6,
0306         *          /10X,'peak current =  ',F8.6,
0307         *          /10X,'negative half-width at half-maxima =  ',F8.6,
0308         *          /10X,'positive half-width at half-maxima =  ',F8.6,
0309         *          /10X,'full-width at half-maxima =  ',F8.6)
0310
0311    C*************************************************************
0312    C       Write the results to the characterization file
0313    C
0314            OPEN (1,FILE=FCHR,STATUS='NEW')
0315
0316            WRITE (1,1100)
0317    1100    FORMAT (23X,'Slow-Scan Linear Sweep Voltammetry',
0318         *          //1X,'Computations based upon:')
0319            IF (SIP.EQ.'Z') THEN
0320                WRITE (1,1110)
0321    1110        FORMAT (10X,'No ion-pairing (kappa=0)')
0322            ELSE IF (SIP.EQ.'S') THEN
0323                WRITE (1,1120)
0324    1120        FORMAT (10X,'Strong ion-pairing (kappa>100)',
0325         *          /10X,'peak potential does not include ln[kappa]')
0326            ELSE
0327                WRITE (1,1130) KAPPA
0328    1130        FORMAT (10X,'General treatment, kappa =  ',D16.9)
0329            ENDIF
0330            IF (SXE.EQ.'Z') THEN
0331                WRITE (1,1140)
0332    1140        FORMAT (10X,'Low fractional loading limit (XE=0)')
0333            ELSE IF (SXE.EQ.'F') THEN
0334                WRITE (1,1150)
0335    1150        FORMAT (10X,'Full fractional loading (XE=1)')
0336            ELSE
```

```
0337                WRITE (1,1160) XE
0338    1160        FORMAT (10X,'General treatment with XE =  ',F8.6)
0339            ENDIF
0340            WRITE (1,1200) DE,EP,CP,HWNEG,HWPOS,FW
0341    1200    FORMAT (/1X,'Resolution in epsilon = ',F8.6,//1X,
0342         *       'Potentials and wave widths expressed in terms ',
0343         *       'of epsilon',/1X,'Peak current expressed in ',
0344         *       'terms of theta',/1X,'Characteristics determined ',
0345         *       'by quadratic interpolation:',
0346         *       /10X,'peak potential =  ',F10.6,
0347         *       /10X,'peak current =  ',F8.6,
0348         *       /10X,'negative half-width at half-maxima =  ',F8.6,
0349         *       /10X,'positive half-width at half-maxima =  ',F8.6,
0350         *       /10X,'full-width at half-maxima =  ',F8.6)
0351
0352            CLOSE (1)
0353
0354            END

0001
0002    C$$$$$$$$$$$$$$$$$$$$$$$$$$$$$$$$$$$$$$$$$$$$$$$$$$$$$$$$$$$$$$$$$$
0003
0004            DOUBLE PRECISION FUNCTION EPSILON(RHO,KAPPA,F0,SIP,SXE)
0005
0006    C       Function returns epsilon given the oxidation state
0007    C            of the coating (RHO), the ion-pairing equilibrium
0008    C            constant (KAPPA), and the fractional loading (F0).
0009    C
0010    C       The switches SIP and SXE indicate the extent of
0011    C            ion-pairing and fractional loading, thereby
0012    C            identifying the proper formulas to be used.
0013    C
0014    C*************************************************************
0015            DOUBLE PRECISION R,RHO,RHO1,KAPPA,F0,F1,F2,F3
0016            DOUBLE PRECISION TMP,A,E
0017            CHARACTER*1 SIP,SXE
0018
0019    C*************************************************************
0020    C       these quantities appear frequently in the formulas for E
0021            F1=F0-1.D0
0022            F2=F0-2.D0
0023            F3=F0-3.D0
0024            RHO1=RHO+1.D0
0025            R=RHO/RHO1
0026
0027            IF (SXE.EQ.'Z') THEN
0028    C            Zero fractional loading
0029                 E=-DLOG(3.D0*RHO)
0030                 IF (SIP.EQ.'G') THEN
0031    C                 Arbitrary degree of ion-pairing
0032                      E=E-DLOG(1.D0+KAPPA)
0033                 ENDIF
0034            ELSE IF (SXE.EQ.'F') THEN
0035    C            Full fractional loading
0036                 IF (SIP.EQ.'Z') THEN
0037    C                 No ion-pairing
```

```
0038                        E=-DLOG(R*RHO)
0039                  ELSE IF (SIP.EQ.'S') THEN
0040      C                 Strong ion-pairing
0041                        E=DLOG(3.D0/(RHO*R**2))
0042                  ELSE
0043      C                 Arbitrary degree of ion-pairing
0044                        TMP=KAPPA*R+3.D0
0045                        A=(DSQRT(12.D0*KAPPA/RHO1+TMP**2)-TMP)/2.D0
0046                        E=-DLOG(R*R*KAPPA/A)
0047                  ENDIF
0048            ELSE
0049      C           Arbitrary fractional loading
0050                  IF (SIP.EQ.'Z') THEN
0051      C                 No ion-pairing
0052                        E=-DLOG(3.D0*RHO*(F2*RHO+F3)/(F0*RHO1))
0053                  ELSE IF (SIP.EQ.'S') THEN
0054      C                 Strong ion-pairing
0055                        E=-DLOG(3.D0*RHO*((F2*RHO+F3)/(F0*RHO1))**2)
0056                  ELSE
0057      C                 Arbitrary degree of ion-pairing
0058                        TMP=F0+KAPPA*(F2*RHO+F3)/RHO1
0059                        A=(DSQRT(4.D0*KAPPA*F0/RHO1+TMP**2)-TMP)/2.D0
0060                        E=-DLOG(3.D0*RHO*KAPPA*(F2*RHO+F3)
0061           *                  /(A*F0*RHO1*RHO1))
0062                  ENDIF
0063            ENDIF
0064
0065            EPSILON=E
0066
0067            RETURN
0068
0069            END

0001
0002      C$$$$$$$$$$$$$$$$$$$$$$$$$$$$$$$$$$$$$$$$$$$$$$$$$$$$$$$$$$$$$$$$$$$
0003
0004            DOUBLE PRECISION FUNCTION CURRENT(RHO,KAPPA,F0,SIP,SXE)
0005
0006      C     Function returns value of dimensionless current given the
0007      C           oxidation state of the coating (RHO), the
0008      C           ion-pairing equilibrium constant (KAPPA), and
0009      C           the fractional loading (F0).
0010      C
0011      C     The switches SIP and SXE indicate the extent of
0012      C           ion-pairing and fractional loading, thereby
0013      C           identifying the proper formulas to be used.
0014      C
0015      C*************************************************************
0016            DOUBLE PRECISION R,RHO,RHO1,KAPPA,F0,F1,F2,F3
0017            DOUBLE PRECISION TMP,A,C
0018            CHARACTER*1 SIP,SXE
0019
0020      C*************************************************************
0021      C     these quantities
0022            F1=F0-1.D0
0023            F2=F0-2.D0
```

```
0024            F3=F0-3.D0
0025            RHO1=RHO+1.D0
0026            R=RHO/RHO1
0027
0028            IF (SXE.EQ.'Z') THEN
0029      C           Zero fractional loading
0030                  C=R/RHO1
0031            ELSE IF (SXE.EQ.'F') THEN
0032      C           Full fractional loading
0033                  IF (SIP.EQ.'Z') THEN
0034      C               No ion-pairing
0035                      C=R/(2.D0+RHO)
0036                  ELSE IF (SIP.EQ.'S') THEN
0037      C               Strong ion-pairing
0038                      C=R/(3.D0+RHO)
0039                  ELSE
0040      C               Arbitrary degree of ion-pairing
0041                      TMP=KAPPA*R+3.D0
0042                      A=(DSQRT(12.D0*KAPPA/RHO1+TMP**2)-TMP)/2.D0
0043                      C=R*(RHO1*A*A+3.D0*KAPPA)/(6.D0*KAPPA
0044           *                +(3.D0+A)*KAPPA*RHO+2.D0*RHO1*A*A)
0045                  ENDIF
0046            ELSE
0047      C           Arbitrary fractional loading
0048                  IF (SIP.EQ.'Z') THEN
0049      C               No ion-pairing
0050                      C=R*(F2*RHO+F3)/(F2*RHO*RHO+2.D0*F2*RHO+F3)
0051                  ELSE IF (SIP.EQ.'S') THEN
0052      C               Strong ion-pairing
0053                      C=R*(F2*RHO+F3)/(F2*RHO*RHO+
0054           *                (2.D0*F0-3.D0)*RHO+F3)
0055                  ELSE
0056      C               Arbitrary degree of ion-pairing
0057                      TMP=F0+KAPPA*(F2*RHO+F3)/RHO1
0058                      A=(DSQRT(4.D0*KAPPA*F0/RHO1+TMP**2)-TMP)/2.D0
0059                      C=R/(KAPPA*RHO*(A+F0)/(RHO1*A*A+KAPPA*F0)
0060           *                +(F1*RHO+F3)/(F2*RHO+F3))
0061                  ENDIF
0062            ENDIF
0063
0064            CURRENT=C
0065
0066            RETURN
0067
0068            END
```

Part II References

References

1. For reviews see (a) R. W. Murray, Electroanalytical Chemistry, A. J. Bard, ed., Dekker, New York, 1984, pp. 191-368. (b) A. R. Hillman, Electrochemical Science and Technology of Polymers, R. G. Lindford, ed., Elsevier Applied Science, New York, 1987, Chapts. 5 and 6. (c) M. Kaneka and D. Woerhle, *Adv. Polym. Sci.*, **14** (1988) 142.

2. W. J. Albery, M. G. Boutelle, P. J. Colby, and A. R. Hillman, *J. Electroanal. Chem.*, **133** (1982) 135.

3. (a) N. Oyama and F. C. Anson, *J. Electrochem. Soc.*, **127** (1980) 640. (b) D. A. Buttry and F. C. Anson, *J. Electroanal. Chem.*, **130** (1982) 333. (c) K. Shigehara, N. Oyama, and F. C. Anson, *J. Amer. Chem. Soc.*, **103** (1981) 2552. (d) N. Oyama, S. Yamaguchi, Y. Nishiki, K. Tokuda, H. Matsuda, and F. C. Anson, *J. Electroanal. Chem.*, **139** (1982) 371. (e) D. A. Buttry and F. C. Anson, *J. Amer. Chem. Soc.*, **105** (1983) 685. (f) F. C. Anson, J.-M. Saveant, and K. Shigehara, *J. Amer. Chem. Soc.*, **105** (1983) 1096. (g) F. C. Anson, T. Ohsaka, and J.-M. Saveant, *J. Phys. Chem.*, **87** (1983) 640. (h) D. A. Buttry, J.-M. Saveant, and F. C. Anson, *J. Phys. Chem.*, **88** (1984) 3086.

4. (a) P. J. Peerce and A. J. Bard, *J. Electroanal. Chem.*, **114** (1980) 89. (b) C. R. Martin, I. Rubenstein, and A. J. Bard, *J. Amer. Chem.* Soc., **104** (1982) 4817. (c) H. S. White, J. Leddy, and A. J. Bard, *J. Amer. Chem. Soc.*, **104** (1982) 4811.

5. (a) K. Doblhofer, H. Braun, and R. Lange, *J. Electroanal. Chem.*, **206** (1986) 93. (b) K. Niwa and K. Doblhofer, *Electrochim. Acta*, **31** (1986) 549. (c) R. Lange and K. Doblhofer, *J. Electroanal. Chem.*, **216** (1987) 241. (d) R. Lange and K. Doblhofer, *J. Electroanal. Chem.*, **237** (1987) 13. (e) K. Doblhofer and R. Lange, *J. Electroanal. Chem.*, **229** (1987) 239. (f) K. Doblhofer and R. D. Armstrong, *Electrochim. Acta*, **33** (1988) 453. (g) J. Ye and K. Doblhofer, *Ber. Bunsen Ges. Phys. Chem.*, **92** (1988) 271.

6. C. Elliott and J. G. Redepenning, *J. Electroanal. Chem.*, **181** (1984) 137.

7. (a) M. Majda and L. R. Faulkner, *J. Electroanal. Chem.*, **137** (1982) 149. (b) M. Majda and L. R. Faulkner, *J. Electroanal. Chem.*, **169** (1984) 77. (c) M. Majda and L. R. Faulkner, *J.*

Electroanal. Chem., **169** (1984) 97. (d) X. Chen, P. He, and L. R. Faulkner, *J. Electroanal. Chem.*, **222** (1987) 223.

8. P. He and X. Chen, *J. Electroanal. Chem.*, **256** (1988) 353.

9. (a) F. B. Kaufman and E. M. Engler, *J. Amer. Chem. Soc.*, **101** (1979) 547. (b) A. Schroeder, F. B. Kaufman, V. Patel, and E. M. Engler, *J. Electroanal. Chem.*, **113** (1980) 193. (c) J. Q. Chambers, F. B. Kaufman, and K. H. Nichols, *J. Electroanal. Chem.*, **142** (1988) 277.

10. (a) C. R. Martin and K. A. Dollard, *J. Electroanal. Chem.*, **159** (1983) 127. (b) R. B. Moore III and C. R. Martin, *Anal. Chem.*, **58** (1986) 2569. (c) L. D. Whiteley and C. R. Martin, *J. Phys. Chem.*, **93** (1989) 4650.

11. (a) P. Daum, J. R. Lenhard, D. Rolison, and R. W. Murray, *J. Amer. Chem. Soc.*, **102** (1980) 4649. (b) P. Daum and R. W. Murray, *J. Phys. Chem.*, **85** (1981) 389. (c) J. S. Facci, R. H. Schmehl, and R. W. Murray, *J. Amer. Chem. Soc.*, **104** (1982) 4959. (d) R. H. Schmehl and R. W. Murray, *J. Electroanal. Chem.*, **152** (1983) 97. (e) S. Nakahama and R. W. Murray, *J. Electroanal. Chem.*, **158** (1983) 303. (f) J. C. Jernigan and R. W. Murray, *J. Phys. Chem.*, **91** (1987) 2030. (g) J. C. Jernigan and R. W. Murray, *J. Amer. Chem. Soc.*, **109** (1987) 1138. (h) B. J. Feldman and R. W. Murray, *Inorg. Chem.*, **26** (1987) 1702.

12. (a) I. Rubenstein, *J. Electroanal. Chem.*, **188** (1985) 227. (b) I. Rubenstein, J. Rishpon, and S. Gottesfeld, *J. Electroanal. Chem.*, **133** (1986) 729.

13. (a) C. P. Andrieux and J.-M. Saveant, *J. Electroanal. Chem.*, **111** (1980) 377. (b) C. P. Andrieux, O. Haas, and J.-M. Saveant, *J. Amer. Chem. Soc.*, **108** (1986) 8175.

14. M. Sharp, B. Lindhom, and E. L. Lind, *J. Electroanal. Chem.*, **274** (1989) 35.

15. (a) See References 1 and 11b-e and references cited therein. (b) W. J. Albery and A. R. Hillman, Annual Rep. C (1981), The Royal Society of Chemistry, London, 1983, pp. 347-377. (c) F. C. Anson, C.-L. Ni, and J.-M. Saveant, *J. Amer. Chem. Soc.*, **107** (1985) 3442. (d) A. R. Guadalupe and H. D. Abruna, *Anal.*

Chem., **57** (1985) 142. (e) U. Dogani and A. Heller, *J. Amer. Chem. Soc.*, **111** (1989) 2357.

16. (a) C. P. Andrieux, J.-M. Dumas-Bouchiat, and J.-M. Saveant, *J. Electroanal. Chem.*, **114** (1980) 159. (b) R. W. Murray, *Phil. Trans. R. Soc. Lond. A*, **302** (1981) 253. (c) C. P. Andrieux, J.-M. Dumas-Bouchiat, and J.-M. Saveant, *J. Electroanal. Chem.*, **131** (1982) 1. (d) C. P. Andrieux and J.-M. Saveant, *J. Electroanal. Chem.*, **134** (1982) 163. (e) C. P. Andrieux and J.-M. Saveant, *J. Electroanal. Chem.*, **142** (1982) 1. (f) F. C. Anson, J.-M. Saveant, and K. Shigehara, *J. Phys. Chem.*, **87** (1983) 214. (g) C. P. Andrieux, J.-M. Dumas-Bouchiat, and J.-M. Saveant, *J. Electroanal. Chem.*, **169** (1984) 9. (h) W. J. Albery and A. R. Hillman, *J. Electroanal. Chem.*, **170** (1984) 27. (i) C. P. Andrieux and J.-M. Saveant, *J. Electroanal. Chem.*, **171** (1984) 65.

17. (a) Transient techniques have usually been employed, but in a few cases steady-state measurements have been used. (b) P. G. Pickup and R. W. Murray, *J. Amer. Chem. Soc.*, **105** (1983) 4510. (c) P. G. Pickup, K. Kutner, C. R. Leidner, and R. W. Murray, *J. Amer. Chem. Soc.*, **106** (1984) 1991. (d) C. E. Chidsey, B. L. Feldman, C. Lundgren, and R. W. Murray, *Anal. Chem.*, **58** (1986) 601. (e) D. K. Smith, G. A. Lane, and M. S. Wrighton, *J. Phys. Chem.*, **92** (1988) 2616.

18. (a) If this condition is not fulfilled, restricted diffusive behavior observed. (b) A. T. Hubbard and F. C. Anson, *J. Electroanal. Chem.*, **4** (1970) 129.

19. E. Laviron, *J. Electroanal. Chem.*, **112** (1980) 1.

20. (a) In previous discussions of experimental data, the following expression[20b] has usually been used instead of Equation 5.2:

$$D_{ap} = D_{pd} + \frac{\pi}{4} k_1 \delta^2 C_E$$

This expression was originally derived from a thermodynamic model of the possible enhancement of the diffusion coefficient for physical displacement in solution by electron transfer between the diffusion species.[22b-c] The numerical coefficient of $\pi/4$ has been recently corrected to 1/6 on the basis of the same thermodynamic model that was shown to be equivalent to the stochastic model.[22d-f] (b) I. Ruff and V. J. Friedrich, *J.*

Phys. Chem., **75** (1971) 3297. (c) H. Dahms, *J. Phys. Chem.*, **72** (1968) 362. (d) I. Ruff and L. Botar, *J. Chem. Phys.*, **83** (1985) 1292. (e) L Botar and I. Ruff, *Chem. Phys. Lett.*, **126** (1988) 348. (f) L. Botar and I. Ruff, *Chem. Phys. Lett.*, **149** (1988) 99.

21. (a) J. Newman, Electrochemical Systems, Prentice-Hall, New York, 1973. (b) R. P. Buck, *J. Electroanal. Chem.*, **46** (1973) 1.

22. (a) The appropriate partial differential equations describing the time-dependence of electron hopping have been derived by means of the same fictitious cubic lattice model evoked earlier where the effect of the difference in the electric potential between the two adjacent sites on the rate of electron transfer has been taken into account. (b) J.-M. Saveant, *J. Electroanal. Chem.*, **227** (1987) 299. (c) J.-M. Saveant, *J. Phys. Chem.*, **92** (1988) 4526. (d) J.-M. Saveant, *J. Electroanal. Chem.*, **242** (1988) 1. (e) C. P. Andrieux and J.-M. Saveant, *J. Phys. Chem.*, **92** (1988) 6761.

23. (a) A. Eisenberg, *Macromolecules*, **3** (1970) 147. (b) A. Eisenberg and M. King, Ion-Containing Polymers, Academic Press, New York, 1977. (c) R. A. Komozovski and K. A. Mauritz in Perfluorinated Ionomer Membranes, ACS Symp. Ser. No. 180, A. Eisenberg and H. L. Yeager, eds., American Chemical Society, Washington, D. C., 1982, pp. 113-138 and references cited therein.

24. J.-M. Saveant, *J. Phys. Chem.*, **92** (1988) 1011.

25. G. A. Olah, P. S. Iyer, and G. K. S. Prakash, *Synthesis*, (1986) 513.

26. C. Creutz, M. Chou, T. L. Netzel, M. Okumura, and N. Sutin, *J. Amer. Chem. Soc.*, **102** (1982) 1309.

27. N. Oyama and F. C. Anson, *J. Amer. Chem. Soc.*, **101** (1980) 3450.

28. An early study of $Ru(bpy)_3^{2+}$ in Nafion coatings reported that significant portions of the incorporated complexes were not electroactive.[4b] These results, which depended upon the mixing of the complexes with nonaqueous solutions of Nafion before the deposition of coatings on the electrode surfaces, may have resulted in significantly different internal structures in which pockets of reactants were insulated from the electrode.

29. (a) A very recent report has presented measurements of the diffusion coefficients of a singly charged ferrocenylammonium cation and of $Fe(bpy)_3^{2+}$ in Nafion coatings on ultramicroelectrodes.[10c] The results show a sharp increase in the diffusion coefficient at very low loadings, a region not investigated extensively in the present and in other recent[8,14] studies. The experimental conditions employed were quite different from those of the present study, including the use of much higher supporting electrolyte concentrations. The cationic permselectivity of the coatings was compromised, while in the present study the permselectivity was ideal as has been demonstrated previously.[27] (b) J. G. Redepenning and F. C. Anson, *J. Phys. Chem.*, **91** (1987) 4549.

30. K. A. Mauritz and A. J. Hopfinger, Modern Aspects of Electrochemistry, No. 14, J. O'M. Bockris, B. E. Conway, and R. E. White, eds., Plenum, New York, 1982, Chapt. 6.

31. H. L. Yeager and A. J. Steck, *J. Electrochem. Soc.*, **128** (1981) 1880.

32. H. L. Yeager and R. S. Yeo, Modern Aspects of Electrochemistry, No. 16, J. O'M. Bockris, B. E. Conway, and R. E. White, eds., Plenum, New York, 1985, Chapt. 6.

33. (a) These differential equations are based on the stochastic description of electron hopping mentioned in the introduction of Chapter 5. In the cubic quasi-lattice model, the system is regarded as a completely disordered structure so that the probability of finding one particular species at one node of the lattice is proportional to its concentration. In a recent discussion of electron hopping in redox polymers, a quite different approach was proposed[33b] in which the redox centers are regarded as individually located at the nodes of an actual perfect cubic lattice. The lattice characteristic distance was taken as equal to the average distance between two nearest neighbors and the probability of electron hopping between them as an exponentially decaying function of this distance. The resulting diffusionlike charge propagation is predicted to increase with the concentration of redox sites more rapidly than proportionally. It seems unlikely, however, that such a perfect crystal ordering of the electroactive sites could exist in redox polymer films. For such systems, the stochastic model described above strikes us as more realistic. (b) I. Fritsch-

Faules and L. R. Faulkner, *J. Electroanal. Chem.*, **263** (1989) 237.

34. The rate constants k_1 and k_2 describe the rate of electron hopping across a distance δ. A simple estimate of δ is the separation between redox centers when the equivalent hard spheres are in contact. It would be possible to allow electron transfer to occur at greater distances in consideration of the overlap of the electron donating and receiving orbitals ("extended electron transfer"[29b]), and/or because each redox center may oscillate out of its equilibrium position. In both cases, integration over a distance-dependent probability density function (a decaying exponential function would be the simplest model) would lead to an increase of the average hopping distance.

35. M. W. Verbrugge and R. F. Hill, *J. Electrochem. Soc.*, **137** (1990) 893.

36. (a) H. D. Abruna, P. Denisevich, M. Umana, T. J. Meyer, and R. W. Murray, *J. Amer. Chem. Soc.*, **103** (1981) 1. (b) M. S. Chan and A. C. Wahl, *J. Phys. Chem.*, **82** (1978) 2543. (c) R. Campion, N. Purdie, and N. Sutin, *J. Amer. Chem. Soc.*, **85** (1986) 3528.

37. (a) H. D. Abruna, *Coord. Chem. Rev.*, **86** (1988) 135. (b) R. F. Lane and A. T. Hubbard, *J. Phys. Chem.*, **77** (1973) 1401. (c) E. Laviron, *J. Electroanal. Chem.*, **39** (1972) 1.

38. A. J. Bard and L. R. Faulkner, Electrochemical Methods, Wiley, New York, 1980, pp. 76-78.

39. Reference 38, Chapt. 1.

40. R. L Burden, J. D. Faires, and A. C. Reynolds, Numerical Analysis, 2nd ed., Prindle, Weber, and Schmidt, New York, 1981, pp. 448-455.

41. Reference 40, Chapt. 6.

42. Reference 40, Chapt. 11.

43. C. M. Bender and S. A. Orszag, Advanced Mathematical Methods for Scientists and Engineers, McGraw-Hill, New York, 1978, Chapt. 8.

44. Reference 40, Chapt. 2.